Report No. 1.LC.APL.96

Synchronous Picosecond Sonoluminescence

Lawrence A. Crum

Applied Physics Laboratory
University of Washington
1013 NE 40th Street
Seattle, WA 98105

10 October 1996

FINAL REPORT

1 June 1993 - 31 May 1996

Approved for public release:
Distribution Unlimited.

Prepared for:

Office of Naval Research
ONR 331
800 North Quincy Street
Arlington, VA 22217-5660

DISCLAIMER NOTICE

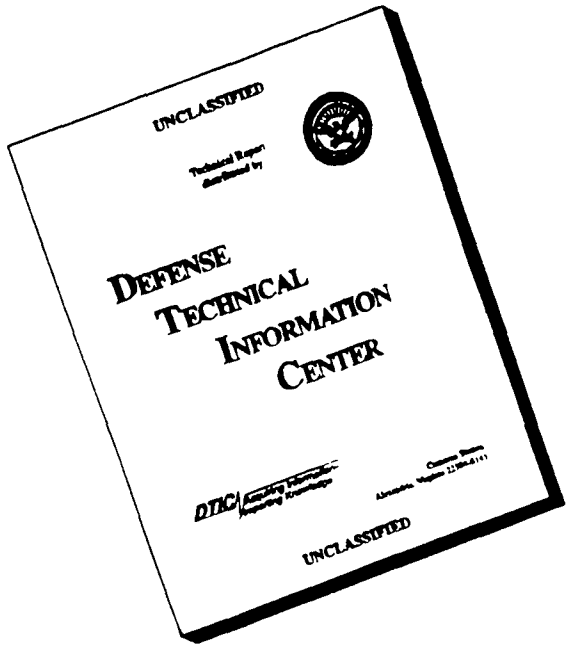

THIS DOCUMENT IS BEST QUALITY AVAILABLE. THE COPY FURNISHED TO DTIC CONTAINED A SIGNIFICANT NUMBER OF PAGES WHICH DO NOT REPRODUCE LEGIBLY.

SUPPLEMENTARY

INFORMATION

ERRATA

Applied Physics Laboratory
College of Ocean and Fishery Sciences, University of Washington

AD-A 317384

26 December 1996
Serial 5C4071

TO: Defense Technical Information Center
8725 John J. Kingman Road
Suite 0944
Fort Belvoir, VA 22060-6218

From: Lawrence A. Crum, Chairman
Acoustics & Electromagnetics Department

Subj: Revision of Previously Submitted 298 Form Page

Ref: (a) "Synchronous Picosecond Sonoluminescence," by Lawrence A. Crum, Applied Physics Laboratory, University of Washington, 10 October 1996, report # 1LC.APL.96, unclassified

Encl: (1) Revised 298 Form page for the report of Ref. (a)
(2) DTIC 50 card for the report of Ref. (a)

1. In October 1996, the report of Reference (a) was submitted to DTIC. However, the 298 Form page bound within the report was incomplete. Since the report satisfied the final report requirement for two interrelated Office of Naval Research grants, both grant numbers should have been cited in block #5, Funding Numbers. Enclosure (1) is a revised 298 Form page that cites both grants.

2. The original submission of the report to DTIC also failed to include a DTIC 50 card. This card for the report is provided as Enclosure (2).

Lawrence A. Crum

LAC:rmb

cc: June Hawley, ONR Administrative Grants Officer
Dr. Logan Hargove, Code 331, Office of Naval Research

1013 NE 40th Street Seattle, Washington 98105-6698 (206) 543-1300

REPORT DOCUMENTATION PAGE

Form Approved
OPM No. 0704-0188

1. AGENCY USE ONLY *(Leave blank)*	2. REPORT DATE	3. REPORT TYPE AND DATES COVERED
	10 October 1996	Final Report 2/1/93 - 5/31/96

4. TITLE AND SUBTITLE

Synchronous Picosecond Sonoluminescence

5. FUNDING NUMBERS

G N00014-93-1-0322

G N00014-93-1-0798

6. AUTHOR(S)

Lawrence A. Crum

ERRATA
ADA 317984

7. PERFORMING ORGANIZATION NAME(S) AND ADDRESS(ES)

Applied Physics Laboratory
University of Washington
1013 NE 40th Street
Seattle, WA 98105-6698

8. PERFORMING ORGANIZATION REPORT NUMBER

1.LC.APL.96

9. SPONSORING / MONITORING AGENCY NAME(S) AND ADDRESS(ES)

Office of Naval Research, Code 331
800 N. Quincy Street
Arlington, VA 22217-5660

10. SPONSORING / MONITORING AGENCY REPORT NUMBER

11. SUPPLEMENTARY NOTES

[redacted]

12a. DISTRIBUTION / AVAILABILITY STATEMENT

Approved for public release, distribution unlimited

12b. DISTRIBUTION CODE

13. ABSTRACT *(Maximum 200 words)*

The discovery of single-bubble sonoluminescence has led to a number of interesting discoveries and provocative claims-among these are that hydrogen isotope fusion could be accomplished with a collapsing cavittaion bubble and that the sonoluminescence emissions are first demonstration of quantum vacuum radiation. This project has sought to understand the nonlinear bubble dynamics associated with the phenomonon, and has specifically involved the conditions necessary for bubble levitation and sonoluminescence extinction.

ERRATA

14. SUBJECT TERMS

acoustic cavitation, sonoluminescence, bubble dynamics

15. NUMBER OF PAGES

175

16. PRICE CODE

17. SECURITY CLASSIFICATION OF REPORT	18. SECURITY CLASSIFICATION OF THIS PAGE	19. SECURITY CLASSIFICATION OF ABSTRACT	20. LIMITATION OF ABSTRACT
unclassified	unclassified	unclassified	unlimited

Report No. 1.LC.APL.96

Synchronous Picosecond Sonoluminescence

Lawrence A. Crum

Applied Physics Laboratory
University of Washington
1013 NE 40th Street
Seattle, WA 98105

10 October 1996

FINAL REPORT

1 June 1993 - 31 May 1996

Approved for public release:
Distribution Unlimited.

Prepared for:

Office of Naval Research
ONR 331
800 North Quincy Street
Arlington, VA 22217-5660

REPORT DOCUMENTATION PAGE

Form Approved
OMB No. 0704-0188

1. AGENCY USE ONLY (Leave blank)	2. REPORT DATE	3. REPORT TYPE AND DATES COVERED
	15 October, 1996	Final Report 5/31/93-6/1/96

4. TITLE AND SUBTITLE

Synchronous Picosecond Sonoluminescence

5. FUNDING NUMBERS

PE 61153N
G N00014-93-1-0322
TA 3126966

6. AUTHOR(S)

Lawrence A. Crum

7. PERFORMING ORGANIZATION NAME(S) AND ADDRESS(ES)

Applied Physics Lab
University of Washington
1013 NE 40th St
Seattle, WA 98105

8. PERFORMING ORGANIZATION REPORT NUMBER

1.LC.APL.96

9. SPONSORING/MONITORING AGENCY NAME(S) AND ADDRESS(ES)

Office of Naval Research
ONR 331
800 N. Quincy Street
Arlington, VA 22217-5660

10. SPONSORING/MONITORING AGENCY REPORT NUMBER

11. SUPPLEMENTARY NOTES

Approved for public release, distribution unlimited.

12a. DISTRIBUTION/AVAILABILITY STATEMENT

Approved for public release; distribution unlimited

12b. DISTRIBUTION CODE

13. ABSTRACT *(Maximum 200 words)*

The discovery of single-bubble sonoluminescence has led to a number of interesting discoveries and provocative claims--among these are that hydrogen isotope fusion could be accomplished with a collapsing cavitation bubble and that the sonoluminescence emissions are first demonstration of quantum vacuum radiation. This project has sought to understand the nonlinear bubble dynamics associated with the phenomenon, and has specifically involved the conditions necessary for bubble levitation and sonoluminescence extinction.

14. SUBJECT TERMS

Acoustic Cavitation, Sonoluminescence, bubble dynamics

15. NUMBER OF PAGES

175

16. PRICE CODE

17. SECURITY CLASSIFICATION OF REPORT	18. SECURITY CLASSIFICATION OF THIS PAGE	19. SECURITY CLASSIFICATION OF ABSTRACT	20. LIMITATION OF ABSTRACT
unclassified	unclassified	unclassified	

Project Title:

Synchronous Picosecond Sonoluminescence

Project Description:

We examined the general problem of sonoluminescence, principally from the viewpoint of single bubble sonoluminescence (SBSL), in which a single stable gas bubble is made to emit electromagnetic emissions each acoustic cycle. We have sought to understand the basic mechanisms that give rise to the existence of this phenomenon, especially from the perspective of bubble dynamics.

Approach:

Two important aspects of SBSL have been examined: (1) the levitation mechanism and (2) the extinction criterion. In terms of bubble levitation, we have examined the Bjerknes force that permits a gas bubble to be levitated in a stationary acoustic field, and have discovered that the nonlinearities in the bubble dynamics practically invalidate the existing equations--we have addressed that issue and modified the equations. In terms of SBSL extinction, we have examined the condition under which the bubble experiences a translational motion even while it is levitated. A coupling between this translation motion and shape deformation of the bubble suggests that the bubble could be destroyed by asymmetrical collapse, and provides an extinction mechanism for SBSL. We have also examined the role of water vapor in the internal gas dynamics of gas bubble oscillations.

Results:

We include in this report copies of the various publications associated with this effort as well as two significant manuscripts: the Doctoral Dissertation of Sean Cordry, which examined the conditions for SBSL levitation and extinction; a manuscript, composed primarily by Yi Mao, on the internal acoustic modes in a binary gas mixture within a gas bubble.

The various publications treat the variety of topics that we addressed during the duration of the grant and will be included without further comment, as they were discussed in some detail in previous annual reports.

In Cordry's dissertation, it was determined that the ordinary equations that describe the force exerted on a bubble in an acoustic standing wave were insufficient to describe the position of the bubble accurately. In fact, the nonlinear nature of the bubble oscillations were such that an increase in acoustic pressure amplitude actually caused the bubble to move away from the pressure antinode rather than toward it as would be expected in the linear case. This result is not insignificant in that the position of the bubble within the sound field is often used to determine the magnitude of the pressure. It was determined that if one accounted for the nonlinearities in the bubble dynamics, the classical expression for the Bjerknes force adequately specified the position of the bubble.

In a second aspect of Cordry's work, it was determined that the translational motion of the bubble was coupled directly to the radial motion; consequently, asymmetries in the bubble collapse could be induced by this coupling. When a specific criterion was used--namely the attainment of a critical Weber number--it was possible to specify a value of the acoustic pressure that would result in bubble break-up and thus sonoluminescence extinction. The calculated values seemed to agree in general with the measured ones.

The manuscript by Yi Mao on the internal acoustic modes in an oscillating gas bubble containing a binary gas mixture is a complicated and detailed examination of this general problem. It provides an archival summary of the important equations, and provides an explanation for the (pseudo) double resonance of a vapor bubble.

Summary of the scholarly activities accomplished during the duration of the grant.

a. List of papers submitted to referred journals but not yet published.

"Modes in an infinite binary-gas mixture", Y. Mao, L. A. Crum and R. A. Roy, submitted to the Journal of the Acoustical Society of America.

"Sonochemistry and sonoluminescence", K.S. Suslick and L.A. Crum, in Handbook of Acoustics, M. Crocker, ed. (submitted, 1991).

b. List of papers published in referred journals.

"Comments on the evolving field of sonochemistry by a cavitation physicist", L. A. Crum, Ultrasonics (Sonochemistry), 2, pp. 147-152 (1995).

"Sonoluminescence, sonochemistry, and sonophysics", L. A. Crum, J. Acoust. Soc. Am. **95**, 559-564 (1994).

"Sonoluminescence", L. A. Crum and R. A. Roy, Science, (Perspectives) **266**, 233-234 (1994).

c. List of book chapters submitted but not yet published.

"Sonoluminescence", S. Cordry and L. A. Crum, to be published in Luminescence in Solids and Liquids, Dr. R. Vij, ed., (Plenum Pub. Co.: scheduled for 1996).

e. List of papers published in non-referred journals.

"Sonoluminescence--History and present status", L. A. Crum, Proc. World Congress on Acoustics, Berlin, 1995, Vol. **1**, pp. 63-69.

L. A. Crum and S. Cordry, "Single-bubble sonoluminescence", in Bubble Dynamics and Interface Phenomena, J. R. Blake, J. M. Boulton-Stone and N. H. Thomas, eds. (Kluwer Academic Publishers: Dordrecht) 1994, pp 287-297.

"Sonoluminescence", L. A. Crum, Physics Today , September, 1994.

"Single bubble sonoluminescence", L. A. Crum, Proceedings Fifth Western Pacific Regional Acoustics Conference, Seoul, Korea, **1**, 17-25 (1994).

"Bubbles hotter than the sun", L. A. Crum, New Scientist, **146**, 36-41 (1995).

"Sonoluminescence", L. A. Crum, Parity, **10**, 13-22 (1995). (Japanese translation of Phyics Today article).

H. List of invited presentations at professional society meetings.

"Popcorn and the role of acoustic cavitation in HIFU surgery", presented at the 130th meeting of the Acoustical Society of America, Indianapolis, IN, December (1995).

"Wave exposure and analysis of cell injury", with J. McAteer, S. Andreoli, A. Evan, D. Denman, C Mallett, R. Cleveland, M. Averkiou, J. Lingeman and D. Lifshitz, presented at the 131th meeting of the Acoustical Society of America, Indianapolis, IN, December (1995).

"Sonoluminescence", with S. Cordry, presented at the 128th meeting of the Acoustical Society of America", Austin, TX, November (1994).

"Single bubble sonoluminescence", presented at the Fifth Western Pacific Regional Acoustics Conference, Seoul, Korea, 23-26 August, 1994.

"Origins of single bubble sonoluminescence", presented at the International Union of Theoretical and Applied Mechanics Symposium on Cavitation and Bubble Dynamics, Birmingham, England, September (1993).

"Hot topics in physical acoustics", presented at the Fall Meeting of the Acoustical Society of America, Denver, CO, September (1993).

"Sonoluminescence--History and present status", L. A. Crum, Plenary Paper presented at the World Congress on Ultrasonics, Berlin, September (1995).

"Single bubble Sonoluminescence", Plenary paper presented at the Conference of the American Physical Society Topical Group on Shock Compression of Condensed Matter, Seattle, WA, August (1995).

I. List of contributed presentations at professional society meetings.

"Some light emission features of single bubble sonoluminescence", with W. M. Cordry and R. A. Roy, presented at the 126th meeting of the Acoustical Society of America, Denver, CO, September (1993).

"A novel technique for measuring the maximum radius of a sonoluminescing bubble, with S. M. Cordry, presented at the 127th meeting of the Acoustical Society of America, Cambridge, MA, June (1994).

"Nonlinear bubble oscillations and Bjerknes forces", with S. M. Cordry and R. A. Roy, presented at the 129th meeting of the Acoustical Society of America", Washington, DC, May (1995).

"Mass diffusion in spark-induced vapor bubbles", with J. S. Allen, M. A. Averkou, C. M. Young and G. R. Hess, presented at the 128th meeting of the Acoustical Society of America, Austin, TX, November (1994).

"Acoustic modeling of plasma-induced vapor bubbles", with G. R. Hess, A. E. Rodriguez, N. K. Winsor, C. M. Young and R. F. Stellingwerf, presented at the 128th meeting of the Acoustical Society of America, Austin, TX, November (1994).

"Temperature-related effects in single-bubble sonoluminescence", with S. Cordry and R. A. Roy, presented at the 131st meeting of the Acoustical Society of America, Indianapolis, IN, December (1995).

j. Honors/Awards/Prizes

- L. A. Crum was elected to the positions of Vice President Elect and President-Elect of the Acoustical Society of America.

- L. A. Crum was elected a member of the International Commission on Acoustics.

Comments on the evolving field of sonochemistry by a cavitation physicist

Lawrence A. Crum

Applied Physics Laboratory, University of Washington, 1013 NE 40th Street, Seattle, WA 98105, USA

Received 17 November 1994

Sonochemistry is an evolving field that has shown recent rapid growth and increasing interest. Although this field concentrates on chemistry and uses acoustics principally as a tool, the basic mechanism that gives rise to sonochemistry – acoustic cavitation – is often ignored or given little attention. This paper addresses some of the relevant aspects of cavitation and physical acoustics that apply to sonochemistry.

Keywords: sonochemistry; cavitation; bubble dynamics

The field of sonochemistry has existed for over 50 years and excellent work has been steadily produced by a variety of investigators. However, there has been a recent upsurge of interest in the topic, brought about particularly by some exciting scientific developments[1–4]. A prime example of the evolution of this field is the efforts toward the development of a scientific community, notably the European Society of Sonochemistry, which has now had four highly successful meetings. This particular paper reflects on the subjective views of one individual who attended the most recent meeting held in Blankenberg, Belgium, and presented a plenary paper at that meeting.

Acoustics

The developing field of sonochemistry has an interesting parallel with that involving the medical and biological effects of ultrasound. In early papers on this topic, it was not uncommon to see research articles that described a particular bioeffect in great detail but a limited and incomplete description given of the acoustic system that gave rise to that effect. Because it was generally difficult to duplicate such experiments in other laboratories, this inadequate description of the acoustic field soon resulted in the insistence by editors and reviewers that their deficiency be remedied. Currently, it is difficult to have a bioeffects paper accepted in a major journal without a full description given of the characteristics of the acoustic field that gave rise to such an effect.

Currently, most sonochemistry reaction vessels are designed by chemists, with an emphasis on facilitating the chemistry rather than simplifying the acoustics. Consequently, these systems are mechanically complex and difficult to model from an acoustics perspective. Moreover, these systems are designed to produce a particular yield in a minimal time and thus tend to seek acoustic sources that provide high acoustic power into small (and often geometrically complex) volumes. Further, a probe hydrophone that would be used to characterize acoustically such systems suffers the destructive effect of this mechanically and chemically active region. Efforts to develop instrumentation for the acoustic characterization of such systems have met with a similar lack of success. Nonetheless, it is extremely important that the acoustic systems that give rise to sonochemistry be characterized in as much detail as possible.

Cavitation and bubble dynamics

It is generally assumed that sonochemistry cannot occur without cavitation. Although it is clear that acoustic cavitation plays a major role in most of the sonochemical reactions studied, it is also clear that there are cases in which the high intensity ultrasound acts principally to increase convection (an ultrasonic stirrer); accordingly, it is possible that cavitation, in such cases, in undesirable and actually reduces yields. Of course, Luche *et al.*[5] contend that this is not 'true sonochemistry'; nevertheless, it is often difficult to determine when cavitation is involved and when it is not. Further, it seems reasonable to assume that there will be many cases in which both the mechanical and the chemical effects of cavitation are important in reaction yields. In order that this field can advance, efforts to determine the existence and intensity of cavitation should be given high priority. We turn now to the important phenomenon of cavitation.

Hot spot or not!

The concept of a 'hot spot' as a necessary ingredient of sonochemistry was originally conceived by Noltingk and Neppiras[6] and has more recently been promoted by

SSDI 1350-4177(95)00018-6

Suslick *et al.*[7] Of course, there have been a variety of alternative explanations for the origin of sonochemical effects, most notably those involving various electrical hypotheses, and in particular those of Margulis[8] and LePoint and Mullie[9].

It is important to recognize that the very nature of (violent) acoustic cavitation demands a hot spot. Whenever acoustic pressure amplitudes in excess of about 0.1 MPa exist in a liquid that is saturated with gas, there is a rapid growth of the equilibrium size of the bubble during the rarefaction phase of the sound field, to volumes at least one (and usually several) order(s) of magnitude larger. (By equilibrium size is meant the size of the bubble in the absence of a sound field.) Thus, there is considerable potential energy supplied to the expanded bubble by the acoustic source. Again, by the very nature of acoustic cavitation, this potential energy is converted to kinetic energy in a very short time period (i.e. short with respect to the period of the acoustic field, which is itself fairly short). Consequently, such a collapse cannot be isothermal, even for liquid metals with large thermal conductivities, but rather must be adiabatic. Finally, the relatively small volume of gas contained within the initial nucleation site, and the relatively long times required for gas diffusion from the liquid into the bubble, require that this fluid volume be relatively small (volumes of the order of microns cubed!). Consequently, acoustic cavitation results in an amazing degree of energy concentration, reported by some to be as high as eleven orders of magnitude[10]. Thus, even though there may be a variety of mechanisms for chemical kinetics, there *must* be a hot spot. It is simply reasonable to assume that this region of high temperature and pressures is the origin of chemical reactions.

Homogeneous sonochemistry

In many sonochemical reactions, the majority of chemical activity occurs in the bulk of the homogeneous liquid. In this case, the cavitation field is likely to be composed of many active cavitation bubbles that grow from a variety of nucleation sites to sizes large with respect to these sites.

Since an air–liquid interface is unstable under compression (this effect is generally described as a Rayleigh–Taylor intability and explains why the surface of ocean has waves when the wind blows), a bubble that collapses from an initially spherical configuration must eventually become unstable to surface instabilities sometime before it reaches minimum size. [Of course, there appears to be a rare and intriguing exception to this rule, evidenced by single-bubble sonoluminescence (SBSL), which will be discussed below.] These asymmetries are likely to be enhanced by neighbouring bubbles in a multi-bubble cavitation field, and evidenced by multiple bubble sonoluminescence (MBSL), but nonetheless will occur also in bubbles isolated from other bubbles or boundaries. Consequently, microscopic jets of liquid will be injected into the interior of the collapsed bubble. It is likely that these jets will often break up into microscopic droplets that have large surface to volume ratios. An example of such behaviour is shown in *Figure 1a*[11].

It is important to recognize that if a bubble did remain spherically symmetric throughout its collapse and rebound cycle, computations by Prosperetti and co-workers[12,13] indicate that sonochemistry would occur only within the vapour phase because (a) the liquid has a large heat capacity compared with the gas, (b) the thermal conductivity of liquids is also large, compared with that of most gases, and (c) the total energy existing within a collapsed cavitation bubble is relatively high but absolutely low (measured in units of MeV, rather than joules or ergs)[14]. Accordingly, liquid temperature rises only in the tens (or perhaps hundreds) of kelvin are to be expected. In contrast, for microscopic jets and droplets that are injected into the collapsed bubble interior, the temperature rise can be shown to be fairly large. A sample calculation illustrates this effect.

Suppose a collapsed cavitation bubble results in the generation of 300 MeV of total thermal energy created by a transient-cavitation collapse[14]. If 30 droplets of water of initial radius of 1.0 μm are contained within the collapsed bubble, and only 10% of this energy is used to raise the temperature of these droplets to superheated vapour, then a simple application of Joules' law shows that a temperature increase of 10 000 K is expected.

Heterogeneous sonochemistry

Whenever cavitation bubbles collapse in the vicinity of a surface, the asymmetry of the hydrodynamic flow field results in a preferential geometry for jet development. For both hard and soft (pressure-release) boundaries, a liquid jet is generated that is directed toward the surface. This well known phenomenon[15] of high-velocity liquid jets striking the boundary has demonstrated that enormous energy density is deposited at microscopic sites on the bubble surface; see *Figure 1b*. However, not only mechanical dmage is produced by the impacting jet; for example, it has also been demonstrated that sonoluminescence (SL) is also produced from the vortex ring that results as a topological residue of the asymmetric collapse[16]. The eventual collapse of this ring can result in free radical production in the near vicinity of the solid surface, a rich region for sonochemical reactions.

A second aspect of cavitation bubble collapse near a boundary that is often neglected is the intense microstreaming that results from bubble pulsation. If liquid flow occurs near a plane boundary, a viscous boundary layer develops that is related to the liquid viscosity and the velocity of the flow. The thickness of this boundary layer is inversely proportional to the square root of the velocity[17]. For flow velocities typical of a mechanical stirrer, say $v = 1\ \mathrm{cm\ s^{-1}}$, this boundary layer can be of the order of hundreds of microns. For the surface to act as a catalyst for a particular chemical reaction, diffusion through this layer must occur. Since diffusion is an inherently slow process, this boundary layer probably presents an important limit to the rate of chemical reactions.

Suppose, however, that acoustic cavitation can be caused to occur near the surface of a catalyst or reacting surface. According to the observation of Elder[18], intense microstreaming can occur around bubbles located on the surface of the boundary. This microstreaming will dissipate the boundary layer in the vicinity of the bubble, and thus chemical species can be rapidly convected to the surface of the catalyst. This microconvection should be very effective in increasing its reactivity. Of course, this effect, even though it involves cavitation, is not 'true sonochemistry' according to Luche *et al.*[5], because it does not involve electron exchange. Nonetheless, cavitation-

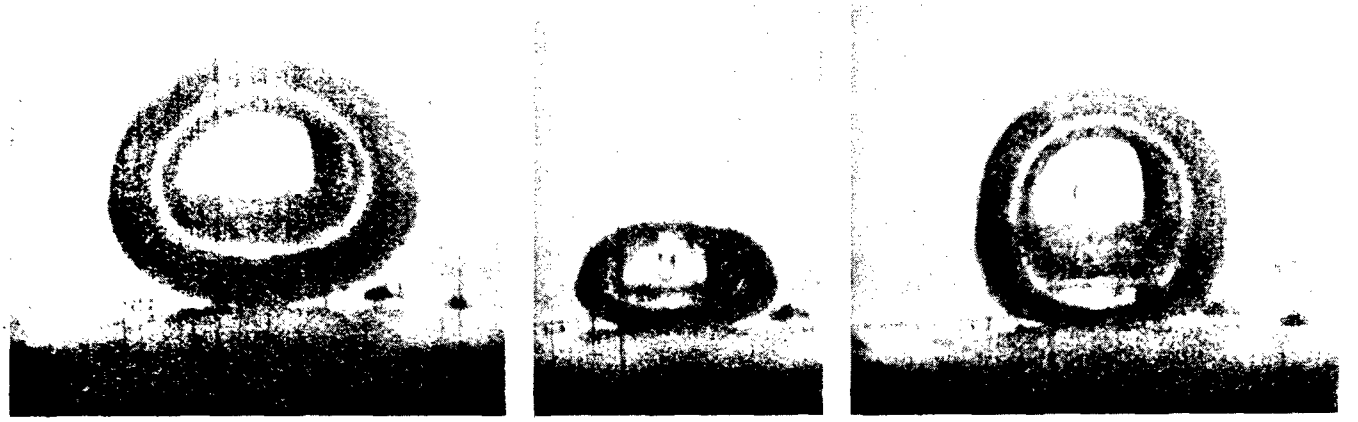

(a) **Homogeneous Sonochemistry**

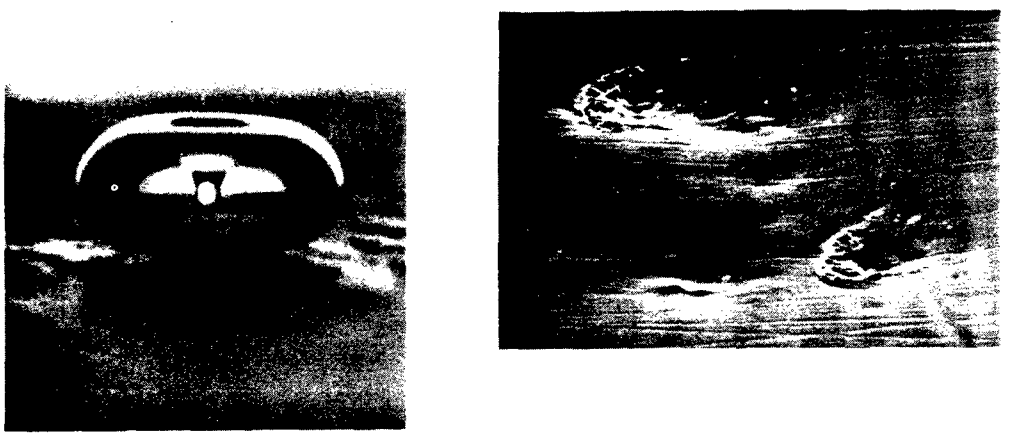

(b) **Heterogeneous Sonochemistry**

(c) **Single Bubble Sonoluminescence**

Figure 1 (a) Homogeneous sonochemistry: because the liquid surrounding a cavitation bubble is a large heat sink, the temperature of the gas–liquid interface can be elevated only slightly[13]; however, if microdroplets or microjet filaments are inserted into the hot bubble interior, as shown, the liquid phase can be elevated to high temperatures. (b) Heterogeneous sonochemistry: when a cavitation bubble collapses near a boundary (either soft or hard), liquid jets develop that impact the boundary (left) and cause damage to the surface[15] (right). These jet impacts can remove surface coatings, convect liquid readily to the surface and produce localized high temperatures and pressures. (c) Symmetric bubble collapse: in rare circumstances, cavitation bubbles can collapse symmetrically, generating high temperatures and pressures at the very centre of a cavity. This photograph shows a time exposure of single-bubble sonoluminescence[19], showing the maximum size of the bubble (approximately 100 μm in diameter) and light emissions from the geometric centre

induced microconvection may play an important role in influencing the yield in heterogeneous sonochemistry.

Symmetric bubble collapse

As indicated earlier, the compression of a liquid–gas interface is inherently unstable and any perturbation in the radial dimension can grow without bound. There appears to be a rare phenomenon that occurs within a relatively small parameter space in which this asymmetric collapse is somehow prevented; see *Figure 1c*. In studies of SBSL[19,20], it appears as if an imploding shock wave develops within the gas contained within the collapsing bubble. It has been conjectured that this shock wave terminates further collapse of the liquid–gas interface and prevents asymmetric bubble collapse from destroying the bubble's geometric integrity. Although these speculations have yet to be firmly tested, they appear to be the only plausible explanations for the short SL pulse durations and high level of synchronicity observed in SBSL.

Although the phenomenon of SBSL is of considerable interest owing to its many extraordinary features, its limited parameter space suggest that it probably plays a minor role in sonochemistry. However, the use of this well controlled phenomenon to study various aspects of the sonochemical reactions itself could be of some utility.

Other cavitation considerations

Frequency dependence. In theory, a cavitation bubble grows during the negative portion of the acoustic cycle and is forced to collapse by the positive portion. Except for frequencies in excess of a few megahertz, such behaviour is approximately followed. For similar acoustic intensities and pressure amplitudes, this behaviour would suggest that cavitation bubbles at low frequencies (say, 20 kHz) would grow for about one half cycle or about 25 μs. Similarly, cavitation bubbles at high acoustic frequencies (say, 1 MHz) would have only 0.5 μs for growth. These significantly different times for growth result in small maximum sizes at high frequencies and thus less violent collapses. On the other hand, because there are more acoustic cycles at higher frequencies, there are more cavitation collapses and, thus, presumably more free radicals produced. This increased free-radical yield at higher frequencies is mitigated somewhat by the fact that the cavitation threshold increases with increase in frequency. It would seem reasonable to assume that cavitation collapses would be fewer but more violent at lower frequencies, and more frequent and less violent at higher frequencies. Thus, if a particular reaction is favoured by larger numbers of radicals, high frequencies should be desirable. Conversely, if the reaction is favoured by higher temperatures and pressures, then low frequencies are probably desirable. There are recent reports[21] of a nearly 30-fold increase in the oxidation rate of iodide when the frequency was increased from 20 to 900 kHz; is this evidence in support of arguments presented above? It would be useful for sonochemists to report reaction rates as a function of frequency, for equivalent acoustic intensities, to test this simple hypothesis.

Shock waves. It was shown by Vogel and Lauterborn[22] that shock wave amplitudes of the order of kilobars could be developed within the liquid by laser-produced cavitation bubbles. Further, since white noise is associated with impulsive sources (such as shock waves), the presence of extensive white noise at low frequencies (the audible 'frying' sound) indicates the likely presence of extensive shock waves. It is noted that cavitation at high frequencies has significantly less audible white noise, and thus probably less shock waves (both in number and in intensity). Since shock waves provide a potentially useful reaction-enhancement mechanism, it would be of interest to attempt experiments that would ascertain the role (if any) of shock waves in sonochemical yields.

Cavitation clouds. A cavitation area probably contains many individual cavitation bubbles. It is known from studies in ocean acoustics[23] that bubble clouds can act as discrete entities with a different sound speed velocities (in cases of large numbers of bubbles, this sound speed reduction can easily be an order of magnitude). Accordingly, clouds of bubbles can act as efficient scatterers of acoustic energy and can cause significant modification of the acoustic impedance provided to the acoustic source. In exceptional cases, it can even result in an effective decoupling of the source and the liquid medium.

Because bubble clouds are composed of individual pulsating bubbles, they can acoustically interact with each other. In studies of cavitation bubble dynamics, it is known that clouds of bubbles can collapse in such a cooperative manner that they develop cavitation jet velocities and shock wave intensities much in excess of individual bubbles[24]. It is possible that this phenomenon could be used to advantage in sonochemistry.

Theoretical bubble dynamics. The field of cavitation bubble dynamics has been active for many years and has reached a considerable level of maturity (measured, if by no other manner, by the complexity of the analytical development and by the number of papers published on the subject annually.) However mature the field, the direct transfer of this knowledge to sonochemistry is not a simple matter. It would seem that increased interaction between those who are interested in sonochemistry for its yields and reaction rates (sonochemists?) with those more interested in the physical mechanisms that result in sonochemistry (sonophysicists?) would be of considerable benefit to both communities. It is clear that there is still a wide gulf between the two camps and meetings such as those held by the European Society of Sonochemistry (ESS) are of considerable benefit in enhancing communication between sonochemists and sonophysicists.

Pulsed enhancement. Because most sonochemists are concerned about reaction yields, it would seem of little benefit to pulse the acoustic field. However, because cavitation bubble dynamics is such a complex phenomenon, there are very likely certain situations in which sonochemistry could be enhanced by operating the acoustic source under pulsed conditions. As demonstrated in the studies of Flynn and Church[25] and Henglein and Gutierrez[26], certain effects are enhanced under pulsed conditions. A brief explanation for the phenomenon is as follows: a cavitation bubble grows from a nucleation site, and while expanded, gathers extra gas that diffuses into the bubble from the liquid. When the bubble collapses, it shatters into many smaller bubbles, which in turn can act as extra nucleation sites. However, there

is an optimal size for gas bubbles to act as seeds for more nucleation sites. If the collapse produces bubbles that are too large and thus unfavourable for subsequent bubble growth, a delay in the time between pulses can be of benefit. Of course, a delay that is too long will result in the dissolution of these potential cavitation nuclei, which is clearly undesirable. Thus, certain pulse lengths and repetition frequencies can lead to an optimization of the effect. Because total energy consumption is a major factor in the industrial application of sonochemistry, there appears to be con-siderable promise for research efforts in this area.

Start-up time. If one observes the SL produced by a cavitation field, then turns off the field, and then again re-establishes the field, there is a readily observable 'start-up time', of the order of seconds before the SL is again observed. Since transient cavitation can occur within an acoustic cycle, it is difficult to explain the reason for this time delay. Apparently there are some steady-state conditions that need to be established. Because the characteristic time-scales for diffusion are of this order, it appears likely that gas diffusion plays an important role. This delay time appears to have no positive consequences for sonochemistry, but its understanding may be of benefit to the global understanding of the general phenomenon.

Recommendations

It is presumptuous of the author, who is at best a novice in the field of sonochemistry, to offer recommendations; however, as an aspiring sonophysicist, and one accustomed to offering opinions on any topic, he boldly proceeds:

1 'Know thy sound field'. One of Apfel's golden rules[27] of cavitation is directly applicable here. Sonochemistry will not mature or gain acceptability as a science until discoveries in one laboratory can be duplicated in another laboratory (or industrial reactor). Since the sound field is the source of sonochemistry, it is recommended that accurate measurements be made and careful descriptions be presented of the characteristics of the field. Of course, in many cases, these measurements are either very difficult or nearly impossible. Hence, reactor designs that permit this determination are clearly desirable.

2 'Know thy liquid'. The second of Apfel's golden rules applies less directly but is still of considerable importance. Cavitation bubble dynamics is very dependent on such variables as the dissolved gas concentration (and composition) and liquid vapour pressure. It is less dependent on such parameters as viscosity, electrical conductivity, density and velocity of sound. Again, one could obtain radically different results for different values of some of these parameters. In a similar sense to the preceding paragraph, it is recommended that those liquid properties be measured and presented whenever possible.

3 'Know thy dirt'. It is more appealing for sonophysicists to attempt first an understanding of homogeneous sonochemistry because of the increased complexity of the heterogeneous systems. However, as Apfel suggests in a corollary of his golden rule, the source of cavitation nucleation is most likely to originate on inhomogeneities that exist within the liquid. Further, heterogeneous sonochemistry would seem to have greater promise for industrial applications. Hence it is recommended that efforts be made to understand the nucleation process as fundamental to the phenomenon of cavitation, and therein sonochemistry.

4 'Establish some benchmarks'. Before sonophysicists can make progress in understanding why sonochemistry works, they must be able to work with a few simple reactions that are easily performed and provide repeatable results. Therefore, it is recommended that a future committee of the ESS or some other interested organization provide a description of a few simple reactions with expected yields under carefully and thoroughly specified conditions of the sound field and the liquid. At least one reaction should involve heterogeneous sonochemistry.

5 'Establish an International Society'. At this nascent period in the development of the science of sonochemistry, there is considerable benefit associated with a professional community that provides opportunities for the diffusion of knowledge through meetings and written communication; further, it can lead to the establishment of standards, foster collaboration among scientists and between scientists and engineers, and effectively promote the general welfare. Additionally, there is a critical mass in terms of the number of individuals before such Societies, with their inevitable ups and downs, can not only endure but prevail. The ESS is currently on the road to success in reaching this critical mass and should now be ready to serve as the nucleus of an international society. Accordingly, it is recommended that the ESS combine with representatives of other budding national and regional societies to form the International Society of Sonochemistry.

Acknowledgements

This article is an outgrowth of ideas and concepts from a plenary paper presented by the author at the Fourth meeting of the European Society of Sonochemistry held in Blankenberg, Belgium, 19–22 September, 1994. He acknowledges that he has borrowed extensively from the comments of many of the participants but personally accepts responsibility for all the views contained herein. He also gratefully acknowledges the financial support of the European Society of Sonochemistry, the Office of Naval Research and the National Science Foundation.

References

1 **Suslick, K.S.** The chemical effects of ultrasound *Sci Am* (1989) **260** 80
2 **Suslick, K.S.** Sonochemistry *Science* (1990) **247** 1439
3 **Suslick, K.S. (Ed.)** *Ultrasound: Its Chemical, Physical and Biological Effects* VCH, New York, USA (1988)
4 **Mason, T.J. and Lorimer, J.P.** *Sonochemistry: Theory, Applications and Uses of Ultrasound in Chemistry* Ellis Horwood, Chichester, UK (1989)
5 **Luche, J.L., Einhorn, C., Einhorn, J.H. and Sinisterra-Gago** Organic sonochemistry: a new interpretation and its consequences *Tetrahedron Lett* (1990) **31** 4125
6 **Noltingk, B.E. and Neppiras, E.A.** Cavitation produced by ultrasonics *Proc Phys Soc* (1950) **63** 674
7 **Suslick, K.S., Cline, R.E. and Hammerton, D.A.** The sonochemical hot spot *J Am Chem Soc* (1956) **108** 5641
8 **Margulis, M.A.** Fundamental aspects of sonochemistry *Ultrasonics* (1992) **30** 152

9 **LePoint, T. and Mullie, F.** What exactly is cavitation sonochemistry? *Ultrasonics Sonochem* (1994) **1** 13

10 **Barber, B.P. and Putterman, S.** Observation of synchronous picosecond sonoluminescence *Nature* (1991) **352** 318

11 **Crum, L.A.** Sonoluminescence, sonochemistry and sonophysics *J Acoust Soc Am* (1994) **95** 559

12 **Prosperetti, A., Crum, L.A. and Commander, K.W.** Nonlinear bubble dynamics *J Acoust Soc Am* (1988) **83** 502

13 **Kamath, V., Prosperetti, A. and Egolfopoulas, F.N.** A theoretical study of sonoluminescence *J Acoust Soc Am* (1993) **94** 248

14 **Apfel, R.E.** Possibility of microcavitation from diagnostic ultrasound *IEEE Trans UFFC* (1986) **33** 139

15 **Benjamin, T.B. and Ellis, A.T.** The collapse of cavitation bubbles and the pressures thereby produced against solid boundaries *Philos Trans R Soc London Ser A* (1966) **260** 692

16 **Walton, A.J. and Reynolds, G.T.** Sonoluminescence *Adv Phys* (1984) **33** 595

17 **Olson, R.M.** *Engineering Fluid Mechanics* International Textbooks, Scranton, PA, USA (1961) 133

18 **Elder, S.A.** Cavitation microstreaming *J Acoust Soc Am* (1959) **31** 54

19 **Crum, L.A.** Sonoluminescence *Phys Today* September (1994) 22

20 **Barber, B.P., Wu, C.C., Lofstedt, R., Roberts, P.H. and Putterman, S.J.** Sensitivity of sonoluminescence to experimental parameters *Phys Rev Lett* (1994) **72** 1380

21 **Entrezari, M.H. and Kruus, P.** Effect of frequency on sonochemical reactions. I: Oxidation of iodide *Ultrasonics Sonochem* (1994) **1** S75

22 **Vogel, A. and Lauterborn, W.** Acoustic transient cavitation by laser-produced cavitation bubbles near solid boundaries *J Acoust Soc Am* (1988) **84** 719

23 **Roy, R.A., Carey, W., Nicholas, M., Schindall, J. and Crum, L.A.** Low-frequency scattering from submerged bubble clouds *J Acoust Soc Am* (1992) **92** 2993

24 **Morch, K.A.** On cavity cluster formation in a focused acoustic field *J Fluid Mech* (1989) **201** 57

25 **Flynn, H.G. and Church, C.C.** A mechanism for the generation of cavitation maxima by pulsed ultrasound *J Acoust Soc Am* (1984) **76** 505

26 **Henglein, A. and Gutierrez, M.** Chemical effects of continuous and pulsed ultrasound. A comparative study of polymer degradation and iodide oxidation *J Phys Chem* (1990) **94** 5169

27 **Apfel, R.E.** Acoustic cavitation. In *Methods in Experimental Physics* (Ed. Edmunds, P.) Academic Press, New York. USA (1981) 360

Sonoluminescence, sonochemistry, and sonophysics

L. A. Crum
Applied Physics Laboratory, University of Washington, Seattle, Washington 98105

(Received 8 June 1993; accepted for publication 11 August 1993)

Recent measurements of sonoluminescence produced by a single, stable, pulsating gas bubble indicate that the spectrum can be modeled by that for a blackbody at a temperature of nearly 40 000 K [R. Hiller, S. J. Putterman, and B. P. Barber, "Spectrum of synchronous picosecond sonoluminescence," Phys. Rev. Lett. **69**, 1182 (1992)]. These results are in contrast with earlier measurements of the spectrum which is modeled by electronic transitions of rotational and vibrational bands within specific elements of the host liquid [E. B. Flint and K. S. Suslick, "The temperature of cavitation," Science **253**, 1397 (1991)]. It is suggested that the single-bubble SL observed by Hiller *et al.* is intrinsically different from the multiple-bubble SL observed by Flint and Suslick. In the former case, symmetric bubble collapse leads to shock wave formation in the gas; in the latter case, asymmetric bubble collapse leads to liquid jets that penetrate the hot bubble interior and result principally in incandescence of the host liquid.

PACS numbers: 43.35.Ei

INTRODUCTION

The phenomenon of sonoluminescence (SL) has been of considerable recent interest due to some exciting discoveries that have lately come to light! Although this phenomenon has been known for over 60 years (Marinesco and Trillat, 1933; Frenzel and Schultes, 1935), it is only recently that it is beginning to be understood. The standard paradigm for its existence is that the electromagnetic emissions are associated with the collapse of cavitation bubbles produced within the host liquid by an acoustic field: gas contained within microscopic nucleation sites is made to grow explosively during the negative portion of the acoustic cycle and then these gas and vapor-filled cavities are driven to an implosive collapse during the positive portion. Consequently, the cavity's contents are heated adiabatically to incandescence temperatures. However, as this phenomenon is examined in continuing depth, there appear to be intrinsic inconsistencies in the results of various investigators.

For example, Suslick and others have revitalized the discipline of sonoluminescence chemistry (sonochemistry) in which SL plays a major role (for example, see Suslick, 1989, 1990; Suslick *et al.*, 1990; Berlan and Mason, 1992; Luche, 1992). In some recent experiments, Flint and Suslick (1991) have measured the "temperature of cavitation" and discovered that the SL emissions correspond to a value of approximately 5000 K (surface of sun ~7000 K); furthermore, they have demonstrated that the spectrum can be characterized by spectral peaks that correspond principally to electronic transitions in the host liquid, rather than the gas contained within the bubble. Because the liquid, in addition to the gas, can be elevated to high temperatures, chemical effects of considerable magnitude can be attained: thus, the discipline of sonochemistry.

In contrast, recent measurements of the physical aspects of cavitation by Gaitan *et al.* (1992) and in greater depth and detail by Putterman and his colleagues (Barber and Putterman, 1991; Barber and Putterman, 1993; Barber *et al.*, 1992; Hiller *et al.*, 1992; Lofstedt *et al.*, 1993) have demonstrated that SL can occur in a single, stable, pulsating gas bubble and that the SL spectrum is devoid of major peaks and can be fitted only by a blackbody spectrum with temperatures as high as 40 000 K. These high temperatures, rapid SL pulse rise times, and remarkable synchrony imply the operation of some exciting new physical acoustics—sonophysics. Both the sonochemistry and the sonophysics groups have performed careful and repeatable experiments, with no inconsistencies within their own measurements. This brief communication purports to resolve these inconsistencies by proposing that there are two different forms of SL, in which the physical mechanisms that give rise to SL emissions are shown to be fundamentally different.

I. SONOCHEMISTRY

In the sonochemistry experiments of Suslick and his colleagues, cavitation is typically generated by an acoustic horn that is immersed within the host liquid and driven at relatively large amplitudes. As a consequence there is much cavitation at the tip of the horn, and throughout the bulk of the fluid (see, for example, Crum and Reynolds, 1985). The cavitation is seen to be "transient" in the normal use of the word, appearing and disappearing, often as rapidly as an acoustic cycle. In many cases the SL can be seen by the naked eye to be a faint glow that is distributed throughout the bulk liquid. Although measurements of the temporal duration of the SL flashes are difficult to obtain because of the transient nature of the SL, reported lifetime of several nanoseconds are typical (Jarman, 1960; Taylor and Jarman, 1970; Margulis, 1992). Individual flashes appear to be random and uncorrelated in time. Furthermore, the SL spectrum tends to be characteristic of the liquid rather than the gas. Figure 1 shows a typical spectrum obtained from an acoustic horn.

If the various atomic transitions are known, then synthetic spectra can be generated that can be matched to the

 0001-4966/94/95(1)/559/4/$6.00

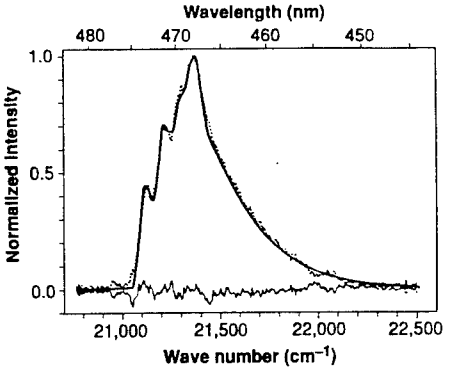

FIG. 1. Sonoluminescence spectrum of silicone oil under continuous Ar sparge at 0 °C as generated by an acoustic horn. The dotted line shows the experimental spectrum; the boldface line shows the best fit synthetic spectrum, assuming emissions from the Swan band of C_2, with $T=4900$ K; the thin line shows the difference spectrum [from Flint and Suslick (1991)].

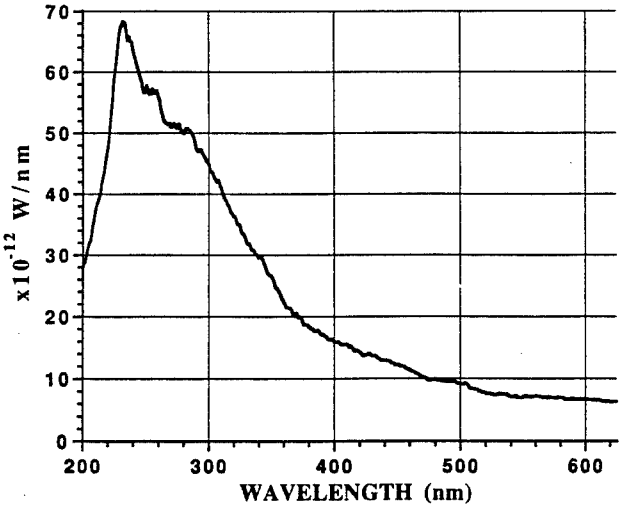

FIG. 2. Calibrated spectral density of the synchronous picosecond flashes of sonoluminescence at 22 °C for an air bubble in water. The fall-off below 240 nm is thought to be due to absorption in the liquid and the containing system. If this spectrum is assumed to be that of a blackbody, and a best fit made to the data, an "effective temperature" of approximately 40 000 K is obtained [from Hiller *et al.* (1992)].

measured spectra, with the single fitting parameter being the temperature. Flint and Suslick (1991) have obtained excellent fits to spectra such as these and have thus determined the "temperature" of sonoluminescence. With a fit similar to this one, a temperature of 4900 °C was obtained for an argon bubble in silicone oil. It is important to note that this spectra is characteristic of the host liquid, not the gas. In particular, the spectrum in Fig. 1 represents the Swan band emissions from C_2 in the $d^3\Pi_g$ excited state. This "effective temperature" may not necessarily represent the temperature of the gas because this excited state may not be fully equilibrated with other species within the cavitation bubble. In particular, one should expect significant temporal and spatial variability for this system.

Thus, in general, we see that in sonochemistry, using an acoustic horn or a similar source to generate extended (in space and time) regions of acoustic cavitation, SL spectra can be obtained that have well-defined peaks that correspond to atomic transitions in the host liquid, and can be associated with a temperature of roughly 5000 K.

II. SONOPHYSICS

In the recent sonophysics experiments of Putterman and his colleagues, significantly different results are obtained for the behavior of SL. In this latter case, a single gas bubble is acoustically levitated in a liquid contained within a resonant chamber. The gas bubble is driven in a volume mode at relatively large radial excursions and is observed to be remarkably stable, remaining at a fixed position and oscillation about an equilibrium size that remains unchanged over millions of cycles. Under relatively easily attainable but considerably specialized conditions, the bubble is observed to emit a steady light which can be determined by photometry to be reproduced repetitively every acoustic cycle.

One of the most remarkable discoveries by Putterman's group was that the lifetime of the SL flash was not measurable by standard techniques, i.e., currently available photodetectors were unable to resolve the rapid rise time of the flash. A conservative value of 50 ps was assigned as a best estimate of an upper bound. Furthermore, the synchrony of the flashes was also found to be remarkably stable, with an intrinsic "jitter" of less than 50 ps.

Shown in Fig. 2 is a spectrum obtained by Hiller *et al.* (1992) for a stable air bubble in water. Note the absence of any major spectral peaks and also the apparent extension of the spectrum into the ultraviolet. When Fig. 2 is compared with Fig. 1, it appears as if these two phenomena are fundamentally different.

Thus, we see that for sonoluminescence physics (sonophysics), in which a single, stable, gas bubble is made to emit electromagnetic emissions, the spectrum is representative of a blackbody, there are no spectral peaks, the lifetime of the pulse is very short (<50 ps), and the effective temperature is on the order of 40 000 K.

III. RESOLUTION OF THE PROBLEM

These intrinsic inconsistencies can be resolved only if the physical mechanisms that give rise to the respective SL emissions are fundamentally different. It is well known that when cavitation bubbles are permitted to collapse near a boundary, either soft or hard, the collapse is asymmetric and instabilities develop that grow without bound. Consider Fig. 3 which shows high-speed photographs of a cavitation collapse near a rigid boundary.

Note that for an asymmetrical collapse, portions of the host liquid are delivered to the center of the bubble. Because the liquid is an immense heat reservoir, a typical temperature profile within the bubble indicates that although the temperature at the center of the bubble may be several thousands of degrees, the temperature near the bubble wall must be near that of the liquid [Kamath *et al.*, 1993]. For the case shown in Fig. 3, it is seen that a liquid jet develops that penetrates into the interior of the gas bubble where the temperature is elevated. In this rather atypical case, it is also seen that small droplets of liquid can

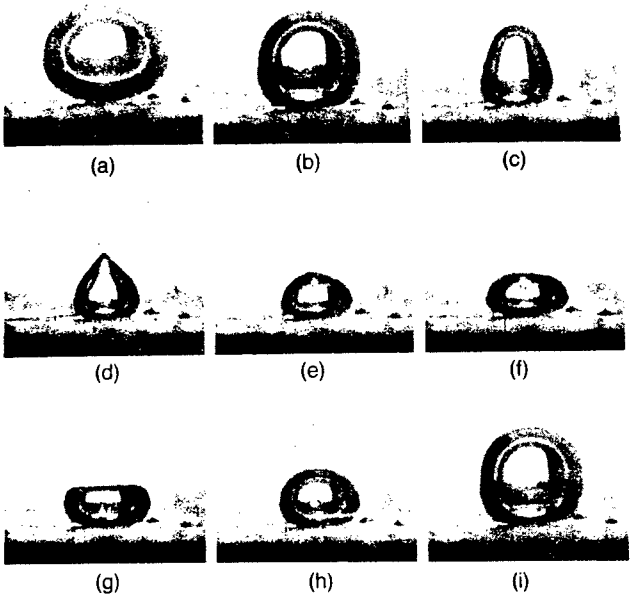

FIG. 3. Cavitation bubble collapse near a rigid boundary. In this case, the liquid was an aqueous solution of glycerin (30% by volume), the ambient pressure was near that of the vapor pressure of water, and the driving frequency was approximately 60 Hz. The maximum size of the bubble was approximately 2 mm [from Crum (1979)].

be deposited within the interior of the bubble, which would then be heated much more effectively during a subsequent collapse than would the liquid near the bubble interface. Thus, when asymmetrical bubble collapse occurs, the liquid can be elevated to high temperatures and spectra characteristic of the liquid rather than the gas can be observed.

The conditions under which asymmetrical bubble collapse would be more common are those in which an acoustic horn or a similar source is used to generate extended areas of cavitation throughout the bulk of the liquid. In this case, the presence of many bubbles triggers the collapse asymmetry by providing many pressure-release boundaries within the liquid itself. If a bubble is caused to collapse in the vicinity of another bubble, then the presence of this pressure release surface itself is an effective boundary. Asymmetrical bubble collapse due to the presence of other bubbles has been demonstrated by Tomita and Shima (1990). Thus, when "multiple-bubble" sonoluminescence occurs, the following behavior is observed.

(1) The cavitation bubbles tend to collapse asymmetrically, thus introducing liquid into the interior of the bubble, which is heated by adiabatic compression.

(2) The spectrum of multiple-bubble SL is dominated by the characteristics of the liquid rather than the gas.

(3) Because the symmetry of the collapse is destroyed, the final temperatures achieved in this case are relatively low.

Consider next the case in which a single, stable gas bubble is driven at sufficiently large volume oscillations to produce SL. In "single-bubble" sonoluminescence, symmetric bubble collapse is much more likely to occur, and conditions can develop that are unachievable in the multiple-bubble case. In fact, considerable evidence has been presented (Barber and Putterman, 1993) that a shock wave develops within the gas and is responsible for the enormous temperatures achieved. Thus, when "single-bubble" SL occurs, the following behavior is observed.

(1) The cavitation bubbles tend to collapse symmetrically, thus developing an imploding shock wave within the gas.

(2) The spectrum of single-bubble SL is dominated by the characteristics of the gas (and vapor) and tends to approach that of a blackbody.

(3) Because the symmetry of the collapse is preserved, the final temperatures achieved for this case are relatively high.

Finally, if the scenarios proposed here are correct, there are several experimental tests that could demonstrate the differences between these two phenomena. For example, in single-bubble SL, the shock wave that develops within the gas should also exist within the liquid, even at these low driving amplitudes. Similarly, these shock waves would probably not exist in *low-amplitude* multiple-bubble SL. (Of course, when driving amplitudes become large, shock waves appear to exist even in cavitation fields involving many bubbles.) A second test would be the duration of the SL flash. In single-bubble SL, it has been determined to be very short—as a consequence of the shock wave; in multiple-bubble SL, it should be much longer—because the temperature elevation comes from adiabatic heating. Finally, the rapidity of the collapse in single-bubble SL should eliminate the effects of heat conduction, while the longer collapse times in multiple-bubble SL should enable it to be expressed. Thus, in single-bubble SL, the presence of high thermal conductivity gases such as xenon should not have much effect on the final temperature, while in multiple-bubble SL, it should have a considerable effect.

IV. CONCLUSIONS

There are two types of sonoluminescence: multiple-bubble SL and single bubble SL. The former is important in sonochemistry and cases in which the cavitation is extended throughout the liquid. In multiple-bubble SL, cavitation bubble collapse is asymmetrical, which results in lower SL temperatures, but elevates the temperature of the liquid to incandescence temperatures. In single-bubble SL, in which a single, stable, pulsating gas bubble is driven at large radial excursions, cavitation bubble collapse is symmetrical, which results in higher SL temperatures. These effects occur principally within the gas and are of interest for their fundamental sonophysics.

ACKNOWLEDGMENTS

The author wished to acknowledge many helpful discussions with Ron Roy, Seth Putterman, Ken Suslick, and Andrea Prosperetti, who suggested to the author the important distinctions between symmetrical and asymmetrical bubble collapse, and to the Office of Naval Research, Code 1112, for financial support.

Barber, B. P., and Putterman, S. J. (**1991**). "Observation of synchronous picosecond sonoluminescence," Nature **352**, 318.

Barber, B. P., Hiller, R., Arisaka, K., Fettermann, H., and Putterman, S. (**1992**). "Resolving the picosecond characteristics of synchronous sonoluminescence," J. Acoust. Soc. Am. **91**, 3061.

Barber, B. P., and Putterman, S. J. (**1992**). "Light scattering measurements of the repetitive supersonic implosion of a sonoluminescing bubble," Phys. Rev. Lett. **69**, 3839.

Berlan, J., and Mason, R. J. (**1992**). "Sonochemistry: From research laboratories to industrial plants," Ultrasonics **30**, 203.

Crum, L. A. (**1979**). "Surface oscillations and jet development in pulsating air bubbles," J. Phys. (Paris) **40**, 131.

Crum, L. A., and Reynolds, G. T. (**1985**). "Sonoluminescence from stable cavitation," J. Acoust. Soc. Am. **78**, 137.

Flint, E. B., and Suslick, K. S. (**1991**). "The temperature of cavitation," Science **253**, 1397.

Frenzel, H., and Schultes, H. (**1935**). Z. Phys. Chem. **27B**, 421.

Gaitan, D. F., Crum, L. A., Roy, R. A., and Church, C. C. (**1992**). "Sonoluminescence and bubble dynamics from a single, stable, cavitation bubble," J. Acoust. Soc. Am. **91**, 3166.

Hiller, R., Putterman, S. J., and Barber, B. P. (**1992**). "Spectrum of synchronous picosecond sonoluminescence," Phys. Rev. Lett. **69**, 1182.

Jarman, P. (**1960**). "Sonoluminescence: A discussion," J. Acoust. Soc. Am. **32**, 1459.

Kamath, V., Prosperetti, A., and Egolfopoulos, F. N. (**1993**). "A theoretical study of sonoluminescence," J. Acoust. Soc. Am. **94**, 248. (*Note added in proof:* We note that these authors have also suggested that asymmetrical collapse conditions can lead to insertion of liquid into the hot interior of a bubble and thus result in spectra characteristic of the liquid.)

Lofstedt, R., Barber, B. P., and Putterman, S. J. (**1993**). "Towards a hydrodynamic theory of sonoluminescence," Phys. Fluids A (to be published)

Luche, J. L. (**1992**). "Development of the new 'experimental theory' of sonochemistry initiated in Grenoble," Ultrasonics **30**, 154.

Margulis, M. A. (**1992**). "Fundamental aspects of sonochemistry," Ultrasonics **30**, 152.

Marinesco, N., and Trillat, J. J. (**1933**). C. R. Acad. Sci. Paris **196**, 858.

Suslick, K. S. (**1989**). "The chemical effects of ultrasound," Sci. Am. **260** (2), 80 (1989).

Suslick, K. S. (**1990**). "Sonochemistry," Science **247**, 325.

Suslick, K. S., Dokytcz, S. J., and Flint, E. B. (**1990**). "On the origins of sonochemistry and sonoluminescence," Ultrasonics **28**, 280.

Taylor, K. J., and Jarman, P., D. (**1970**). "The spectra of sonoluminescence," Aust. J. Phys. **23**, 319.

Tomita, Y., and Shima, A. (**1990**). "High-speed photographic observations of laser-induced cavitation bubbles in water," Acustica **71**, 161.

Reprint Series
14 October 1994, Volume 265, pp. 233–234

SCIENCE

Sonoluminescence

Lawrence A. Crum and Ronald A. Roy

Sonoluminescence

Lawrence A. Crum and Ronald A. Roy

When trapped in sufficiently intense acoustic fields, single bubbles of gas can emit luminescence bright enough to be visible in an undarkened room. The large number of intriguing results recently published about such single-bubble sonoluminescence (SBSL) (*1*–*9*) suggests that this phenomenon awaits a full explanation. And as reported by Hiller *et al.* on page 248 of this issue (*10*), some exciting atomic physics may be occurring within the collapsing cavitation bubble that gives rise to SBSL. However, many of the results they present are also anomalous and defy immediate explanation.

Sonoluminescence (SL) was discovered nearly 60 years ago when Frenzel and Schultes (*11*) found that photographic plates became exposed when submerged in water and irradiated with ultrasonic waves. Since then, the phenomenon of SL has been associated with the presence of (relatively) intense sound fields within liquids. The light emission implies existence of high local temperatures (the ambient temperature of the liquid remains relatively constant), temperatures high enough to incandesce gas and influence chemical reactions. Thus arose sonochemistry, which has resulted in an active field of both basic research and emerging technology development (*12*).

When an intense sound field is produced within a liquid, microscopic cavities of gas or vapor can be generated when the liquid fails under tensile stress. The subsequent acoustic compression cycle forces these cavities to collapse violently, which results in a remarkable concentration of mechanical energy, estimated to be as high as 12 orders of magnitude (*3*, *4*, *10*). In the process, the gas contained within these cavities is heated to luminescence. In some cases, the light emissions appear to come from a distributed region surrounding the tip of the acoustic source. This multiple-bubble sonoluminescence (MBSL) results from the collapse of many separate, individual cavitation bubbles. Because MBSL occurs randomly and transiently, it has been difficult to study in much detail. Recently, Gaitan and co-workers discovered the unique conditions necessary for a single bubble, pulsating stably, to emit SBSL each acoustic cycle (*1*, *2*) (see figure); its robust stability and simplicity has permitted detailed studies of this "hydrogen atom of sonoluminescence" (*1*–*4*, *10*).

Theoretical calculations of the time interval during which the contents of a gas bubble, driven to collapse by the sound field, is sufficiently heated to emit light tend to be on the order of tens of nanoseconds. However, when Barber and Putterman sought to measure the duration of the light flash, they discovered that they were in fact measuring the impulse response of their photomultiplier tube (PMT) (*3*). Even subsequent measurements obtained with the world's fastest multichannel plate PMT led to results that were rise time–limited. Their best measurements to date indicate an upper bound of about 50 ps, about 1/1000 of that predicted by conventional theory of cavitation bubble collapse. In addition, Barber and Putterman measured the statistics of the flash-to-flash interval for a bubble driven at 30 kHz and discovered that it had an average value of 33 μs with a root-mean-square fluctuation of only 50 ps (*3*). This remarkable stability, 1 part in 10^6, exceeds the rated stability of the frequency generator that drove the acoustic system.

The spectrum of MBSL contains molecular emission bands associated with the liquid in which the sonoluminescence occurs (*12*). For example, if MBSL occurs in an organic liquid such as dodecane, one sees diatomic carbon bands; if MBSL occurs in an inorganic liquid such as water, one observes the spectral bands of the OH radical; these bands suggested temperatures within the cavities on the order of 5000 K. However, when Hiller *et al.* (*4*) and Atchley and coworkers (*5*) studied SBSL emissions, they discovered a smooth spectrum, devoid of any distinct bands. This suggests the presence of much higher temperatures, perhaps orders of magnitude greater than those encountered in MBSL systems.

To date, only one viable explanation has been offered for the short pulse duration of the SBSL flash and for the seemingly extreme temperatures involved: a

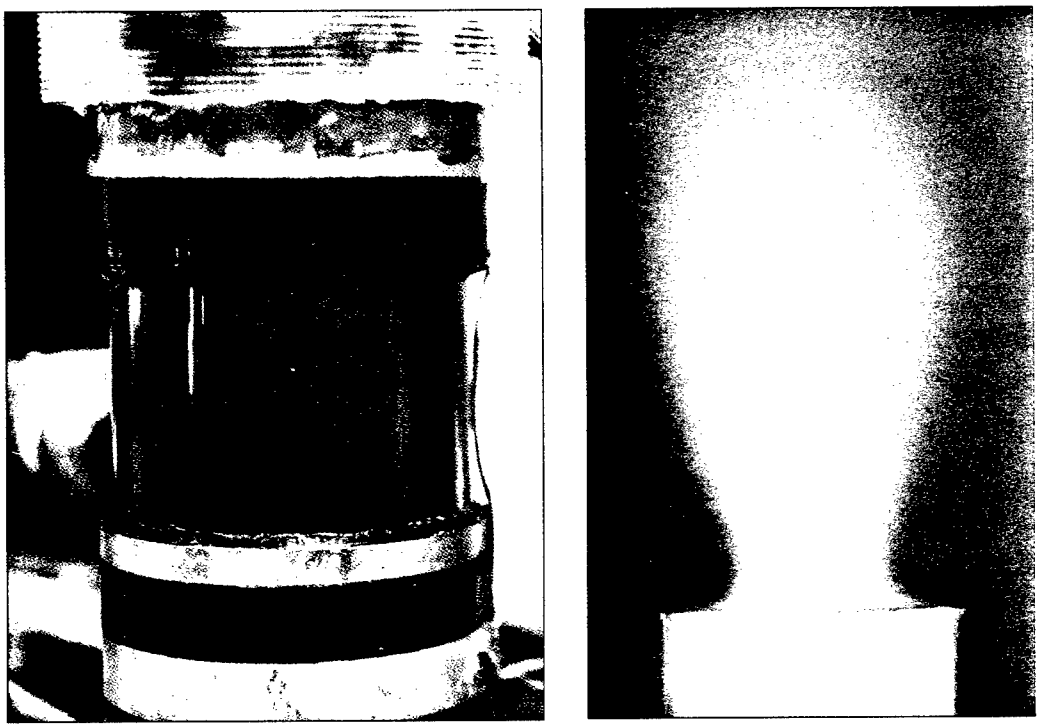

Bright bubbles. An acoustic standing wave levitates a small gas bubble near the center of a glass cell **(left)** and drives that bubble to radial excursions of sufficient amplitude to generate sonoluminescence each and every acoustic cycle. Note the bright spot at the center of the cell, which can easily be seen without darkening the room; no chemical enhancement is required. This bubble was driven at a frequency of 22.3 kHz and at a pressure amplitude of about 1.3 bar. In an example of MBSL **(right)**, the intense sound field near the tip of an acoustic source produces many transient cavitation bubbles that grow and collapse with such violence that they heat their respective interiors to incandescence. Because the individual bubbles persist for only a few acoustic cycles (at 22 kHz), they are not visible in this photograph. Luminol, a wavelength shifter, was added to enhance the light emission, which is normally too faint for unaided photography.

The authors are in the Department of Acoustics and Electromagnetics, Applied Physics Laboratory, University of Washington, Seattle, WA 98105, USA.

spherically converging shock wave generated within the collapsing bubble. Wu and Roberts (7) as well as Greenspan and Nadim (8) have demonstrated numerically that such an imploding shock should exist in the SBSL bubble and that extremely short pulse durations (0.1 ps) and high temperatures (1000 eV; 1 eV = 11,600 K) should occur. Using a more accurate equation of state, Moss *et al.* (9) have confirmed predictions of extreme temperatures and pressures, obtaining values more in line with the (crude, at this time) experimental measurements, namely, pulse durations on the order of 10 ps and peak temperatures on the order of 10 to 100 eV. Furthermore, their computations suggest that at various locations within the imploded core at the center of the bubble, pressures can be as high as 200 Mbar (1 Mbar = 10^{11} Pa), and densities as high as 13.4 g/cm^3 (at these levels, it is possible that the compressed air near the center of the bubble will have properties similar to that of a metal). Note that all the calculated results cited above are based on one-dimensional calculations assuming a perfectly symmetrical bubble collapse and are mitigated by the effects of dissociation and ionization [which are accounted for in the Moss *et al.* (9) computations] and by various radiation and mass transport mechanisms (which are not accounted for by Moss *et al.*).

As indicated in figure 2 of Hiller *et al.* (10), a small quantity of argon introduced into a pure nitrogen bubble increases the luminosity of SBSL by nearly two orders of magnitude. What effect does argon have on this system? Does it strongly influence the dissociation, ionization, and radiation transport within the core? Does it have a catalytic effect on electronic transitions within the plasma or material composing the core? Does it readily conduct heat from the hot interior of the core to the outer layers and thus increase the radiated energy or the total volume of high-temperature gas? These questions are difficult to answer with the existing data and clearly require additional measurements and computations.

Figure 3 of Hiller *et al.* (10) demonstrates that if the bubble contains certain gas species, the spectra show broad peaks near 300 nm, whereas for other species, no peaks exist and the spectrum monotonically increases down to the water cutoff (the transmissivity of the ultraviolet through water is greatly reduced below 200 nm). Why is it that a maximum exists at all? If the gas core is heated and compressed to the degree predicted by recent theories, then only the outer shell should radiate (like the sun). If there is a broad maxima for xenon, then shouldn't there also be one for helium? These again are anomalous results and perhaps have something to do with the heat transport through the compressed gas.

Finally, the data displayed in figure 5 either have a trivial explanation (for example, a periodic detuning of the cell) or they are truly remarkable. These data suggest that some mechanism, possibly gas diffusion across the gas-liquid interface, is causing the luminosity and equilibrium bubble radius to cycle with a period on the order of seconds. It seems remarkable to us that such long-term memory (on the order of 100,000 acoustic cycles) could exist in a mechanical system.

As we currently understand it, single-bubble sonoluminescence may result in temperatures in excess of 10^5 K, pressures in excess of 10^7 bar, light emissions lasting less than 50 ps, and mechanical energy concentrations of up to 12 orders of magnitude; all this from a simple acoustical system costing a few hundred dollars to construct. It is a remarkable laboratory for physics and chemistry.

References

1. D. F. Gaitan and L. A. Crum, in *Frontiers of Nonlinear Acoustics*, 12th ISNA. M. Hamilton and D. T. Blackstock, Eds. (Elsevier, New York, 1990), pp. 459–463; D. F. Gaitan, L. A. Crum, R. A. Roy, C. C. Church, *J. Acoust. Soc. Am.* **91**, 3166 (1992).
2. L. A. Crum, *J. Acoust. Soc. Am.* **95**, 559 (1994); *Physics Today* **47**, 22 (September 1994); R. A. Roy, *Ultrason. Sonochem.* **1**, S5 (1994).
3. B. P. Barber and S. J. Putterman, *Nature* **352**, 318 (1991); B. P. Barber, R. Hiller, K. Arisaka, H. Fetterman, S. J. Putterman, *J. Acoust. Soc. Am.* **91**, 3061 (1992); R. Lofstedt, B. P. Barber, S. J. Putterman, *Phys. Fluids A* **5**, 2911 (1993); B. P. Barber and S. J. Putterman, *Phys. Rev. Lett.* **69**, 3839 (1992).
4. R. Hiller, S. J. Putterman, B. P. Barber, *Phys. Rev. Lett.* **69**, 1182 (1992); R. Hiller and B. P. Barber, *J. Acoust. Soc. Am.* **94**, 1794 (1993).
5. A. A. Atchley, in *Advances in Nonlinear Acoustics*, H. Hobaek, Ed. (World Scientific, Singapore, 1993), pp. 36–42; R. G. Holt, D. F. Gaitan, A. A. Atchley, J. Holzfuss, *Phys. Rev. Lett.* **72**, 1376 (1994).
6. T. Lepoint and F. Mullie, *Ultrason. Sonochem.* **1**, S13 (1994); M. A. Margulis, *Ultrasonics* **30**, 152 (1992); J. Schwinger, *Proc. Natl. Acad. Sci. U.S.A.* **89**, 4091 (1992); *ibid.*, p. 11118; V. Kamath, A. Prosperetti, F. N. Egolfopoulos, *J. Acoust. Soc. Am.* **94**, 248 (1993).
7. C. C. Wu and P. H. Roberts, *Phys. Rev. Lett.* **70**, 3424 (1993).
8. H. P. Greenspan and A. Nadim, *Phys. Fluids A* **5**, 1065 (1993); A. Nadim, A. D. Pierce, G. V. H. Sandri, *J. Acoust. Soc. Am.* (*suppl.*) **95**, 2938 (1994).
9. W. C. Moss, D. B. Clarke, J. W. White, D. A. Young, *Phys. Fluids* **6**, 2979 (1994).
10. R. Hiller, K. Weninger, S. J. Putterman, B. P. Barber, *Science* **266**, 248 (1994).
11. H. Frenzel and H. Schultes, *Z. Phys. Chem. B* **27**, 421 (1934).
12. K. S. Suslick, *Science* **247**, 1439 (1990); K. S. Suslick, E. B. Flint, M. W. Grinstaff, K. A. Kemper, *J. Phys. Chem.* **97**, 3098 (1993).

SONOLUMINESCENCE--HISTORY AND PRESENT STATUS

L. A. Crum
Applied Physics Laboratory, University of Washington, 1013 NE 40th St.
Seattle, Washington 98105-6698, USA

PREFACE

The author was asked to present a Plenary Paper at this Congress on the general topic of Sonoluminescence, and as these things go, to keep it quite general. Consequently, this written communication is meant to follow the same concept--to be informative and broad rather than rigorous and specific. The interested reader is referred to the citations for more detail.

INTRODUCTION

Sonoluminescence was discovered when the German scientists Frenzel and Schultes [1] noticed that a photographic plate was darkened when it was exposed to ultrasonic waves in a water bath --not unlike the discovery of radioactivity by Becquerel. Thus, it was determined that sound gave rise to light--and hence sonoluminescence.

This is an amazing phenomenon when one considers that the energy density in an acoustic field is on the order of 10^{-11} eV/molecule, while light emissions tend to be on the order of an eV or so. Thus, one has a phenomenon which gives rise to an energy concentration of 11-12 orders of magnitude--perhaps even higher. There are few physical processes that we know of that can concentrate mechanical energy so efficiently.

So why does this happen? How is the sound field able to concentrate such energy? The answer lies in the phenomenon of cavitation, in which microscopic gas bubbles present in the liquid are made to grow to quite large relative volumes by the rarefaction portion of the acoustic cycle. For example, a cavitation bubble may grow from a few microns in diameter to over a hundred microns, thus resulting in a volume increase of many orders of magnitude. The subsequent compressional portion of the sound field then leads to an implosive collapse of this (mostly) vapor-filled cavity. It is easy to see that if the initial size of the bubble is quite small, and thus the total number of gas molecules contained inside the bubble also quite small, the collapse will proceed essentially unimpeded--the vapor can provide no stiffness--until the very end; thus, the relatively large amount of work done by the sound field on the bubble during its growth is concentrated in a relatively small volume at collapse. Of course, the violent nature of cavitation is well know among acousticians and is responsible for the rapid destruction of poorly designed ship propellers, the unmatched scouring capabilities of ultrasonic cleaners, and the *in vivo* destruction of kidney stones in shock wave lithotripters. However, it has been the contributions of chemists that have renewed much of our recent interest in cavitation, and, particularly, in sonoluminescence.

SONOCHEMISTRY

The unique environment provided by cavitation collapse is ideally suited to the study of exotic chemical processes. First of all, there is the capacity to generate enormous temperatures and pressures in a cold liquid! Second, the apparatus, at least to get started, is relatively inexpensive--one needs only a reaction vessel and some means of generating lots of cavitation. A particularly favored device is an acoustic horn. Third, the field is mostly unexplored, with lots of interesting things still to discover.

An innovator in this field is Prof. K. Suslick of the University of Illinois, in the USA. Not only has he made some significant contributions, but he has also popularized the field; the interested reader is referred to two particular publications of general interest [2,3]. Of course, the field of sonochemistry has been around for quite some time also, but permit me to mention a class of recent discoveries that have renewed interest in cavitation in general and sonoluminescence in particular.

When Suslick and his colleagues radiated with high intensity ultrasound a compound that contained a dissolved but volatile form of iron, microscopic particles of *free* iron were generated [4]; furthermore, these particles were found to be amorphous iron--without a crystalline structure, and potentially of considerable industrial importance. So how does one get amorphous iron particles out of a cavitation bubble? Apparently, when the bubble collapses, the interior of the bubble gets so hot that the molecules all dissociate into their constituent atoms, including the volatile iron-containing vapor. When this hot system starts to cool, the iron atoms begin coalescing into little particles of molten iron--but here's the interesting portion--the rebounding cavitation bubble cools so fast--like thousands of degrees per nanosecond--that the iron atoms don't have time to crystallize, and amorphous iron results. With interior temperatures of tens of thousands of degrees, with interior pressures of

thousands of atmospheres, and with these remarkable cooling rates -- clearly, the interior of a cavitation bubble is one of the unique laboratories on earth.

But back to sonoluminescence--what does sonochemistry tell us about this phenomenon? It is obviously very difficult to insert some probe into an imploding cavitation bubble. However, the collapsed bubble is in such an elevated level of temperature and pressure, it radiates electromagnetic waves, i.e., it produces sonoluminescence. Our best chance to learn something about the interior of the bubble is to examine these emissions. Suslick and his colleagues have done that by examining their spectroscopic characteristics; Fig. 1 gives some indications of their results.

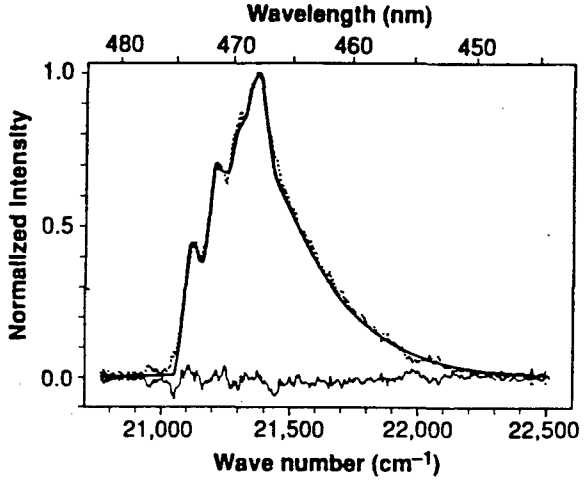

Fig. 1. Sonoluminescence spectrum of silicone oil under continuous Ar sparge at 0°C generated by an acoustic horn. The dotted line shows the measured spectrum; the solid line shows the best fit synthetic spectrum, assuming emissions from the Swan band of C_2, with T=4900 K; the jagged line at the bottom shows the difference spectrum (from Flint and Suslick [5]).

This analysis goes something like this: One measures the radiated sonoluminescence spectrum. Knowing what the constituents are within the bubble, one can assume a particular spectrochemical reaction--such as electronic transitions in the diatomic carbon complex--and then calculate the spectrum that one would expect, with temperature as a fitting parameter. One then varies the temperature until a good fit is achieved, as is observed in this particular case, and now--*voila*--one has measured "the temperature of sonoluminescence". Nicely done! At this stage, it was assumed that sonoluminescence was pretty well understood, particularly, since computations by bubble theorists such as Prosperetti and his colleagues [6] gave similar results. However, the fortuitous discovery of "Single Bubble Sonoluminescence" (SBSL), has led us to reevaluate much of what we thought we once knew.

SINGLE BUBBLE SONOLUMINESCENCE

One of the difficulties associated with a more complete understanding of sonoluminescence is that it is normally associated with thousands of individual cavitation bubbles, presumably all behaving in an independent fashion. A picture of a cavitation field displaying sonoluminescence (see, e.g., Fig. 2 of Ref. [7]) shows light emissions arising from a variety of locations in which there is active cavitation. Thus, one has to assume either that all the cavitation events are generating nearly identical conditions, or that we are simply sampling a statistical average of the many different events. It was obvious that if we could generate sonoluminescence from a single cavitation bubble, then we would have a much more precise laboratory to study the phenomenon.

After a laborious search, Felipe Gaitan, in my laboratory, was able to find the conditions necessary to obtain a single, stable cavitation bubble that gave rise to sonoluminescence emissions each cycle, and rather remarkably, was so stable that it would continue to radiate these emissions for as long as the liquid and acoustic conditions didn't measurably change. This discovery should have enabled us to understand the phenomenon of sonoluminescence in great detail; however, as nature is wont to do, this discovery has raised many more questions than it has answered and now most of us feel that we understand very little about the phenomenon.

First, let me describe the experimental conditions under which one can generate single bubble sonoluminescence: Suppose one acquires a small spherical flask, attaches a ceramic transducer to the outside, fills the flask with water or some other liquid, and drives the system in one of its resonant modes. A small gas bubble inserted into the liquid in this standing wave system will experience radiation pressure forces that will tend to propel it along a pressure gradient. Under the right conditions--not very difficult to achieve--the acoustic forces will balance the buoyancy forces and the bubble will remain at a fixed position within the standing wave system. At this point the bubble is said to be "acoustically levitated". Of course, there are several effects that end to destabilize this system. For example, a bubble undergoing radial oscillations within a liquid containing dissolved gas will tend to

force additional gas into its interior because of a phenomenon called "rectified diffusion". Simply stated, this effect results from the fact that the outward diffusion that would result from the increased gas pressure within the bubble is not matched by the inward diffusion when the bubble is compressed, because the diffusion rate is proportional to the area of the bubble--and it is larger during the inward diffusion (expanded) stage than during the outward diffusion (compressed) stage. Consequently, a bubble oscillating in a liquid containing dissolved gas will tend to undergo a rectification of diffusion due to this area asymmetry. Of course, a non-oscillating bubble would normally dissolve due to the outward diffusion resulting from the added interior pressure arising from surface tension. Thus, one has two competing processes for gas diffusion, and the point at which these balance is a point of unstable equilibrium only; accordingly, a slight change in the conditions will result in the bubble growing or dissolving without bound.

When Gaitan discovered that under certain rather restricted conditions a bubble would generate sonoluminescence emission each acoustic cycle, *and the bubble seemed to neither grow or dissolve*, we found the result rather remarkable. The following figure demonstrates the phenomenon of single bubble sonoluminescence:

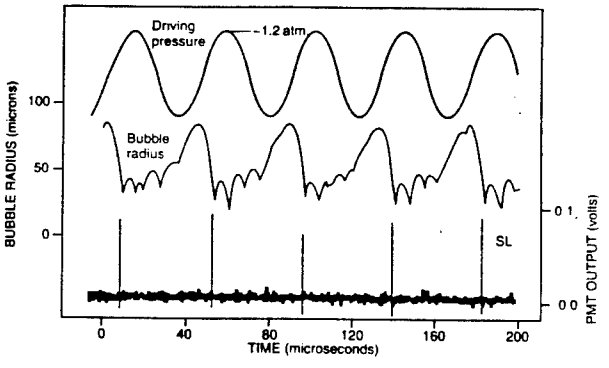

Fig. 2. Original plot obtained by Gaitan demonstrating the synchronous relationship between the acoustic field, top trace, the measured radius-time curve, middle trace, and the sonoluminescence emissions, bottom trace. Note that the emissions occur at a fixed phase of the acoustic field. Though not shown in this figure, such behavior will tend to continue without change for an unlimited period of time.

Although this phenomenon was quite interesting in and of itself, it was Seth Putterman and his colleagues at UCLA who discovered some truly remarkable aspects of SBSL [9-11].

When Putterman's group tried to measure the duration of the light emission, they discovered that there were no photomultiplier tubes fast enough to record the event [9]. Eventually they settled on a value of 50 ps as an upper bound! 50 picoseconds is a rather short time, compared to the period of oscillation of the sound field--about a million times shorter--and even short with respect to the expected duration of the time for which the bubble is collapsed--about 50 ns, when calculated by the best available theories of bubble dynamics. How is it that the bubble can radiate for only one thousandth of the time the gas is presumably compressed within the interior of the bubble.

Over 35 years ago, Peter Jarman [12] suggested that sonoluminescence may be due to a shock wave that is generated within the gas in the interior of the bubble. This speculation was largely ignored until these recent discoveries, but now we have resurrected it. Furthermore, they have given rise to some bold speculations, and some detailed calculations, that suggest the possibilities of rather exotic physics occurring within the interior of the sonoluminescing bubble.

In particular, there has been speculation that under the right conditions, nuclear fusion could result from an implosive collapse of a sonoluminescing bubble containing the appropriate hydrogen isotopes. Indeed, Moss and his colleagues [13] at Lawrence-Livermore National Laboratories in the USA have made some detailed calculations that are reproduced in Fig. 3. below:

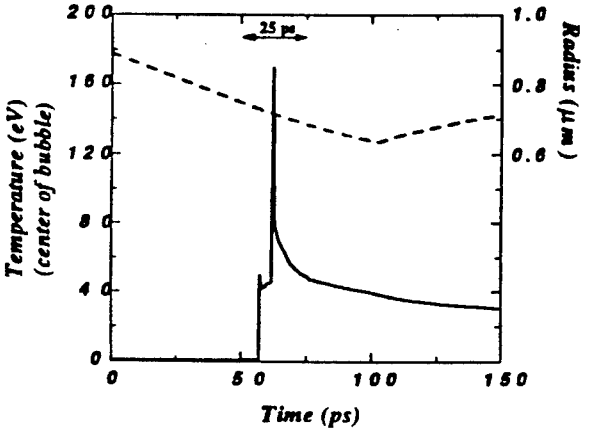

Fig. 3. Calculated variation of the radius-time curve for the bubble and the temperature of the gas within the imploded core with the assumption of an imploding shock waves within the gas (after Moss, et al. [13])

Single-bubble sonoluminescence

Lawrence A. Crum and Sean Cordry
Applied Physics Laboratory, 1013 NE 40th Street
University of Washington, Seattle WA 98105

Abstract. The discovery of single-bubble sonoluminescence [Gaitan and Crum, 1990] has lead to several interesting and remarkable observations [Barber and Putterman, 1991]. Among these are picosecond-length light flashes and a level of syncronicity several orders of magnitude greater than the period of the applied acoustic field. Although new and unique observations concerning this phenomenon are being rapidly reported, an adequate explanation for the physical mechanisms that give rise to single-bubble sonoluminescence has never been given. We present here evidence that this phenomenon arises from nonlinear aspects of bubble dynamics coupled with the process of rectified diffusion. Our results suggest the presence of multiple stability locations that depend upon the driving acoustic pressure and the equilibrium size of the bubble.

1 Introduction

When an acoustic wave propagates through a liquid, certain conditions can be attained in which the mechanical energy associated with the acoustic field is converted into electromagnetic energy. This process, typically intermediated by acoustic cavitation, is called *sonoluminescence*, and is the principal focus of this article.

When cavitation is generated in a liquid, multiple cavitation sites appear with the result that the process is not localized but spatially and temporally distributed over a relatively large parameter space. Fig. 1 shows a photograph of sonoluminescence (SL) generated by a therapeutic ultrasound device [Crum et al., 1987]. Note the localization of SL into bands associated with standing waves in the liquid, but also the distributed nature of the process throughout the bulk of the fluid. Further, this photograph is a time-exposure (about 15 sec.); on an instantaneous basis, one sees random flashes of light from the SL zone that gradually build into the geometrical configuration presented here [Crum et al., 1986].

It has been difficult to determine the basic physical processes that give rise to SL, partly because it has been practically impossible to spatially and temporally control the production of cavitation, the origin of SL. It appears to occur randomly over a relatively large spatial area, as shown in Fig. 1. However, the fortuitous discovery of SL from a single stable cavitation bubble by Gaitan et al., [1988] has now made it possible to study the phenomenon in much more detail than was previously possible. With this system, the dynamics of a single cavitation bubble can be studied simultaneously with the physical processes that lead to SL, thus isolating the critical temporal and spatial parameters that give rise to SL. We shall first present some background material on SL in general, and then describe the process of single-bubble SL. Finally, we shall present some preliminary evidence that suggests the reason for the existence of this phenomenon.

J. R. Blake et al. (eds.), Bubble Dynamics and Interface Phenomena, 287–297.

Fig. 1. Photograph of sonoluminescence produced by a therapeutic ultrasound transducer, shown at the top; here the driving frequency was about 1 MHz and the acoustic pressure amplitude was about 0.15 MPa. The width of the transducer is approximately 2.5 cm.

2 Background

SL was discovered nearly 60 years ago [Marinesco and Trillat., 1933; Frenzel and Schultes, 1935], and since then there have been a variety of explanations given for the origin of the electromagnetic emissions. Electrical discharge theories of various types were at first quite popular. As early as 1940, Frenkel [1940] suggested that electrical charges known to exist on the surfaces of bubbles (see for example, [Watmough, et al., 1992]) were somehow made to discharge. This model, though seriously challenged by the experiments of Suslick [Suslick, 1989;1990], also has its modern advocates [Margulis, 1992; Lepoint and Mullie, 1993]. However, the results summarized below strongly support the hot-spot model of Noltingk and Neppiras [1950] which posits SL to be the result of incandescence of the bubble's contents. Nonetheless, there are still many unanswered questions concerning the origin of this phenomenon.

In 1959, Strasberg [1959] discovered that a stationary sound field could be used to levitate a gas bubble in a liquid. Since then, this technique has been used by a number of researchers to determine various aspects of bubble dynamics [Crum, 1980; 1983; Crum and Prosperetti, 1983]. Recently, Holt and Crum [1987; 1992] developed a technique that enabled real-time measurements of the radius–time curve for an oscillating gas bubble to be obtained; they used this technique to investigate the behavior of bubbles that were driven into nonlinear volume oscillations — a major aspect of acoustic cavitation and SL.

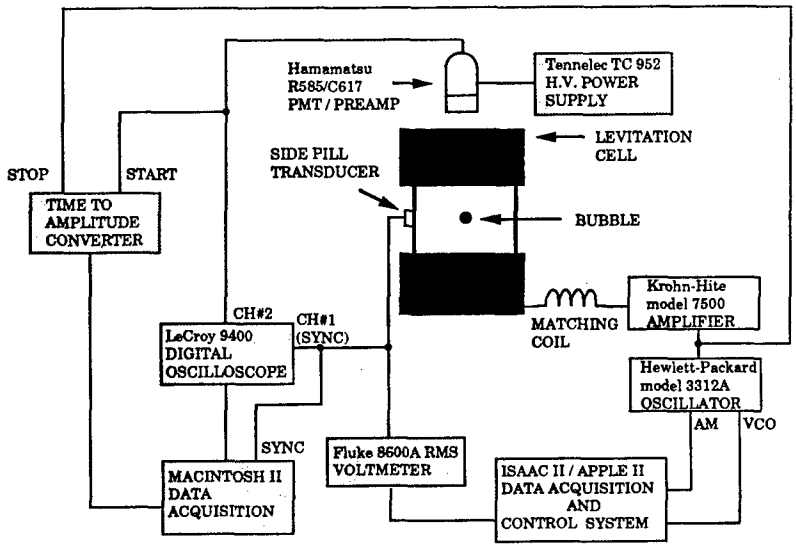

Fig. 2. Experimental arrangement used to levitate a gas bubble and to obtain SL emissions.

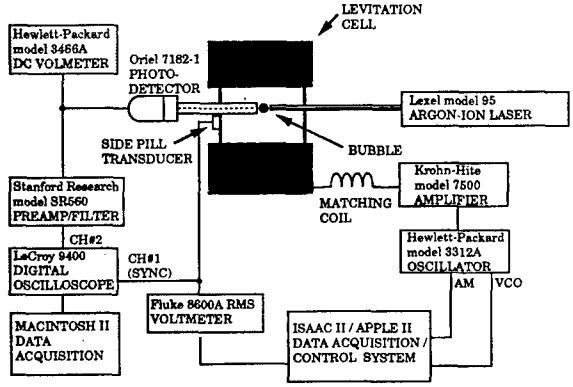

Fig. 3. Experimental arrangement used to obtain the radius–time curve for a luminescing bubble.

In 1988, when Gaitan was studying the conditions necessary for sonoluminescence (SL) during stable cavitation, he discovered that under certain fairly restrictive conditions, a single, stable gas bubble could produce SL emissions each cycle [Gaitan et al., 1988]. Using the light-scattering technique developed earlier [Holt and Crum, 1987; 1992], Gaitan was able to demonstrate the SL emissions were indeed coming from a single gas bubble and that they were being emitted at the final stages of gas bubble collapse. Figs. 2 and 3 show the experimental system used to obtain the phase of the SL emissions and the light scattering technique used

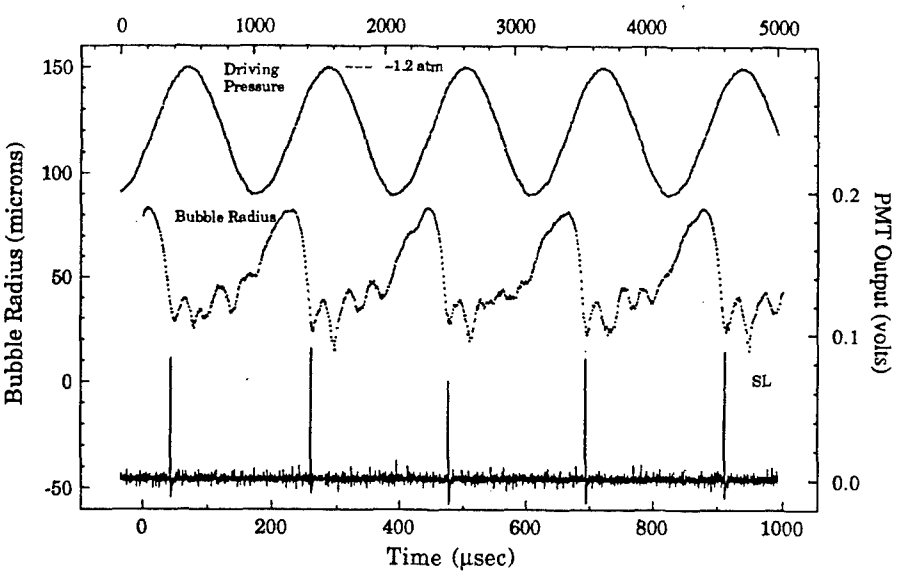

Fig. 4. Synchronous relationship between the driving acoustic pressure (top trace), the bubble radius–time curve (middle trace) and the sonoluminescence emissions (bottom trace) for a gas bubble of approximately 25 μm in radius driven at an acoustic pressure amplitude of approximately 0.12 MPa and at a frequency of 22.3 kHz. Here the liquid was an aqueous solution of glycerin.

to obtain the radius–time (R–t) curve, respectively. (These experimental systems are described in considerable detail in previous publications, [Gaitan and Crum, 1990; Gaitan, et al., 1992] and will not be described again here.)

These two sets of apparatus were combined to obtain Fig. 4 which shows "simultaneous" measurements of the R–t curve and the SL emissions. These are not truly simultaneous, but by synchronizing both the R–t curve and the SL emissions with the acoustic pressure, all three of these variables could be plotted as shown in Fig. 4. This technique was observed by Putterman in our laboratory and then duplicated in his own. A series of remarkable discoveries [Barber and Putterman, 1991; Barber, et al., 1992; Hiller, et al., 1992] were then made that has caused this phenomenon to attract international attention [Levi, 1991].

Barber, Putterman and their coworkers, working in clean, degassed water, have discovered that these light emissions are extremely short and remarkably repetitive. Shown in Fig. 5 is the response of a state-of-the-art photodetection system. It is seen that the SL pulse is no more easily resolved than that of a 35 ps pulsed laser. It should be noted, however, that the PMT was not fast enough to resolve either of these events. From this data, Barber and Putterman estimated that the maximum duration of the SL pulse was 50 ps.

An equally intriguing result is the phenomenon shown in Fig. 6, which shows

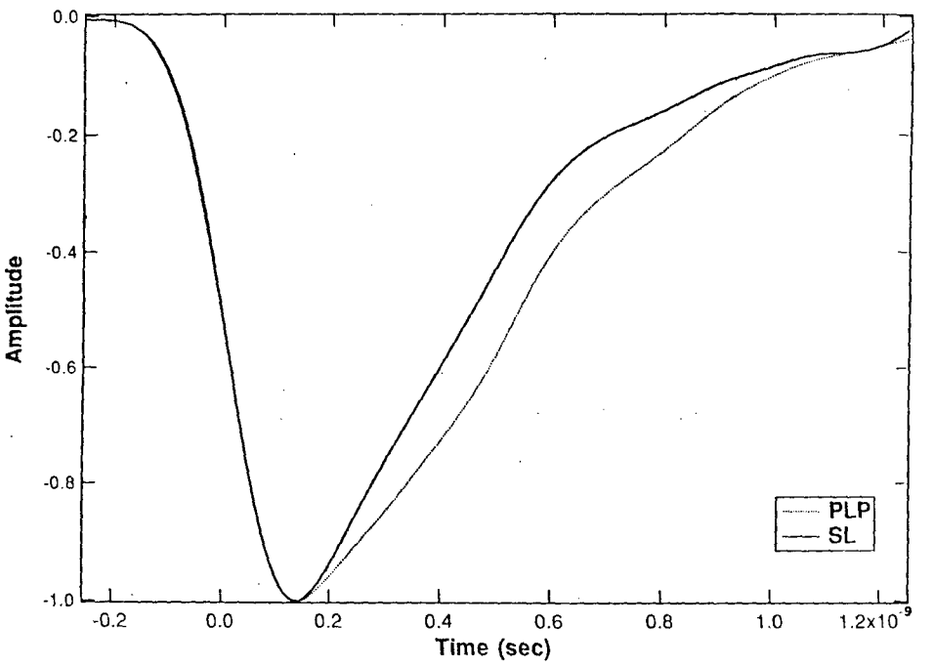

Fig. 5. Response curve of the PMT for SL and a pulsed laser (PLP). The tail in the response of the PLP compared to SL is thought to be due to ringing in the laser. From Barber et al. [1992]

the temporal "jitter" in the SL pulse from cycle to cycle.

This result is remarkable because the half-width of the jitter is estimated to be on the order of 50 ps. Since the electrical voltage that drives the transducer is operated at a frequency of 20 kHz, this jitter represents an instability of only one part in 106 of the acoustic cycle! Surely the electronics of this system has an intrinsic jitter larger than this value. For unknown reasons, the bubble has "mode-locked" to an incredible precision; moreover, the jitter seems to be independent of the stability of the oscillator. Single-bubble SL is like a light source emitting 1.5 cm long light bursts, with a separation between the bursts of 15 km, and with an uncertainty in the position of the bursts of only 1.5 cm. Truly, this is an amazing natural phenomenon!

3 Results and Discussion

If one were to ask, *a priori*, if stable, single-bubble SL could exist — as it does now — most of us would be quite skeptical, because of rectified diffusion. It is difficult to imagine that a bubble of 5 microns, say, could remain at a fixed size for essentially an infinite amount of time. It should either grow or dissolve, but it

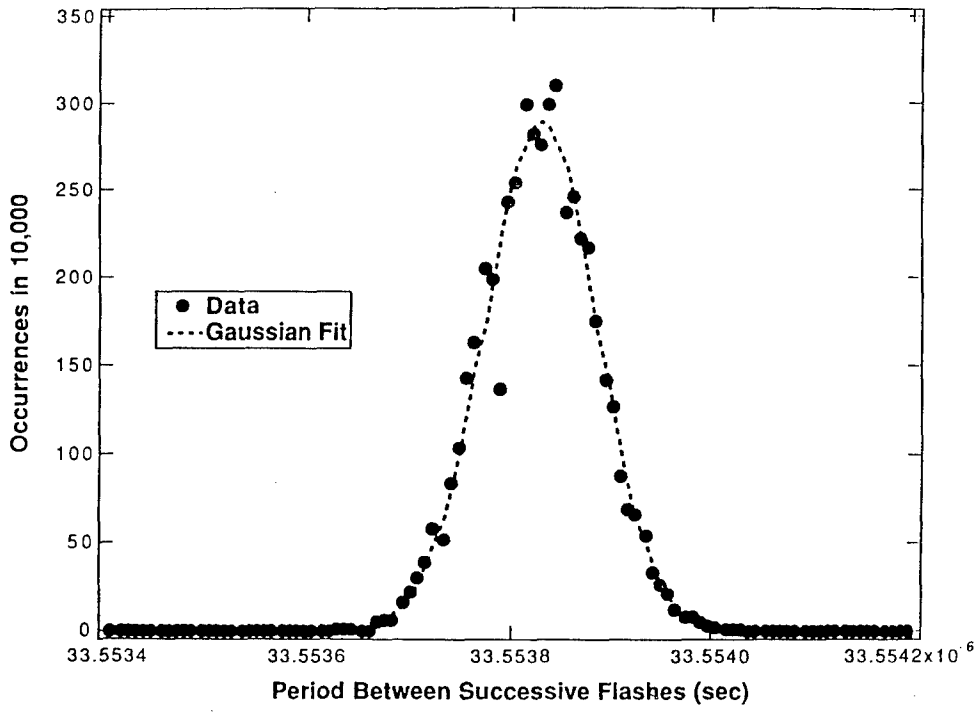

Fig. 6. Distribution of events versus the period between flashes for SL emissions. From Barber et al. [1992]

seems unlikely that it would remain at a fixed size.

Using the nonlinear rectified diffusion code developed by Church, [1988], we have investigated this phenomenon for bubbles under the set of parameters similar to those experiencing sonoluminescence. Figure 7 shows what we believe is an important result.

Note that when one reduces the dissolved gas concentration to the level desirable for single-bubble SL, a couple of "notches" appear in the threshold curve that could be very meaningful (these notches or depressions or valleys are due to the nonlinear response of the bubble and represent harmonic resonances). Consider the notch near 3.5 μm; this value of the radius is near that of the value measured by Barber and Putterman [1993] in their light scattering experiments. Suppose that a bubble were "positioned" within this notch (above the threshold), by selecting a bubble of about 3.5 μm in radius and driving it at a pressure amplitude of 0.115 MPa (1.15 bars) and at a frequency of 20 kHz. This particular bubble would then grow until it engages the threshold curve at about 3.7 μm. At this point, if it grew further, it would pass into a region for which the threshold is higher than 0.115 MPa, and it would start to dissolve. As it got smaller, it would cross the threshold line once again, and get larger, etc. Thus, a positive slope on the rectified

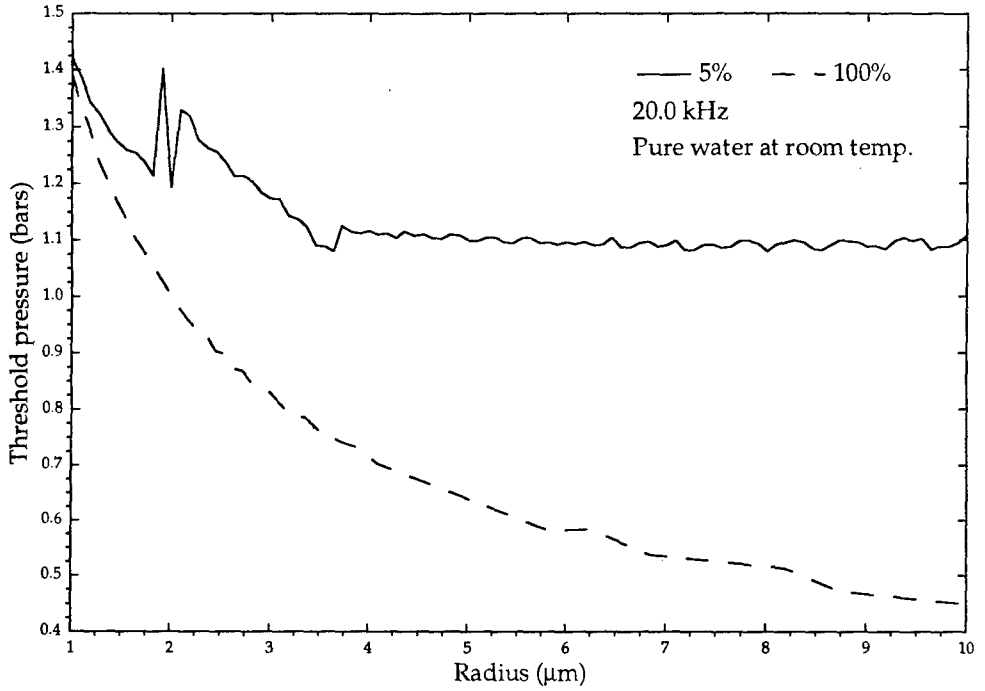

Fig. 7. Calculations of the threshold for rectified diffusion of gas bubbles in water for a driving frequency of 20.0 kHz and dissolved gas concentration of 5 % (solid line) and 100 % (dashed line).

diffusion threshold curve is a point of stable equilibrium for a bubble driven at a fixed acoustic pressure amplitude.

For this bubble to produce SL flashes each cycle, it would seem necessary that shape oscillations not occur, because that should lead to asymmetrical bubble collapse, which would in turn, tend to prevent SL. It is difficult to make measurements in this region, of course, but the extrapolations of our earlier measurements and calculations [Horsburg, et al., 1990] suggest that the threshold for shape oscillations is larger than 0.115 MPa in this radius range (2–5 μm). Thus, it is plausible that this general region of parameter space is the location for single-bubble sonoluminescence.

Consider some further support for this contention. Figure 8 shows the response of a PMT to the "initiation" of single-bubble SL. For this case, a bubble was generated by electrolysis and allowed to rise into the antinodal region of a standing wave field (with the field inactivated); at this point, the field was activated and the time-averaged SL intensity observed as single-bubble SL was initiated.

Figure 8 shows three separate traces taken at different times and under slightly different conditions. Note that similar behavior was observed in each case: A small burst of light occurred for a second or so, followed by a rapid rise to a value in

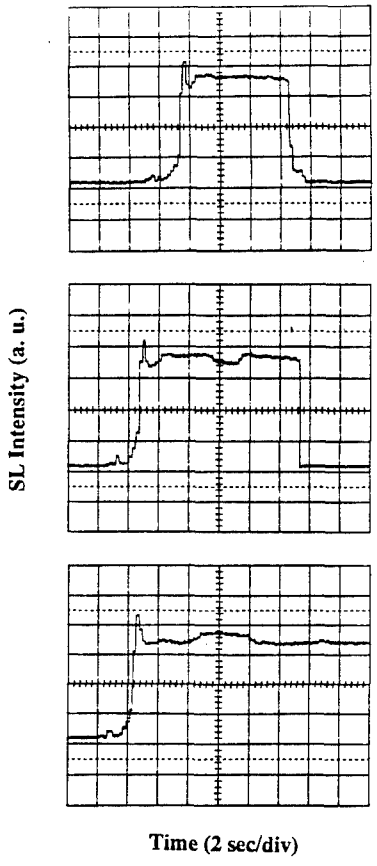

Fig. 8. PMT outputs for the initiation of single-bubble SL. In this case a bubble was introduced into a standing wave field and the time-averaged SL intensity measured as a function of time. These traces are for three different events under approximately the same conditions. Note the repeatability in the structure of the initiation phase. In the top figure, the bubble went unstable, in the middle trace the field was deactivated, and in the bottom trace the bubble remained stable for the duration of the trace.

excess of the equilibrium value, and then a relaxation to a steady output. This behavior seems consistent with the proposed idea that the bubble will adjust its radius by rectified diffusion to reach some stable state. The time scales for bubble growth by rectified diffusion are on the order of seconds for this range of acoustic parameters [Crum and Hansen, 1983]. A second region of notches is also observed in Fig. 7 for a range of bubble radii from 1.5–2.5 μm . This lower-radius region occurs at a higher value of the acoustic pressure amplitude, and could represent a second (and even third, because there are two separate notches here) region of rectified diffusion stability. We believe we have seen evidence of this region.

Consider Fig. 9, which represents a long-term time series for the initiation and

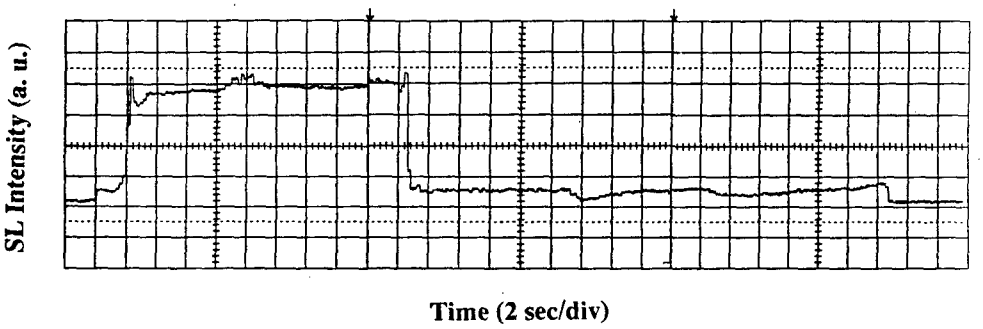

Fig. 9. PMT output for the initiation and stabilization of single bubble SL. In this case the bubble was initiated and stabilized, remaining in this state until the position of the arrow at the top. At this point the system was perturbed, and a transition occurred from a high SL output to a low SL output. The bubble stabilized again in this low output state and remained until the time indicated by the second arrow at the top. At this point, the system was again perturbed, and a transition from this particular state to the noise floor soon occurred.

subsequent deactivation of single-bubble SL.

In this instance, a bubble was activated; it followed the general behavior for initiation as seen in Fig. 8, and then was stabilized. However, in this particular case, the local conditions were slightly perturbed to the extent that after a few minutes, the bubble's intensity dropped to about 15 % of its stable value. It remained at this level, with some slight drifts, for a few more minutes, and then dropped to the noise floor.

We wish to suggest that the bubble could have made a transition from the larger-radius location for single-bubble SL to the smaller-radius one. Keep in mind that it is difficult to maintain equilibrium in the liquid parameters. For example,

a slight increase (or decrease) in temperature will significantly change the level of the dissolved gas concentration. If the temperature of the liquid changes, then the threshold curve moves down (or up) with a shift in the location of the stability regions. Furthermore, slight drifts in the temperature result in resultant changes in the modal frequency and antinodal position. Accordingly, although it may have been fortuitous that a transition from one stability location to another occurred, it is not an unlikely possibility. Finally, it seems likely that a smaller radius bubble would have a lower SL intensity output, which would account for the observed behavior shown in Fig. 9.

These suggestions for the behavior of single-bubble SL are admittedly speculative. However, there seems to be some justification for the general arguments presented here. Related arguments have been presented previously by Kamath, et al., [1993]. A consistent and detailed explanation for this general phenomenon, however, awaits further research.

Summary

We have presented some preliminary evidence that single-bubble SL is the result of nonlinear bubble dynamics in which regions of positive slope occur on the rectified diffusion threshold curve. It appears that bubbles can be entrapped in these regions and, provided liquid and acoustic parameters remain unchanged, furnish locations where individual bubbles can radiate SL emissions each cycle for indefinite periods of time.

Acknowledgment

The authors wish to acknowledge many helpful discussions with Ron Roy, Pierre Mourad, and Andrea Prosperetti, and the financial support of the Office of Naval Research, Physics Division.

References

Barber, B. P. and Putterman, S. J., "Observation of synchronous picosecond sonoluminescence", Nature 352, 318 (1991).

Barber, B. P., Hiller, R., Arisaka, K., Fettermann, H. and Putterman, S., "Resolving the picosecond characteristics of synchronous sonoluminescence", J. Acoust. Soc. Am. 91, 3061 (1992).

Barber, B. P. and Putterman, S. J., "Light scattering measurements of the repetitive supersonic implosion of a sonoluminescing bubble", Phys. Rev. Lett. (in press — preprint).

Church, C. C., "Predictions of rectified diffusion during nonlinear bubble pulsations at biomedical frequencies", J. Acoust. Soc. Am. 83, 2210 (1988).

Crum, L. A., "Measurements of the growth of air bubbles by rectified diffusion", J. Acoust. Soc. Am. 68, 203 (1980).

Crum, L. A., "The polytropic exponent of gas contained within air bubbles pulsating in a liquid", J. Acoust. Soc. Am. 73, 116 (1983).

Crum, L. A. and Hansen, G. M., "Generalized equations for rectified diffusion", J. Acoust. Soc. Am. 72, 1586 (1983).

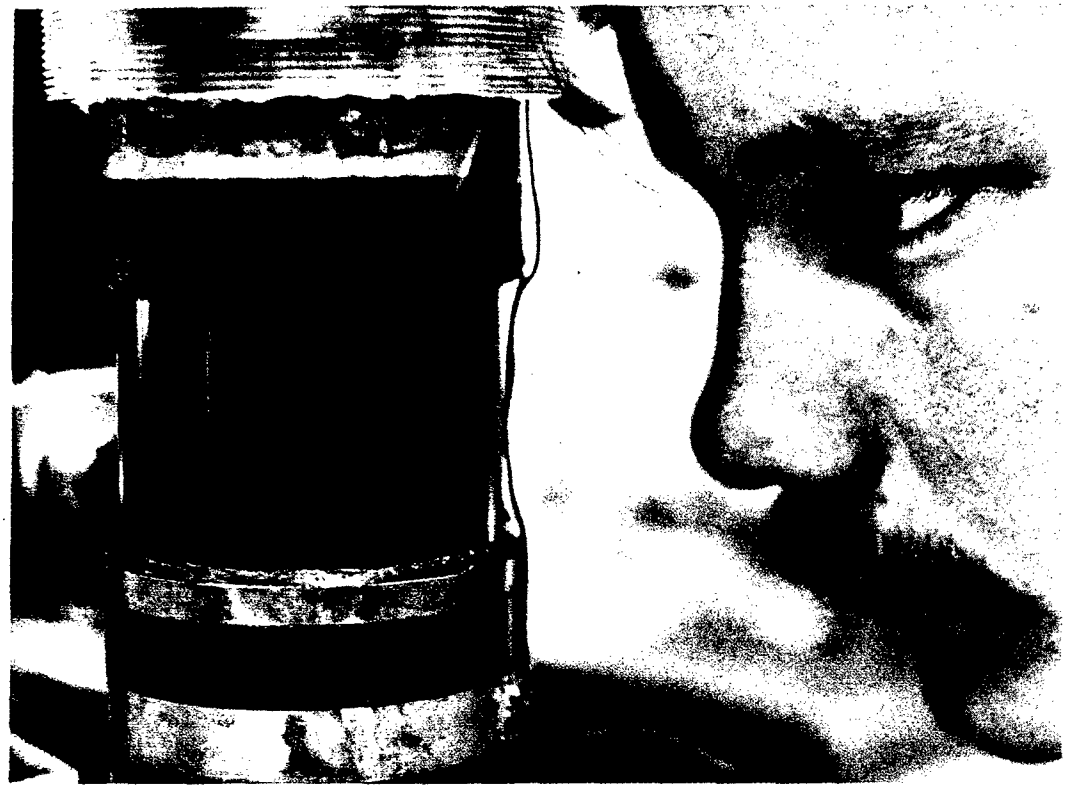

Acoustic cavitation and Sonoluminescence. This acoustic resonator consists of two transducers separated by a thin glass cylinder. Standing waves with frequencies from about 20 kHz to over 100 kHz and acoustic pressures up to about 3 bars can be generated in the liquid. If the acoustic-pressure amplitude is sufficiently large, many cavitation bubbles can be generated near the pressure antinodes of the standing-wave system. If the pressure is considerably lower, it is possible to "acoustically levitate" individual gas bubbles, which under conditions described in the text can generate light each acoustic cycle. Graduate student Sean Cordry watches the blue sonoluminescence from such a bubble. The red streak is an artifact of the lighting.
Figure 1

bles grow and collapse throughout the regions of most intense acoustic stress. Figure 2 shows typical MBSL, with a relatively large area of sonoluminescence activity containing many separate cavitation events, each emitting discrete bursts of light.

Sonoluminescence has been poorly understood because it is associated with the random growth and collapse of large numbers of cavitation bubbles. Moreover, the spatial scale of an individual event is on the order of a micron, and the temporal scale is on the order of a few nanoseconds. Thus, until recently, studies of sonoluminescence involved the time-averaged analysis of a cavitation field. Such a field contains many bubbles of various sizes, probably loosely coupled to each other in their dynamic behavior. These analyses were helpful in understanding gross aspects of the phenomenon, and proved useful in sonochemistry; however, because of the random nature of MBSL it was difficult to learn much about the physics of not only the individual cavitation events but also the resulting electromagnetic emissions.

Single-bubble sonoluminescence

This situation was substantially improved in 1988 when Felipe Gaitan,[3] after a painstaking search, discovered the conditions under which a single, stable cavitation bubble would produce sonoluminescence each acoustic cycle. The achievement of repetitive single-bubble sonoluminescence enabled this phenomenon to be examined in considerable detail. That analysis has led to some remarkable discoveries.[4]

To attain SBSL, it is first necessary to drive a single bubble with an acoustic field intense enough to lead to relatively large radius excursions yet not so intense as to lead to self-destructive instabilities. The procedure Gaitan followed was to levitate a bubble in an acoustic standing wave. As the acoustic-pressure amplitude is slowly increased, a levitated gas bubble progresses through an evolution of states that can lead to SBSL; figure 3 diagrams this evolution. The "equilibrium radius" is obtained in the limit of no bubble oscillations. For relatively low pressures, the bubble undergoes low-amplitude radial pulsations and is positioned between the nodal and antinodal regions of the standing-wave field, where the buoyancy force is balanced by the acoustic radiation-pressure force. As the pressure amplitude is increased, the bubble moves closer to the antinode and eventually undergoes nonspherical pulsations (surface oscillations evidenced by a type of dancing motion of the bubble), which typically split the bubble into a number of small microbubbles. However, if the liquid is sufficiently degassed (say, to 10% of saturation), the dancing motion suddenly ceases. For an air bubble in pure water this happens at a pressure amplitude of about 1.1 bars. The bubble then becomes remarkably stable and emits a faint glow. This glow becomes brighter and brighter as the pressure amplitude is increased, eventually becoming

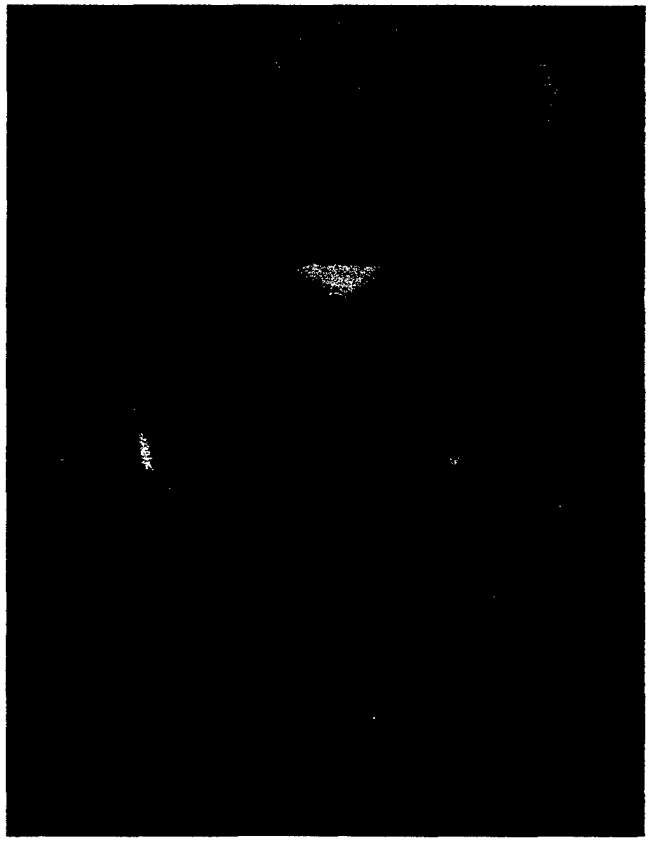

Multiple-bubble sonoluminescence produced by an ultrasonic horn at a frequency of 20 kHz. This is a double exposure: The thin, filamentary lines exist when the horn is driven at low acoustic intensity (2 W/cm^2) and are associated with microscopic cavitation bubbles located near the antinodes of the standing-wave pattern. The bright, triangular-shaped area directly below the horn exists when the system is driven at a higher acoustic intensity (7 W/cm^2); in this case there are no standing waves. For these photographs, Luminol was added to the water to produce more light in the visible region of the spectrum. Each exposure time was about 5 minutes at f/2.8. **Figure 2**

bright enough to be visible even with the lights on in the room. (See figure 1.) When the pressure is increased above about 1.5 bars, the brightly glowing bubble suddenly disappears.

It is likely that diffusion of gas through the liquid–bubble interface plays an important role in bubble stability and restricts the conditions under which SBSL can occur.[5–7] Consider an oscillating bubble in a liquid that contains dissolved gas. When the bubble is in its expansion phase, gas will diffuse into the bubble; conversely, when it is in its compression phase, gas will diffuse out of the bubble. For small-scale oscillations and linear excursions of the bubble radius, the total acoustically induced mass flux of gas over one complete cycle will be zero, and the bubble will dissolve slowly as a consequence of surface tension. However, for larger oscillations (at higher acoustic-pressure amplitudes) there is considerable temporal asymmetry in these radius excursions: The time that the bubble spends in its expansion phase is large compared with the time it spends in its compression phase. Thus over a complete cycle, more gas will diffuse into the bubble than will diffuse out, and the bubble will grow.

This "rectified diffusion" is reduced if the amount of gas dissolved in the liquid is less than the saturation level. Consequently, if the liquid is considerably undersaturated with gas, stable bubble size can be achieved only for large displacement amplitudes. Of course, a balance of diffusion should occur only for a unique pair of values of the dissolved gas concentration and the driving pressure amplitude—which implies that the equilibrium is unstable. However, apparently because of nonlinearities in the bubble response, stable equilibrium conditions can occur.[5,7] Hence greatly reducing the dissolved gas concentration makes it possible to produce a single, stable cavitation bubble that undergoes large radius excursions each cycle. Gaitan was able to find the conditions necessary for these radial excursions to produce sonoluminescence in each oscillation. Once those conditions are achieved the system is amazingly robust: Unless there are significant changes in the acoustic or liquid parameters, SBSL can be maintained for unlimited periods of time.

One can determine the conditions for the bubble dynamics that lead to SBSL rather straightforwardly with light-scattering techniques.[3,8] Using a laser, a photodetector and the applicable Mie-scattering algorithms, one can invert the scattered intensity and obtain a radius-versus-time curve for the bubble. One finds that the light emissions occur on bubble collapse and that the phase of those emissions stays rigorously fixed over a number of acoustic cycles. (See figure 4.)

A group headed by Seth Putterman at the University of California, Los Angeles, has used the constant-phase result and a much improved light-scattering technique to obtain radius–time curves for SBSL to a high level of precision.[8,9] These curves, shown in figure 5, illustrate the transition from a nonsonoluminescing bubble to a sonoluminescing one and are very useful for understanding critical aspects of this phenomenon. As the acoustic-pressure amplitude is increased, there is a transition point at which the bubble's equilibrium radius (apparent at early and late times in figure 5), its maximum radius and its rebound from implosive collapse are all suddenly reduced. At this pressure sonoluminescence emissions begin to occur. Computations of these radius–time curves using standard models of nonlinear bubble dynamics predict the rebound reduction at the reduced bubble size; however, the sudden decrease in equilibrium radius is still not clearly understood. It is known that in most cases surface waves exist on the bubble just prior to the onset of sonoluminescence. However, when sonoluminescence conditions are met, the bubble becomes amazingly stable and shows no evidence of shape instabilities. The parameter space for SBSL occurrence is a topic of current interest. To date, no liquids other than water and

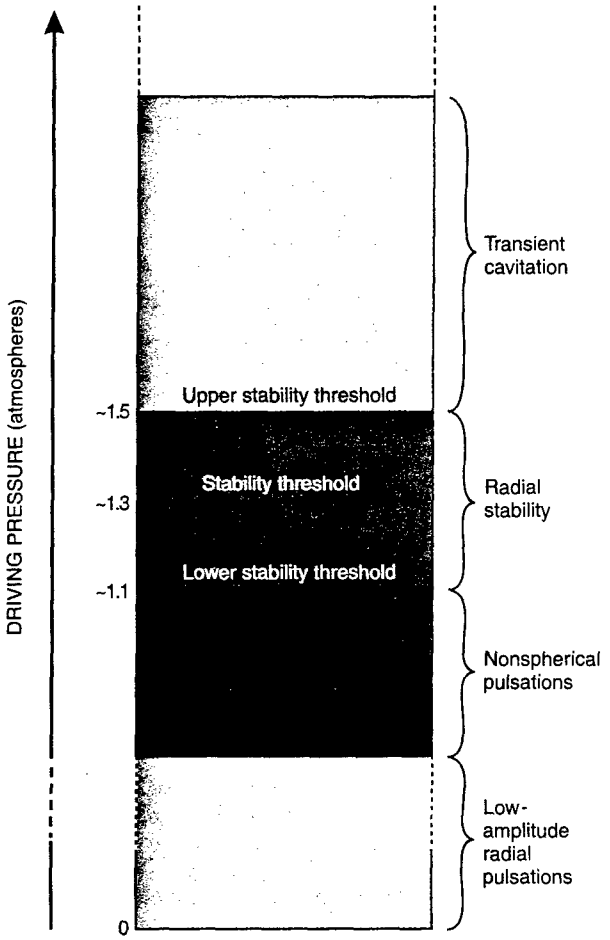

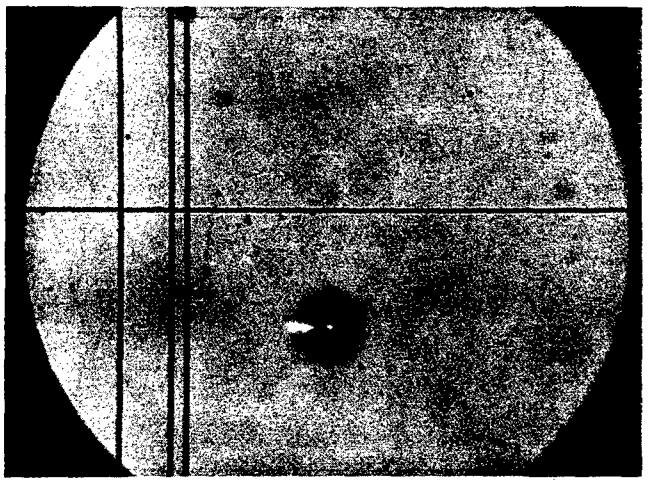

Pressure regimes of single-bubble sonoluminescence. The behavior of an acoustically levitated bubble in an aqueous liquid changes with acoustic driving pressure, as shown schematically at left and described in the text. A photograph of SBSL (above) shows light emissions from a single, stable cavitation bubble that is oscillating about an equilibrium radius of a few microns and emitting blue light each acoustic cycle. The sonoluminescence appears to be coming from the very center of the bubble. The diffuse background light shows that the maximum radius of the bubble is on the order of 50 microns (the outer fiducial lines are 105 μm apart). Over this 1-second exposure, the bubble underwent about 20 000 complete cycles. The horizontal white line is reflected light from an illuminator aimed directly at the bubble. **Figure 3**

glycerin–water mixtures have been shown to demonstrate this phenomenon, although there is no *a priori* reason why it shouldn't exist in many liquids.

Putterman and his colleagues have examined SBSL in some detail and have discovered some of its remarkable properties.[2,6,8–11] One particularly interesting discovery arose from their attempts to measure the pulse duration of the sonoluminescence flash. They found that as they selected photomultiplier tubes with increasingly faster response times, they continued to measure only the impulse response of the tubes. Even when they used the world's fastest microchannel-plate photomultiplier tube they were unable to obtain a direct measurement of the SBSL pulse duration.[2] Furthermore, when they compared the impulse response of the SBSL flash with that of a 34-picosecond pulsed laser, they determined that the SBSL flash is extinguished faster than that of the laser, probably due to some residual ringing in the laser that is absent in SBSL. Attempts to measure the pulse duration with streak cameras and other high-speed devices have been unsuccessful. Although a precise value for the pulse duration has not yet been obtained, Putterman's group estimates an upper bound of 50 psec (see PHYSICS TODAY, November 1991, page 17). This extremely short time (as compared with the acoustic period of about 40 microseconds) is difficult to explain in terms of our conventional understanding of bubble dynamics.

A second remarkable aspect of SBSL is the degree of synchronicity of the flashes. If the relative phase angle between the zero-point crossing of the acoustic field and the emission of the sonoluminescence burst is measured, it is found to be stable to within a degree for periods of several minutes.[3] When the pulse-to-pulse jitter was measured,[9] the standard deviation of the Gaussian curve that defines the jitter was on the order of 50 psec. This remarkable clock-like synchronicity is amazing when one considers that the jitter in the synchronous output of the frequency synthesizer used in the experiment was on the order of 3 nanoseconds. Phase-locking of the flashes is no longer guaranteed, however, if the levitation vessel is driven slightly off resonance.[12] In fact, for that case analysis of successive intervals between flashes shows period-doubling, quasiperiodic and even chaotic behavior.

Sonoluminescence spectra

Because sonoluminescence is indicative of the high temperatures and pressures generated by cavitation collapse, measuring the spectrum of this light has been of interest for many years. Figure 6 shows some representative spectra. In the spectrum of MBSL generated within an organic liquid such as dodecane, one sees well-defined spectral bands that are characteristic of the host liquid. For example, the well-defined peaks in the dodecane spectrum shown in figure 6 are associated with diatomic carbon. By generating synthetic spectra that closely approximate the measured spectra, Kenneth Suslick and his colleagues[13] have obtained the "effective temperature" of the constituents that give rise to the sonoluminescence. This technique depends upon the ability to resolve recognizable emission bands generated by atomic and molecular transitions. Indeed, in hydrocarbon solutions containing dissolved metallic compounds or salts, one sees discrete metal line emissions. When the spectrum of dodecane was measured, with argon as the dissolved gas, the synthetic spectrum indicated that the effective temperature of the C_2 excited state was 5100 K. These measurements

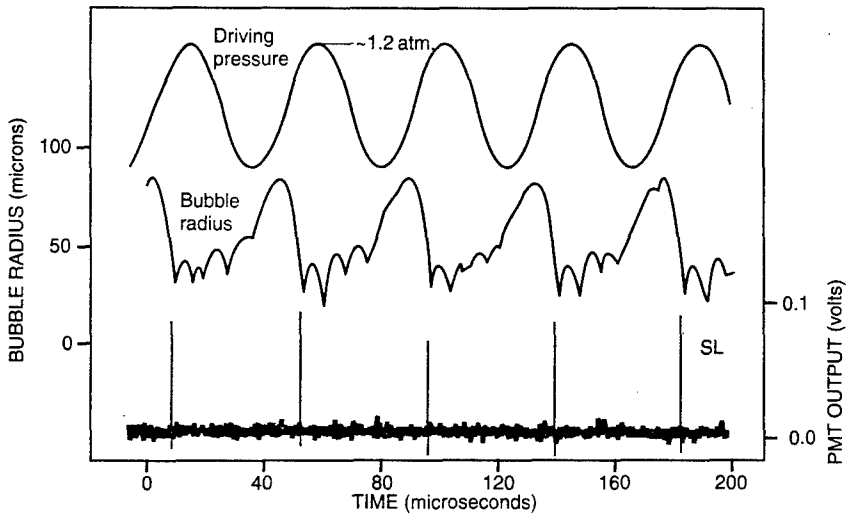

Synchronous relationship between the acoustic field (top), the measured radius-versus-time curve (middle) and the SBSL emissions measured with a photomultiplier tube (PMT) (bottom). The emissions occur at a fixed phase of the acoustic field. (Adapted from ref. 3.) **Figure 4**

were all performed under conditions of MBSL, as in figure 2. In this case bubble–bubble interactions are likely to occur.

Figure 6 also shows the spectrum of water generated under MBSL conditions.[14] This spectrum is considerably different from that of dodecane and shows a well-defined peak at 310 nm. This peak can be associated with molecular bands of the OH free radical, which is likely to be produced by the high temperatures and pressures within the bubble.

Extensive spectroscopic measurements of SBSL in water have also been undertaken[11] and show some intriguing results. For example, the SBSL spectrum is remarkably smooth, containing no significant peaks, and can be fit quite closely by a blackbody curve—giving an effective temperature as high as 30 000 K under some conditions. Furthermore, the sonoluminescence intensity of a pure nitrogen bubble is only a few percent of that of an air bubble, but with the addition of only 1% argon (its approximate abundance in air), the sonoluminescence intensity returns to that for air. With a pure xenon gas bubble, a broad maximum in the spectrum is observed near 300 nm. No such maximum is observed for a pure helium bubble. For both pure Ar and He the intensity increases with decreasing wavelength until the ultraviolet cutoff for water is reached. These results suggest that complicated physical chemistry is occurring within the sonoluminescing bubble.

A typical spectrum of SBSL in water, obtained by Anthony Atchley and his colleagues,[15] is shown in figure 6. When one compares this spectrum with that of MBSL in water, one sees that the 310-nm peak is barely visible and that the spectrum now extends deeply into the ultraviolet. In fact, there is still uncertainty about whether the peak at about 230 nm in the SBSL spectrum is real or is simply the result of the uv attenuation within the water and the measurement apparatus.

The SBSL spectrum doesn't appear to have any spectral bands or emission lines indicative of well-known atomic and molecular transitions and thus doesn't lend itself to a comparison with synthetic spectra. (Perhaps the bands are there but are so broadened by the high temperatures and pressures that they aren't recognizable.) It may be that the spectrum is more closely approximated by that of a blackbody and that the temperature of sonoluminescence is relatively high. The blackbody fit[15] of the SBSL spectrum in figure 6 indicates an effective temperature of approximately 16 000 K. When one lowers the temperature of the water, the SBSL spectrum shifts toward shorter wavelengths; indications of temperatures as high as 30 000 K are then found, provided the blackbody assumption is made.[11] This issue of the temperature of sonoluminescence is still unresolved. Of course, whether one can even have a "temperature" (which implies some sort of equilibrium) of 30 000 K for 50 psec is debatable.

Some basic theory

The theoretical analysis of acoustic cavitation and bubble dynamics in general is reasonably mature,[16] having been initiated, in some sense, by Lord Rayleigh. While MBSL is complicated by the presence of many bubbles, SBSL, in which a single bubble is driven into spherical pulsations at a relatively low driving pressure, seems to represent an idealized case that would be adequately described by existing theoretical models. Hence the discovery of SBSL has provided an exceptional opportunity to test existing theories of bubble dynamics.

Because the gas bubble is an inherently nonlinear system, the theoretical treatment of cavitation-bubble dynamics is necessarily complicated and is best approached through numerical methods. These analytical–numerical approaches usually involve an equation of motion for the bubble interface, an energy equation for both the liquid and the gas, and the application of momentum conservation across the gas–liquid interface. These coupled nonlinear differential equations are then solved, using an equation of state for the gas in the interior of the bubble. The solution describes the motion of the interface and allows one to infer values for the internal pressure and temperature.[5,16] Using such an approach, Bradley Barber and Putterman[8] obtained excellent agreement with their measured radius–time curves. (To be sure, because neither the equilibrium radius of the bubble nor the acoustic-pressure amplitude at the site of the bubble can be measured precisely, these variables were treated as adjustable parameters.) Thus it seemed reasonable to assume that the temperature and the sonoluminescence pulse duration also ought to be describable with this theoretical analysis.

Unfortunately, there is a major failure in the analysis. Figure 7 shows the predicted behavior of the radius and temperature as a function of time for typical conditions that give rise to SBSL: an acoustic-pressure amplitude of 1.3 bars, an equilibrium bubble radius of 5 microns and a driving frequency of 25 kHz. The initial 5-micron bubble radius expands to nearly 40 microns and then rapidly collapses to a value on the order of 0.1 micron. The temperature within the bubble is predicted to rise to

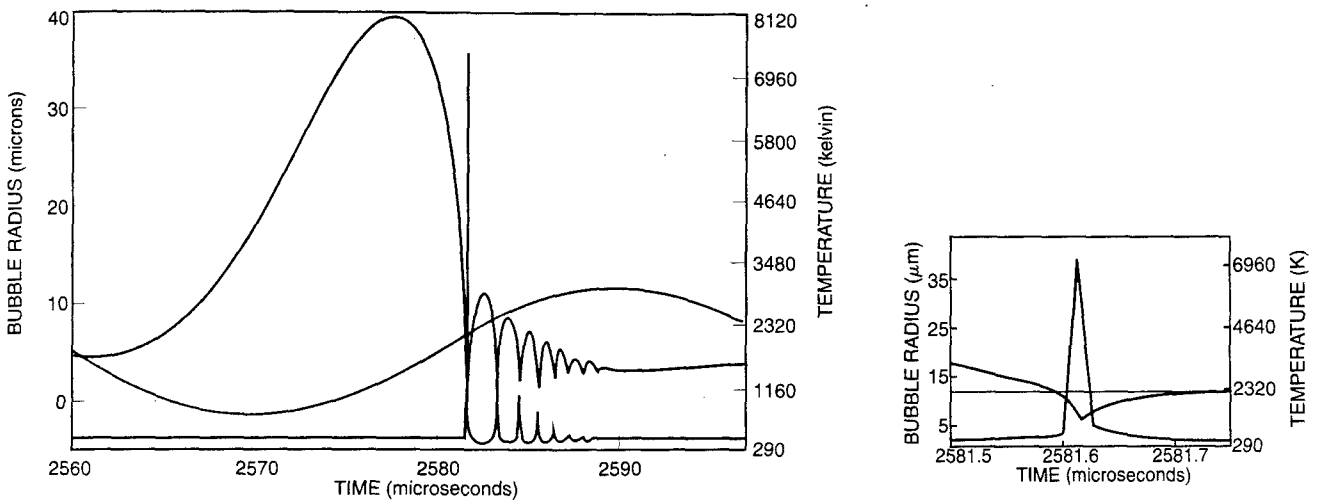

Expected behavior of the bubble radius and internal temperature during SBSL. The purple curve is the acoustic pressure with a driving frequency of 25 kHz. The pressure amplitude is 1.3 bars. The red curve is the bubble radius after the transients have died down (about 60 cycles into the oscillations). Temperature is shown by the green curve. On the right is an expansion of the data around the bubble collapse region. Theory predicts that the temperature of the contents of the bubble should be about 2000 K for over 20 nsec; however, the measured sonoluminescence pulse duration is only 50 psec—a time so short that it can't be drawn to scale on the figure. (Results courtesy of Vinod Kamath.) **Figure 7**

species will revert back to its initial constituents before the high temperatures can be reduced. In acoustic cavitation, on the other hand, the rapid quenching of the reaction "freezes out" the new species. Consider the production of amorphous (noncrystallized) iron, a product of considerable commercial interest for its catalytic capabilities. It is difficult to cool a liquid metal rapidly enough to prevent crystallization. However, in the chemical reactor within a cavitation bubble, ferrous compounds can be decomposed into free atoms and then quenched on such short time scales that solidification of the iron can occur before crystallization.[23] Amorphous iron is easily produced on a laboratory scale by this technique.

To date, SBSL has been demonstrated only in water and mixtures of glycerin and water. It is known from MBSL studies that the intensity of sonoluminescence scales with σ^2/p_v, where σ is the surface tension and p_v is the vapor pressure.[24] MBSL is known to occur in liquid metals such as mercury. If SBSL could be demonstrated in mercury, and the σ^2/p_v scaling parameter holds, then one should expect sonoluminescence intensities nearly 10 000 times greater than what one finds for water.

Energy concentrations of 10^{11}, temperatures of 30 000 K, optical pulse synchronicities to a few parts in 10^{11}, pulse durations of 50 psec, production of exotic chemical species and imploding shock waves—all this from a simple mechanical system costing a few hundred dollars to construct! Although the phenomenon of light from sound has been known for 60 years, the recent discovery of single-bubble sonoluminescence has enabled us to access a remarkable laboratory for physics and chemistry.

* * *

I wish to acknowledge helpful discussions with many individuals, including Andrea Prosperetti, Seth Putterman, Ken Suslick, Anthony Atchley, Logan Hargrove, Sean Cordry, Pierre Mourad and especially Ron Roy. I also acknowledge the financial support over the years of the Office of Naval Research, Physics Programs.

References

1. H. Frenzel, H. Schultes, Z. Phys. Chem. **27B**, 421 (1934).
2. B. P. Barber, R. Hiller, K. Arisaka, H. Fetterman, S. J. Putterman, J. Acoust. Soc. Am. **91**, 3061 (1992).
3. D. F. Gaitan, L. A. Crum, in *Frontiers of Nonlinear Acoustics*, Proc. 12th Int. Symp. on Nonlinear Acoustics, M. Hamilton, D. T. Blackstock, eds., Elsevier, New York (1990), p. 459. D. F. Gaitan, L. A. Crum, R. A. Roy, C. C. Church, J. Acoust. Soc. Am. **91**, 3166 (1992).
4. L. A. Crum, J. Acoust. Soc. Am. **68**, 203 (1980); **95**, 559 (1994). R. G. Holt, L. A. Crum, J. Acoust. Soc. Am. **91**, 1924 (1992).
5. V. Kamath, A. Prosperetti, F. N. Egolfopoulos, J. Acoust. Soc. Am. **94**, 248 (1993).
6. R. Lofstedt, B. P. Barber, S. J. Putterman, Phys. Fluids A **5**, 2911 (1993).
7. L. A. Crum, S. Cordry, in *Proc. IUTAM Symp. on Bubble Dynamics and Interface Phenomena*, J. R. Blake, N. H. Thomas, eds., Kluwer, Dordrecht, The Netherlands, in press.
8. B. P. Barber, S. J. Putterman, Phys. Rev. Lett. **69**, 3839 (1992).
9. B. P. Barber, C. C. Wu, R. Lofstedt, P. H. Roberts, S. J. Putterman, Phys. Rev. Lett. **72**, 1380 (1994).
10. B. P. Barber, S. J. Putterman, Nature **352**, 318 (1991).
11. R. Hiller, S. J. Putterman, B. P. Barber, Phys. Rev. Lett. **69**, 1182 (1992). R. Hiller, B. P. Barber, J. Acoust. Soc. Am. **94**, 1794 (1993). R. Hiller, K. Weninger, S. J. Putterman, B. P. Barber, Science, in press.
12. R. G. Holt, D. F. Gaitan, A. A. Atchley, J. Holzfuss, Phys. Rev. Lett. **72**, 1376 (1994).
13. K. S. Suslick, Science **247**, 1439 (1990). K. S. Suslick, E. B. Flint, M. W. Grinstaff, K. A. Kemper, J. Phys. Chem. **97**, 3098 (1993).
14. K. J. Taylor, P. D. Jarman, Aust. J. Phys. **23**, 319 (1970). P. D. Jarman, J. Acoust. Soc. Am. **32**, 1459 (1960).
15. A. A. Atchley, in *Advances in Nonlinear Acoustics*, H. Hobaek, ed., World Scientific, Singapore (1993), p. 36.
16. A. Prosperetti, L. A. Crum, K. W. Commander, J. Acoust. Soc. Am. **83**, 502 (1988). W. Lauterborn, J. Acoust. Soc. Am. **59**, 283 (1976). R. E. Apfel, J. Acoust. Soc. Am. **69**, 1624 (1981).
17. J. Schwinger, Proc. Natl. Acad. Sci. USA **89**, 1118, 4091 (1992).
18. T. Lepoint, F. Mullie, Ultrasonics Sonochem. **1**, S13 (1994). M. A. Margulis, Ultrasonics **30**, 152 (1992).
19. C. C. Wu, P. H. Roberts, Phys. Rev. Lett. **70**, 3424 (1993).
20. H. P. Greenspan, A. Nadim, Phys. Fluids A **5**, 1065 (1993).
21. A. Nadim, A. D. Pierce, G. V. H. Sandri, J. Acoust. Soc. Am. (Suppl.) **95**, 2938 (1994).
22. R. J. Zanetti, Chem. Eng. **99**, 37 (1992).
23. K. S. Suslick, S. B. Choe, A. A. Cichowlas, M. W. Grinstaff, Nature **353**, 414 (1991).
24. A. J. Walton, G. T. Reynolds, Adv. Phys. **33**, 595 (1984). ■

29 April 1995 No1975 Weekly £1.70

NewScientist

Molecular movies

When planes fall out of the sky

17
9 770262 407060

Bubbles hotter than the Sun

Bubbles hotter than the Sun

Hit water with a blast of sound and tiny bubbles start to glow. This astonishing phenomenon has enormous potential, says *Lawrence A. Crum*

TAKE a jar of water, pass sound waves through it and, hey presto, it gives off light. How can this be? For one thing, visible light has so much more energy than sound waves that to turn sound into light you would have to boost the sound's energy a trillionfold, roughly equivalent to focusing all the sunlight striking the Earth onto about 100 square metres.

It turns out that when sound waves are passed through water, they generate tiny bubbles that are expert at focusing energy. And in the process, these bubbles can reach temperatures that are hotter than the surface of the Sun and pressures tens of thousands of times that of the Earth's atmosphere, opening the way to exotic chemical reactions using astonishingly simple equipment (see Box "Sounding out chemistry"). And researchers now suspect that they may get hotter still—perhaps even hot enough to achieve the elusive nuclear fusion.

Sonoluminescence, the process of turning sound into light, was discovered over 60 years ago, but it was not until 1959 that Erwin Meyer and Heinrich Kuttruff from the University of Göttingen in Germany, discovered that the light came from the collapse of tiny bubbles produced by the sound field, a process called acoustic cavitation.

Concentrated energy

Bubbles can unleash extraordinary amounts of energy when they collapse; for example, if water passes over an obstruction such as a ship's propeller or a turbine blade, bubbles can be generated which, when they collapse, can punch a hole in solid brass or steel. But the concentration of energy needed to turn sound into light is even higher than this.

Sound waves are simply pressure waves alternately compressing and expanding the medium through which they move. Imagine what happens if they pass through liquid. When the pressure drops the liquid effectively boils, forming a bubble that begins to expand, and when the pressure rises again the bubble is forced to collapse. At this stage, the gas inside it is greatly compressed and heated to a very high temperature, and light is emitted.

In 1986, Ken Suslick at the University of Illinois used chemical rate equations to infer that collapsing bubbles in a sound field could reach temperatures of around 5000 K. In 1993, using sophisticated computer models of bubble collapse, Andrea Prosperetti of Johns Hopkins University in Baltimore calculated even higher temperatures of around 7000 K, approximately the temperature of the surface of the Sun, and higher than the temperature of an acetylene torch used to cut hardened steel. Chemists were thrilled at the prospect of such high temperatures from such simple equipment—a jar of liquid and a sound field. Even though the overall temperature of the liquid stays about the same, there are many thousands of tiny gas bubbles that reach temperatures of thousands of degrees, which makes it possible to break apart molecules and produce chemical reactions that would otherwise be very hard in an ordinary laboratory.

Meanwhile, physicists have been trying to understand exactly how sonoluminescence works. One clue comes from the way the light emissions are distributed, sometimes evenly throughout the water, and sometimes concentrated as intense bands of light at certain points. It turns out that these intense bands coincide with the regions where sound is most intense, in the acoustic "standing waves". These are combinations of forward and reverse waves that look like a single stationary wave, and that occur when a wave moving in one direction is reflected back from a boundary.

But whether it is concentrated in the bands or not, the light comes from so many different parts of the liquid that it must involve the collapse of many different bubbles. And any attempt to understand what is really going on in more detail runs up against the problem that this multiple bubble sonoluminescence is just too messy—imagine trying to understand what is happening in a thousand different bubbles, emitting light at different places.

Fortunately, in 1990 Felipe Gaitan, a graduate student at the University of Mississippi

Illustration by Pol Turgeon

As a bubble in a liquid is forced to collapse by a passing sound wave, a shock wave is launched which heats the molecules at the centre of the bubble to enormous temperatures and causes them to give off light

managed to come up with a way out of the messiness when he devised a simple system containing a single "levitated" sonoluminescing bubble. If there is an acoustic standing wave in the middle of the liquid, the forces associated with this standing wave try to move the bubble towards the strongest part of the sound field—that is, towards the middle of the container.

But the bubble is also trying to rise to the surface of the liquid because of its inherent buoyancy. Gaitan tweaked the sound field until the two forces exactly balanced, and levitated the bubble at a fixed position in the liquid. By reducing the amount of gas that was dissolved in the liquid, he could force a single bubble to grow and collapses reaching a bigger size during each successive cycle. Eventually, he found just the right conditions and the bubble glowed like a tiny star.

'The temperatures in the imploded shock wave could still reach 2 million degrees, roughly half of what is needed for fusion'

The discovery of single bubble sonoluminescence (SBSL) made it possible to study sonoluminescence in much more detail than before. By scattering light from a laser beam off the bubble, we watched the violent oscillations, and discovered that, true to our expectations, the light flash was emitted when the bubble imploded. More surprisingly, though, the bubble didn't destroy itself when it collapsed, but reappeared out of the ashes of the implosion.

There were other surprises in store. According to Prosperetti's calculations, the light flash should last about 20 billionths of a second. But in 1991, Seth Putterman and his colleagues at the University of California, Los Angeles, had shown that Prosperetti's predictions were out by a factor of a thousand. They discovered that the light flash lasted for less than 50 trillionths of a second, and the spectrum of the emitted light seemed to show that the temperature inside the bubble was not thousands of degrees, as suggested by Prosperetti, but tens of thousands.

In his calculations, Prosperetti had assumed that when the bubbles collapse, the gas inside is compressed by thousands of times its normal pressure, heating it dramatically. This, he believed, would cause the gas to give off light to shed its newly acquired energy. His calculations and our light-scattering experiments showed that the bubble takes about 20 billionths of a second to collapse, so he assumed that the gas would be heated for the same length of time. But if the hot gas is responsible for the light flash, why should the flash be so much shorter than the time the gas is heated? And why should the temperature be so much hotter than predicted?

One possible explanation is that the inside of the bubble is not heated all at once. Back in 1960, Peter Jarman, an Australian physicist, suggested that a shock wave developed inside the sonoluminescing bubble and that this was responsible for heating the gas. At the time there was no evidence to support this, and Jarman's views were largely ignored. But in the light of Putterman's 1991 experiments and some more recent research by Mike Moran and Willie Moss of the Lawrence Livermore Laboratory in California many physicists began to wonder whether Jarman was right after all.

Two years ago, Cheng Chin Wu and Paul Roberts of UCLA tried to work out what would happen to the gas if a shock wave were created. They assumed that things behave more or less according to Prosperetti's theory until the final stage of collapse. By then, the outside of the bubble could be moving towards the centre faster than the speed of sound, which would launch a shock wave into the centre of the bubble, in much

Sounding out chemistry

NEARLY seventy years ago, Princeton scientist Alfred Loomis first noticed the chemical effects of ultrasound—sound waves whose frequency is too high to be audible to humans. But the field of sonochemistry lay fallow until the 1980s when inexpensive and reliable laboratory generators of high-intensity ultrasound became available.

Sonochemistry occurs because of acoustic cavitation—the formation, growth, and implosive collapse of bubbles in a liquid irradiated with high-intensity sound or ultrasound. The collapse generates intense local heating and extreme pressures, but for very short timespans, typically less than a millionth of a second.

Because the bubbles are tiny, the hot regions that they generate then cool very rapidly, at rates of more than 10^{10} degrees per second—a million times faster than cooling a red-hot metal poker by plunging it into ice water. The immense local temperatures and pressures and the extraordinary heating and cooling rates generated by the collapsing bubble mean that ultrasound is an extremely unusual and potentially very useful method of generating high-energy chemistry.

One of many exciting applications of sonochemistry lies with amorphous metals. If a molten metal alloy can be cooled quickly enough, it can freeze into a solid before it has a chance to crystallise properly. Unlike normal metals or alloys, the resulting amorphous alloys have no crystalline structure on a scale of more than a few hundred atoms. They thus can have unique electronic and magnetic properties, and can also resist corrosion, but are hard to make because the cooling has to be very rapid.

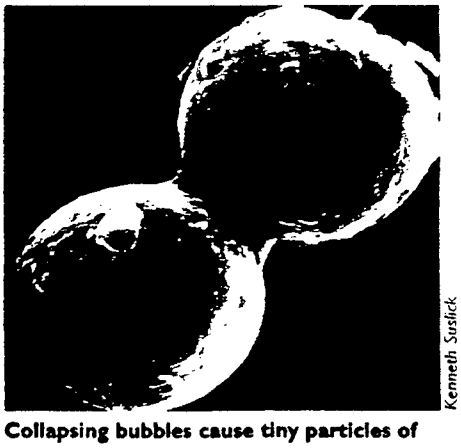

Kenneth Suslick

Collapsing bubbles cause tiny particles of metal powder to crash together and fuse

In 1992, three researchers in my group at the University of Illinois managed to capitalise on the rapid cooling rates that sonochemistry offers. Seok-Burm Choe, Andrzej Cichowlas and Mark Grinstaff used ultrasound to decompose solutions of organometallic compounds and create hot clusters of metal atoms, which amalgamated and cooled very rapidly to form amorphous metal powders made up of nanometre-sized metal clusters.

This means that it may be possible to make unusual materials at low overall temperatures. For example, we used iron pentacarbonyl to produce amorphous iron, which has a very high surface area and is an active catalyst for several important reactions, for example converting carbon monoxide from coal into liquid fuel. And magnetic measurements reveal that the amorphous iron is a very soft ferromagnet—in other words, it quickly forgets its original magnetisation and adopts a new one when a magnetic field is applied. Such materials are excellent for electrical trans-

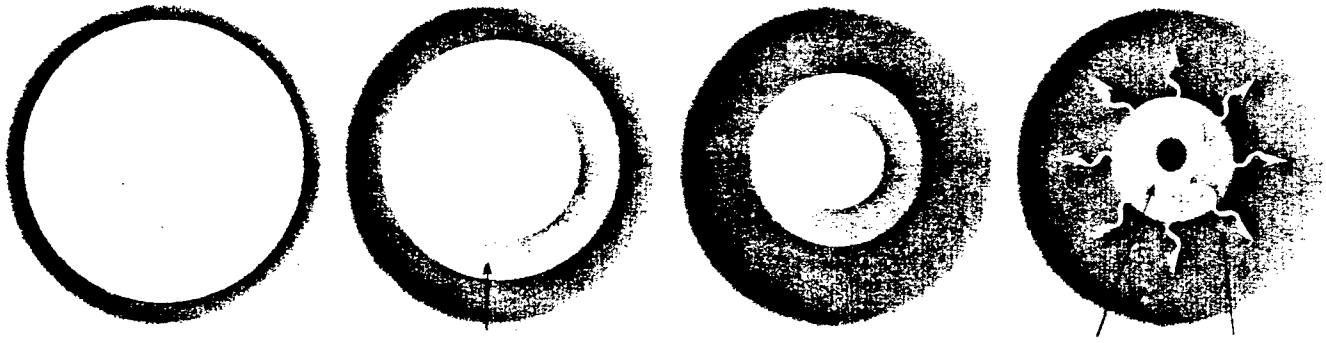

the same way that Concorde's supersonic speeds generate sonic booms. As the molecules in the shock wave all try to arrive at the centre of the bubble at once, they bounce against one another causing the shock wave to rebound. During the implosion, the gas at the centre is heated, but when the shock wave rebounds it allows the gas to expand and cool very rapidly.

Wu and Roberts decided that the gas would therefore be heated for only a very short time, in line with the experimental measurements of the flash duration. They also realised that the energy generated when the bubble collapsed would be distributed over a much smaller volume than had been assumed previously—only the molecules in the very centre would be affected. This would give a higher concentration of energy, and therefore higher temperatures. Wu and Roberts decided that shock waves were the answer, explaining both the rapid flash and the high temperatures seen in experiments.

Noble mystery

Investigations of SBSL have also raised plenty of new questions. For example, in October last year Robert Hiller, from Putterman's group at UCLA, reported in *Science* that the presence of noble gases such as argon, helium or xenon seemed to be crucial for the sonoluminescence. They discovered this almost by accident. When they filled their luminescing bubble with air they saw plenty of light, but when they filled it with nitrogen or oxygen—the two main constituents of air—there was hardly any light. They realised that air contains a small but significant impurity of argon and so they tried adding a small amount of argon to the nitrogen. To their surprise, they discovered that a mixture containing just 0·1 per cent argon boosted the luminosity by a factor of nearly 30. Helium or xenon worked just as well. For now, no one knows why a small amount of a noble gas should produce such a dramatic change.

Meanwhile, the extreme conditions created during sonoluminescence have raised the exciting, albeit highly controversial idea that SBSL could be used to create nuclear fusion. Nuclear fusion is the energy source that drives the Sun and other stars. Deep inside the Sun, where the gravitational force is enormous, the nuclei of deuterium, a heavy isotope of hydrogen, are forced to fuse to form helium nuclei, releasing tremendous amounts of energy in the process. For many years, physicists have been trying to produce controlled fusion on Earth, because hydrogen is so plentiful here that this could provide a virtually unlimited energy source. But although billions of dollars have been spent on fusion research, we are still at least twenty or thirty years from a commercial process.

The main problem is that before fusion can take place the temperatures and pressures must be extremely high, conditions

former cores or magnetic recording heads.

At the other end of the scale, sonochemistry's extreme temperatures could also benefit industries or governments struggling to clean up water sources contaminated by small amounts of halocarbons, pesticides, or other toxic or carcinogenic compounds. Everyone knew that applying ultrasound to aqueous solutions yielded hydrogen and hydrogen peroxide, but Peter Riesz at the US National Institutes of Health recently proved that aqueous sonochemistry also yields the hydroxyl radical, which is an extremely potent oxidising agent normally formed in flames. In other words, the high temperatures of cavitation create flame-like conditions inside the liquid water, breaking the water's hydrogen-oxygen bond and forming the hydroxyl—normally a very difficult feat.

Other researchers have also been hard at work in similar areas. Over at the Hahn-Meitner Institute in Berlin, Arnim Henglein's team has turned up many other similarities between sonochemistry and combustion chemistry, and Michael Hoffmann at the California Institute of Technology is exploring applications for these extremely high-energy chemical reactions for cleaning up contaminated water supplies.

High-intensity ultrasound can be used to increase the speed of reactions at metal surfaces substantially, and this has become an important synthetic technique for many chemical reactions, especially those involving reactive metals such as magnesium, lithium or zinc, which are particularly important for synthesising pharmaceuticals and rare chemicals. This approach was first advocated by Pierre Renaud in France in the 1950s, and has been developed more recently by Jean-Louis Luche at the University of Toulouse.

Chemists are also excited by the shock waves generated when the bubbles collapse. These are like tiny depth charges in the liquid. If they occur in the presence of metal powder, they can smash nearby powder particles together at such high speeds that the particles actually melt at the points where they collide. This was discovered in 1990 by Stephen J. Doktycz and Dominick Casadonte in my group at the University of Illinois. Such collisions can produce striking changes in surface texture, composition, and reactivity of the powders.

Recently, Gareth Price at the University of Bath has been studying how to use sonochemistry to break up polymers dissolved in organic solvents. The polymer chains are split mechanically by shock waves when the solvent is irradiated with ultrasound. Price has used this to synthesise block copolymers, long-chain polymers with two or more different, but linked, parts—like a train made up of passenger cars in front and freight cars at the back. The idea is that block copolymers can combine the useful properties of their constituent parts.

Ultrasound is also useful for synthesising biomaterials, particularly micrometre-sized spheres with shells made from protein molecules that are bonded together sonochemically. Such microspheres are smaller than red blood cells and can be used to carry drugs and medical imaging agents through the bloodstream. One recent example is the use of high-intensity ultrasound by Mike Wong, a student at Illinois, to make long-lived haemoglobin microspheres suspended in water, which could act as a blood substitute to carry oxygen from the lungs to the rest of the body (Technology, 17 December 1994). **Kenneth S. Suslick**

Abstract

The role of the Bjerknes force, which enables an underwater bubble to be levitated acoustically against gravity, was examined for the case of single-bubble sonoluminescence (SBSL). It was found that the analytical expression obtained by Eller [Eller, A., J. Acoustical Soc. America, **43**, 170 (1968)] for the position at which bubbles can be stably levitated was insufficient for describing SBSL bubbles since the theory was based on linear bubble motion. The levitation of bubbles with nonlinear radial oscillations was examined numerically and found to agree with experimental data. The dynamic translational motion of SBSL bubbles was also examined numerically. It was found that in certain circumstances the translation would lead to a shape deformation of the bubble which, upon collapse, would destroy the bubble. The role of temperature in SBSL was also examined for different frequencies and dissolved gas concentrations. Comparisons were made between the bubble's acoustic and electromagnetic radiation. The results of these comparisons suggest that the observed temperature-related effects are related to the interior gas dynamics of the bubble during light emission.

Contents

List of Figures

Chapter 1

Introduction

Sonoluminescence (SL) literally means "light from sound." In practice, it means that a sound field of sufficient intensity applied to a liquid can cause the liquid to emit light – in both the visible and invisible portions of the electromagnetic spectrum. This conversion of mechanical energy to electromagnetic energy can result in an energy density amplification of 10^{12}! The facilitator of this effect is the ubiquitous bubble: the pressure fluctuations in the sound cause small bubbles to expand and then collapse violently, focusing their energy. This chapter will provide a brief overview of single-bubble sonoluminescence, discuss the significance of the work to be presented and, finally, outline the composition of this dissertation.

1.1 Overview of Sonoluminescence

There are two different classes of SL phenomena: multiple-bubble sonoluminescence (MBSL) and single-bubble sonoluminescence (SBSL). As the name implies, MBSL denotes cavitation fields filled with large numbers of bubbles, whereas SBSL involves just one bubble. The observed properties of the two different classes are similar in some ways, yet quite different

in others. The difference in the nature of the light emitted lies primarily in the observed optical spectra. SBSL has very smooth spectra, suggesting temperatures greater than ten-thousand degrees Kelvin [1, 2]. This smoothness is contrasted by the spectra of MBSL, which show many vibrational and rotational transition lines superimposed on a continuum. These discrete spectral lines suggest temperatures of only a few thousand degrees [3, 4]. Crum [5] discusses these differences at length and suggests that the difference is due to the spherical vs. non-spherical bubble collapses expected in SBSL and MBSL, respectively.

1.1.1 History

Evidence of SL was first observed and reported by Marinesco and Trillat [6], who had been studying the effects of ultrasound on the development of photographic emulsions. They attributed latent spots of light on the photographic plates to intense chemical actions caused by the ultrasound. Frenzel and Schultes [7] performed similar experiments and concluded that the anomolous images were due to some light source, possibly cavitation. Soon it was obvious that cavitation was necessary (but not sufficient) for SL.

MBSL is usually so weak that it must be observed with photomultiplier tubes (PMT's) or other similar low-level light detectors. By studying the light emission from cavitation regions with PMT's, it was learned that SL light emission was composed of discrete flashes synchronized with the sound field. Meyer and Kuttruff [8] were able to take a series of photographs of cavitation with SL on the end of a vibrating nickel rod and demonstrate that the SL flashes occurred near the end of the bubbles' collapse.

One of the many difficulties involved in the study of SL produced by a field of bubbles is the number of individual bubbles involved in the process. When some aspect of the SL behavior is investigated, only averaged or group behavior can be measured. In analogy,

this is like trying to learn English by hanging a microphone over New York: much can be learned about the timing of certain holidays, "rush-hour" traffic, etc., but individual behavior remains obscured. In a given cavitation field, there are bubbles of different sizes, all of which respond differently to the driving sound field. This "discord" then affects all aspects of SL behavior, including the fact that the bubbles may not be collapsing in a spherically symmetric manner. Thus, trying to understand SL on a fundamental level is difficult at best in a MBSL context.

1.1.2 Single-Bubble Sonoluminescence

In 1990, Gaitan *et al.* [9] discovered the "hydrogen atom" of SL by generating light in a single bubble acoustically levitated in a standing wave. Then, via Mie-scattering of laser-light from the bubble, they were able to obtain a time-history of the bubble's motion which showed that a single flash of light was emitted each acoustic period when the bubble collapsed. Barber and Putterman [10] studied the techniques used by Gaitan and were able to expand upon those first results by employing time-averaging techniques and improving the physical optics.

Barber *et al.* [11] have studied the pulse length and synchronization of SBSL flashes. They found the pulse-length of the SBSL flashes to be less than 50 picoseconds with the jitter in the time-interval between flashes to be of the same value. This remarkable synchronization is several orders of magnitude better than the electronic oscillator used to generate the sound-field. The reason for this synchronicity is still not understood. More recently, though, Moran, *et al.* [12], found the flash duration to be less than 15 picoseconds through the use of a streak camera.

The role of the kind and quantity of dissolved gas in the water is not clearly understood.

There are several observations that have been made, but a clear explanation for them is lacking. Arakeri [13] has reported that decreasing gas concentrations lead to enhanced light production; Hiller [14] has made similar observations, but has observed that there is a limit to this effect. Arakeri [15] also reports that bubbles in air-saturated water are brighter than that of those with a single gas, except for oxygen-saturated water. Furthermore, Hiller [14] has demonstrated that the addition of as little as 1% of argon to nitrogen-saturated water increases light production nearly 100-fold.

1.1.3 Mechanisms of SL

By far the most successful theory for explaining the emission of light from a collapsing bubble, historically speaking, has been the "Hot-Spot" theory [16, 17]. This theory states that the internal contents of the bubble are adiabatically heated during the final stages of bubble collapse. This heating results in light production; however, from this point, the exact method by which the hot contents are able to emit light is not clearly understood. For example, the discrete spectra in MBSL suggest that the light emission originates from atomic or molecular de-excitation and chemical recombination processes, but then electronic transition lines would be expected to be observed in SBSL, and (so far) they are not.

An obvious explanation for the smoothness of the SBSL spectra is that the light is produced by black-body radiation; however, the measured temperatures (obtained from the spectra), along with the brief emission times, would suggest that black-body radiation may not be a plausible explanation since it requires an equilibrium state. Indeed, Wu and Roberts [18] and Greenspan and Nadim [19] have proposed that imploding shockwaves could heat the contents of the bubble to the point at which the gas ionizes, thus forming a light-emitting plasma. Their calculations have also shown that such a shock wave could also

account for the extremely brief light-emission times. In an interesting extrapolation of the shock-wave theory, Barber *et al.* [20] have shown that with the proper deuterium-tritium mixture of gas inside the bubble, fusion-induced neutron production may be possible.

Another idea that has been proposed for the smoothness of the SBSL spectra is that the light emission is solely due to chemiluminescence of water. In this theory, the light primarily is emitted by H_2O^*, OH^*, $H+OH$ and $H+HO_2$ molecules. Saksena and Nyborg [21] have calculated the rates of various reactions and found that the decay constant for $H+OH$ in a SBSL bubble with a temperature of ten thousand degrees is about one half of a picosecond. However, it should be pointed out that at temperatures of ten thousand degrees, all the molecules would be completely ionized, casting some doubt on the method used in the calculation.

There have been several theories promoting electrical discharges as being the mechanism for light production and chemical behavior inside a SL bubble. Margulis [22], and LePoint and Mullie [23] each have proposed corona discharge theories utilizing the ζ-potential surrounding a bubble. The ζ-potential arises from charge accumulation near the surface of the bubble due to the orientation of water molecules at the bubble's surface. Water is a dipole molecule and the negative end of the dipole points toward the bubble; negative ions in the liquid then are attracted by the outward facing positive ends. Thus, a double layer of charge surrounds all bubbles. As the bubble collapses, instabilities in the surface develop and microbubbles are ejected. According to these theories then, as the microbubbles are ejected, a charge separation occurs leading to large, localized electric fields. These fields can be strong enough to overcome the dielectric strength of the interior of the bubble, resulting in a discharge. It is important to note that the Margulis and LePoint/Mullie theories, although both involve an electrical discharge mechanism, are distinctly separate and different.

More experimental information is necessary to determine which of the theories , if any, is correct. Roy [24], Crum [25], and Cordry and Crum [26] give reviews of both single-bubble and multiple-bubble sonoluminescence.

1.2 Overview of This Research

The research presented here had a two-fold aim: to understand the acoustic levitation of SBSL bubbles and what role levitation might play in the existence of the extinction threshold, and, to explore the effects of temperature and frequency on the light emitted by the bubble.

The extinction threshold presents a barrier to the amount of light that can be produced by a SBSL bubble. The amount of light produced is proportional to the acoustic pressure amplitude of the applied sound field: the higher the amplitude, the more light produced. However, there is a maximum pressure amplitude at which a bubble can be driven. Beyond this pressure, the bubble will simply cease to exist; it is extinguished. Just beyond this maximum pressure amplitude lies the extinction threshold. Once the threshold is crossed, the bubble is apparently destroyed. There is no explanation for this sharply defined threshold. The Bjerknes force is responsible for acoustic levitation and will be linked to the extinction threshold.

Historically, it has been known that the temperature of a solution which is being ensonified has a strong effect on the amount of light, or even the amount of sonochemical product, produced. The relationship is an inverse one: cooler temperatures result in higher yields. This inverse-temperature dependence applies to both MBSL and SBSL. Hiller [1] observed that cooling the water in a levitation cell by twenty degrees could improve light production by a factor of twelve. This temperature dependence remains unexplained.

The two hypothesis presented in this work are as follows:

1. The extinction threshold is caused by the effects of the Bjerknes force,
2. The observed temperature-related effects in SBSL are associated with the changes in vapor pressure of the water with the temperature.

Numerical and experimental techniques were employed in examining the first hypothesis. In treating this hypothesis, the role of the Bjerknes force was examined both from an equilibrium and non-equilibrium point of view. The second hypothesis was explored experimentally and involved the use of the sound radiated by the bubble.

1.3 Overview of This Dissertation

The principal chapters of this dissertation are Chapters 3, 4 and 5, which detail the three different aspects of the research performed. Chapter 3 discusses in detail the nature of the forces which allow a bubble to be levitated and how they change as a bubble enters a state of SBSL. Whereas Chapter 3 treats the levitation effects statically, Chapter 4 treats them dynamically, allowing the bubble to translate as it pulsates radially. Chapter 5 details the results of several experiments examining the role of the temperature, frequency and dissolved gas concentration on the light and sound emitted by a SBSL bubble. Experimental data presented will be represented in graphs as points and theoretical data will be represented by lines.

This chapter, of course, serves as a prelude and introduction to the whole work. Chapter 2 discusses all of the apparatus used in the experiments to be presented in the principal chapters. The final chapter, Chapter 6, provides a brief recapitulation of the experiments and conclusions of each of the principal chapters.

Chapter 2

Apparatus, Calibration and Measurement Techniques

2.1 Introduction

This chapter will present the different apparatus and methods used in the experiments. The chapter is presented in two segments: the first describes the apparatus, and the second, calibration and measurement techniques, including a new way of measuring the equilibrium radius of a SBSL bubble. Most of the technical details of the experiments are presented here.

2.2 General Apparatus

The apparatus used in the experiments will be discussed in several parts: the fluid system, the electronic systems, the light-tight housing, the needle hydrophone, and the levitation cell. The apparatus has been designed so that measurements of the light and sound produced by a SBSL bubble can be measured in addition to its vertical position inside the levitation

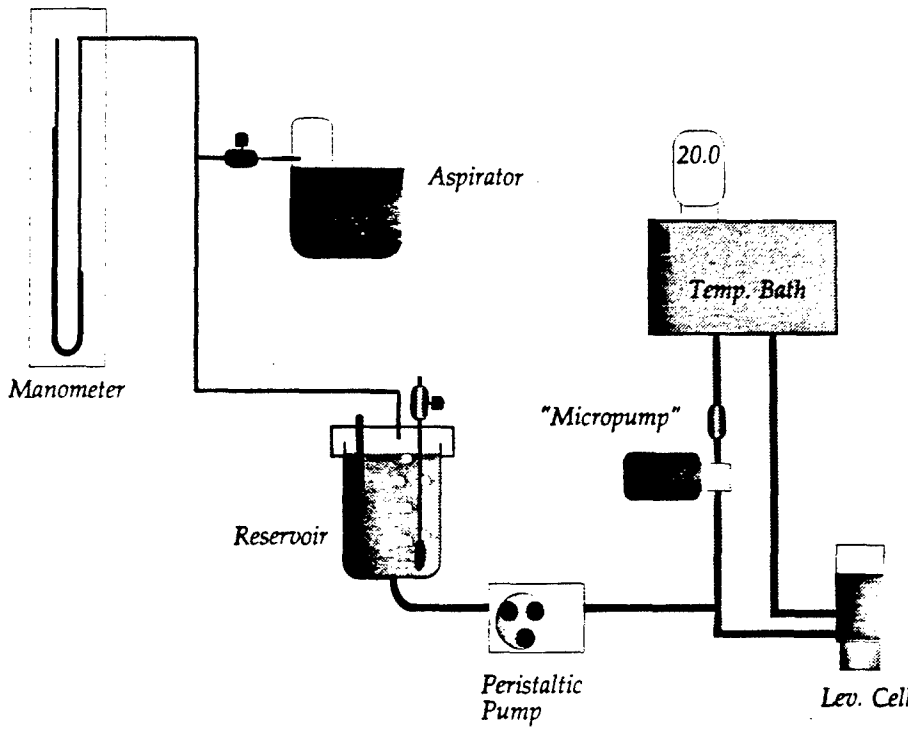

Figure 2.1. Overview of the fluidics layout. The small unlabeled components correspond to filters or valves.

cell. Additionally, the apparatus was designed to perform these measurements over a variety of temperatures and other fluid conditions.

2.2.1 Fluidics

Figure 2.1 shows a general overview of the fluid system. To produce SBSL, the majority of dissolved gas must be removed from the water; the reservoir is the vessel for "degassing" the liquid. Filtered, de-ionized water is placed in the reservoir, then the aspirator is used to reduce the gas pressure inside, a value monitored by the manometer. The degassing process usually required an hour's time.

After degassing, the ambient pressure is restored in the reservoir and the conditioned water is pumped out with a peristaltic pump. The water is pumped into the cell where, after filling – or flushing, it can be recirculated through a temperature bath. The water can be drained from the cell by a tube (not shown) connected to the recirculating circuit.

2.2.2 Electronics

The electronics system is comprised of four different components: the photomultiplier tube system, the hydrophone system, and the bubble and sound generating systems; Figure 2.2 provides an overview. The photomultiplier tube (PMT) system is simply the PMT and the high-voltage power supply required to operate it. The output of the PMT is directed into both the analogue and digital oscilloscopes. Electrolysis was used to generate the bubbles inside the levitation cell by using a DC-voltage source and two platinum wires located within the cell.

The sound generating system is comprised of an electronic oscillator, power amplifier and lead-zirconium-titanate (PZT) ceramic transducer, which acoustically excites the cell. The acoustic pressure generated inside the cell was monitored by a needle hydrophone (described below); the hydrophone was also used to monitor the sonic signature of the SBSL bubbles (also described below). Not shown in Fig. 2.2 is a mechanical switch that would simultaneously open the circuit to the PZT transducer and close that of the bubble generator, and vice versa.

2.2.3 Light-Tight Housing

Figures 2.3 and 2.4 show side and top views, respectively, of the light-tight housing which was constructed. The dimensions of the box are $7.0 \times 11.5 \times 22.0$ inches. It is constructed primarily of $\frac{3}{4}$-inch plywood and has two hinged doors that open at ninety-degrees to each other; the doors can be locked in the closed position with three clamps. The housing is fixed to an optical bread-board along with the x-y-z translator upon which the camera and microscope (described below) are mounted. A mirror is also mounted opposite the camera and microscope so that light from a fiber-optic illuminator can be used to back-light the

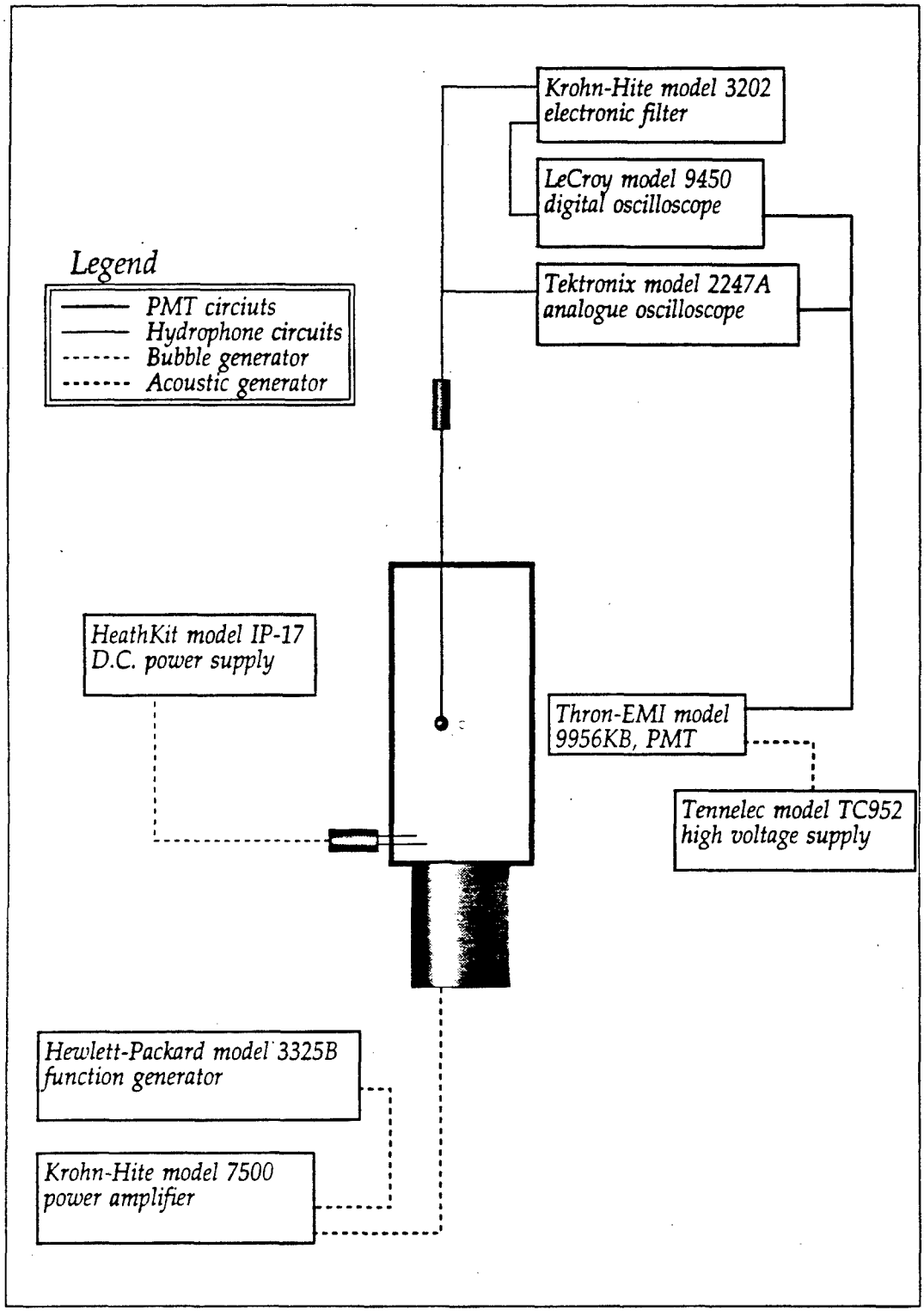

Figure 2.2. Overview of the electronics layout. The four different systems are the PMT circuit, hydrophone circuit, bubble generating system and sound generating system.

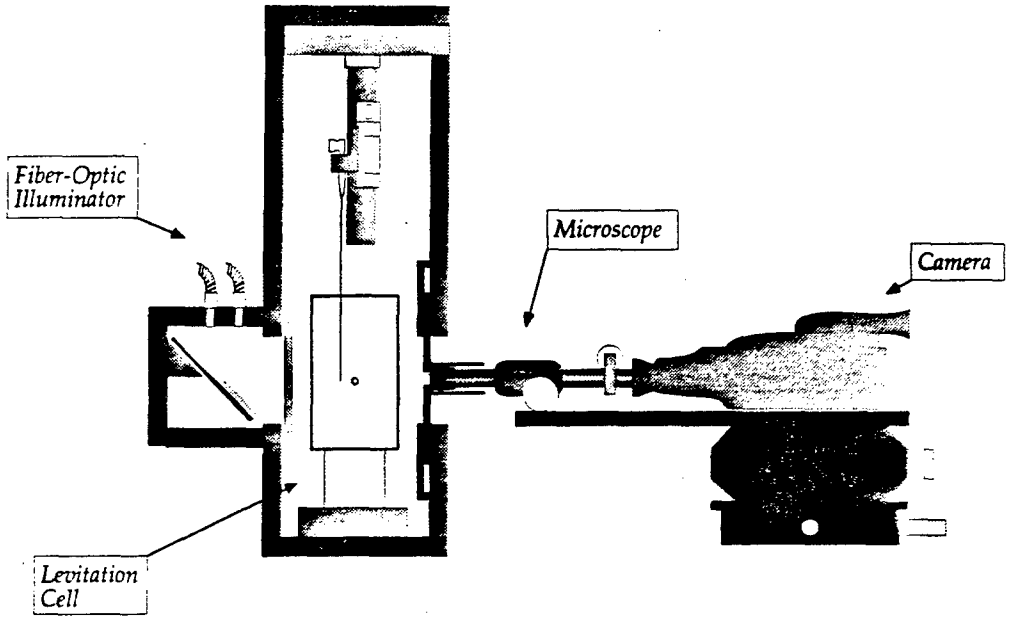

Figure 2.3. Diagram illustrating the light-tight housing used (side view with camera).

bubble.

The light-tight qualities of the housing were determined to be very effective – just a few photons of stray light per second. Two layers of thick, black felt cloth were glued with silicone-sealant to all the contact areas of the doors in order to prevent light-leaks. The PMT rests in a stainless-steel housing attached to the box; this housing has its own shutter. The barrel of the microscope is inserted into a light-tight port which can move in the plane of the housing wall. The port is constructed of black Delrin plastic with an aluminum insertion tube for the microscope barrel; the barrel is held securely inside the tube with 'O'-rings.

2.2.4 Needle Hydrophone

A needle hydrophone was used to monitor the sound field and the sonic signature of SBSL bubbles. It is mounted to an x-y-z positioner attached to the ceiling of the light-tight

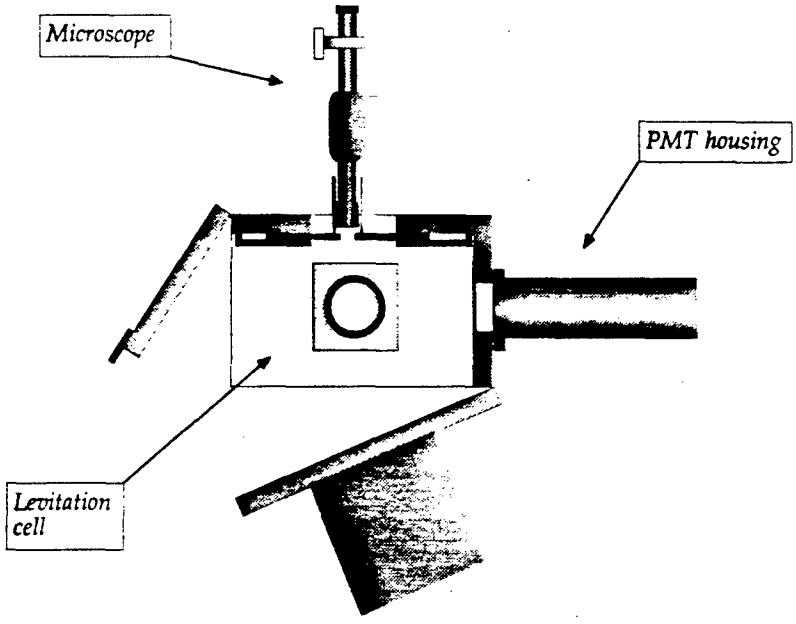

Figure 2.4. Diagram illustrating the light-tight housing used (top view with doors open).

housing. A cartoon illustrating the hydrophone construction is shown in Fig. 2.5: a PZT ceramic cylinder – 0.05 *inch* diameter by 0.05 *inch* long – is epoxied to a 20 *gauge* needle which is epoxied to a BNC cable connector. The inner conductor of the ceramic element is cold-soldered to an insulated wire which connects it to the center-pin of the BNC connector. The ceramic's outer conductor uses the needle to connect it to the BNC connector; a silver painted coating completes the connection. The BNC connector is soldered to the needle. A thin, electrical-insulating coating is applied to the tip; and finally, the tip is covered in silver paint.[1]

The low-frequency calibration of the needle hydrophone is described in detail below in Section 2.3. At 19 kHz the sensitivity of the hydrophone is 708.9 mV/MPa and can vary by approximately 6% with temperature. The high-frequency sensitivity of the needle

[1] Since the outer connection of the BNC connector is grounded, the entire hydrophone is then electrically shielded.

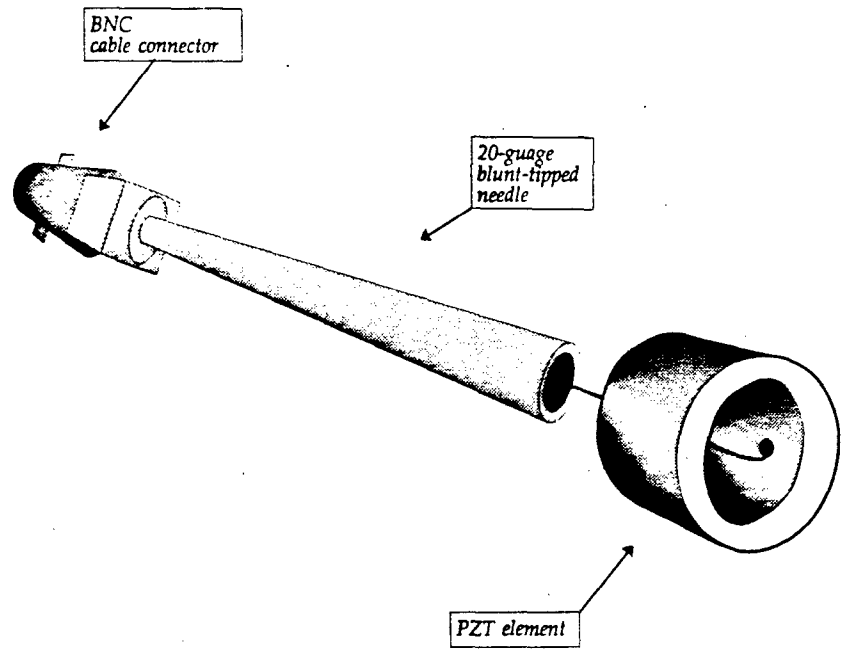

Figure 2.5. Cartoon illustrating construction of the needle hydrophone. The PZT element is epoxied to the end of the needle which is epoxied to the BNC connector. Silver-paint connects the outside of the PZT element to the needle; the inside PZT electrode is connected to the center-pin of the BNC connector via a tiny wire.

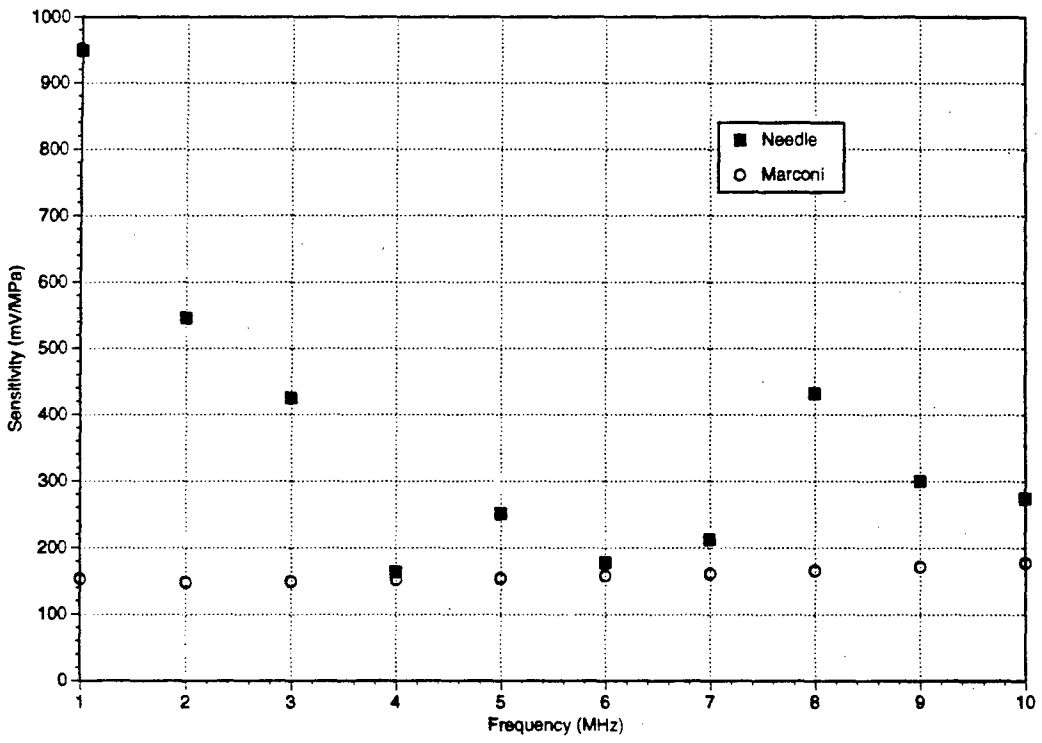

Figure 2.6. Sensitivity of needle hydrophone compared to the calibration of a PVDF-membrane hydrophone.

hydrophone is shown in Fig. 2.6. The hydrophone was calibrated by a substitution calibration using a factory-calibrated Marconi PVDF-membrane[2] hydrophone and two different approaches. The first approach was to use different acoustic sources at a variety of frequencies. The second approach, the results of which are shown here,[3] utilized the non-linear propagation of high-amplitude ultrasound.

A high-amplitude acoustic wave can distort as it propagates [27]. This distortion is the process of shock-wave formation and results in the generation of harmonics of the driving frequency. By driving a sound source at $1 MHz$, one can generate harmonics at 2, 3, $4 MHz$, etc. These different harmonics serve as sound sources for each frequency.

2.2.5 Levitation Cell

A diagram of the acoustic levitation cell used in these experiments is shown in Fig. 2.7. The levitation cell provides the acoustic environment in which the bubbles will be levitated against gravity via the use of an acoustic standing wave.[4] The main part of the cell is a rectangular container made from polycarbonate; it is approximately $16.0 \times 8.5 \times 8.5\, cm$. A PZT-ceramic cylinder has been epoxied to the bottom in order to generate the sound. The first and third eigenmodes of this cell are the most convenient to use since they have pressure antinodes in the center of the cell; the higher, odd eigenmodes were less well-defined.

The cell has fluid inlet and outlet ports so that the fluid can be recirculated through the temperature bath; a thermocouple inserted into the cell is used to monitor the temperature. A pair of platinum wires serves as the electrodes for the electrolysis used in generating the bubbles. Finally, in order to control the dissolved gas concentration in the fluid, the cell

[2] Polyvinylidine flouride

[3] The results of the two approaches were in close agreement, but the sensitivities found in this second method are the actual values used.

[4] The phenomenon is studied in detail in the next chapter.

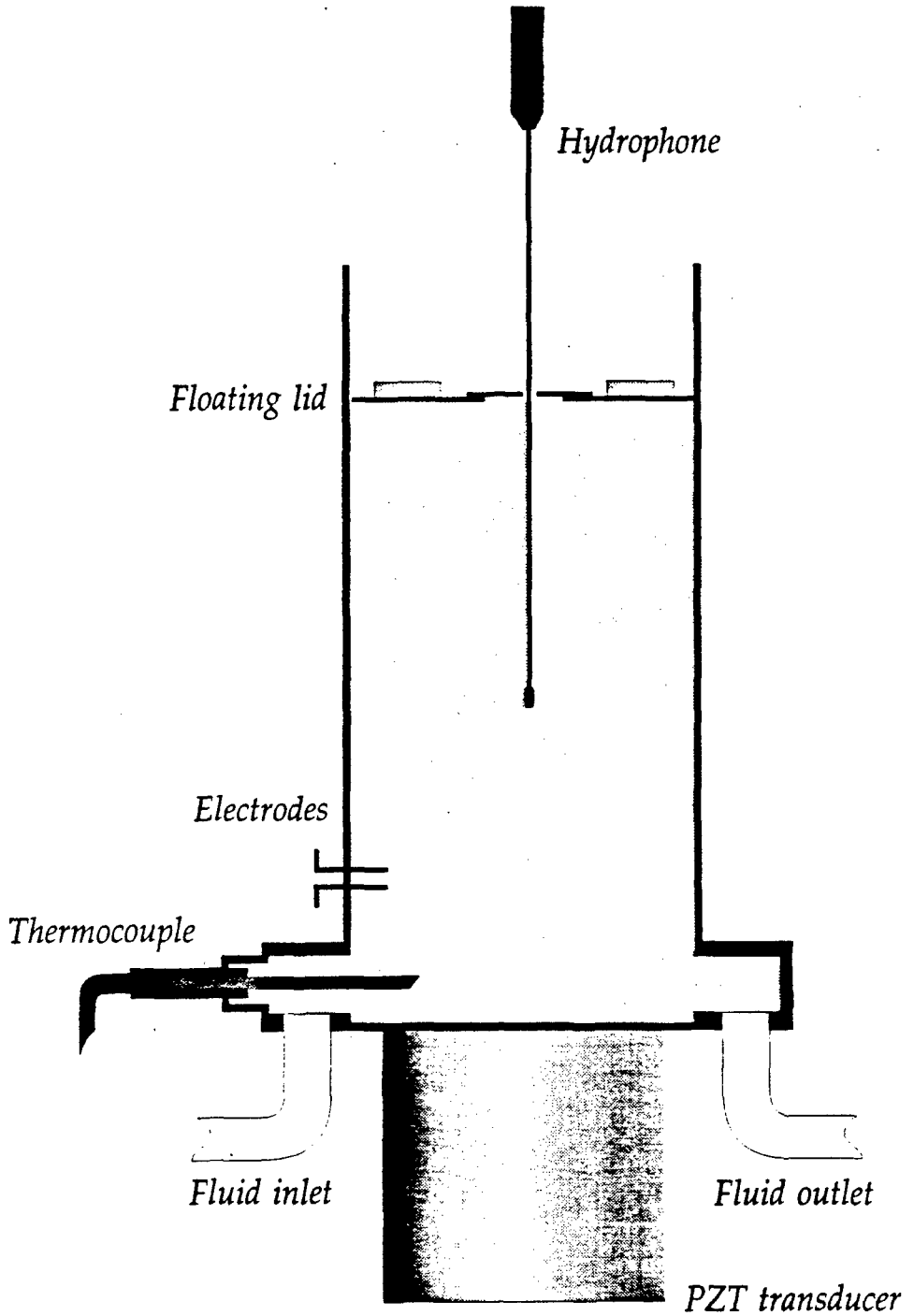

Figure 2.7. Diagram of the levitation cell. See text for details.

has a floating lid. The lid significantly reduces the diffusion of gas from the air into the fluid. In order to position the hydrophone inside the cell, the lid has a movable port – much like the light-tight housing. Since the lid cannot perfectly seal the water against air dissolution, the degree of "contamination" from the outside air must be considered. It was determined that the system was stable for about five to six hours, depending upon the amount of recirculation, a time more than adequate to perform the desired experiments.[5]

2.3 Measuring R_0 and P_A

When conducting research aimed at understanding the nature of SBSL, the two most important quantities to know are the acoustic pressure on the bubble, P_A, and the bubble's equilibrium radius, R_0. These two quantities, however, turn out to be the hardest quantities to measure. In this section, a method developed by this author and used throughout this work will be discussed.

2.3.1 The Sonic Signature of SBSL

One of the original motivations for studying cavitation bubbles was the observation that they could severely damage ship propellers. The large-amplitude pressure fluctuations in the water associated with the rotating propellers can cause tiny bubbles to expand and collapse violently on the surface of the propellers blades. This "cavitation" damage was thought to be caused by a shock-wave radiated by a bubble upon its collapse. Several investigators have studied this phenomenon, particularly Hickling and Plesset [28]. They found that

[5] Although this point was not studied quantitatively, it was noted that experiments were repeatable over this length of time. Furthermore, apparatus was not available for quantifying the dissolved gas concentration.

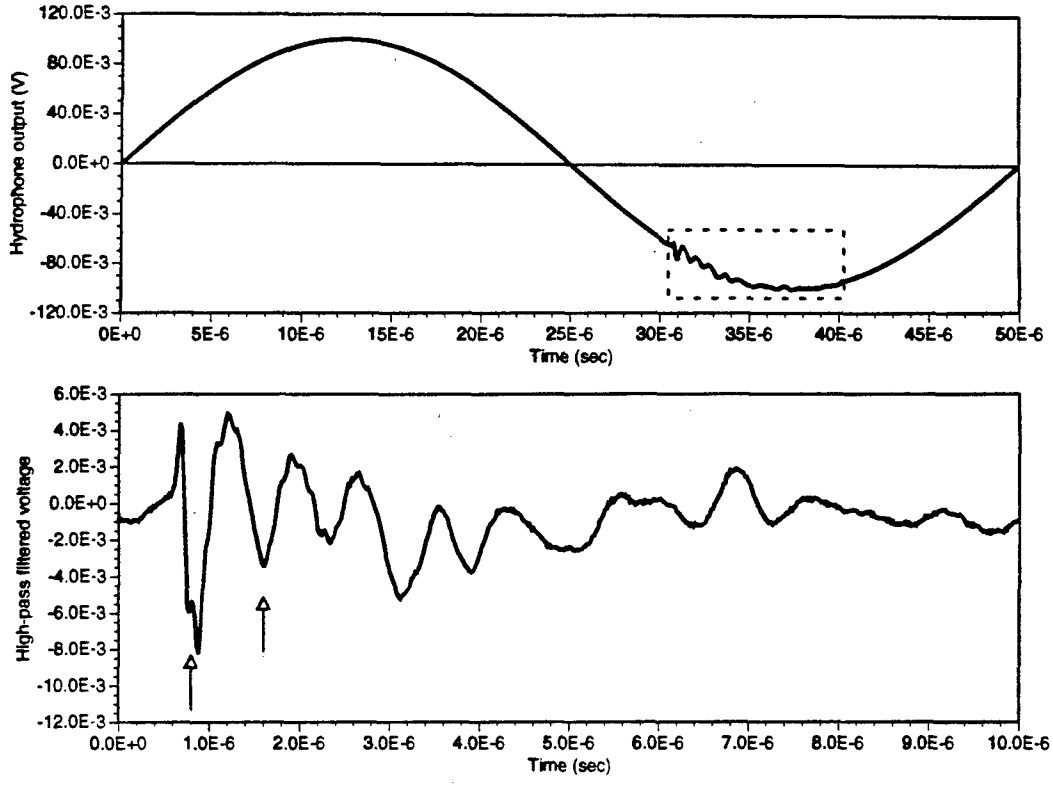

Figure 2.8. The sonic signature of a SBSL bubble. The top plot in this figure is the hydrophone output; the boxed portion is the sonic signature of a SBSL bubble. The bottom trace shows the sonic signature after the signal has been "high-pass" filtered. (Note that the polarity of the hydrophone is reversed.)

inploding – collapsing – cavities generate shock-waves with an amplitude of many *bars*.[6]

The phenomenon of acoustic radiation by bubbles can also be observed in SBSL. If a small hydrophone is placed in the acoustic levitation cell in the presence of a SBSL bubble, a high-frequency noise appears in the hydrophone signal which is not present when the bubble is absent. Upon closer examination, one notices that the "noise" is in fact not random, but identical from one acoustic cycle to the next. If the hydrophone is positioned near the bubble – within about 5 mm, an oscillogram such as the one shown in the upper-half in Fig. 2.8 can be obtained. (The polarity of this hydrophone is such that positive voltages represent negative pressures and vice versa.)

[6] However, it turned out that most cavitation damage is caused by tiny jets of water which penetrate a bubble's interior as it collapses. [29]

The lower-half of Fig. 2.8, which is the hydrophone signal after the low-frequency component has been removed, is referred to as the sonic signature of a SBSL bubble. The characteristic frequency of the sonic signature corresponds to the frequency at which the bubble rings after it collapses. The bubble rings because the collapse shock-excites it – a phenomenon which usually happens when a bubble is formed, *e.g.* rain-drop impacts, bubble splitting, or the emergence of a bubble from a submerged needle. In these examples, the ringing frequency has also been used to size the bubble [30, 31].

The ringing frequency of a shock-excited bubble usually corresponds exactly to the resonance frequency of the bubble. For the case of a SBSL bubble, however, the two frequencies are slightly different; the ringing frequency is higher than the resonance frequency. The reason for this difference is that in the examples mentioned, the bubbles rang in the absence of a high-amplitude acoustic field [32]. SBSL bubbles ring in the presence of a high-amplitude standing wave; the bubble collapses shortly after the acoustic pressure becomes positive.

The linear resonance frequency of a freely oscillating bubble is given by the relation

$$\omega_0 = \frac{1}{R_0}\sqrt{\frac{3\gamma P_0}{\rho}}, \tag{2.1}$$

with R_0, γ, P_0 and ρ being the equilibrium radius, polytropic exponent, ambient pressure and fluid density, respectively. This linear resonance frequency for a typical SBSL bubble is just above $700\,kHz$, much higher than the driving frequency of about $20\,kHz$. Thus, the bubble may ring for several cycles before the $20\,kHz$ sound field can change significantly. The ringing frequency, ω_c, is given approximately by

$$\omega_c = \frac{1}{R_0}\sqrt{\frac{3\gamma(P_0 - P_A sin(\omega t_c))}{\rho}}, \tag{2.2}$$

where t_c is the time of the bubble collapse when the bubble was shock-excited. In Eq. 2.2, the total pressure on the bubble is given by the ambient pressure plus the acoustic pressure.

(The acoustic pressure is defined such that the first half of the acoustic cycle is negative.)

2.3.2 Making the Measurement

The values of t_c and w_c can be measured using a photomultiplier and hydrophone. These values could be used with Eq. 2.2 if the amplitude of the acoustic pressure was known. Fortunately, the values t_c and ω_c depend on the values of both P_A and R_0 and can be used to solve for P_A and R_0 if simulations of radial bubble motion are performed: P_A and R_0 can be used as input parameters and varied until the simulation returns the measured values of t_c and ω_c. There are several good equations of bubble dynamics; Flynn's equation will be used [33, 9]; viz:

$$(1-M)R\ddot{R} + \frac{3}{2}\dot{R}^2(1-M) = \\ (1+M)\left[P_B(R,t) - P_A(\mathbf{r},t) - P_0\right] + \frac{R}{\rho c}(1-M)\frac{dP_B(R,t)}{dt}, \tag{2.3}$$

where R is the instantaneous radius and the dots refer to time-derivatives; $M = \dot{R}/c$, with c being the speed of sound in the liquid. The pressure just outside the bubble, $P_B(R,t)$, is given by

$$P_B(R,t) = P_g(R,t) - 2\sigma/R - 4\mu(\dot{R}/R), \tag{2.4}$$

where μ and σ are the viscosity and surface tension, respectively. The gas pressure, P_g, is given by

$$P_g = (P_0 + 2\sigma/R_0)(R_0/R)^{3\kappa}, \tag{2.5}$$

with κ the polytropic exponent, which varies in value from 1.0 to 1.4 depending upon the equilibrium size of the bubble [34]. Figure 2.9 shows the motion of a bubble whose equilibrium radius is $5\,\mu m$ in a $20\,kHz$ sound field of amplitude $1.5\,bar$; conditions known to result in SBSL behavior. Notice the ringing of the bubble after its collapse; this ringing

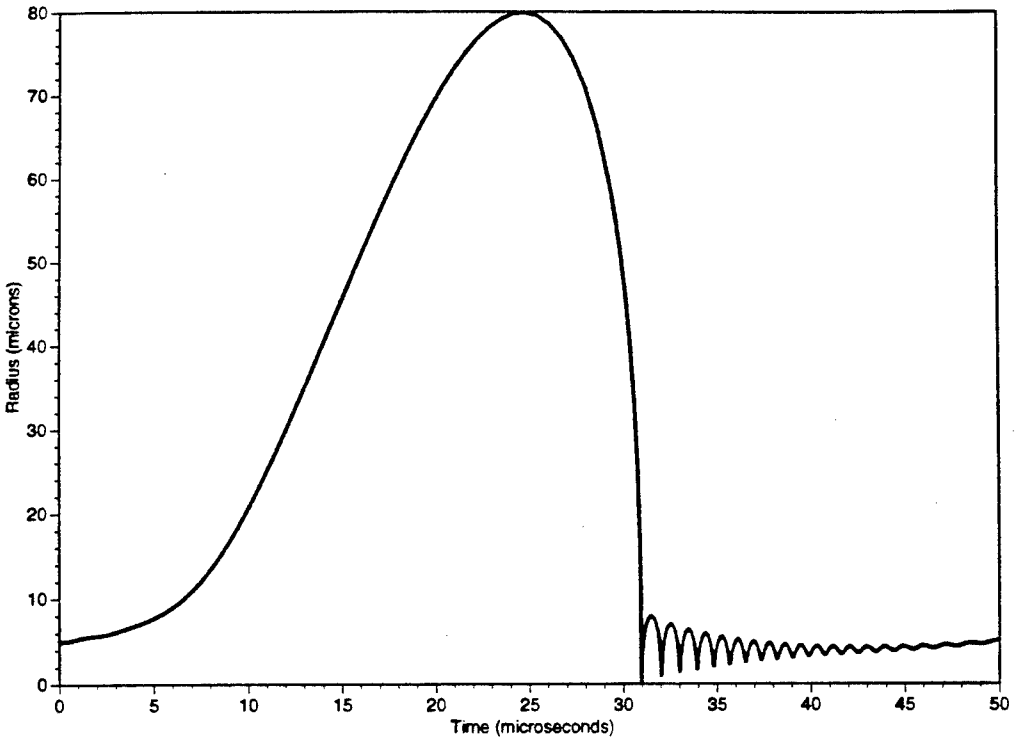

Figure 2.9. Computed radial motion of a $5\mu m$ bubble. This solution to the equation of motion, Eq. 2.3, uses values $f = 20.0\,kHz$ and $|P_A| = 1.5\,bar$

is responsible for the sonic signature. All of the differential equations presented in this dissertation were solved using an adaptive time-step Adams-Moultan routine written in Fortran.

The light from this SBSL-type bubble motion in Fig. 2.9 would be emitted at the time of collapse, t_c, when the bubble's radius is at its minimum. The light-flash will cause the PMT to emit a voltage pulse. The time between this voltage pulse and the maximum in the driving signal can be measured; this value is denoted t_{PMT}. The maximum in the driving signal is exactly a quarter of an acoustic period of the driving frequency, $t_{\frac{1}{4}}$. The time-interval t_c is then given simply as $t_c = t_{\frac{1}{4}} + t_{PMT}$. The measurement is performed on an analogue scope; trial time-interval measurements indicate that such measurements made manually can be performed accurately to within $\pm 1\%$ of the time-base setting.

The arrows in the lower-half of Fig. 2.8 show the measured time-interval which would

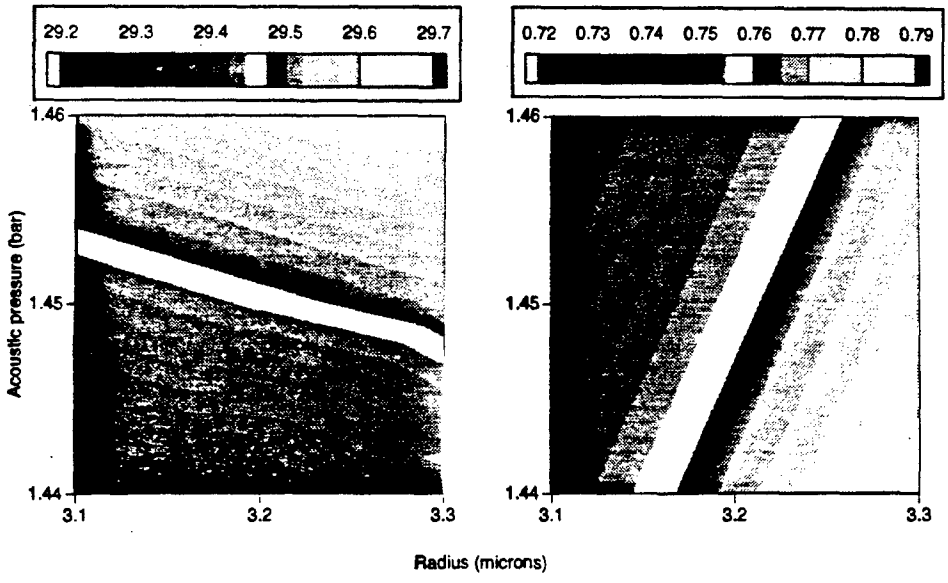

Figure 2.10. Calculated contours showing the variation of t_c and ω_c with R_0 and P_A. For the left figure, the different shades represent the values of the collapse time, t_c. For the right, they represent the periods of different ringing frequencies. See text for details.

be the period of w_c, the ringing frequency; again, the accuracy in this measurement is $\pm 1\%$ of the time-base. The two measurements, t_c and ω_c, are adequate for determining a unique combination of P_A and R_0. The value of t_c increases with both P_A and R_0, but the period of ω_c increases with R_0 and decreases with P_A. These trends in t_c and the period of ω_c are shown in Fig. 2.10. The gradiations in the left half of the figure represent values of t_c, while those of the right represent values of the period of ω_c. The values used in generating Fig. 2.10 are shown in Table 2.3.2.

Measurements of t_c and the period of ω_c have been made for a variety of conditions. These measurements are represented by the blank-strip in each half of Fig. 2.10; the measured value for t_c is 29.46 μsec and that of the period of ω_c is 0.76 μsec. If the two halves of the figure were overlayed, the intersection of the blank strips is the solution, i.e., the appropriate values of R_0 and P_A. The accuracy to which R_0 and P_A can be known

Table 2.1. Table of values used in Fig. 2.10.

Equilibrium Radius (μm)	Acoustic Pressure (bar)	Period of ω_c (μsec)	Collapse Phase t_c (μsec)
3.2	1.45	.757	29.456
	1.44	.767	29.234
	1.46	.747	29.633
3.1	1.45	.735	29.403
	1.44	.745	29.221
	1.46	.725	29.581
3.3	1.45	.779	29.506
	1.44	.789	29.326
	1.46	.768	29.682

is limited by the accuracy of the measurement in t_c and the period of ω_c. An accuracy of $\pm 1\%$ of the time-base in each measurement corresponds to $\pm 0.1\ \mu sec$ for the value t_c and $\pm 0.01\ \mu sec$ for the period of ω_c. From Fig. 2.10, the error in R_0 and P_A is seen to be approximately $\pm .05\ bar$ and $0.05\ \mu m$ for the pressure and equilibrium radius, respectively.

2.4 Measuring Luminosity

The duration of the light flash from a SBSL is quite brief; Barber, *et al.* [11] found the flash-length to be approximately 50 *picoseconds* and more recently, this value has been reduced to 15 *picoseconds* [12]. The flash time is less than the impulse response-time of the PMT, which is about 15 *nanoseconds*. Thus, effectively all the photons emitted by the

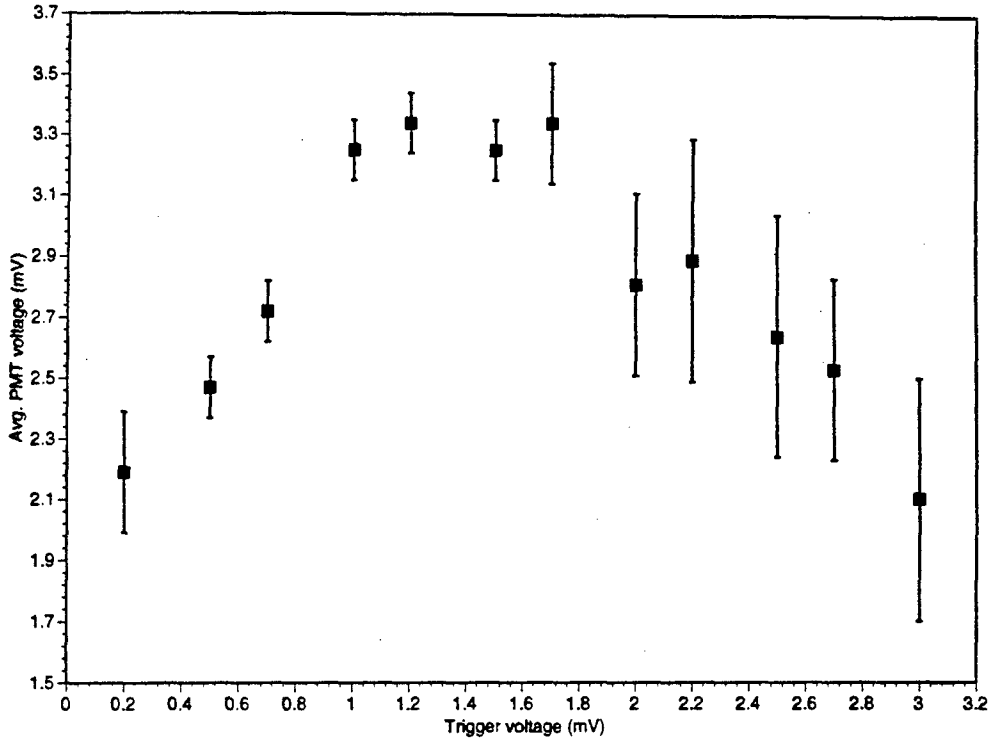

Figure 2.11. The average PMT voltage-pulse as a function of trigger level. The digital oscilloscope was set to trigger on "auto;" in this way the average voltage-pulse is related to the number of events.

bubble enter the PMT simultaneously.

If the PMT responds linearly to the number of simultaneous photons entering it, then counting those incident photons is simply a matter of knowing the response of the PMT to a single photon. Figure 2.11 shows how the voltage-pulse from a single photon event was determined by using a digital oscilloscope. For this figure, the average magnitude of the single-photon voltage-pulse is ploted as a function of the oscilloscope's trigger level when a small amount of light is incident on the PMT. The oscilloscope's triggering was also set to "auto." The "auto" setting is such that the scope will correctly trigger if a valid signal is present, but if there is no valid signal, the scope will trigger freely. In this way, if there were a valid signal, the value of that voltage-pulse would be figured into the average value; if there were no valid signal, a value of zero would be figured into the average value. Thus, Fig. 2.11 has properties similar to a histogram in that the average voltage-pulse value is

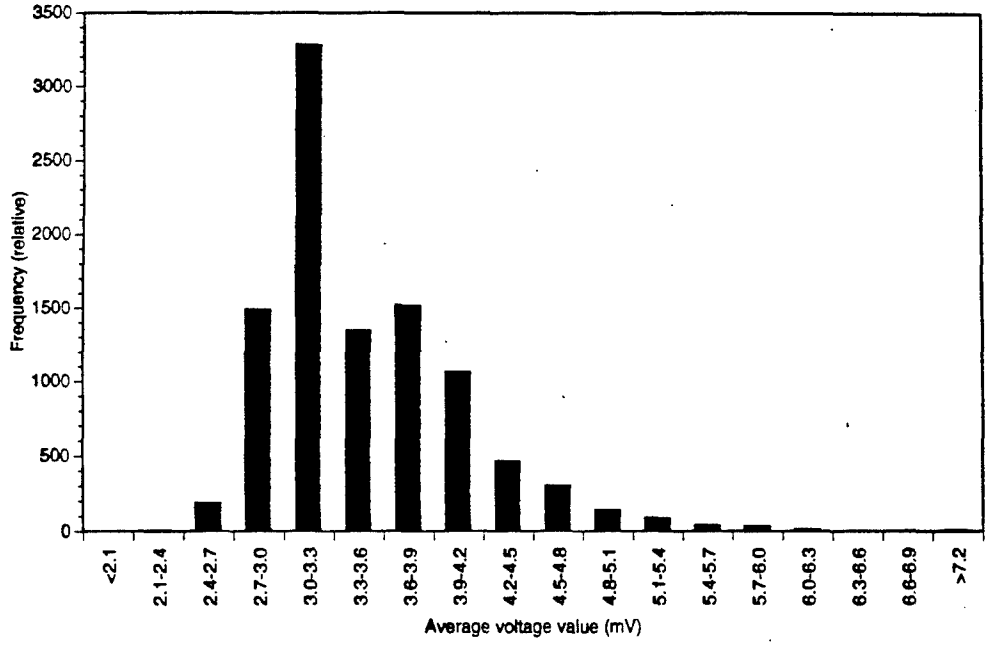

Figure 2.12. The average PMT voltage-pulse histogram.

related to the number of pulses. This figure indicates that the most likely value for voltage pulse from a single photon is about $3.3\,mV$. A more rigorous technique for finding the magnitude of the single-photon voltage involves generating a histogram such as the one shown in Fig. 2.12. To get this histogram, a Macintosh Quadra 650 was used to collect the magnitudes of PMT signal voltages from a LeCroy 9450 digital oscilloscope. These values were then used by a graphing program to generate the histogram. Notice that the most likely voltage pulse is again about $3.3\,mV$.

Once the most probable single-photon voltage was known, it was a simple matter to divide the voltage produced by the PMT by this value to obtain an estimate of the number of photons incident on the photosensitive element. The distance, d, from the PMT photosensitive element to the glowing bubble is approximately $18.0 \pm 1.0\,cm$. The value of d is important since its value is used to correct for the fact that the PMT only collects a small fraction of the total amount of light emitted by the bubble. The total number of photons

emitted by the bubble for a given PMT voltage, V_{PMT} is given by

$$N_{photons} = \frac{V_{PMT} A'}{\epsilon V_{single-photon}}, \tag{2.6}$$

where A' and ϵ correct for the small fraction of photons collected and the quantum efficiency, respectively. The value of A' is given by the ratio $4\,\pi d^2/a$, where a is the area of the photocathode. The error in the value of $N_{photons}$, 10%, is due to the uncertainty in the knowledge of d. Additionally, it should be noted that there may be some systematic error of a few percent in measuring the number of photons due to refraction or reflection inside the cell or light-tight box.

2.5 Measuring Vertical Position

Chapter 3 deals with the vertical equilibrium position of a SBSL bubble in a standing acoustic wave. The experimental data shown in that chapter was obtained using a Gäertner measuring microscope, a Sony Handycam video camera, and a computer with a video digitizing card.

The camera was set to focus at infinity and was aimed through the microscope. The microscope has a spider-silk filar measuring apparatus, which was set at a distance of $100\mu m$ using a calibrated microscope slide. The camera and microscope were mounted together on an x-y-z translating platform and the end of the microscope was inserted into a light-tight, x-z translating portal in the light-tight housing, see Fig. 2.3. Figure 2.13 shows a digitized image of a SBSL bubble as seen through the camera and microscope system. Depending on the "zoom" setting of the camera, the resolution is approximately 2 - 3 μm per pixel. In Fig. 2.13, the bubble has been illuminated from behind so that the outline of the bubble's maximum radius can be seen. The white dot in the center of the bubble is in fact the light

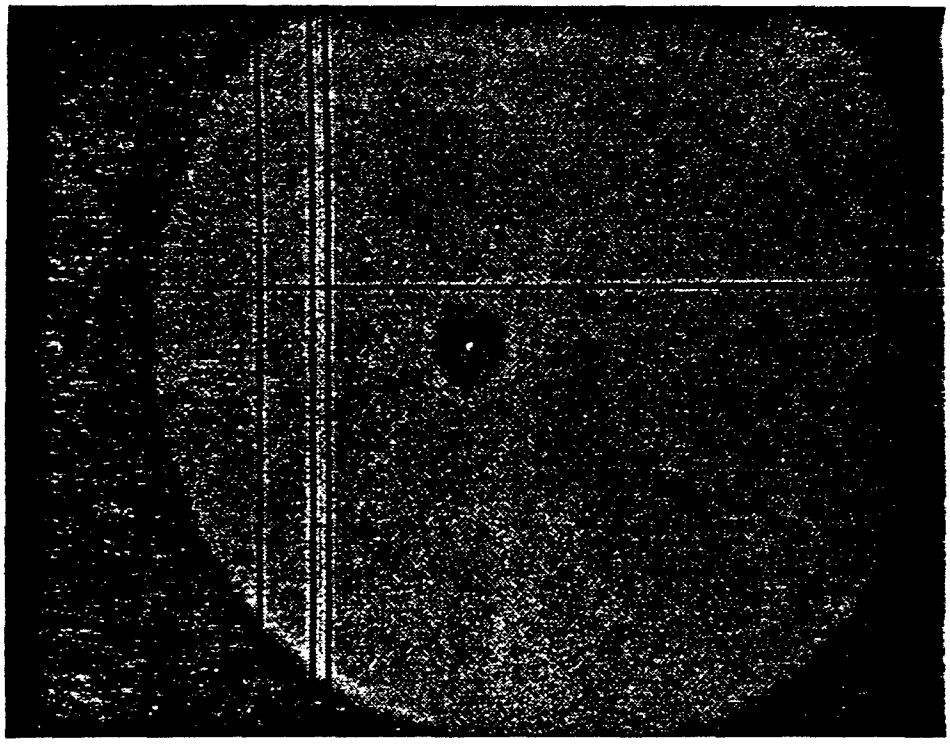

Figure 2.13. The digitized image of a SBSL bubble as seen with a video camera through a microscope. The distance between the single vertical line and inside line of the pair of lines is 101 μm.

emitted by the bubble.

It had originally been hoped that this optical system would be able to resolve the maximum size of the bubble; however, optical diffraction and the rapid motion of the bubble wall produce a bubble image with a poorly-defined edge. Using the procedure described above, simulations utilizing the experimentally-obtained values of R_0 and P_A, indicate a 5 - 6μm discrepancy between the measured value of R_{max} and the calculated one. Even though the maximum radius is difficult to measure, the center of the bubble is simply measured by locating the white dot, which is the light being emitted by the bubble. The accuracy in measuring the center point is estimated to be two pixels.[7] The field of view is approximately $2 \times 2\ mm$, sufficient to capture the full range of the bubble's motion.

[7] For lower values of the acoustic amplitude, the white dot was not easily apparent; however, the center of the bubble could still be located to within approximately three pixels.

2.6 Conclusion

The apparatus and methods described in the this chapter are very versatile and can avail themselves to many different types of experiments. The most important item developed in this chapter is the new method for acquiring the values of R_0 and P_A. The important significance of this new method is its extreme versatility. The traditional method of finding these values has been to use Mie-scattering of laser-light to get a time-history of the bubble's radial motion. The Mie-scattering technique, however, limits the geometry of the levitation cell to transparent cylinders or spheres. The technique described here could be used in a cell of any geometry or even one that was opaque if a fiber-optic cable was used with the PMT. An additional difficulty of Mie-scattering is the fact that it can be rather tedious to get precise data, and positioning of the bubble in the laser-beam is important; problems not present with this new technique. In the next chapter, the nature of the process which allows a SBSL bubble to be acoustically levitated against gravity will be examined in detail.

Chapter 3

Acoustic Levitation of Sonoluminescing Bubbles

3.1 Introduction

Acoustic levitation allows a bubble to be suspended in a sound field in such a way that it is free from the influence of boundaries. It provides a controlled environment for studying bubble dynamics and makes possible the phenomenon of single-bubble sonoluminescence (SBSL). Though SBSL has been known since 1989 [35], a thorough examination of the role of acoustic levitation as it relates to SBSL has been overlooked. This chapter will treat the problem of static levitation of single sonoluminescing bubbles.

Strasberg first reported acoustic levitation of bubbles against gravity in 1959 [36]. The force opposing gravity arises from the interaction between the sound field and the bubble; it is known as the Bjerknes force. Bjerknes forces were first reported by C. A. Bjerknes and his son V. J. K. Bjerknes, after observing bubbles being attracted to one another in the presence of a sound field [37, 38]. (Some researchers had hoped to explain gravity in

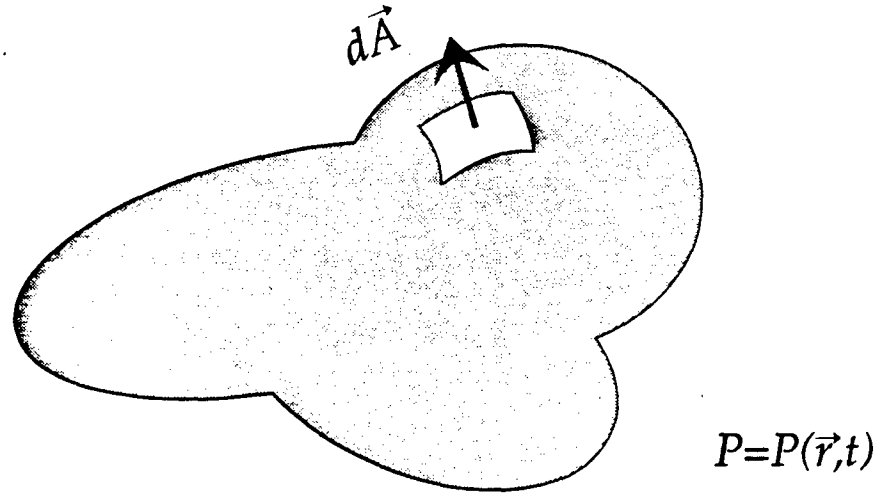

Figure 3.1. Pressure gradients within a sound field are responsible for Bjerknes forces. The force on element $d\mathbf{A}$ is given by Eq. 3.1. The Bjerknes force can be found by integrating the force over the entire surface. .

an analogous way.) Simply put, the Bjerknes force is the force exerted upon an oscillating body because of the existence of acoustic pressure gradients in a fluid: a dynamic buoyancy.

To understand how a pressure gradient can result in a force, consider Fig. 3.1 which shows an arbitrarily shaped object in a pressure field. The differential force, $d\mathbf{F}$, on an area element, $d\mathbf{A}$, due to an external pressure is given by

$$d\mathbf{F} = -P(\mathbf{r},t)\,d\mathbf{A}. \tag{3.1}$$

(Notice that the direction of $d\mathbf{A}$ is away from the surface while the force acts against the surface, hence the minus sign.) To get the total force, the differential force is integrated over the entire surface of the object:

$$\mathbf{F} = \int d\mathbf{F} = -\int_{Surf.} P(\mathbf{r},t)\,d\mathbf{A}. \tag{3.2}$$

Stoke's law can be invoked to transform the surface integral to a volume integral:

$$\mathbf{F} = -\int_{Volume} \nabla P(\mathbf{r},t)\, dV. \tag{3.3}$$

The wavelength is very long compared to the size of the object. Thus, the pressure gradient can be treated as a constant and removed from inside the integral, which, upon integrating, simply yields the volume. Therefore, the total force – that is, the Bjerknes force – is expressed as

$$\mathbf{F}_{Bj} = -V(t)\, \nabla P_A(\mathbf{r},t), \tag{3.4}$$

where $V(t)$ is the instantaneous volume of the bubble and $P_A(\mathbf{r},t)$ is the acoustic pressure.

3.2 The Linear Problem

Eller [39] formulated a simple and elegant way to describe mathematically how the Bjerknes force from a standing acoustic wave could levitate a bubble against gravity. He assumed that the bubble's volume responded linearly to changes in the acoustic pressure. By equating the Bjerknes force and the buoyancy force, he then was able to obtain an expression for the vertical equilibrium position, z_{eq}, of the levitated bubble. Before rederiving his results here, a qualitative look at the behavior of the Bjerknes force is useful.

Figure 3.2 represents the physical situation of a small[1] bubble in a standing acoustic plane wave. The pressure field is described by

$$P_A(z,t) = -|P_A|\, sin\, \omega t\, cos\, kz. \tag{3.5}$$

$|P_A|$ represents the magnitude of the acoustic pressure at the antinode; ω, the cyclic frequency of the sound field; and $k = 2\pi/\lambda$, is the vertical [2] wave number. For convenience,

[1] "Small," as it is used here, means a bubble which pulsates in phase with the sound field.
[2] The vertical, or z-axis, direction is the direction in which gravity is acting.

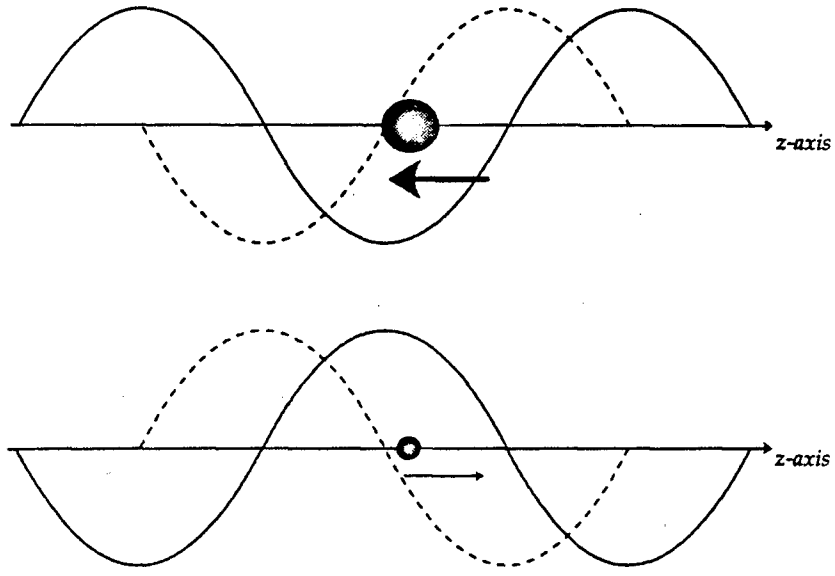

Figure 3.2. Illustration of the Bjerknes force on a bubble in a standing wave. The solid line represents the acoustic pressure, the dashed line the acoustic pressure gradient. The top half represents a time during the first half of the acoustic cycle when the bubble is directed toward the antinode, while the bottom half represents a time one half of an acoustic period later when the bubble is directed away from the antinode.

the acoustic pressure is defined in such away that it is negative during the first half of the sound cycle. During this first half, the bubble expands due to the negative pressure (solid curve). The product of the bubble's volume and the pressure gradient (dashed line) results in a Bjerknes force (large arrow) directed toward the antinode. While the top half of Fig. 3.2 illustrates the first half of the acoustic cycle, the bottom half illustrates the second half of the cycle: positive acoustic pressure compresses the bubble and the resulting Bjerknes force (small arrow) directs the bubble away from the antinode.

Figure 3.3 shows the *instantaneous* Bjerknes force on a $5\,\mu m$ bubble[3] in a $20.0\,kHz$ sound field for one period of motion. $|P_A|$ is $0.2\,bar$ and the vertical wavelength is $9.73\,cm$. When the Bjerknes force is negative, the bubble is directed toward the antinode. When

[3] The phrase "a $5\,\mu m$ bubble" means that the resting, or equilibrium, radius of the bubble is $5\,\mu m$.

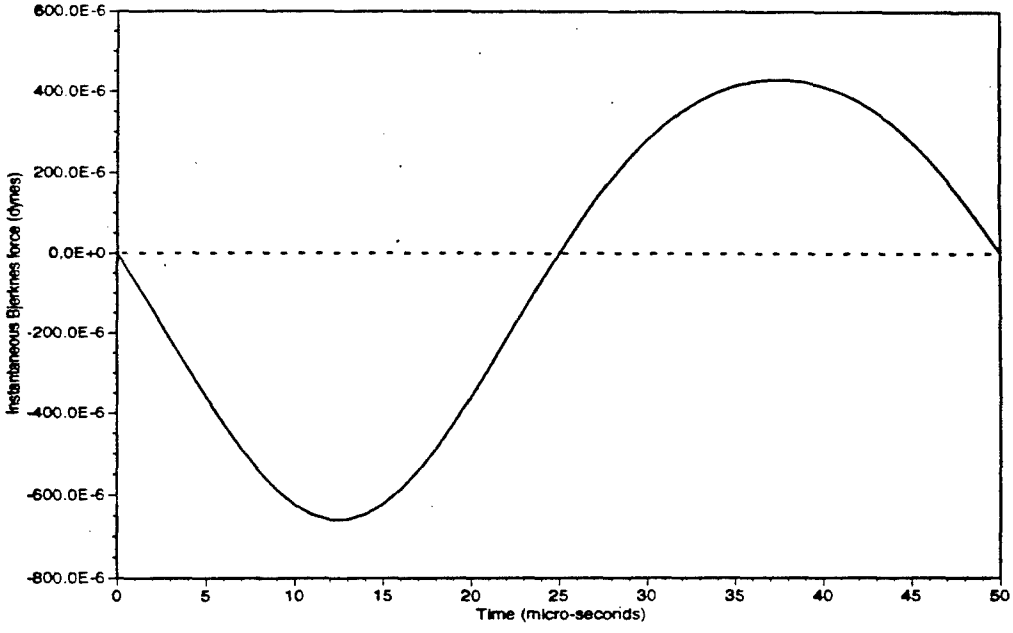

Figure 3.3. The instantaneous Bjerknes force on a 25 μm bubble. The volume of the bubble is larger during the first half of the acoustic cycle than it is during the latter half. Note that the negative and positive values of the force do not balance. ($f = 20.0\,kHz$ and $|P_A| = 0.2\,bar$)

positive, the Bjerknes force directs the bubble away from the antinode. The total force can be obtained by integrating the instantaneous force. Because the volume is always greater during the first half of the acoustic cycle than the second half, the magnitude of the force is greater during former than the latter. Thus, the net Bjerknes force will be negative, forcing the bubble toward the antinode. Notice in Fig. 3.3 that during the first half of the acoustic cycle, the magnitude of the Bjerknes force is more than 600 $\mu dynes$, but it is only about 450 $\mu dynes$ during the second half of the cycle.

The gradient of the pressure field of Eq. 3.5 is given simply as

$$\nabla P_A(z,t) = k\,|P_A| sin\,\omega t\; sin\,kz. \tag{3.6}$$

In Eller's derivation, the bubble is assumed to behave as $R(t) = R_0(1 + \alpha\; sin\,\omega t)$ with α

given by

$$\alpha = -\frac{|P_A| \cos kz}{\rho R_0^2(\omega^2 - \omega_0^2)}, \tag{3.7}$$

and a linear resonance frequency given by the relation $R_0^2\omega_0^2 = 3\kappa P_0/\rho$ [39, 32], where ρ is the density of the fluid, P_0, the ambient pressure and κ is the polytropic exponent, which is related to the thermal damping inside the bubble. R_0 is the equilibrium radius of the bubble. With the specification that α be small, the time dependent volume becomes $V(t) = \frac{4}{3}R_0^3(1 + 3\alpha \sin wt)$. In order to find the equilibrium condition under which a bubble can be successfully levitated against gravity, the time-averaged Bjerknes force, $\mathbf{F}_{Bj}$, must be equal in magnitude to that of the time-averaged buoyancy force, $\mathbf{F}_b$. This equilibrium condition is expressed mathematically as

$$\frac{1}{T}\int_0^T |\mathbf{F}_{Bj}|\, dt = \frac{1}{T}\int_0^T |\mathbf{F}_b|\, dt. \tag{3.8}$$

T is the period of the sound field. Using expressions for the Bjerknes and buoyancy forces, Eq. 3.8 becomes

$$k|P_A|sin(kz_{eq})\int_0^T V(t)\, \sin\omega t\, dt = \rho g \int_0^T V(t)\, dt, \tag{3.9}$$

where g is the acceleration due to gravity. Inserting the time dependent volume yields

$$k|P_A|sin(kz_{eq})\int_0^T (1 + 3\alpha\, sin\,\omega t)\, \sin\omega t\, dt = \rho g \int_0^T (1 + 3\alpha\, sin\,\omega t)\, dt. \tag{3.10}$$

It should be noted that the phase relationship between the time-dependent volume and the sound field is very important, although for the linear case, the relationship is trivial. Evaluating Eq. 3.10 gives

$$k\,|P_A|\, sin\, kz_{eq}\frac{3\alpha}{2} = \rho g. \tag{3.11}$$

Using the expression for α and the relation for the resonance frequency, Eller's solution relating $|P_A|$ to z_{eq} is obtained:

$$|P_A|^2 = \frac{4\rho g}{k}\frac{\gamma P_0}{sin\, 4kz_{eq}}(1 - \frac{\omega^2}{\omega_0^2}). \tag{3.12}$$

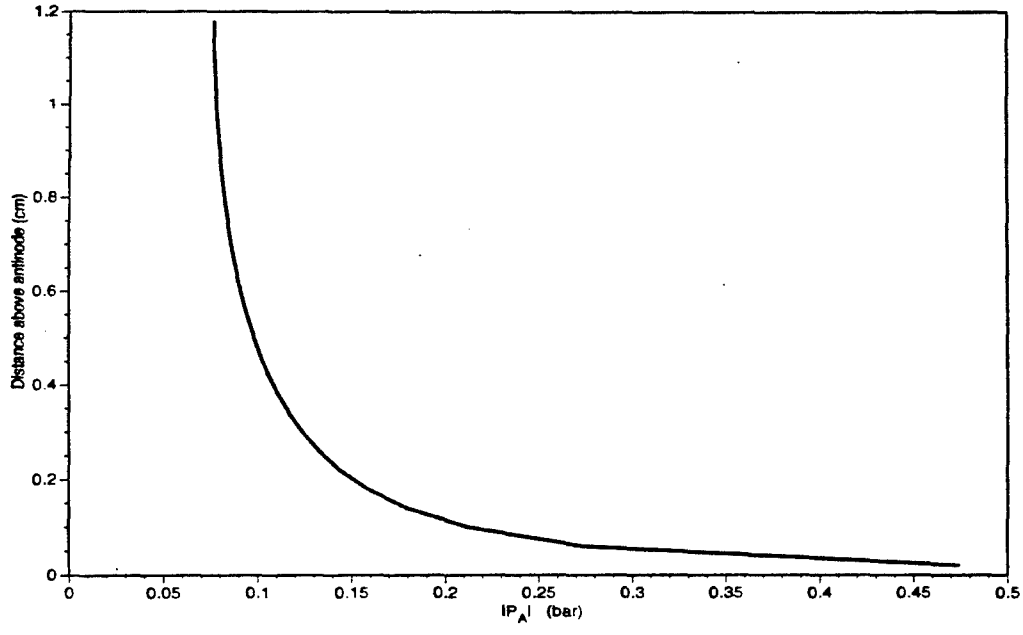

Figure 3.4. The vertical equilibrium position, v_{eq}, for a $25\,\mu m$ bubble as calculated from Eq. 3.12. Note the asymptotic behavior of the curve as $|P_A|$ increases and the bubble approaches the pressure antinode. ($f = 20\,kHz$, $\lambda = 9.73\,cm$)

For bubbles whose resonance frequency, ω_0, is much larger than ω, the parenthetical term of Eq. 3.12 is approximately one. Bubbles large enough that $\omega > \omega_0$ will oscillate "out-of-phase" with the sound field[4] and the final term of Eq. 3.12 is negative. The only real solution then for Eq. 3.12 is one such that $sin\,4kz_{eq}$ is negative. This solution implies that these large bubbles are suspended just above pressure nodes rather than above pressure antinodes. For further information on levitating bubbles larger than resonance size, see Ref. [40].

Figure 3.4 shows values of z_{eq} for a $25\,\mu m$ bubble in a $20\,kHz$ sound field with a vertical wavelength of $9.73\,cm$. Note in Eq. 3.12 that as z_{eq} decreases, $|P_A|$ increases. This asymptotic behavior can be seen in Fig. 3.4. Incidentally, by knowing how z_{eq} behaves with $|P_A|$, one can in fact use acoustic levitation of bubbles for the calibration of small

[4] These "large" bubbles are usually described as being "larger than resonance size."

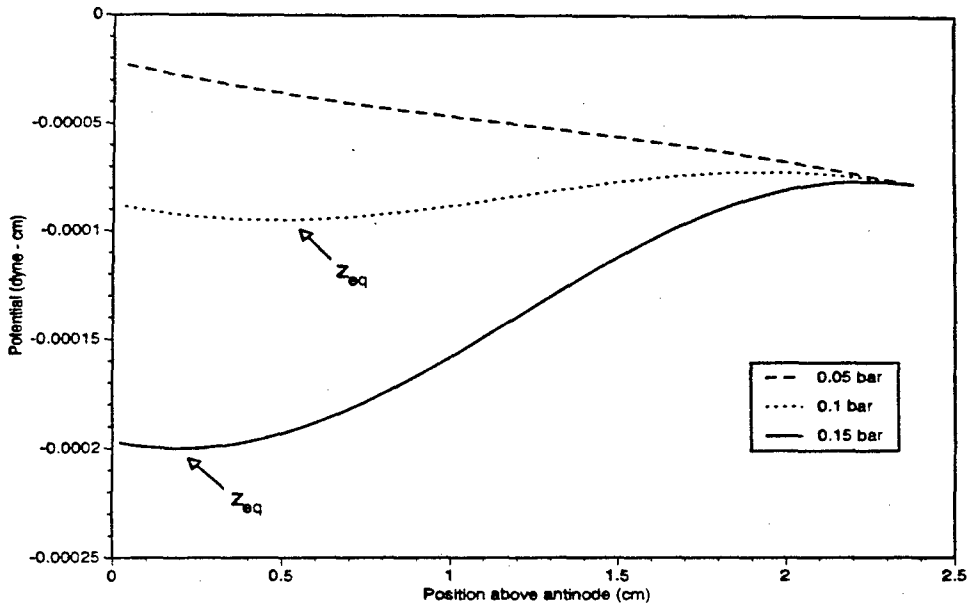

Figure 3.5. Time averaged potential energy for the net Bjerknes force on the bubble in Fig. 3.4. The two lower curves have stability wells corresponding to values of z_{eq}, yet the upper curve does not; the lack of a stability well implies that there is a minimum trapping pressure. ($P_A = 0.05$, 0.01 and $0.15\,bar$)

hydrophones [41].

In general, a force can be expressed as

$$\mathbf{F} = -\nabla U, \tag{3.13}$$

where U is the potential energy of the system. U_{Bj} for the Bjerknes force is given by

$$U_{Bj} = P_A(\mathbf{r}, t)V(t) - \rho g z V(t). \tag{3.14}$$

The time-averaged potentials for three values of $|P_A|$ are shown in Fig. 3.5. Notice that the curve corresponding to $|P_A| = 0.05\,bar$ does not have a "stability well." Between $|P_A| = 0.05$ and $|P_A| = 0.1\,bar$ lies the minimum acoustic pressure necessary to trap the bubble. The locations of the stability wells correspond to values of z_{eq}. Also, the potential wells deepen and shift closer to the antinode for pressures above the minimum trapping pressure.

Incidentally, there are expressions more complicated than Eq. 3.12 describing the force on a body in an acoustic wave. Various authors include King [42], Gorkov [43], Marston [44] and Löfstedt and Putterman [45]. One of the more notable and oft quoted results is that of Yosioka and Kawasima [46]. There has, however, been some discrepancy between the predicted results of Yosioka and Kawasima and those of Eller. Lee and Wang [47] have recently investigated this discrepancy and found that with the correction of a small mistake in Yosioka and Kawasima's result, the two results are in agreement for bubbles.

3.3 The Nonlinear Problem

For small values of P_A, such as that used in Fig. 3.3, the linear approximation for $R(t)$ used in obtaining Eller's result describes the bubble's behavior fairly well; however, for higher amplitude sound fields, e.g. those used for SBSL, the bubble's radial motion must be found numerically – by solving a differential equation of motion for the bubble wall. There are several equations that can be used; Flynn's equation will be used here [33, 9]:

$$(1-M)R\ddot{R}+\frac{3}{2}\dot{R}^2(1-M)= \\ (1+M)\left[P_B(R,t)-P_A(\mathbf{r},t)-P_0\right]+\frac{R}{\rho c}(1-M)\frac{dP_B(R,t)}{dt}. \qquad (3.15)$$

For Eq. 3.15, R is the instantaneous radius and the dots refer to time-derivatives; $M=\dot{R}/c$, with c being the speed of sound in the liquid. The pressure just outside the bubble, $P_B(R,t)$, is given by

$$P_B(R,t)=P_g(R,t)-2\sigma/R-4\mu(\dot{R}/R), \qquad (3.16)$$

where μ and σ are the viscosity and surface tension, respectively. The gas pressure, P_g, is given by

$$P_g=(P_0+2\sigma/R_0)(R_0/R)^{3\kappa}. \qquad (3.17)$$

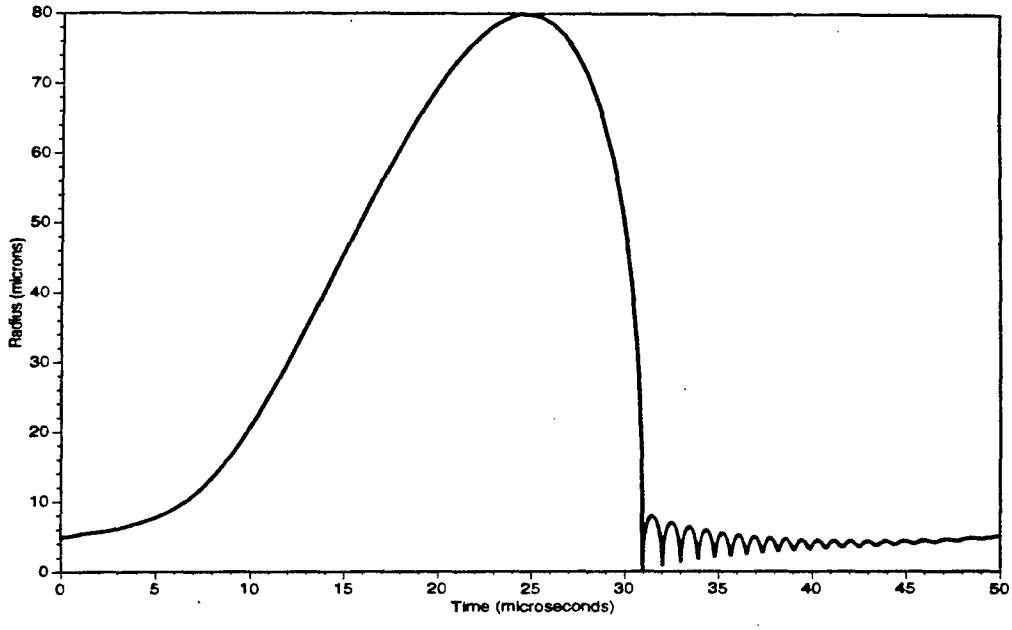

Figure 3.6. Radial motion of a $5\,\mu m$ bubble. ($f = 20.0\,kHz$ and $|P_A| = 1.5\,bar$)

The polytropic exponent, κ, varies in value from 1.0 to 1.4, depending upon the equilibrium size of the bubble [34].

Figure 3.6 shows an R-t (Radius-time) curve for a bubble oscillating in a highly nonlinear fashion. The equilibrium radius is $5.0\mu m$, the frequency, $20.0kHz$, and $P_A = 1.5atm$ – values consistent with conditions for single bubble sonoluminescence. (The behavior of the bubble in Fig. 3.6 would obviously be poorly modeled by a simple harmonic approximation.)

3.3.1 The General Case

To calculate the Bjerknes force in general, the time-dependent volume must be known, which entails calculating $R(t)$ from Eq. 3.15 for a given set of parameters. The instantaneous Bjerknes force for a bubble behaving as in Fig. 3.6 is shown in Fig. 3.7 for three values of P_A. Two primary features can be seen in Fig. 3.7. First, the amplitude of the force is several orders of magnitude larger than that illustrated in Fig. 3.3 for the linear case. The

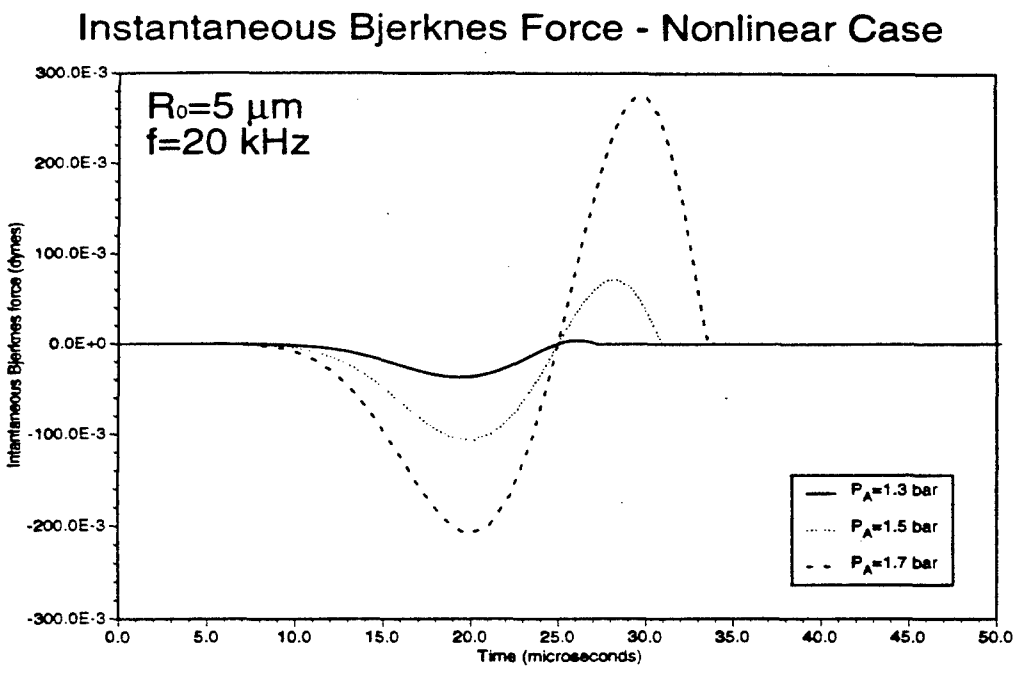

Figure 3.7. Instantaneous Bjerknes force on a 5 μm bubble, $f = 20.0\,kHz$ and $|P_A| = 1.3$, 1.5 and 1.7 bar. As $|P_A|$ increases, the net Bjerknes force shifts from being almost entirely negative to having strong components in both directions.

second is that as P_A increases, the imbalance between positive and negative forces begins to shift. Indeed, for values of P_A greater than about 1.76 bar, the net Bjerknes force is positive and the bubble is forced away from the antinode.

It is important to understand completely the trend seen in Fig. 3.7. Figure 3.8 shows R-t curves for a 5 μm bubble with $P_A = 1.3, 1.5$, and 1.7 bar: the bubble expands to a maximum radius, then rapidly collapses and "rings." Due to the inertia of the growth, the collapse of the bubble occurs during the positive phase of the sound field. Recall that it is during the positive phase of the acoustic cycle that the Bjerknes force directs the bubble away from the antinode. It is the fact that the bubble is still in an inflated stage during the second half of the acoustic cycle that shifts the imbalance of the Bjerknes force: the trend seen in Fig. 3.7. As P_A is increased, the collapse of the bubble is delayed further in time, thus shifting the imbalance even more. Figure 3.9 shows the net Bjerknes force on a 5.0 μm

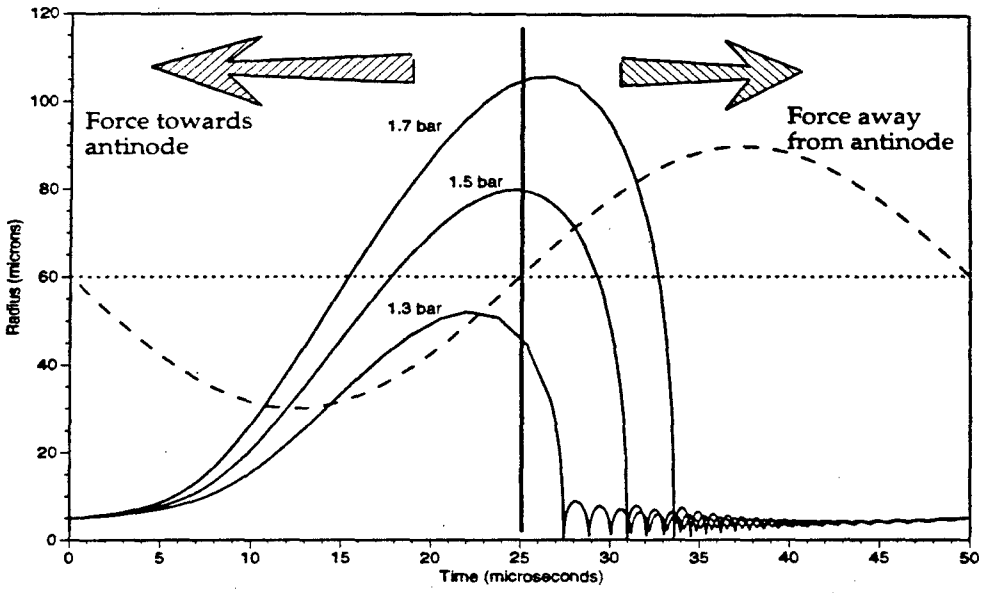

Figure 3.8. Explanation of the trend seen in Fig. 3.7. As the $|P_A|$ increases, the collapse point is delayed in time, extending the expanded phase of the bubble's motion into the second half of the acoustic cycle – when the Bjerknes force is positive. (Dashed line illustrates the time-varying pressure.)

bubble as a function of P_A, illustrating this cumulative effect.

The shifting imbalance of the Bjerknes force is the result of the phase relationship between the sound field and motion of the bubble. The buoyancy force, however, has no such phase dependence. Thus, unlike the net Bjerknes force, the buoyancy force increases monotonically with P_A. In order to find z_{eq}, Eq. 3.9 must be numerically integrated. Fig. 3.10 shows z_{eq} as a function of $|P_A|$. Eller's equation predicts that z_{eq} approach the antinode asymptotically, yet the non-linear case diverges from this behavior.

The solid curve in Fig. 3.10 shows an important implication of the divergent behavior of the non-linear case. The solid curve represents the acoustic pressure amplitude at the location of the bubble, in other words $|P_A| cos\, kz_{eq}$. If P_A is greater than a critical value of approximately $1.76\, bar$, then the net Bjerknes force is positive. This fact implies that for acoustic pressure amplitudes at the antinode, $|P_A|$, exceeding $1.76\, bar$, the vertical

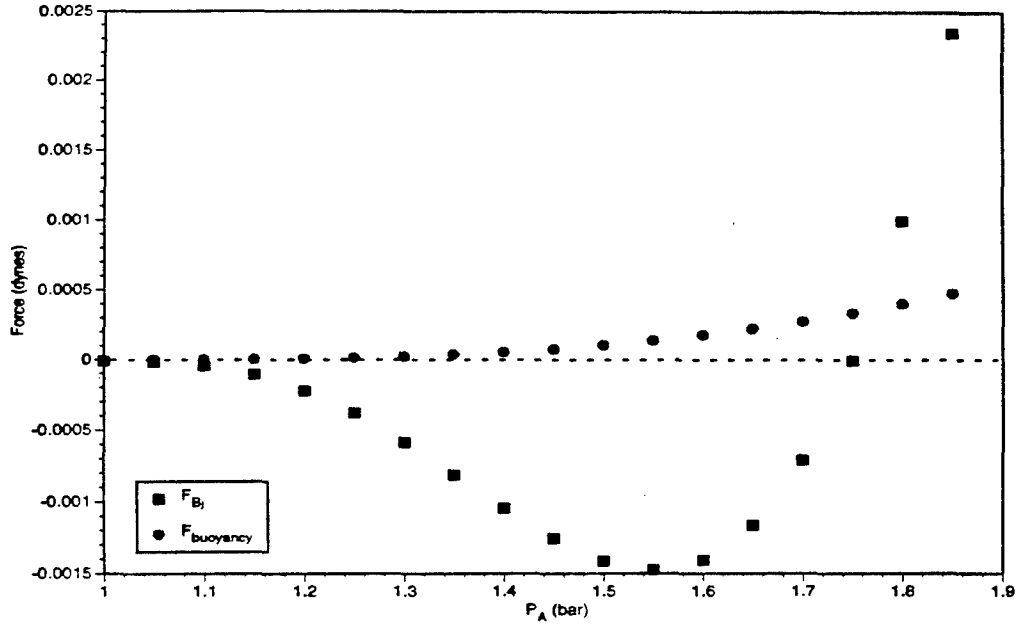

Figure 3.9. The net Bjerknes and buoyancy forces on a bubble as a function of P_A. The magnitude of both increases with acoustic pressure until the acoustic pressure exceeds $1.55\,bar$. At that point, the buoyancy force continues to increase monotonically, but the slope of the Bjerknes force changes sign. ($R_0 = 5.0\,\mu m$, $z = 0.1\,cm$ and $f = 20.0\,kHz$)

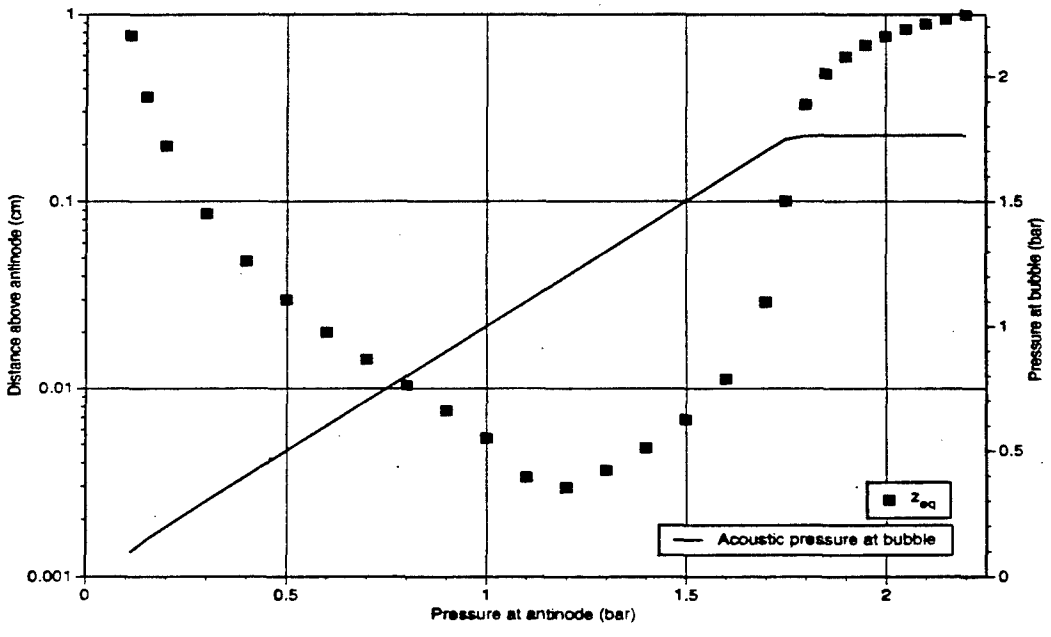

Figure 3.10. The vertical equilibrium position, z_{eq}, for a $5\,\mu m$ bubble as a function of $|P_A|$. The left axis corresponds to values of z_{eq}, while the right axis, that of the solid line, which represents the acoustic pressure amplitude at the location of the bubble. ($f = 20kHz$)

equilibrium position, z_{eq}, must be such a value that P_A is less than the critical value. Thus, there is an intrinsic limit on the acoustic pressure amplitude that can be used to excite a bubble in a state of SBSL.

3.3.2 Bubbles Near the Antinode

For regions near the antinode such that $cos\, kz \approx 1$, the amplitude of the acoustic pressure is constant. A simple and useful result can then be obtained for z_{eq} by starting with Eq. 3.9:

$$k|P_A|\, sin\, kz_{eq} \int_0^T V(t)\, sin\, \omega t\, dt \;=\; \rho g \int_0^T V(t)\, dt.$$

The R.H.S. contains an integral which will be denoted by $\mathcal{V}$; it is similar to the time-averaged volume. The L.H.S. contains a similar integral – a modulated time-averaged volume, $\mathcal{V}'$. Using this notation and the relation that $sin\, kz \approx kz$, Eq. 3.9 can be rewritten as

$$k^2 z_{eq}\, |P_A| \mathcal{V}' = \rho g \mathcal{V}. \tag{3.18}$$

The variable ξ can then be defined as $\xi = \mathcal{V}/\mathcal{V}'$[5]. This further simplifies the expression to

$$|P_A| = \frac{\rho g}{k^2\, z_{eq}} \xi. \tag{3.19}$$

Equation 3.19 is a useful equation because ξ is constant in the region near the antinode for a given value of $|P_A|$. Once the value of ξ is obtained, z_{eq} can be known for a variety of wavelengths. The values for z_{eq} shown in Fig. 3.10 were obtained by calculating Eq. 3.9 for different values of z_{eq} and $|P_A|$ until the equality was true – a computationally intensive process requiring many iterations. With Eq. 3.19, the process is greatly simplified since the iterative element has been removed. Also, the effect of the wavelength can be seen. That effect is to scale the values of z_{eq} with λ^2. Hence, z_{eq} is sensitive to the wavelength.

[5] Note that the values of $\mathcal{V}$, $\mathcal{V}'$, and hence ξ, depend on $|P_A|$ and R_0.

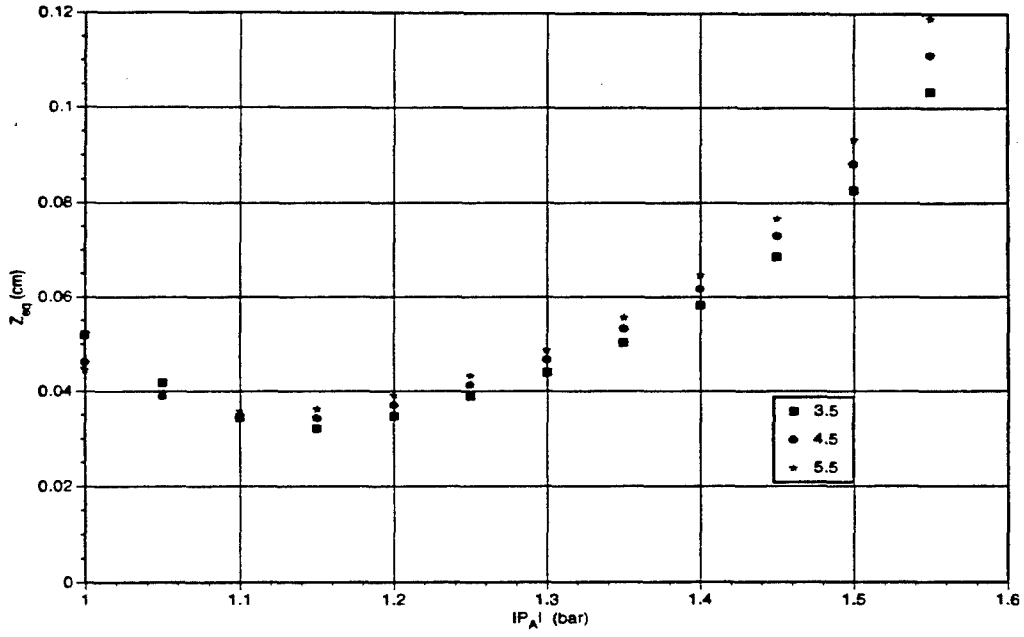

Figure 3.11. The vertical equilibrium position for three different sized bubbles. The vertical equilibrium position, z_{eq}, was calculated using Eq. 3.19 after having numerically obtained values for ξ, the ratio of the time-averaged and modulated time-averaged volumes. Values are shown for $R_0 = 3.5, 4.5$ and $5.5\mu m$. ($f = 20kHz$ and $\lambda = 3.5 \times 9.73cm$)

Figure 3.11 shows how z_{eq} varies for three different bubble sizes. It can be seen from this figure that the dependence on R_0 is weak. (Note that the wavelength is different in this figure than in Fig. 3.10; the reason for this choice will be discussed in the next section.) It is instructional to look briefly at the variation of $\mathcal{V}$ and $\mathcal{V}'$ with $|P_A|$. Figure 3.12 shows the divergent behavior of the two quantities. For the linear case, values of $\mathcal{V}'$ would not "plateau."

It is of interest to examine the potential energy of the levitated bubble for the non-linear case, as was done for the linear case. The instantaneous potential energy is given in Eq. 3.14 as:

$$U_{Bj} = P_A(\mathbf{r}, t)V(t) - \rho g z V(t).$$

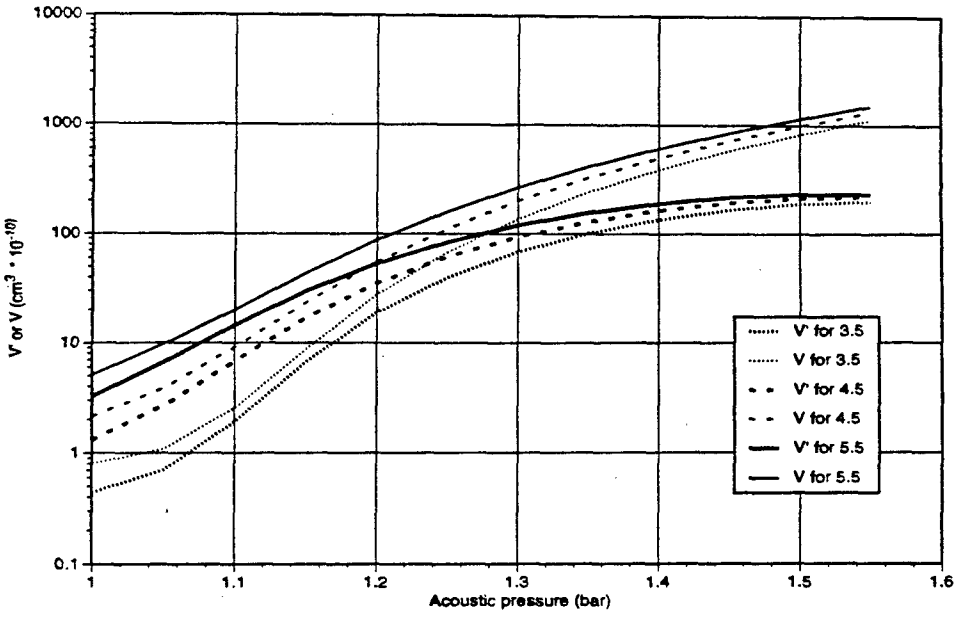

Figure 3.12. The time-averaged volume, $\mathcal{V}$, and modified time-average volume, $\mathcal{V}'$, for Fig. 3.11. The divergent behavior is clearly seen here. Note that the pressure at which the distance of closest approach occurs in Fig. 3.11 corresponds to approximately the same pressure at which the divergence begins.

If this equation is time-averaged, it becomes

$$\int_o^T U_{Bj}\,dt = \int_o^T P_A(\mathbf{r},t)V(t)\,dt - \rho g z \int_o^T V(t)\,dt, \tag{3.20}$$

the values of $\mathcal{V}$ and $\mathcal{V}'$ can be utilized. Figure 3.13 shows the time-averaged potential energy for a $3.5\,\mu m$ bubble in a $20\,kHz$ sound field. There are three different values of $|P_A|$ shown. Notice that the location of the stability point varies in location and depth with $|P_A|$.

It would be useful to put several graphs of the type shown in Fig. 3.13 together into a single three-dimensional surface. However, the large variation in the potential with $|P_A|$ would obscure the variation of that with position. In order to high-light the variation with position, the following procedure was employed: the graphs shown in Fig. 3.13 represent potentials for constant values of $|P_A|$. Each of these "slices" is then normalized to its own average. The normalized slices are then assembled into the surface shown in Fig. 3.14.

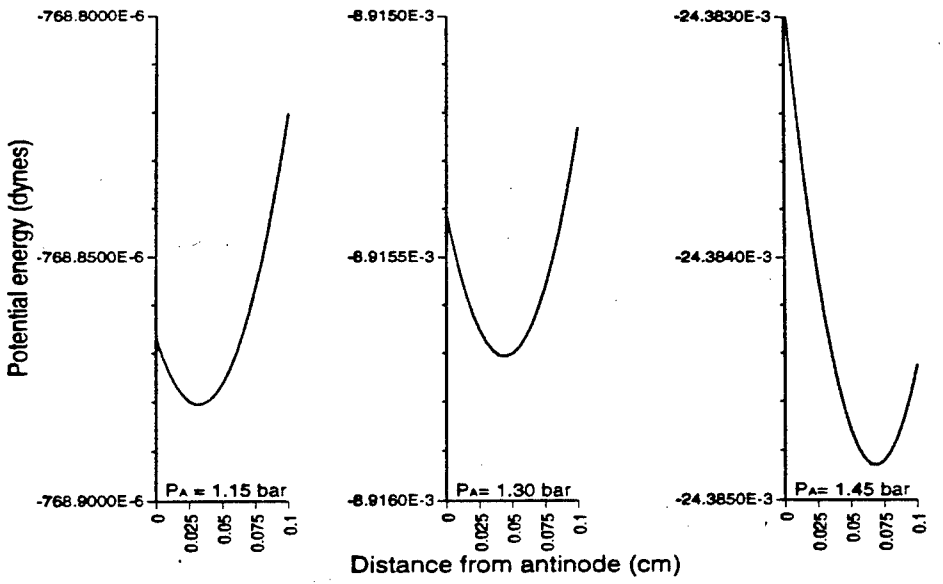

Figure 3.13. The time-averaged potential energy for 3 different values of $|P_A|$ as calculated from Eq. 3.20. Both the depth and location of the stability point for each of these graphs varies with $|P_A|$. ($R_0 = 3.5\,\mu m$ and $f = 20\,kHz$)

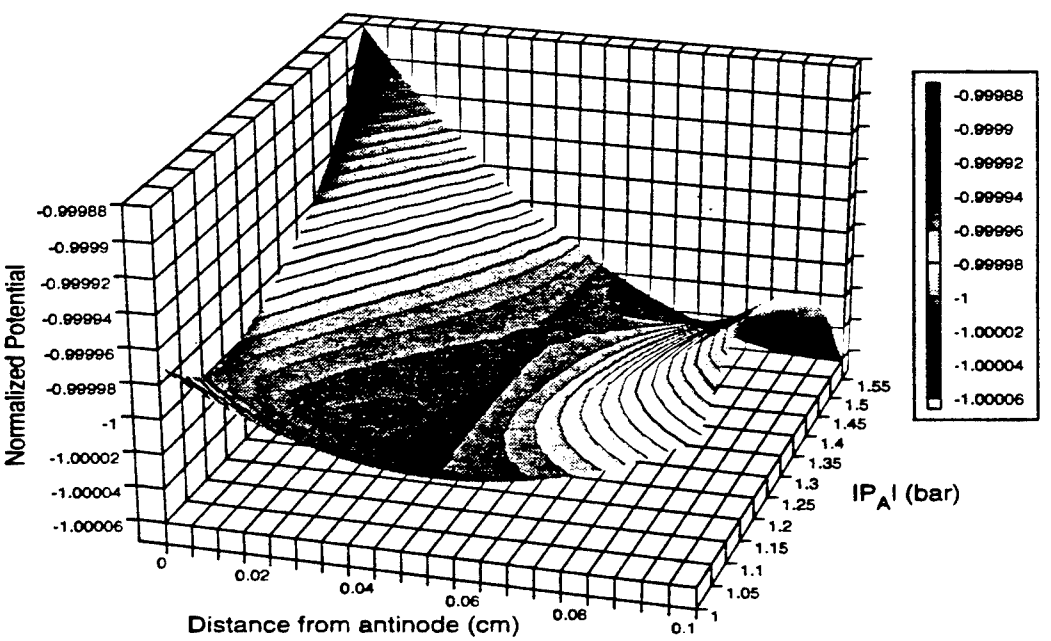

Figure 3.14. "Normalized" potential surface. (See text for details.)

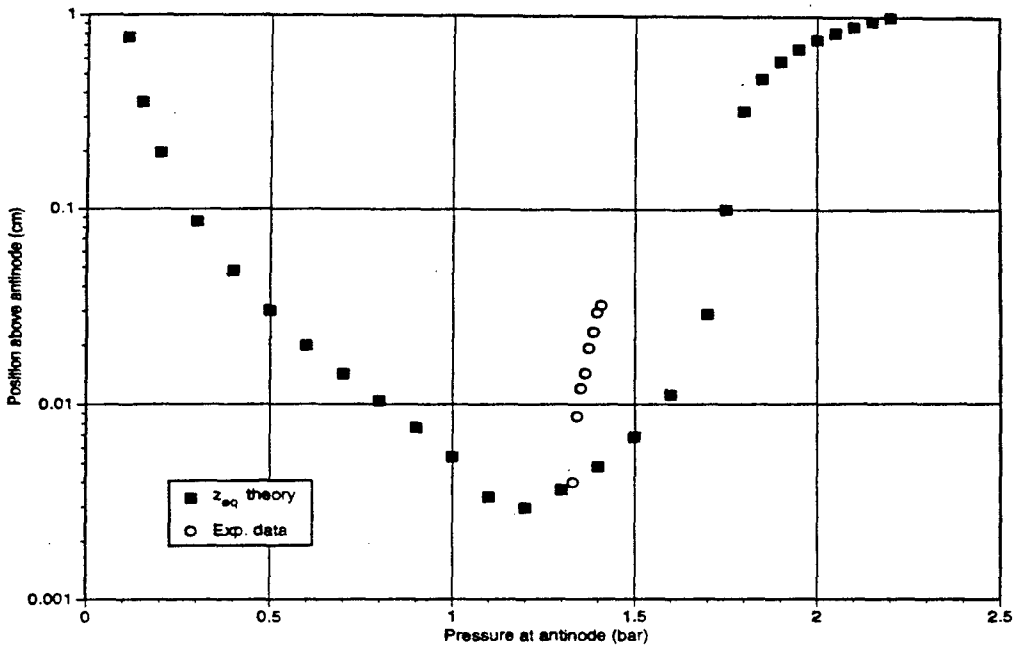

Figure 3.15. Theoretical prediction of z_{eq} of a 5 μm bubble along with experimental data points. Though the fit between experiment and theory is poor, the trend is correct. Use of the correct effective wavelength can significantly improve the fit. ($f = 20.0\,kHz$ and $\lambda = 9.73\,cm$)

Notice in Fig. 3.14 that the potential "valley" approaches the antinode as $|P_A|$ increases, but then as $|P_A|$ is increased further, the valley bends away from the antinode. This behavior was seen in Fig. 3.10. A similar surface for the linear problem discussed above would resemble a trough that would asymptotically approach the antinode.

3.4 Experimental Verification

The camera/microscope and digitizing system described in an earlier chapter were used to obtain data supporting the theoretical conclusions discussed above. Figure 3.15 shows the theoretical predictions seen in Fig. 3.10 along with experimental values of z_{eq} for a single sonoluminescing bubble. It can be seen that although the trend is correct, the quantitative fit is poor.

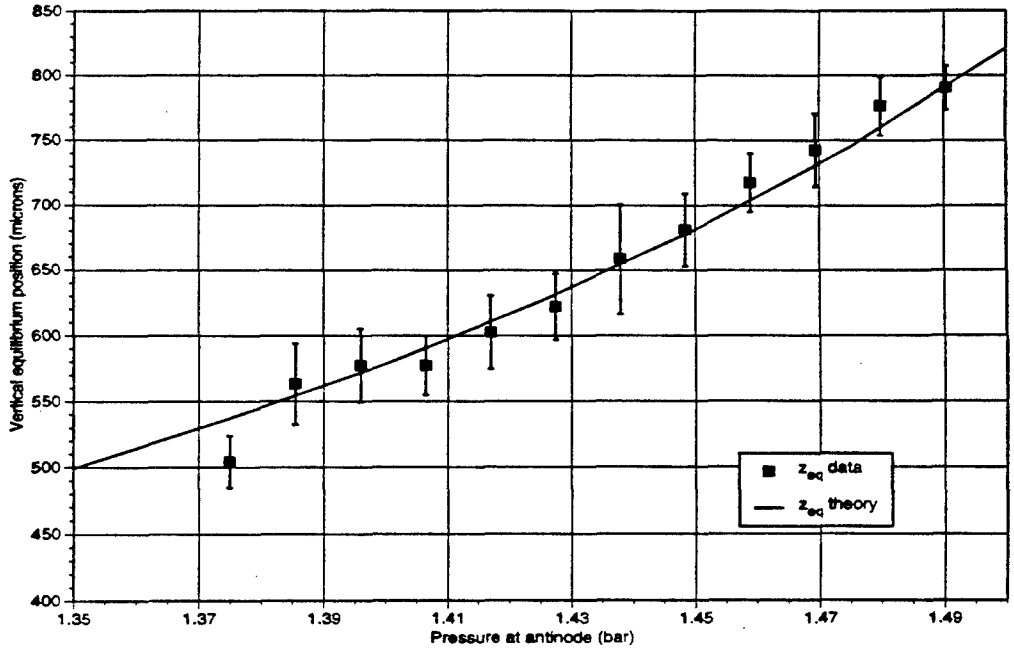

Figure 3.16. Experimental and theoretical data for z_{eq} of a sonoluminescing bubble using the effective vertical wavelength. The bubble was not stationary during these measurements and the error bars correspond to the extent of the wander experienced by the bubble. ($R_0 = 3.2\,\mu m$ and $f = 19.5\,kHz$)

Since the trend is correct and the theory seems robust, the physical parameters involved in the measurement must be scrutinized to determine the source of the discrepancy seen in Fig. 3.15. The most suspect parameter is the vertical wavelength used to make the calculations, since perfect boundary conditions do not exist within the cell, and since the presence of bubbles is known to affect the quality factor of a resonator. The water height in the acoustic levitation cell is typically $14.6\,cm$, which would yield a vertical wavelength of $9.73\,cm$ for a frequency of $19.5\,kHz$[6]. A careful consideration of the experimental data along with Eq. 3.19 indicates that the pressure gradients may not be as steep as the geometry would predict. In other words, the local pressure field may behave as if the wavelength (and corresponding pressure gradient) were longer (and shallower) than $9.73\,cm$. By using an effective wavelength of $\lambda' = 3.5\lambda$ in the theoretical calculations, the theory and the data

[6] A frequency of about $20\,kHz$, depending upon the temperature, excites the third eigenmode of the levitation cell.

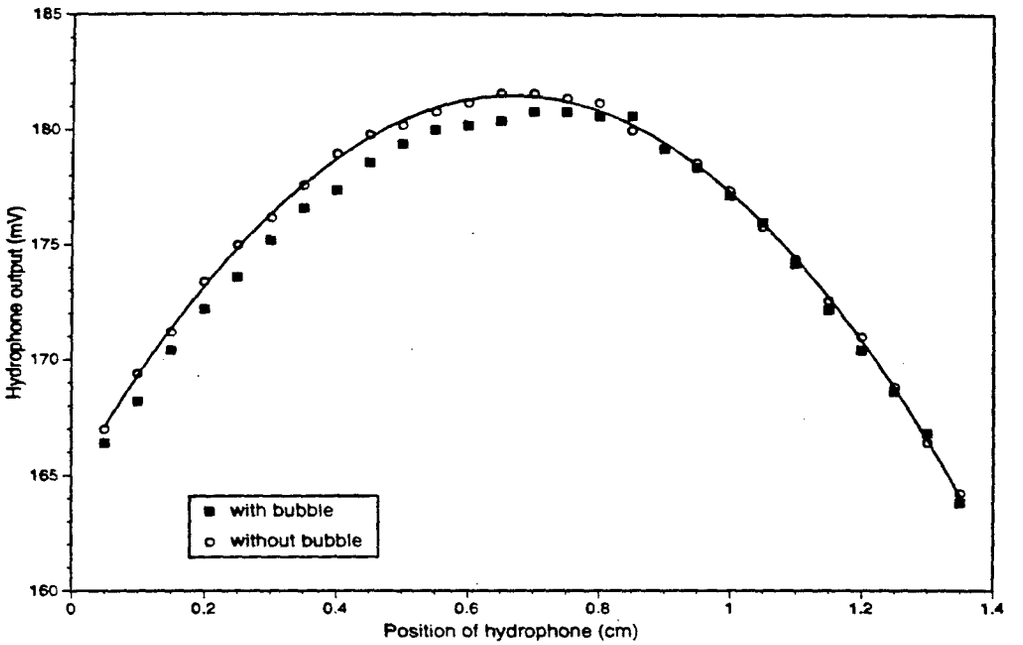

Figure 3.17. Hydrophone response as a function of vertical position near the antinode both with and without a sonoluminescing bubble present. The solid line is a fit to the equation $Acos(kz + \phi)$ with $\lambda = 9.73\,cm$.

match well. Figure 3.16 shows the excellent agreement between the theoretical predictions and the data using the modified wavelength.

Pressure profiles with and without a sonoluminescing bubble present are shown in Fig. 3.17. (The signal was low-pass filtered in order to remove the high frequency acoustic signature radiated by the bubble.[7]) This pressure profile proved difficult to acquire since evaporation and temperature fluctuations have dramatic effects on the tuning of the cell. Additionally, the frequency response of the PZT driver is not flat in the operational range of frequencies. As a consequence, if the cell detunes by as much as $10\,Hz$, adjusting the driving frequency alone will not return the acoustic environment to its previous condition.

These difficulties aside, it is apparent that the peak in the pressure profile is flatter than expected, accordingly, the pressure gradients are not as steep as expected. Figure 3.18

[7] The acoustic signature of a sonoluminescing bubble will be discussed in a later chapter.

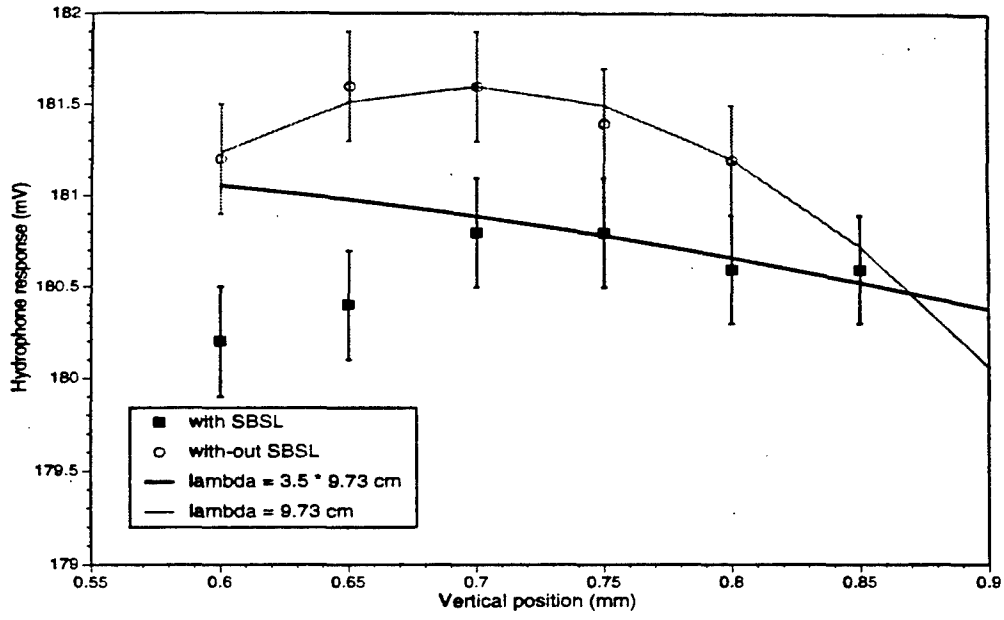

Figure 3.18. Close-up of Fig. 3.17. The data points obtained in the presence of a bubble fit a longer wavelength than that which is predicted by the geometry of the cell.

shows an expanded view of the peak in Fig. 3.17. The data points taken without a bubble present fit the geometrically predicted wavelength well; but, the data points taken in the presence of a bubble fit a wavelength that is greater by a factor of 3.5 – just as predicted by the experimental data for z_{eq}.

Figure 3.19 is similar to Fig. 3.16 except that the frequency used was $13.3\,kHz$, corresponding the the first eigenmode of the levitation cell. Again, a modified wavelength was used; whereas λ should have had a value of $29.0\,cm$, a value of $\lambda' = 2.7\lambda$ fit the data well.

The error bars in Fig. 3.16 are due to the fact that the bubble was not stationary for a given $|P_A|$ while the measurements were made. The length of the error bars corresponds to the magnitude of the wander experienced by the bubble. While the measurements for Fig. 3.19 were being made, the bubble was stationary and the error in the measurements corresponds to the resolution of the optical system, a value too small to appear on the scale of the figure.

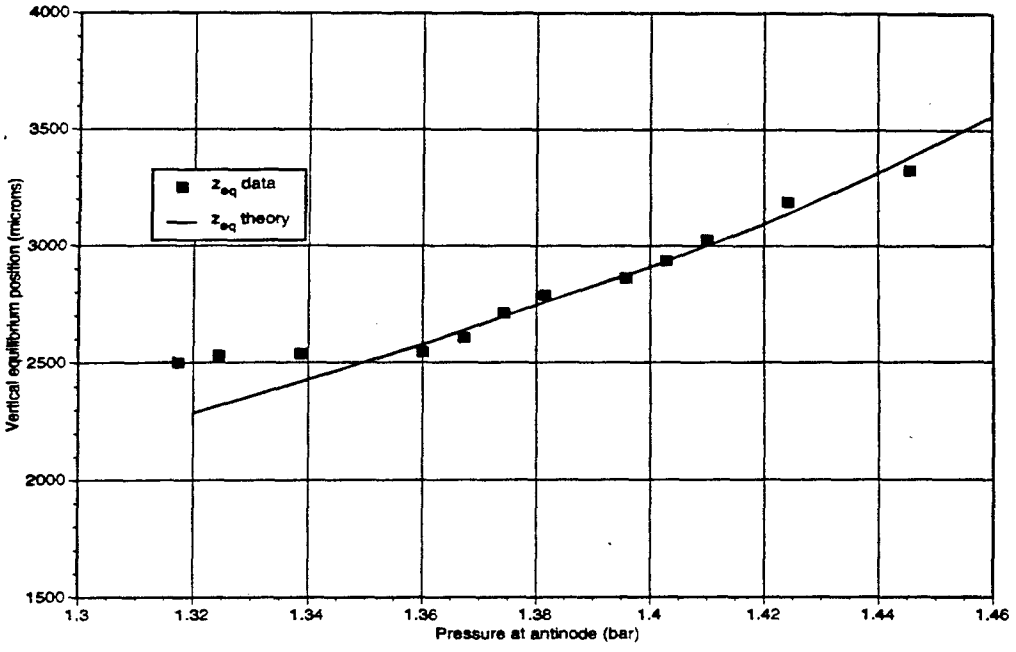

Figure 3.19. This figure is similar to Fig. 3.16 except that $f = 13.3\,kHz$. When this data was obtained the bubble was stationary and the error corresponds to the resolution of the optical system, a value too small to be seen on this scale.

The fit in both of these figures is good, but each figure has experimental data points at the lower values of $|P_A|$ which deviate from the theoretical predictions. For each set of data, the equilibrium radius of the bubble was determined at one pressure and then assumed to be fixed throughout the measurements. This is a good approximation because data by other authors [20] show that the R_0 varies by only a few tenths of a micron with $|P_A|$ during sonoluminescence. However, at the lower pressures, the bubble begins to dissolve as it can no longer support its size via rectified gas diffusion. The equilibrium size at these lower values of $|P_A|$ should be significantly different than that at the higher values. Thus, this deviation is expected.

3.5 Conclusions

In this chapter it was shown that standard linear theory for predicting the equilibrium position of a bubble fails for the case of a sonoluminescing bubble. Once the non-linear nature of the bubble's behavior was taken into account, an equilibrium position could be found by balancing the Bjerknes and buoyancy forces acting on the bubble. The predictions for the equilibrium position given by this non-linear approach proved to be accurate when certain corrections were made for a local detuning of the cell resonance caused by the bubble itself. Furthermore, it was demonstrated that the balance between Bjerknes and buoyancy forces provides a limit to the amplitude of the acoustic pressure that can be applied to a bubble.

Whereas in this chapter the bubble's center of mass was treated in a static manner, in the next chapter a dynamic treatment will be made. Experimental measurements suggest that the limiting acoustic pressure amplitude mentioned above is never reached; SBSL bubbles simply cease to exist beyond some lower threshold acoustic pressure amplitude. It will be shown that the translational motion of the bubble can introduce instabilities that could lead to the demise of the bubble.

Chapter 4

Bubble Translation and the Extinction Threshold

4.1 Introduction

One of the many things not clearly understood about SBSL is the existence of the extinction threshold. This threshold is a sharply defined acoustic pressure amplitude beyond which a bubble in a state of SBSL will simply cease to exist. Theoretically, the threshold remains anomalous; there are continuing attempts to explain it, *e. g.*, surface waves on the bubble breaking the symmetry of the collapse, but no single explanation has satisfactorily treated the problem. Experimentally, the threshold can be a nuisance since, if inadvertently crossed, an experiment must be restarted. Practically, the threshold represents a barrier to higher amplitude oscillations and a maximization of the SL temperature.

In this chapter, the vertical location of a SBSL bubble in a standing acoustic wave will be treated dynamically, *i.e.*, the translation of the bubble will be examined. The translation will then be linked to the extinction threshold; translation of the bubble can lead to surface

distortions. If the distortion is of significant size, it will ultimately destroy the bubble.

4.2 Bubble Translation

The translational motion of a radially pulsating bubble has recently been considered by Watanabe and Kukita [48]. They examined the translation of bubbles of various sizes in a standing acoustic wave in the absence of gravity. Bubbles whose size was significantly less than resonance size [1], they found, are attracted to pressure antinodes. Bubbles larger than resonance size are attracted to pressure nodes. Each of those results is easily predicted by Eller's linear theory of the levitation of bubbles in a standing wave [39]. The significant conclusion of their work was that for bubbles slightly less than resonance size, a chaotic pattern of translation was observed. This, they claim, was what was seen by other researchers and described as "zig-zag" motion [49, 46].

The equation of motion used by Watanabe and Kukita for the translation of a bubble is

$$m_B \dot{u}_b = -V(t)\nabla P_A(\vec{r},t) + \rho g V(t) - \frac{1}{2}\rho\frac{d}{dt}(V(t)u_r) - \frac{1}{2}\rho|u_r|u_r A C_d. \qquad (4.1)$$

The symbols represent the following physical quantities: m_B is the mass of the bubble; u_B, the velocity of the bubble; u_r, the relative velocity of the bubble compared to the fluid velocity; A, the area of the bubble; and C_d is the drag coefficient. The first two terms on the R.H.S. of Eq. 4.1 are the driving terms – the Bjerknes and buoyancy forces.

The third term on the R.H.S. of Eq. 4.1 represents what will be referred to as a reactive force. It arises from separating the total momentum when writing the equation of motion:

$$\begin{aligned} \dot{\vec{p}} &= \sum_i \vec{F}_i \\ \frac{d}{dt}(\vec{p}_{air} + \vec{p}_{hole}) &= \sum_i \vec{F}_i \end{aligned} \qquad (4.2)$$

[1] A "resonance size" bubble means a bubble of such a size that its natural frequency of oscillation equals the frequency of the applied sound.

where $\vec{p}_{air}$ and $\vec{p}_{hole}$ represent the momentum of the air within the bubble and the momentum of the "water hole," which is the product of the effective mass of the displaced water and its velocity. This reactive force is very important when the bubble volume is changing rapidly. If a bubble had a given momentum and its volume were shrinking – thus losing effective mass of the water hole, then the bubble would accelerate to conserve momentum. Alternatively, if the bubble volume were expanding, the bubble would decelerate.

The final term on the right-hand-side of Eq. 4.1 is the drag term. The drag coefficient [50] is

$$C_d = 27.0 R_e^{-0.78}, \tag{4.3}$$

with the Reynolds number defined as

$$R_e = 2\rho R(t) u_r / \mu. \tag{4.4}$$

The translational and radial motions of the bubble are coupled. Equation 4.1 must be solved numerically, but also simultaneously with the radial equation of motion, Eq. 3.15; a computer program was written to accomplish this task. A reasonable test of the program was to reproduce Watanabe and Kukita's original results. However, to accurately reproduce their work, the fluid compressibility terms of Eq. 3.15 had to be "turned off." (They used a radial equation of motion which treated the fluid as incompressible.) The "chaotic" behavior reported by Watanabe and Kukita can be seen in Fig. 4.1. The equilibrium size of the bubble, 125 μm, is slightly less than the resonance size of 134 μm.

It was noticed during this work that the "chaotic" motion did not appear when the compressible-fluid terms of Eq. 3.15 were included in the calculation. Figure 4.2 shows the behavior of three different sized bubbles in the same acoustic environment as Fig. 4.1 and in the presence of gravity – but with the compressibility terms "turned on." The smallest

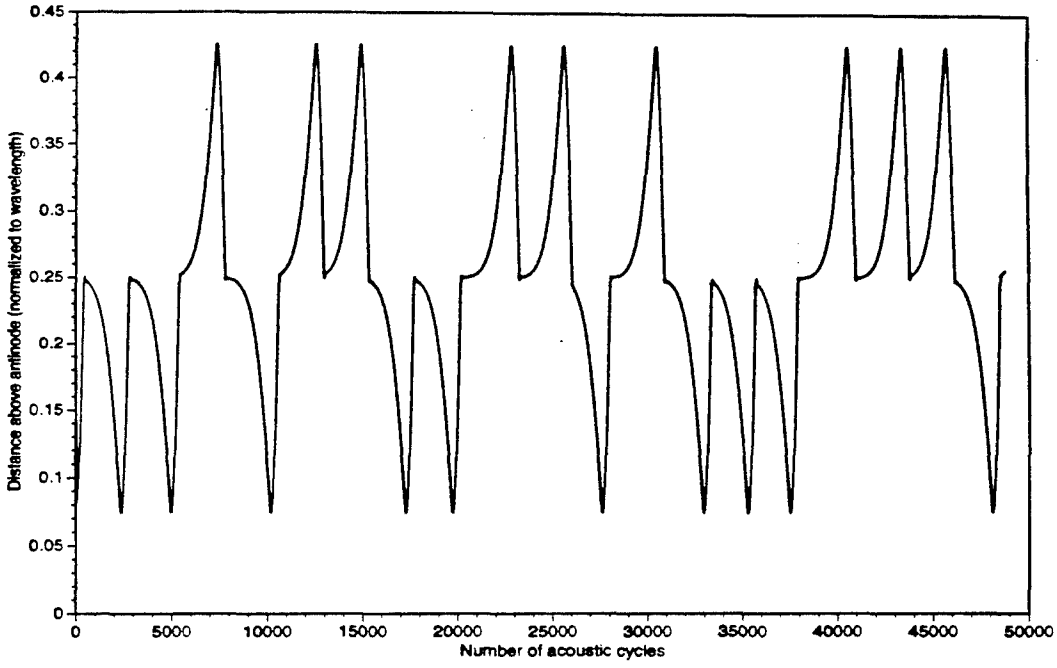

Figure 4.1. "Chaotic" translation reported by Watanabe and Kukita and reproduced here using the author's computer program. It is the coupled relationship between the radial motion and the translation which leads to this kind of behavior – but only for bubbles of very nearly resonance size. ($f = 24.4\,kHz$, $\lambda = 6.1\,cm$, $|P_A| = 1.2\,atm$ and $R_0 = 125\,\mu m$)

bubble attains a vertical position just above the pressure antinode while the largest, a position just above the pressure node; these two bubbles are significantly smaller than and larger than resonance size, respectively. The $125\,\mu m$ bubble does not behave chaotically in this case.

In order to understand the translation of the $125\,\mu m$ bubble seen in Fig. 4.2, it is useful to examine the radial motion concurrently, as is shown in Fig. 4.3. Notice that the bubble requires many acoustic cycles to attain steady-state behavior. It is suggested that Watanabe and Kukita's results may be "chaotic" because there is not enough damping for steady state conditions to develop. Notice the change in the behavior of the bubble when the bubble begins to move toward the antinode. For Fig. 4.4, there is some degree of "aliasing" since not every calculated data point was collected for graphing. For a bubble with radiative damping, a regime of stable, periodic "zig-zag" motion can be found if the

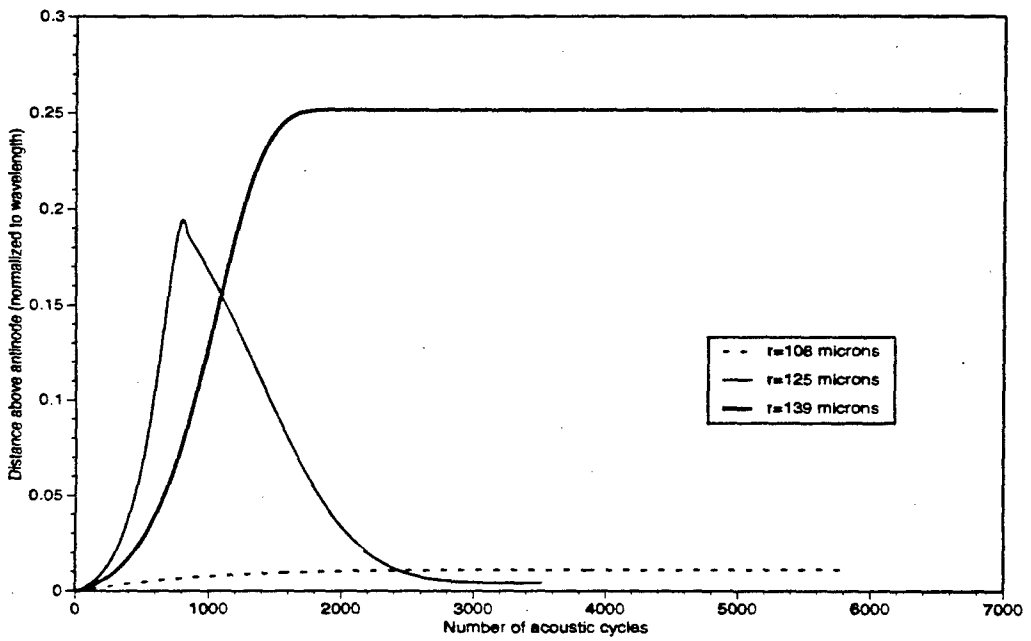

Figure 4.2. Translational motion of three bubbles of different sizes in the same acoustic environment as Fig. 4.1. However, in these calculations, gravity has been added and the radial equation of motion is more sophisticated than the one used in the figure above. Note that the "chaotic" behavior of the mid-sized bubble has disappeared. $R_0 = 108, 125$ and $139\ \mu m$.

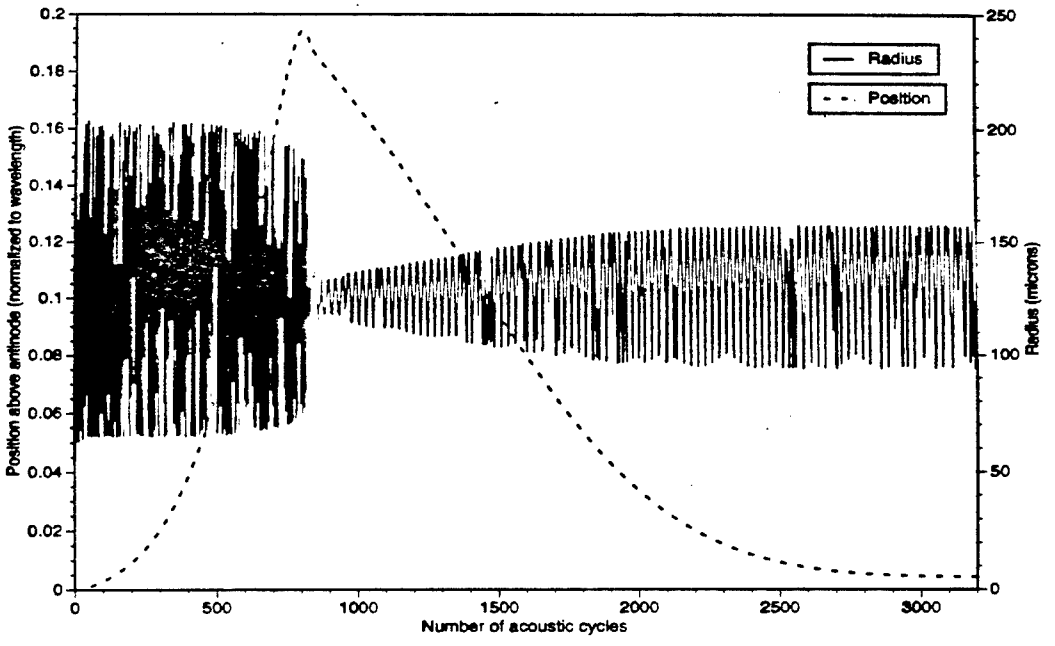

Figure 4.3. Translational motion and radial motion for the 125 μm bubble of the previous figure. Note the relationship between the two types of motion: a change in the radial motion affects the translation. (Note also some aliasing effects since not all calculated data points were recorded.)

acoustic amplitude is sufficiently large. Figure 4.4 shows how a 125 μm bubble may develop periodic behavior once a threshold acoustic pressure has been crossed.

Some have attributed the "dancing" motion of a bubble to the presence of surface waves on the bubble. It should be stressed at this point that in these calculations the bubble has only been allowed to translate and move radially; there are no surface waves involved. The "zig-zag" feature here is purely a function of the coupling between the radial and translational motions of the bubble. (That is not to say that surface waves don't contribute; they can, it's just that they have not been considered here.)

The extent of the translational motion for small bubbles at a position of vertical equilibrium is minute. Indeed, under conditions suitable for SBSL, the dancing motion at acoustic pressures as high as $|P_A| = 1.6\,bar$ is less than one micron; Fig. 4.5 shows the translation of a 5 μm bubble. Notice that there is motion on two different time scales: a shorter time

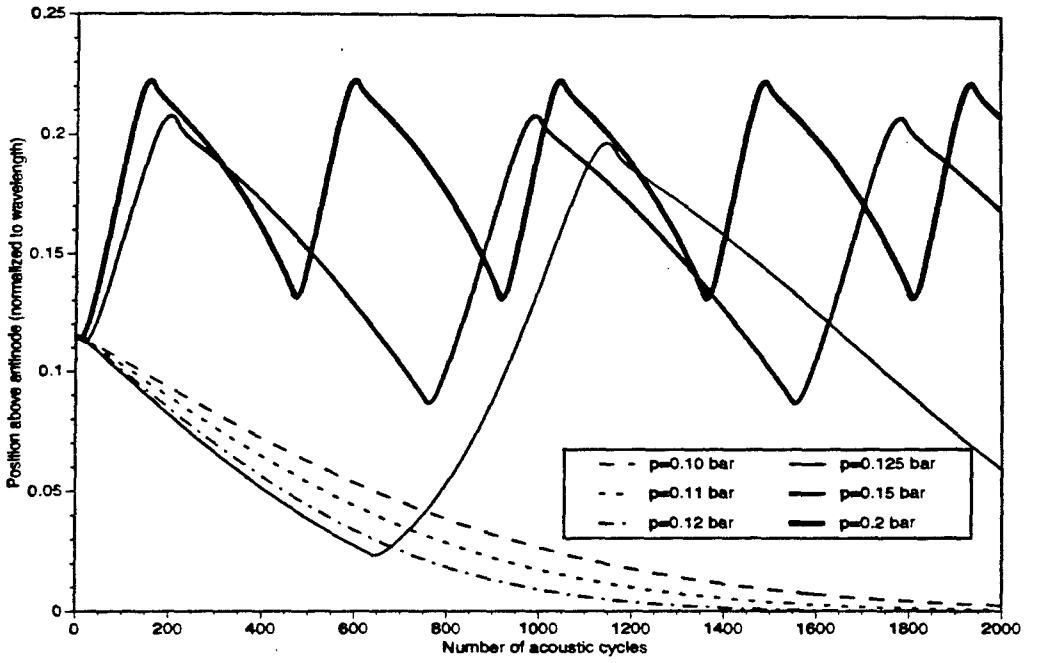

Figure 4.4. Onset of the "zig-zag" behavior in the translational motion of an $125\mu m$ bubble. The period and the amplitude of the translation decrease as the acoustic amplitude is increased. (f=24.4 kHz and $\lambda = 6.1\,cm$)

scale which corresponds to the period of the sound field, and a longer one which oscillates indeterminately.

Figure 4.6 shows the motion of a $3.2\,\mu m$ bubble translating from one position of vertical equilibrium to another. The bubble was started at a position of equilibrium for an acoustic pressure amplitude of 1.43 *bar*. The pressure used in the calculation was 1.44 *bar*. Note that the motion is similar to that of an over-damped simple harmonic oscillator in that the highest velocity occurs at the beginning of the motion. This fact will be important later when trying to understand the role of the vertical wavelength on the translational motion of the bubble.

It is useful to compare the radial and translational motions of the bubble in Fig. 4.5 along with the translational velocity. Figure 4.7 shows such a comparison: the top plot shows the radial motion along with translation, while the bottom plot shows the translational velocity.

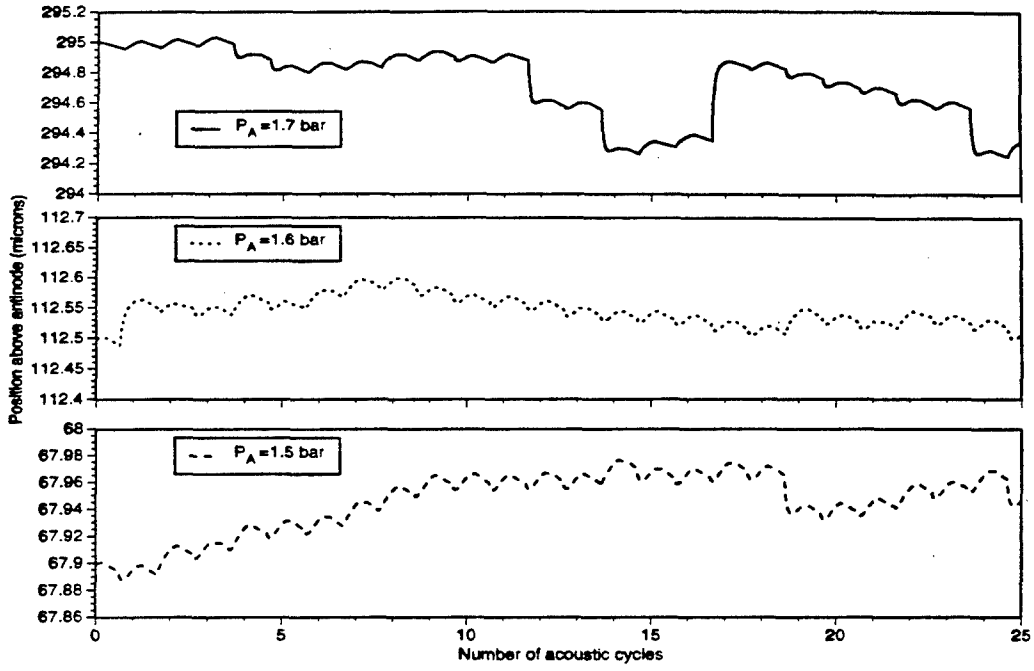

Figure 4.5. Translational motion of an 5 μm bubble in a sound field for different values of $|P_A|$. This is considered stable behavior because the extent of the translation is small. The bubbles are located at appropriate vertical equilibrium positions. $f = 20.0\,kHz$ and $\lambda = 9.73\,cm$

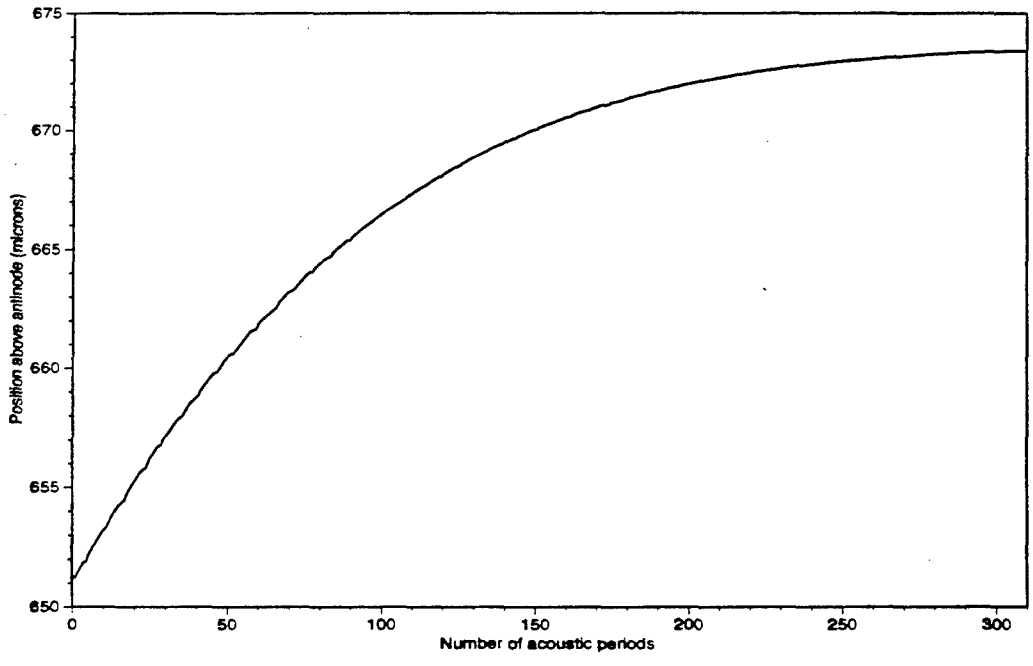

Figure 4.6. SBSL bubble translating from one vertical equilibrium position to another. $3.2\mu m$ SBSL bubble translating from one equilibrium position to the next after increasing the acoustic pressure $0.01\,bar$ to a value of $1.44\,bar$. ($f = 19.3\,kHz$ and $\lambda = 3.5 \times 9.73\,cm$)

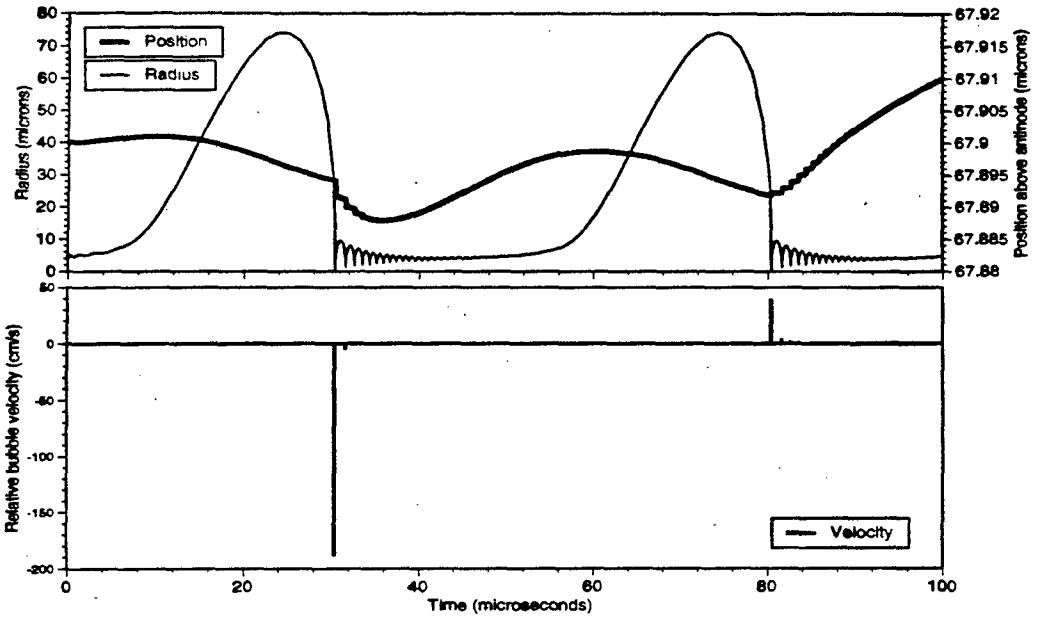

Figure 4.7. Translation, translational velocity and radial motion of one of the bubbles in Fig. 4.5.First two cycles of the lower graph in Fig. 4.5. Note that at one point the speed exceeds 150 m/s. Very high translational velocities put the bubble at risk of destruction from surface distortion.

Note that the magnitude of the translational velocity plotted in Fig. 4.7 exceeds 150 cm/s at one point. Indeed, at times, calculations have indicated that the translational velocity of a bubble can exceed 800 cm/s. These large velocities occur during bubble collapse and are the result of the reactive force term in Eq. 4.1: as the bubble is collapsing very quickly, the term $\frac{d}{dt}(V(t)u_r)$ becomes very large. Given the possibility of such extreme velocities, the spherical integrity of the bubble's surface must be considered during the collapse of the bubble.

4.3 Surface Distortion

Several investigators have, however, studied the deformation of bubbles due to fluid flow. Pelekasis and Tsamopoulos [51, 52] have recently described the attraction of two bubbles to

each other due to so-called secondary Bjerknes forces.[2] Their detailed calculations describe the acceleration experienced by the bubbles and subsequent shape distortion due to rapid translation. The shape distortion is caused by Rayleigh-Taylor instability and causes the bubbles to assume "spherical-bottle-cap" shapes. (The bottle-cap shape deformation of freely rising bubbles was first reported by Davies and Taylor [53].)

Most recently, Longuet-Higgins and Oguz [54] have described micro-jet formation in collapsing cavities. While usually the collapse of a cavity into a micro-jet is described as an event occurring near a boundary [29], Longuet-Higgins and Oguz have described micro-jet formation in collapsing cavities which are not necessarily near a boundary. Their paper describes the process of micro-jet formation as the result of moving hydrodynamic sinks. When a cavity collapses, it is a hydrodynamic sink, drawing fluid from the surrounding area. If the sink location is moving, then there is the possibility of micro-jet formation. (Cavity micro-jet formation near a boundary may be viewed as a moving sink problem.)

The instability of a collapsing cavity has also been studied from the standpoint of surface waves on a bubble [55]. The initial surface can be described as

$$R_s(t) = R(t) + a(t)Y_l^m(\theta, \phi), \tag{4.5}$$

where $a(t)Y_l^m(\theta, \phi)$ is a spherical harmonic of amplitude $a(t)$. As the cavity collapses, the amplitude of the distortion will grow as

$$a = \epsilon R^{-\frac{1}{4}}, \tag{4.6}$$

where ϵ is a constant. Additionally, it should be mentioned that Prosperetti and Seminara [56] have shown that the role of viscosity in the growth of surface waves for a collapsing cavity is to impede the growth of the higher order harmonics.

[2] The secondary Bjerknes force is the force between two bubbles due to acoustic radiation from the bubbles themselves. The primary Bjerknes force was the topic of the subject of the preceding chapter.

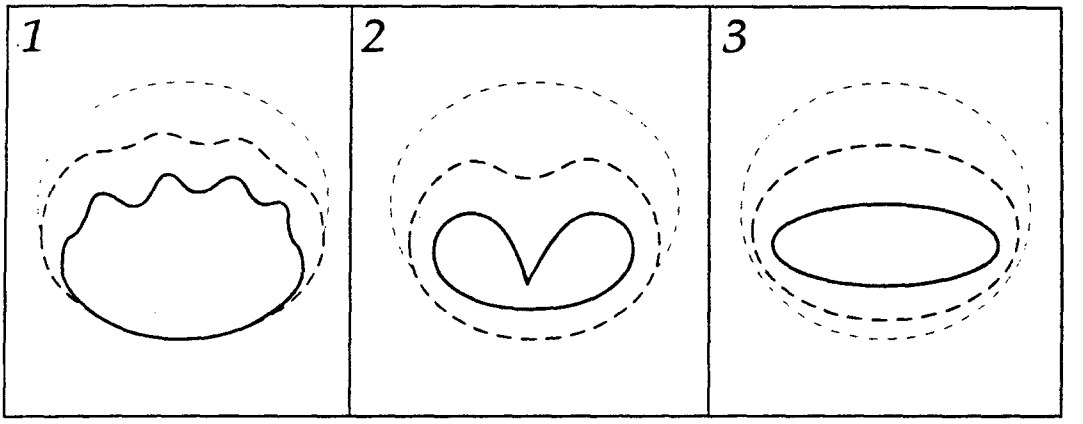

Figure 4.8. Cartoon illustrating the three mechanisms which can lead to the demise of a bubble due to its translation: (1) "bottle-cap" ripples on the back side of the bubble, (2) critical micro-jet formation, and (3) flattening and stretching. (All three bubbles are pictured as moving downward.)

Anilkumar, *et al.* [57], have examined the stability of an acoustically levitated drop and found the point of drop break-up to be directly related to the air flow around the edges of the droplet. In an analogous way, there are then three different mechanisms by which a translating bubble experiencing nonlinear radial motion might meet its demise as a result of a loss of spherical integrity. These are illustrated in Fig. 4.8.

1. The first is the manner of bottle-cap formation as described by Pelekasis and Tsamopoulos which could lead to the destruction of the bubble if the instabilities became large enough. The bubble would develop such instabilities if the Weber number exceeds a value of 1.22. The Weber number is defined as

$$W_e = \rho R u_r^2 / \sigma. \tag{4.7}$$

2. A second mechanism is the moving sink phenomena studied by Longuet-Higgins and Oguz. This mechanism is difficult to employ expediently since it requires difficult computations of the surface of the bubble. More work needs to be done before their mechanism can be put into an *ad hoc* formulation suitable for the problem discussed here.

3. Taylor and Acrivos [58] have derived the following equation describing the radius of a bubble rising through water with a certain velocity

$$R_s = R_0(1 - \frac{5}{96}R_e C_a[3\cos^2\theta - 1]). \tag{4.8}$$

For Eq. 4.8, C_a is the capillary number defined as

$$C_a = \mu u_r/\sigma. \tag{4.9}$$

The third possible mechanism is that a distortion given by Eq. 4.8 could grow as the cavity collapses to a point were the bubble would not survive the collapse.The bracketed term of Eq. 4.8 is a second degree Legendre polynomial – the familiar oblate spheroidal shape of a freely rising bubble, and by comparing Eq. 4.8 with Eq. 4.5 we can see that the amplitude of the harmonic is given by

$$a = \frac{5}{96}R_e C_a R. \tag{4.10}$$

It is then possible to solve Eq. 4.6 for ϵ in terms of the initial surface distortion and radius at which the distortion occurs:

$$\epsilon = a_i R_i^{\frac{1}{4}}. \tag{4.11}$$

Now substitute Eq. 4.10 into Eq. 4.11 to get for Eq. 4.6

$$a = (\frac{5}{96}R_e C_a R_i^{\frac{5}{4}})R^{-\frac{1}{4}}. \tag{4.12}$$

It is then necessary to know the minimum surface distortion amplitude which, if allowed to grow in the manner of Eq. 4.6, would achieve some critical amplitude, a_c, which would

destroy the bubble. Since the distortion amplitude is a maximum at the radial minimum, the critical distortion amplitude is defined by the minimum radius:

$$a_c = R_{min}/2. \tag{4.13}$$

In other words, if the final amplitude of an initial surface distortion equals or exceeds half the minimum radius, the bubble will break-up. Inserting a_c into Eq. 4.12 yields the following result.

$$\frac{5}{96} R_e C_a R^{\frac{5}{4}} = \frac{1}{2} R_{min}^{\frac{5}{4}} \tag{4.14}$$

If the left-hand-side of the equation exceeds the right-hand-side, then the bubble will break-up.

The Weber number from mechanism (1) and the left-hand-side of Eq. 4.14 can be calculated at all times while numerically solving the translational and radial motion of the bubble. Either condition will result in the "death" shown in Fig. 4.9 of a $5\mu m$ bubble. The initial condition of this calculation for a bubble in a standing wave was that the bubble was started at the vertical location of the antinode – a position far from the vertical equilibrium position, z_{eq}, discussed in the last chapter. The calculation was stopped at the point where $W_e \geq 1.22$. The top plot shows the radial motion and the translation, while the bottom plot shows the translational velocity. Note that the velocity increases several orders of magnitude during the collapse of the bubble: from $0.0128\, cm/s$ at the radial maximum, to $269\, cm/s$ at the point the computation was stopped – an average acceleration of nearly $44,000$ "g's"!

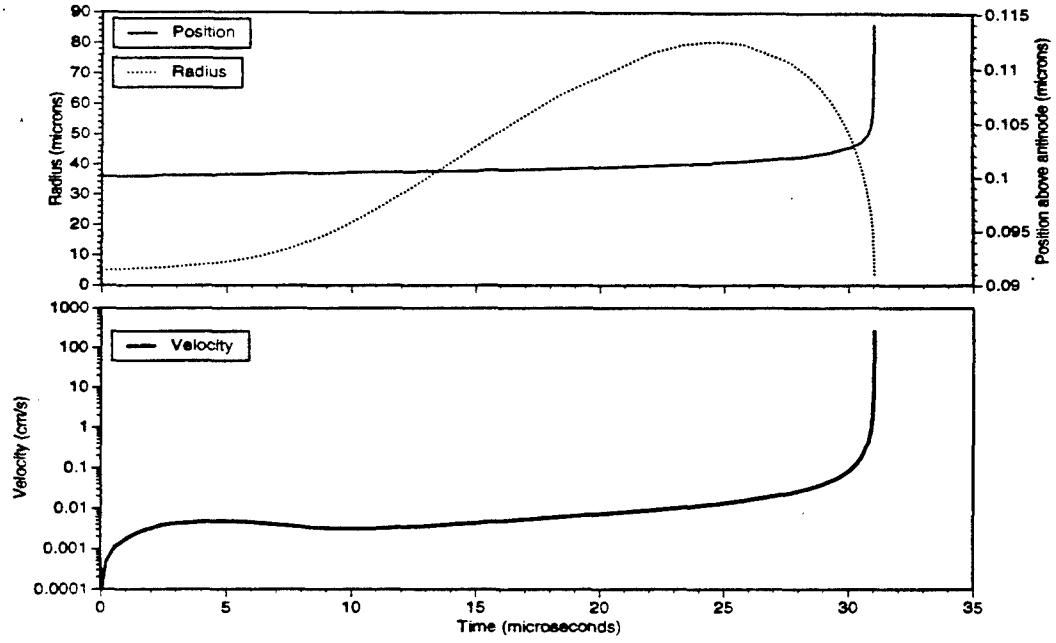

Figure 4.9. Example of bubble "death." A bubble started at a vertical location far from its equilibrium position can achieve translational velocities which result in the destruction of the bubble. An example of this "death" is shown here. This $5\,\mu m$ bubble experienced an average acceleration higher than $40,000$ "g's." ($f = 20.0\,kHz$, $\lambda = 9.73\,cm$ and $|P_A| = 1.3\,bar$.)

4.4 Discussion

4.4.1 Sensitivity to Pressure Increments – The Extinction Threshold

The large acceleration and subsequent "death" experienced by the bubble in Fig. 4.9 were due to the fact that the initial conditions for the calculation were such that the bubble was not started at a vertical equilibrium position. As was discussed in the previous chapter, the values of such equilibrium vertical positions, z_{eq}, depend upon several parameters, one of which is the amplitude of the acoustic pressure at the antinode, $|P_A|$. When the value of $|P_A|$ is changed, the value of z_{eq} must also change, *i. e.* the bubble must translate. It is during these transitions that the bubble is subject to the possibility of surface distortion.

Because the second-derivative of the curve comprising the collection of points z_{eq} is positive in the regime of SBSL, the distance between successive points of equilibrium increases

for a given incremental pressure step. In other words, for a given ΔP_A, the bubble must move from the position z_{eq-old} to z_{eq-new} – a difference of Δz. As $|P_A|$ is incremented ΔP_A, Δz increases. As the value of Δz increases, the force accelerating the bubble to its new equilibrium position increases and the translational speed is larger.

One would expect then that the onset of the surface distortion should be related to the acoustic pressure increment, ΔP_A; and that is indeed the case as is demonstrated in Fig. 4.10. In Fig. 4.10, the calculation of the bubble's translation was initiated with the bubble starting at rest at some equilibrium position, z_{eq-0}, with a corresponding pressure amplitude of P'_A. The acoustic pressure was incremented and the bubble allowed to move to a new equilibrium position, z_{eq-1}. As the bubble translates from the location z_{eq-0} to z_{eq-1}, the computer program, using the criteria stipulated in Eq. 4.14, also checks for a "lethal" combination of translational and radial velocity – a combination which would lead to a compromise of the bubble's spherical integrity.

If the spherical integrity of the bubble remains intact while translating to z_{eq-1}, the pressure amplitude is incremented again and the bubble translates to a newer equilibrium position, z_{eq-2}. If the spherical integrity is still intact after the bubble reaches the point z_{eq-2}, then the pressure amplitude is again incremented. This procedure is repeated as long as the spherical integrity is preserved. However, a point is always reached at which the spherical integrity is lost – the extinction threshold – while the bubble translates from the location z_{eq-N} to z_{eq-N+1}. The value of z_{eq-N} corresponds to the maximum equilibrium location obtained by a given value of ΔP_A.

The maximum acoustic pressure attained with a given value of ΔP_A is

$$|P_A|_{max} = P'_A + N\Delta P_A. \tag{4.15}$$

where P'_A is the initial acoustic pressure. If a smaller incremental pressure step were used,

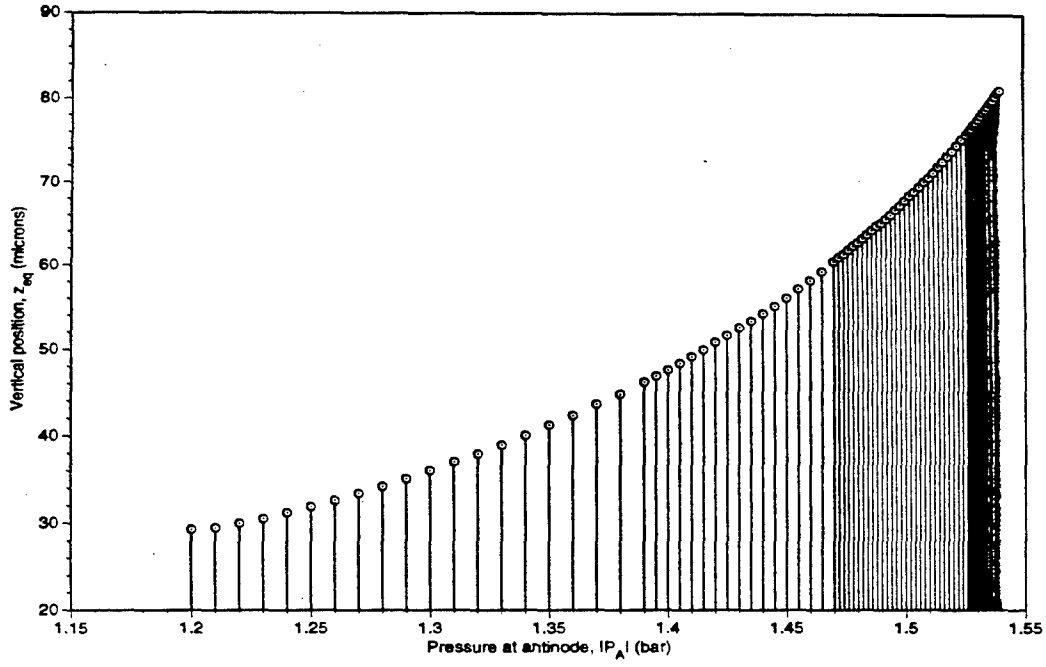

Figure 4.10. Graph illustrating calculations of the bubble's equilibrium position when the possibility of bubble destruction is allowed. For a given incremental step-size there is a maximum attainable pressure amplitude

then the corresponding changes in equilibrium position, Δz, would be less – reducing the chances of the bubble losing spherical integrity. Notice in Fig. 4.10 that different pressure increments were used. Higher values of z_{eq-N} and $|P_A|_{max}$ were obtained by using smaller increments of ΔP_A. Figure 4.11 shows the different values of $|P_A|_{max}$ that can be achieved with various incremental acoustic pressure step-sizes. Figure 4.11 suggests that ever smaller step-sizes must be used to achieve ever higher pressure amplitudes. Smaller step-sizes were not explored in depth since such small step-sizes are difficult to achieve in the laboratory.

4.4.2 SBSL in a Micro-gravity Environment

An appropriate question to address at this point concerns the role of the vertical wavelength. The buoyancy force on the bubble is independent of the wavelength or location of the bubble; it depends only on P_A, the pressure at the location of the bubble.[3] When the bubble is in

[3] For the case of SBSL, $P_A \approx |P_A|$ since the bubble is very close to the antinode.

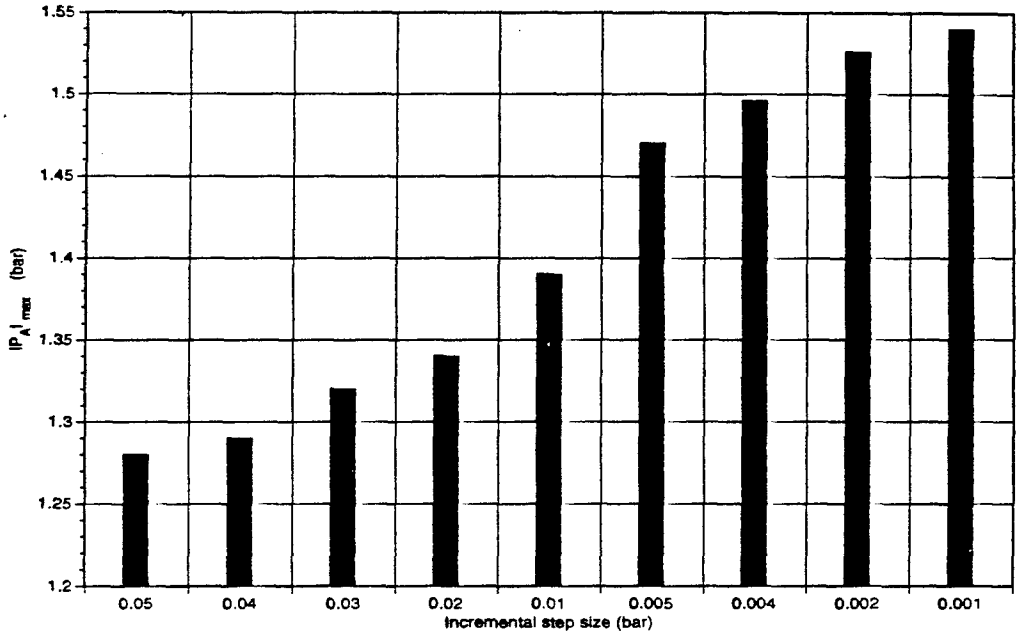

Figure 4.11. Maximum value of $|P_A|$ attained using different ΔP steps. The size of the incremental pressure step determines the extinction threshold. See Fig. 4.10 for details.

vertical equilibrium, the magnitude of the Bjerknes force must equal that of the buoyancy force. While the actual values of z_{eq} depend upon the wavelength, the magnitudes of the forces do not. Thus, the force which accelerates the bubble is also independent of the wavelength.

Recall from Fig. 4.6 that the speed is a maximum at the beginning of the motion, during the first period after the pressure increment. The momentum imparted to the bubble during that first acoustic cycle would be the product of the accelerating force and the period of the sound field. Again, the force and the period, of course, are independent of the wavelength. Thus the maximum speed is independent of the wavelength.

Since the maximum speed is independent of the wavelength, the extinction threshold depends solely on the value of ΔP_A and not on the wavelength. An interesting test of this theory would be to examine the operational ranges of SBSL in a micro-gravity environment. This theory would predict that the operational range should be extended since the buoyancy

force – and hence translation – would be essentially non-existent. It is mostly speculation to predict the extent of the range extension, but certainly one limiting factor will be the fact that the Bjerknes force becomes positive above an acoustic pressure of about $1.76\,bar$; this pressure amplitude limiting effect was discussed in the last chapter.

4.4.3 Experimental Corroboration

Laboratory experiments have yielded the following qualitative observations which indicate that SBSL is sensitive to incremental changes in the value of $|P_A|$.

1. The extinction threshold is sharply defined; once it is reached, it can be crossed by an increase in voltage to the driving transducer of as little as one part in one-hundred-twenty.

2. SBSL is sensitive to the rate of increase of the driving voltage; increasing the driving voltage in incremental steps that are too large has been observed to destroy the bubble prematurely.

3. SBSL must be initiated at some acoustic pressure which is less than the maximum attainable.

4. The luminescing bubble only disappears when the pressure amplitude is increased. If the acoustic environment is left unaltered, the bubble will be stable indefinitely.

Quantitative agreement between the predictions of this extinction theory and experiment has some success. Experiments show the range of SBSL at $19.3\,kHz$ to extend from 1.39 to $1.49\,bar$. Using identical experimental parameters – including $\Delta P_A = .01\,bar$ and $R_0 = 3.2\,\mu m$ – and a minimum radius of $0.5\,\mu m$, the theory presented here indicates that $|P_A|_{max}$ should be $1.49\,bar$. Barber, *et al.*, [20] show experimental data obtained at a frequency of

Table 4.1. Experimental values and theoretical values of the extinction threshold.

R_0	Frequency (kHz)	P_{max} – Theoretical (bar)	P_{max} – Experimental (bar)
4.5	26.4	1.30	1.30
7.0	26.4	1.08	1.08
3.2	19.3	1.49	1.49
3.0	13.3	1.36	1.45

$26.4\,kHz$ for a 7.0 and a $4.5\,\mu m$ bubble. The smaller of the two was in a state of SBSL and had an operational range of 1.13 to $1.30\,bar$. The larger, which did not luminesce, had a range up to $1.08\,bar$. This theory gave a similar level of agreement in predicting each of these bubble's extinction threshold.

However, for data obtained at $13.3kHz$, the agreement was not as good. Experimentally, the operational range of pressures for SBSL at this frequency was about 1.34 to $1.45\,bar$. The extinction theory predicted that the threshold should have been $1.36\,bar$. This disagreement poses a significant challenge to the theory; nonetheless, there appear to be some indications that the extinction model relayed here has merit. Perhaps it will be necessary to apply Longuet-Higgins and Oguz' ideas for critical microjet formation in order to obtain a complete model of SBSL extinction.

4.4.4 Implications for Rectified Diffusion

The term "rectified diffusion" refers to the dynamic transport of gas into and out of a bubble due to its expansion and contraction, respectively. This gas flux is due to the changing partial pressures of gas inside and outside the bubble [59, 60]. Löfstedt, *et al.* [61, 62]. have contended that SBSL necessitates the existence of an anomolous gas transport mechanism.

This is based on the fact that typical rectified diffusion calculations [63] applied to SBSL do not yield an equilibrium state. These equations for rectified diffusion assume that all the mass flow into and out of the bubble takes place within a thin fluid shell surrounding the bubble.

Figure 4.7 shows the vertical translation of a typical SBSL bubble for two acoustic periods. Though small, this translation would set up a circulation pattern in the water. This circulation would undoubtedly alter the mass-flow pattern. No longer could the effects of mass transfer be limited to a thin shell of liquid. The circulating water would continuously "refresh" the thin shell – particularly as the bubble collapses, when the velocity is greatest and mass is diffusing out of the bubble. The fluid flow could carry away this mass thus enabling the bubble to maintain a small equilibrium size instead of growing, as typical rectified diffusion calculations predict.

4.5 Conclusion

In this chapter, the vertical location of a SBSL bubble was treated in a dynamic way, building on the work of Watanabe and Kukita, who investigated the translation of bubbles of near-resonance size and found a tendency toward "chaotic" translation. This work has shown that the motion of such bubbles is probably not "chaotic", but periodic; the difference being due to use by the former of a less-accurate bubble dynamics equation. Investigation of the translation of SBSL bubbles revealed a link to the extinction threshold: rapid translation can lead to a loss of spherical integrity of the bubble. If the extent of the loss of sphericity is significant enough, it can lead to the destruction of the bubble. Implementing these ideas had mixed success when trying to predict the extinction thresholds seen in the laboratory.

The work presented here raises several questions: What is the relationship between R_0.

f and $|P_A|$ to the period and amplitude of the "zig-zag" motion seen in Fig. 4.4? What would happen if 3-dimensional motion were allowed? What are the exact effects of viscosity or surface tension on the extinction threshold? Answering such questions will be left for future work.

In the next chapter, the light and sound emitted by a SBSL bubble will be examined for several different experimental parameters. Simultaneous investigation of these features may give some insight into the observed effects of ambient temperature on SBSL.

Chapter 5

Sights and Sounds of SBSL

5.1 Introduction

It has long been known that fluid temperature has a strong effect on the luminosity of Multi-Bubble Sonoluminescence (MBSL); the cooler the liquid, the brighter the light produced. Recently, this effect was also confirmed for the case of Single-Bubble Sonoluminescence (SBSL) by Hiller [1], who recorded the maximum luminosity of a SBSL bubble as a function of temperature. His results are shown in Fig. 5.1. Notice that the luminosity increases by a factor of 12 for a $20^{o}\,C$ temperature reduction.

One clue to understanding the temperature-related effects was first obtained by Jarman [64], who investigated the amount of light emitted by various liquids under MBSL conditions. He found that the luminosity was related to the quantity σ^2/P_V, where σ is the liquid's surface tension, and P_V, its vapor pressure. The vapor pressure of water varies strongly with temperature. This "Jarman factor" has been fit to the data and is shown as the solid curve in Fig. 5.1 for the case of water; the equation of the curve is $y = a/P_V + b$, with $a = 5.35$ and $b = -1.76$. (The surface tension has been absorbed by the constant a since

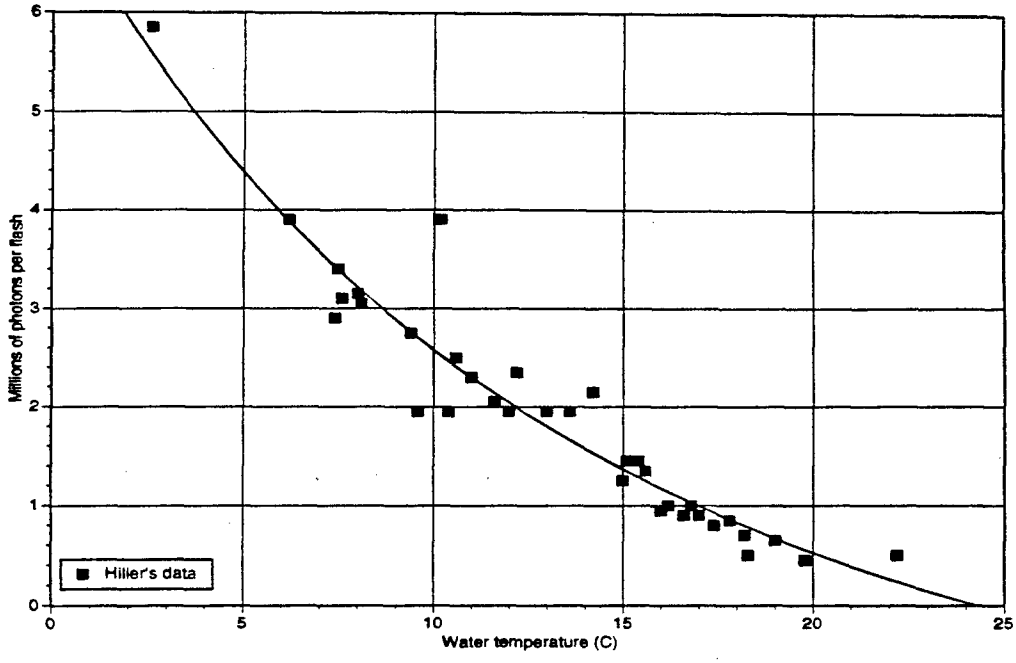

Figure 5.1. The luminosity of SBSL as a function water temperature as obtained by Hiller (squares). The curve $y = a/P_V + b$ fit to the data of with $a = 5.35$ and $b = -1.76$ suggests that the vapor pressure, P_V, may be important.

its value varies little over this range of temperatures used here.) Figure 5.1 is to appear in Ref. [26].

The excellent agreement between the Jarman factor and Hiller's data raises questions concerning the role of the vapor pressure: is the vapor pressure alone responsible for the temperature-related effects? If so, how? In this chapter, the sonic signature of a SBSL bubble will be used to compare the acoustic and electromagnetic energy radiated by the bubble. These comparisons are made over a range of temperatures and dissolved gas concentrations (DGC's). The experimental results are surprising and the interpretation of these results reveals something about the origin of the temperature-related effects.

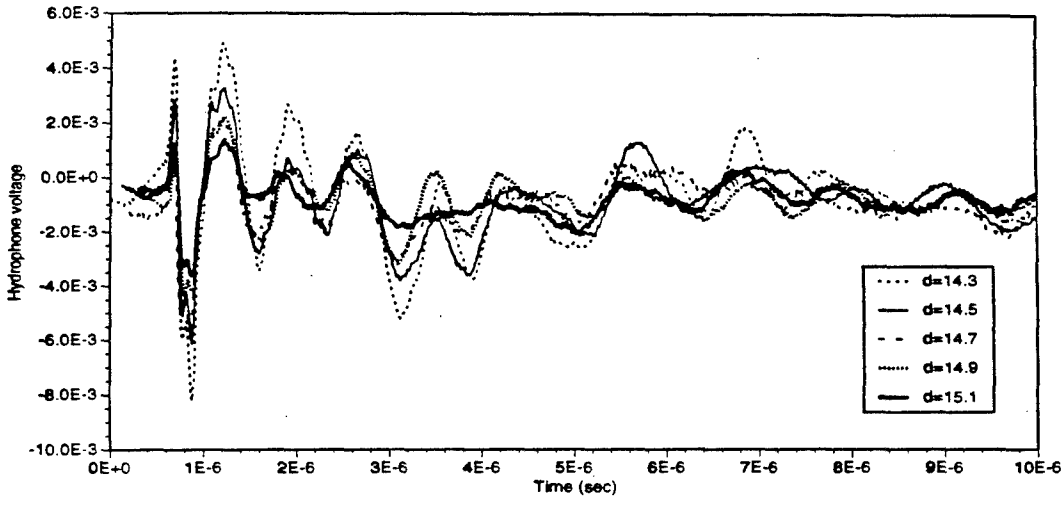

Figure 5.2. The sonic signature of a SBSL bubble received by a hydrophone placed at different distances from the bubble. The distances are given in the legend with units of *cm*; the bubble is located at the position 13.8 *cm*. Each signal has been offset in time in order to compensate for the different arrival times. (Note that the polarity of the hydrophone is reversed.)

5.2 Radiated Acoustic Energy

The sonic signature of a SBSL bubble can be used to measure the acoustic energy radiated by the bubble. During a violent cavity collapse, acoustic radiation is the most significant energy-loss mechanism; after collapsing, a gas-filled cavity will ring. This ringing can be detected by a hydrophone and its amplitude is related to the energy of the collapse. Figure 5.2 shows the sonic signature received by a hydrophone placed at different distances from the bubble. The distance units are *cm* with the bubble being located at the position 13.8*cm*. Each signal has been offset in time in order to compensate for the different arrival times. The acoustic energy flux can be calculated at each location by converting the voltage to a pressure and then, assuming a sinusoidal, spherical source, the pressure to an intensity; finally, the intensity is integrated in time.

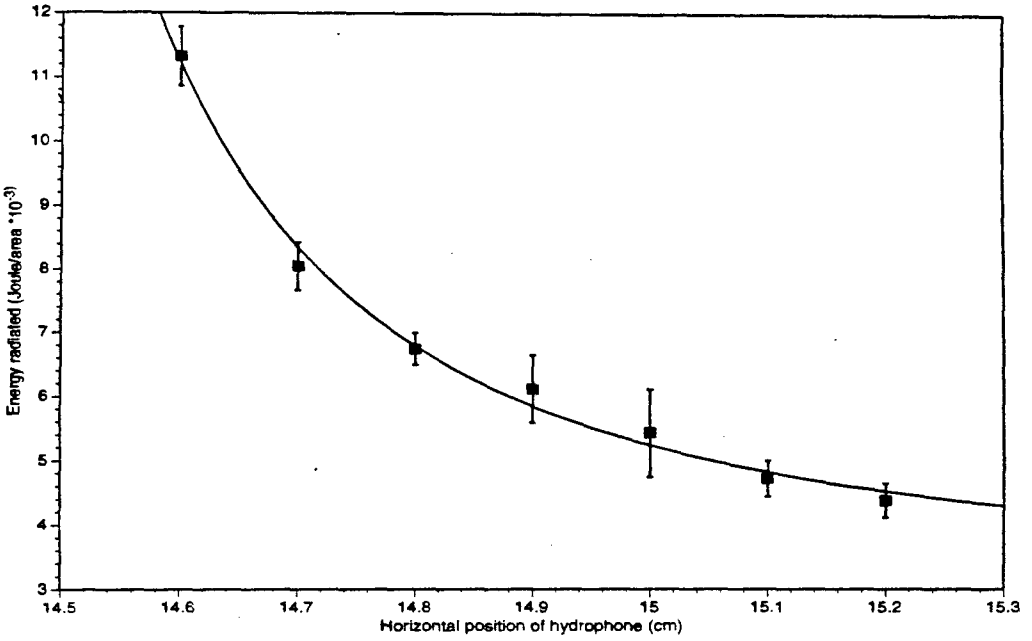

Figure 5.3. After being converted to an intensity, the sonic signature from a SBSL bubble was integrated in time to get the acoustic energy flux. The solid line, a fit to $\frac{1}{r^2}$, demonstrates that the flux is behaving in the manner of the inverse-square-law. The error bars represent the standard deviation in each measurement.

Figure 5.3 shows the acoustic energy flux at several distances from the bubble. (This data was taken at a different time than the data shown in Fig. 5.2, thus the difference in distances. The bubble is located at the position $14.2\,cm$.) The curve through the data is a fit to the equation $y = a/(r - r_0)^2 + b$; the values of a, b and r_0 being 1.3, 3.2 and 13.8, respectively. As expected, the flux decays as $\frac{1}{r^2}$, meaning that the bubble does behave as a spherical source and that there is reasonable certainty that the hydrophone is not being shock-excited by the bubble's collapse, which was a concern.[1] The offset-value, $b = 3.2$ for the decay curve corresponds to the noise floor. Once the acoustic energy flux is known, the total energy can be obtained by multiplying the flux with the area of a sphere centered at the bubble and extending to the hydrophone. The flux-offset corresponds to an offset of

[1] In fact, the risk of shock-exciting the hydrophone is minimal; the hydrophone is many source-radii from the bubble and the shock is expected to have decayed by the time it reaches the hydrophone. Had the hydrophone been shock-excited, a faster decay in the flux would have been observed.

$\approx 1.0^{-6}$ *Joules* in the total acoustic energy radiated by the bubble, but this value is not subtracted from the data to be presented.

5.3 The Experiments

Six sets of acoustic and electromagnetic radiation data were obtained using two different acoustic frequencies and three different DGC's over four different temperatures. A single batch of water with a given DGC could be used for each frequency and temperature, constituting two sets of data.

5.3.1 Procedure

The following procedure was followed when acquiring the data shown below:

(1) Clean[2] water was placed in the reservoir. The atmospheric pressure in the reservoir was reduced to a level just below that of the vapor pressure of water at room temperature and held constant; small bubbles aerated the water to enhance the "degassing" process. The water was degassed for $\frac{1}{2}$-hour, then the pressure in the reservoir was raised to the appropriate level for obtaining the desired DGC.

The value of the DGC's are given in terms of percentages of saturation at room temperature, *e. g.* the DGC of Fig. 5.4 is eight-percent of saturation at $22^{\circ}\,C$, loosely referred to as being 8%. To obtain a given DGC, the gas-pressure in the reservoir was set to the same percentage value as that of the desired DGC, *i. e.* for a DGC of 8%, the gas-pressure was set to be eight-percent of the atmospheric gas-pressure. The atmospheric gas-pressure is simply the barometric pressure minus the vapor pressure of water at room temperature.

[2] "Clean" will refer to de-ionized and filtered – to 0.1 μm – water.

Once the gas-pressure was set in the reservoir, it was held constant and the fluid aerated for another $\frac{1}{2}$-hour.

(2) After completing the degassing-regassing cycle, ambient pressure was restored to the reservoir. The levitation cell was filled with the prepared water via a peristaltic pump; the cell was flushed several times before filling completely, since usually a small amount of water was left in the cell in between batches of water. Since electrolysis was used to generate bubbles, a minute quantity of potassium chloride – about ten grains – was added to the water to bring the conductivity from 2.4 to 11.0 $\mu mho \cdot cm$.

(3) The acoustic energy was measured as described above;[3] the electromagnetic energy was measured by counting the number of photons per flash as described in Chapter 2. The method used to find values of the equilibrium radius and acoustic pressure amplitude was employed at each temperature and each frequency in order to off-set any temperature- or frequency-related effects on the low-frequency calibration of the hydrophone. Data was taken at room temperature, first at one frequency, then the other. The water was cooled and then data recorded again at each frequency. The process was repeated such that data was obtained at temperatures of about 21, 15, 10 and $5^{o}\,C$.

5.3.2 Presentation of Data

The Figs. 5.4 through Fig. 5.9 display the collected data; Table 5.1 has been supplied as a quick reference to the different figures. The upper plot of each figure shows the total number of photons emitted per flash as a function of acoustic pressure for each temperature. The lower plots are similar except that they show the acoustic-pressure-dependence of the total

[3] The distance from the hydrophone to the bubble was obtained by measuring the time delay between the arrival of the light flash and the sonic signature. This distance was needed to know the area through which the flux was passing.

Table 5.1. Summary of data figures.

Figure	DGC (% of Saturation – room temperature)	Acoustic Frequency (kHz)
5.4	8	19
5.5	8	13
5.6	6	19
5.7	6	13
5.8	11	19
5.9	11	13

radiated acoustic energy. To facilitate comparisons between data sets, all the axis have identical limits between the sets.

The saturation concentration of air in water varies with temperature. This fact means that water prepared to have a DGC of 8% of saturation at $22^{o}\,C$ will have a DGC of 6% of saturation when the water has been cooled to $5^{o}\,C$. The reason for the change is that the total quantity of gas in the water was fixed when the water was at a temperature of $22^{o}\,C$ yielding a DGC of 8% of saturation, but that same quantity of gas yields a DGC of 6% of saturation when the water is cooled to $5^{o}\,C$. Similarly a DGC of 11% of saturation at $22^{o}\,C$ will be reduced to 8% of saturation at $5^{o}\,C$. The different values of the DGC – 6, 8 and 11% – were not selected arbitrarily; they were chosen for the very reason mentioned above. By using these values, it was possible to determine whether the temperature-related effects are related to changes in the relative DGC. Whereas the preceding six figures compared absolute quantities of gas, Figs. 5.10 and 5.11 compare relative DGC's.

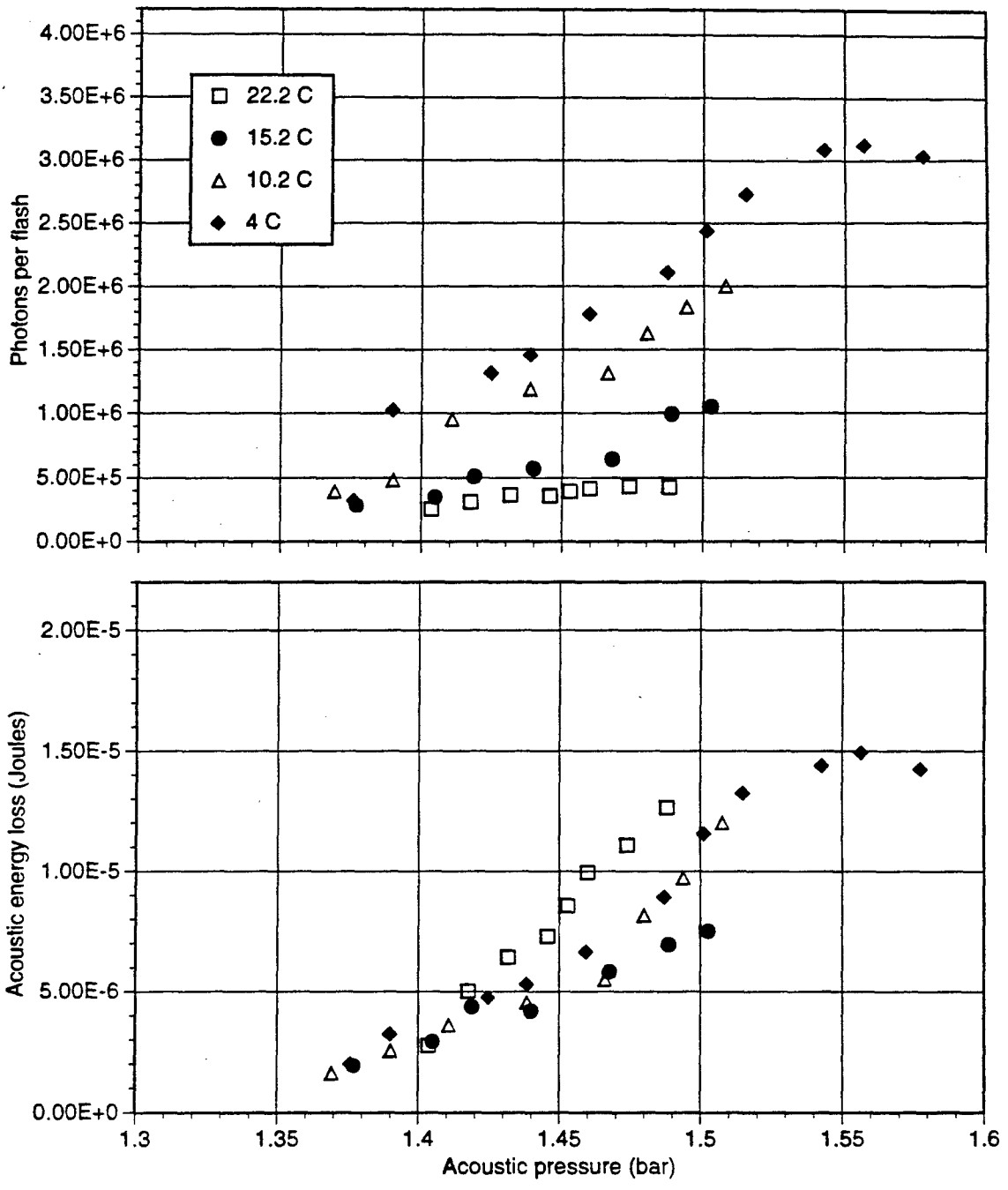

Figure 5.4. Acoustic and electromagnetic emission for water with a dissolved gas concentration (DGC) of 8% at room temperature; the driving frequency is $19\,kHz$. The different symbols represent the different temperatures at which the data was acquired.

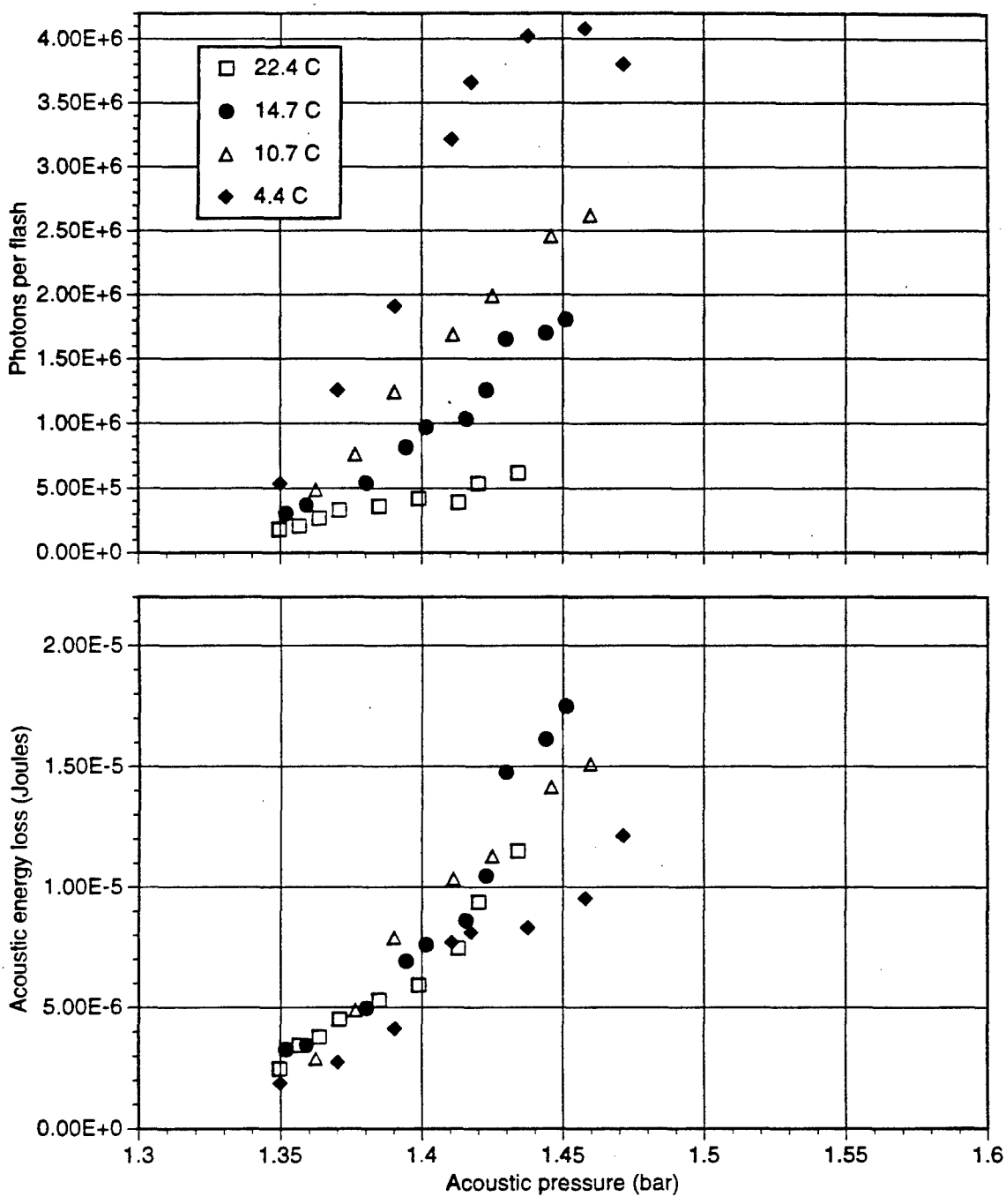

Figure 5.5. Acoustic and electromagnetic emission for water with a DGC of 8% at room temperature; the driving frequency is $13\,kHz$. The different symbols represent the different temperatures at which the data was acquired.

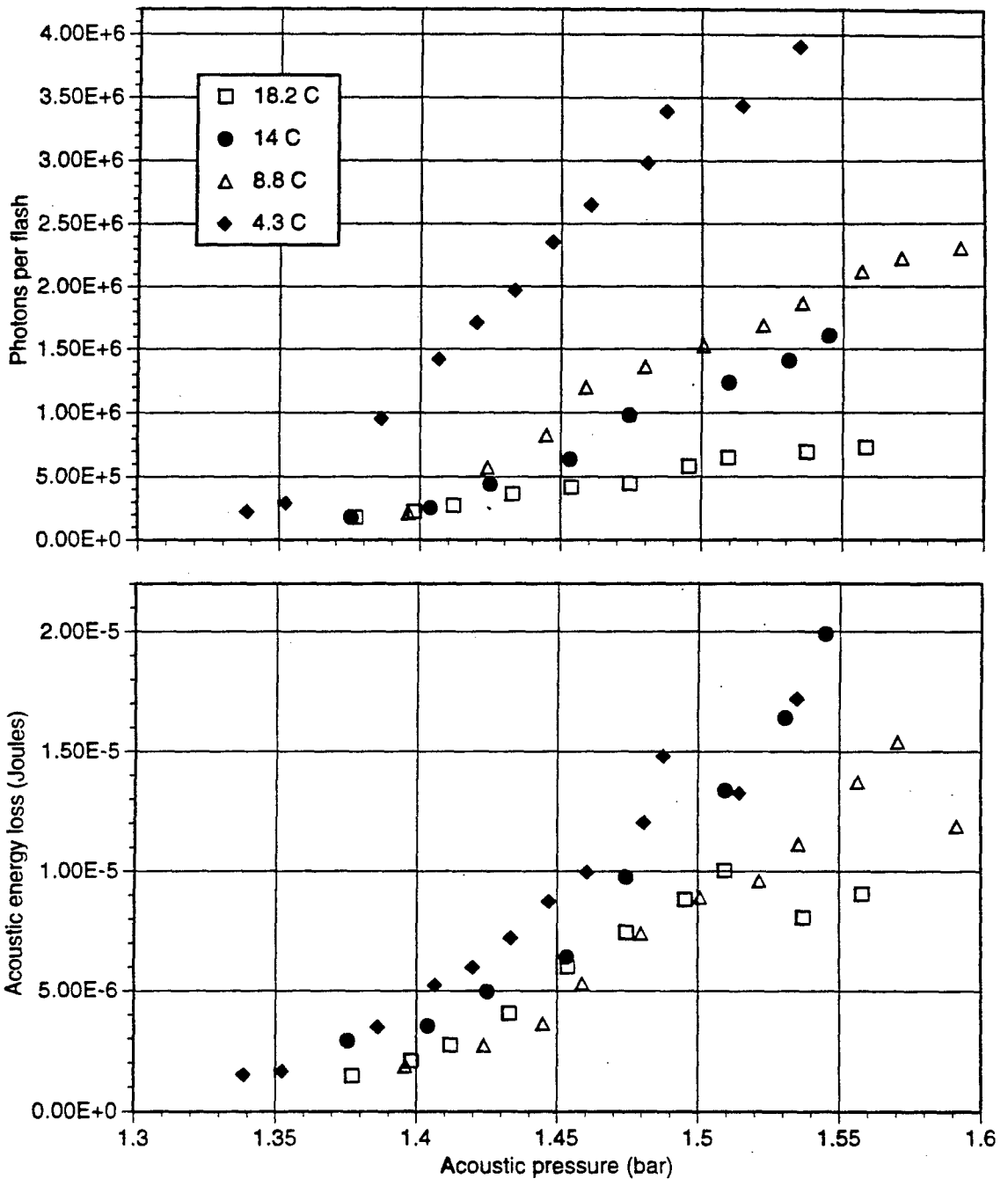

Figure 5.6. Acoustic and electromagnetic emission for water with a DGC of 6% at room temperature; the driving frequency is $19\,kHz$. The different symbols represent the different temperatures at which the data was acquired.

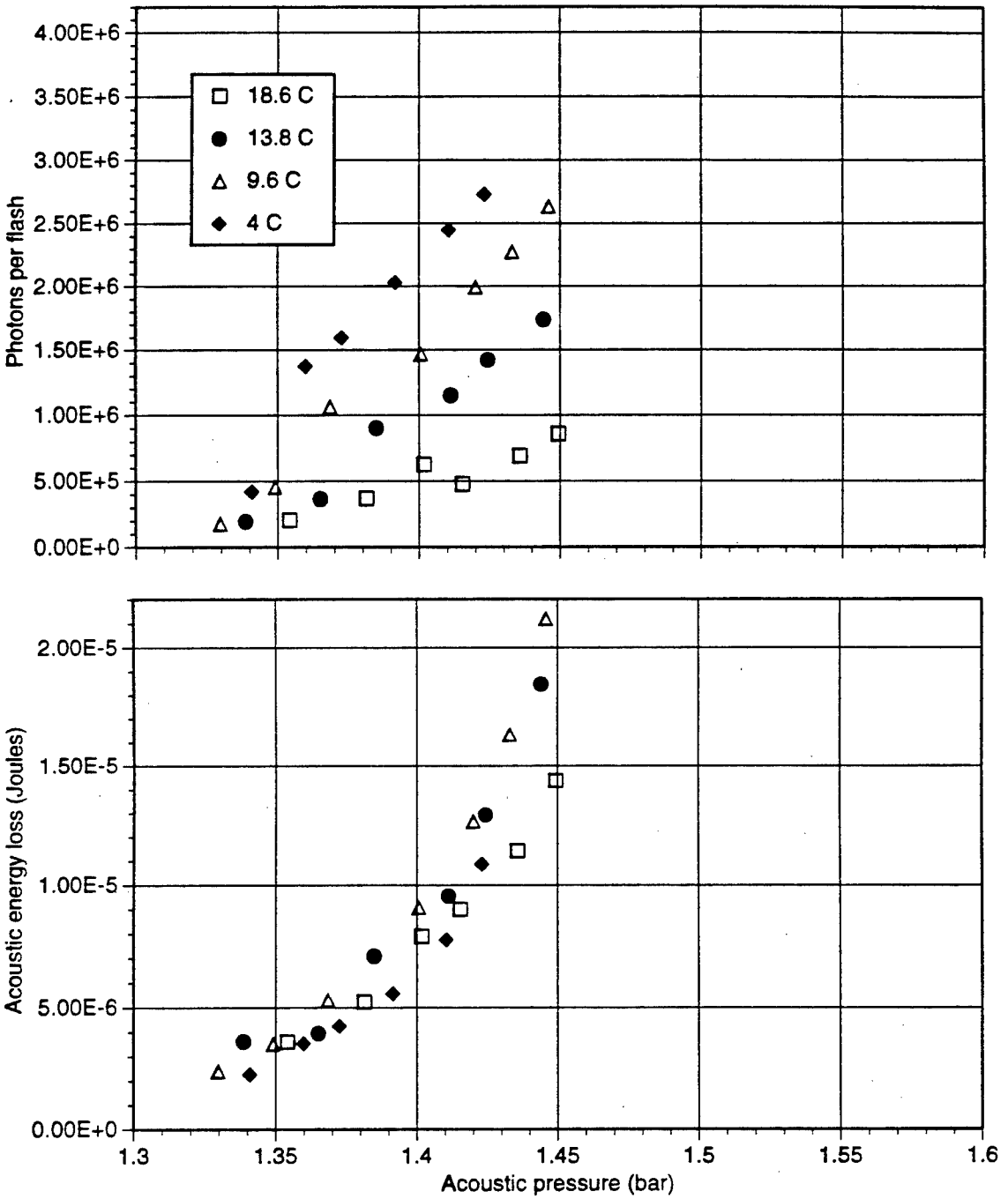

Figure 5.7. Acoustic and electromagnetic emission for water with a DGC of 6% at room temperature; the driving frequency is $13\,kHz$. The different symbols represent the different temperatures at which the data was acquired.

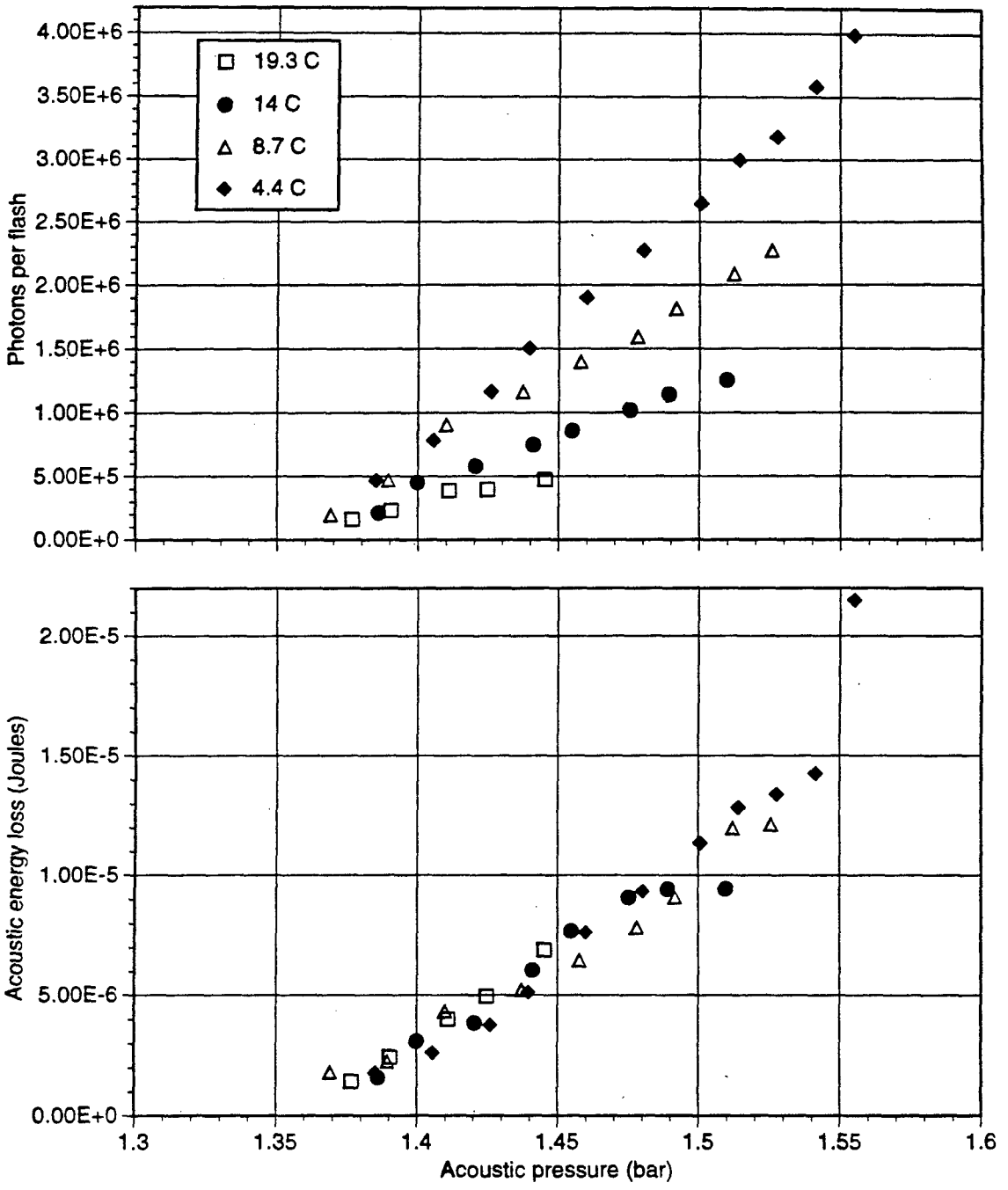

Figure 5.8. Acoustic and electromagnetic emission for water with a DGC of 11% at room temperature; the driving frequency is 19 kHz. The different symbols represent the different temperatures at which the data was acquired.

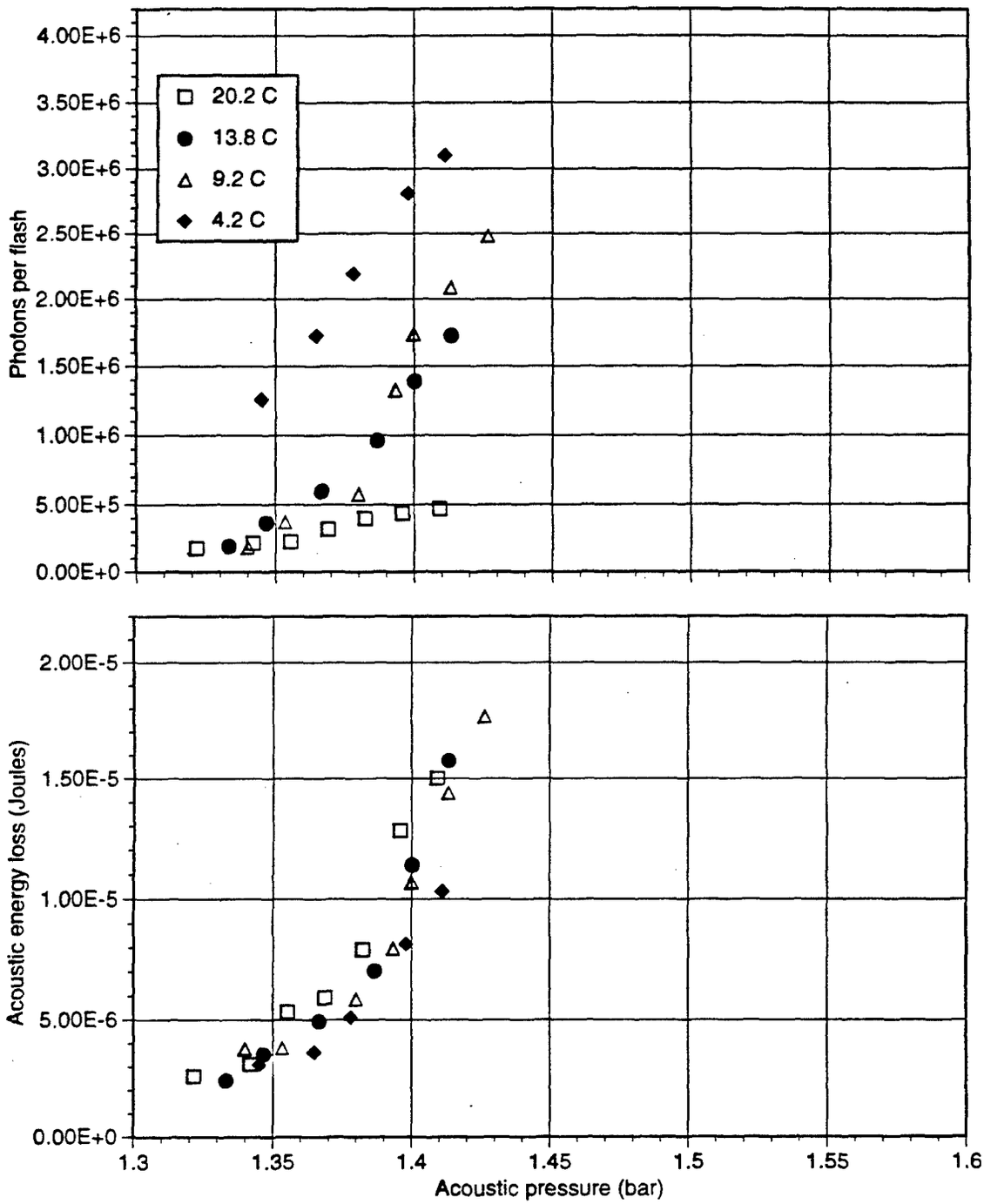

Figure 5.9. Acoustic and electromagnetic emission for water with a DGC of 11% at room temperature; the driving frequency is $13\,kHz$. The different symbols represent the different temperatures at which the data was acquired.

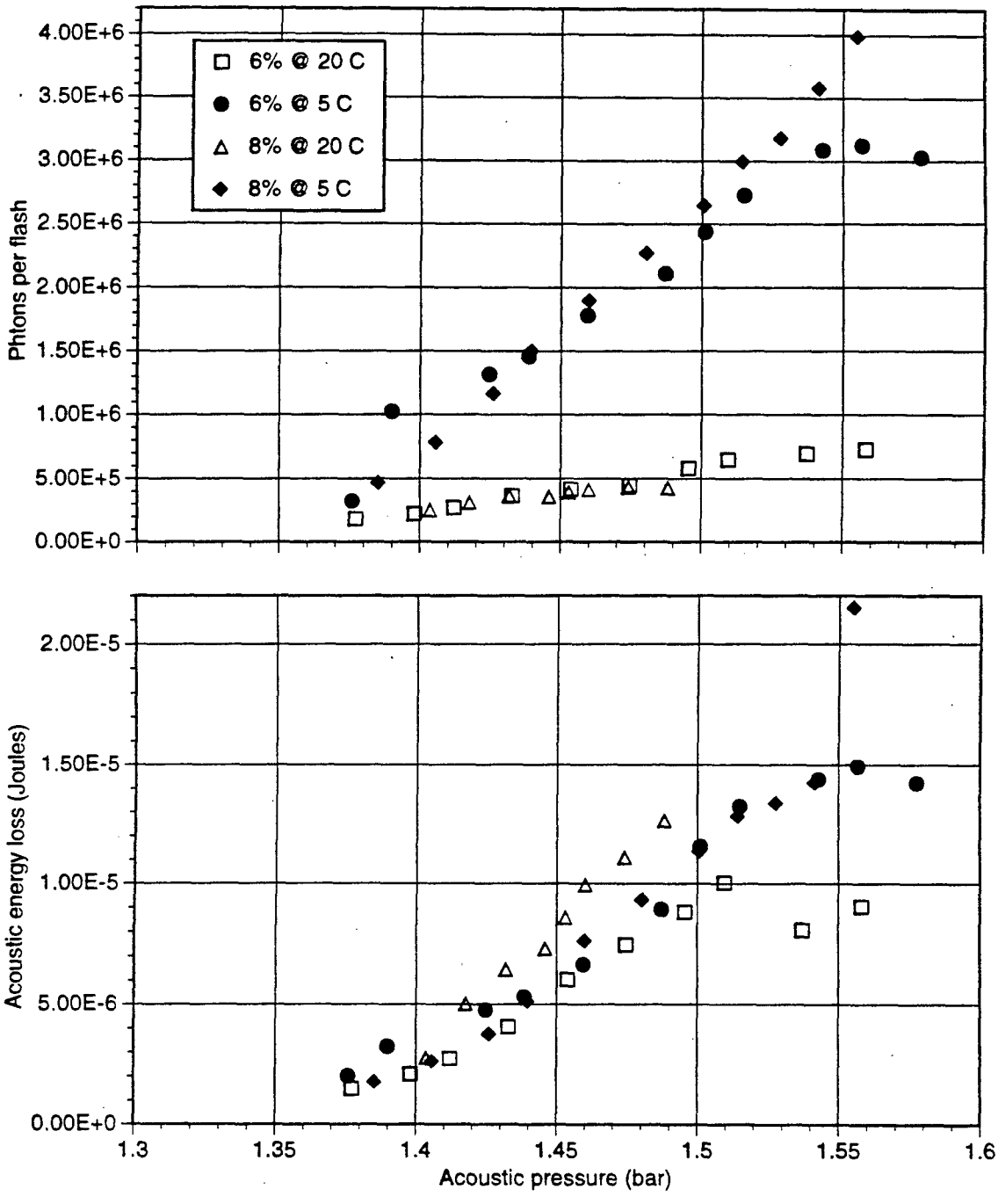

Figure 5.10. Comparison of the effects of the relative DGC for two different temperatures; the frequency is $19\,kHz$. This data is assimilated from data in Figs. 5.4, 5.6 and 5.8. See text for details.

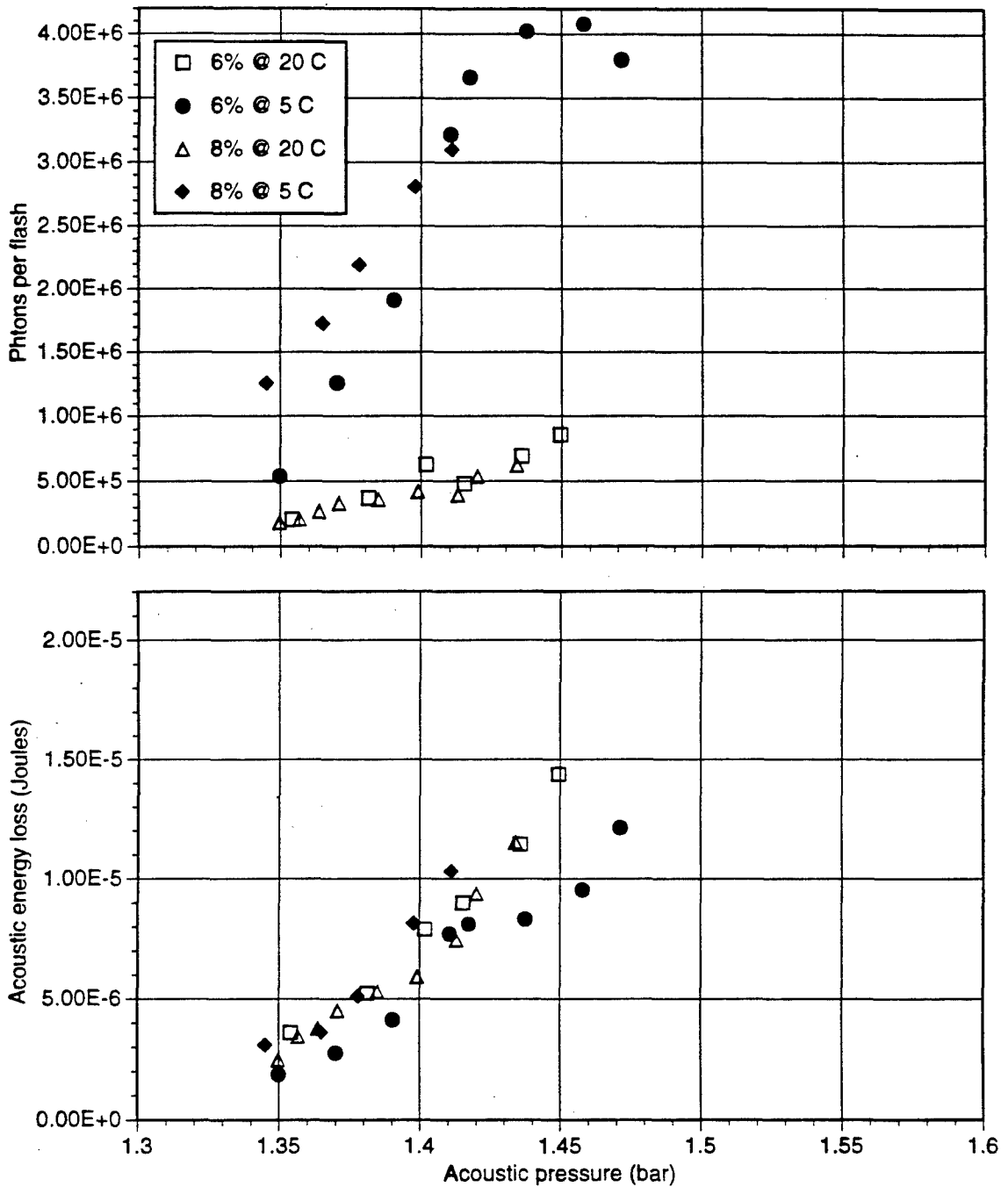

Figure 5.11. Comparison of the effects of the relative DGC for two different temperatures; the frequency is 13 kHz. This data is assimilated from data in Figs. 5.5, 5.7 and 5.9. See text for details.

Table 5.2. Values of the equilibrium radius, R_0; values are given in microns. The average value for $19\,kHz$ is $3.19\,\mu m$; the average for $13\,kHz$, $2.95\,\mu m$.

Water Temperature (C^o)	Frequency (kHz)	R_0 - 6%	R_0 - 8%	R_0 - 11%
20	19	3.30	3.40	3.30
	13	3.4 0	3.10	2.50
14	19	3.30	3.35	3.20
	13	3.30	3.30	2.80
9	19	3.20	3.50	3.00
	13	3.45	2.65	2.50
4	19	3.00	2.60	3.15
	13	2.90	2.70	2.75

5.4 Discussion

In this section, the effects of frequency, temperature, DGC and acoustic pressure will be discussed for the data obtained.

5.4.1 Effects of Frequency

The values of equilibrium radii were measured for the data sets collected; each these values, shown in Table 5.4.1, was found for only one acoustic pressure amplitude and assumed to be constant for that individual set of data. The average equilibrium radius for the $19\,kHz$ data is $3.19\,\mu m$; the average for the $13\,kHz$ data, $2.95\,\mu m$. The Physical Acoustics Group at the University of California at Los Angeles (UCLA) has consistently reported equilibrium radii of about $4.5\,\mu m$ for frequencies around $25\,kHz$ [65, 20]. The trend is that the value of R_0 decreases with decreasing frequency.

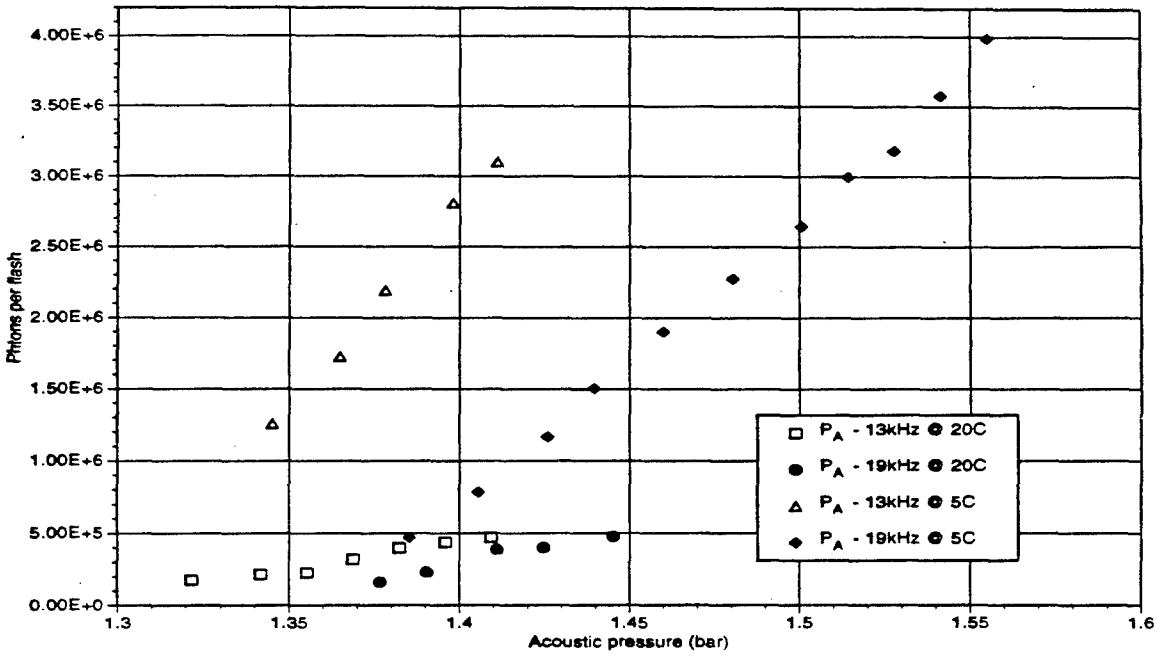

Figure 5.12. Acoustic and electromagnetic emission for water at 5 and 20° C using two different frequencies. The solid symbols are for data using 19 kHz, and the open symbols, 13 kHz.

Although detailed investigations of the maximum radius were not undertaken in this study because of measurement difficulties discussed in Chapter 2, it was noted that the maximum radius increased with decreasing frequency. The UCLA group, working at frequencies around 25 kHz, reports maximum radii of about 40 μm [65, 20]. In this investigation, the maximum radii were typically 55 and 65 μm at the driving frequencies of 19 and 13 kHz, respectively.[4]

Figure 5.12 shows the light emitted by a SBSL bubble and compares two different frequencies, 13 and 19 kHz. The DGC for this data was 11%. The trends seen in this figure can also be seen in the previous figures, but this figure is presented in order to help clarify one particular observation about all of this data. That trend is that for the data obtained in this study, the most notable frequency-related effect appears to be that the

[4] Of course the maximum radius is a function of acoustic pressure.

range of operational acoustic amplitudes changes. For the lower frequency, the range is both smaller and shifted toward lower pressure amplitudes. Thus for a given value of P_A, a bubble driven at a lower frequency would emit more light than that driven at the higher frequency. Note, however, that the maximum amount of light radiated by a bubble for a given set of conditions shows little variation with frequency.

5.4.2 Effects of Temperature

Of the different parameters examined in this study, the temperature had the strongest effect upon a bubble's light-emitting behavior. An unexpected result comes from comparing the luminosity and the acoustic energy over the range of temperatures. That result is this: temperature has a strong effect on the luminosity, but virtually none on the acoustic energy. This suggests that the macroscopic motion of the bubble is not strongly related to the temperature, but that the internal gas dynamics are. In a private communication, William Moss of Lawrence Livermore National Laboratory suggested, prior to getting these results, that the temperature-related effects could be caused by the role played by water vapor in shock-wave propagation inside the bubble. The vapor pressure determines the amount of water vapor inside the bubble. If the vapor pressure is low, then there will be little water vapor inside the bubble. The presence of the water vapor reduces the temperatures and pressures generated by an interior shock-wave. Calculation of the temperatures and pressures inside the bubble is outside the scope of this work.

When all the figures are compared, it is clear that the temperature-related effects are not associated with the relative values of the DGC. The DGC seems to slightly decrease the value of the equilibrium radius, but the scatter in this data prohibits suggesting anything more. The temperature also has a small effect upon the value of R_0, but again, the data is

not good enough to be definitive.

5.4.3 Effects of Pressure Amplitude

As was mentioned above, the operational range of acoustic pressures is strongly dependent upon frequency. The range at 19 kHz extends from 1.35 to more than 1.55 bar; while at 13 kHz the range extends from 1.32 to 1.46 bar. The higher frequency has a more extensive range and is centered at a higher pressure amplitude than the lower frequency. If the trend seen here suggests the possibility that there may exist a low frequency limit to SBSL.

Curiously, the luminosity increases linearly with the pressure amplitude; the slope appears to depend upon the temperature. This linearity suggests that there is a well-defined "turn-on" point at which the bubble will begin to emit light – a luminosity threshold. The threshold has values of 1.3 and 1.35 bar for the frequencies 13 and 19 kHz. The radiated acoustic energy, however, does not exhibit a linear dependence on the pressure amplitude, but a dependence which appears to be exponential; and, it does not appear to go to zero. The fact that the radiated acoustic energy does not go to zero is not surprising, but instead, is expected since acoustic-radiation-damping is experienced by the bubble regardless of luminescence.

5.5 Conclusions

Several observations were made above concerning the acoustic and electromagnetic radiation from a SBSL bubble. Future work would entail investigation of a wider range of frequencies, as was mentioned earlier, and even a broader range of temperatures. Additionally, it would be very interesting to obtain spectra of the emitted light over these ranges of frequencies and temperatures; optical spectra may reveal something about the changes in internal

temperature.

Chapter 6

Final Conclusions

This thesis has examined three different areas of the behavior of SBSL bubbles: acoustic levitation, translational motion, and the light and sound they emit. The purpose has been to address such questions as: Do SBSL bubbles levitate acoustically in the same manner as that of bubbles whose radial motion is linear? What affect would translation have on the behavior of SBSL bubbles? And, what can be learned by examining the acoustic radiation of a SBSL bubble? This chapter presents a brief recapitulation of each of the principle chapters.

6.1 Acoustic Levitation

In this chapter it was shown that standard linear theory for predicting the equilibrium position of a bubble fails for the case of a sonoluminescing bubble. The two forces acting on a bubble in a standing acoustic wave are the buoyancy and the Bjerknes forces. The Bjerknes force is a dynamic buoyancy caused by interaction between the oscillating radial motion of the bubble and a pressure gradient. A bubble can be stably levitated against gravity if the time-average of the net force is zero.

Eller's [39] analytical theory for predicting the vertical equilibrium position at which a bubble can be acoustically levitated is only valid for bubbles with linear radial motion; he used analytical expressions describing the bubble's radial motion in his derivation. His theory predicts that the location of the vertical equilibrium position should approach that of the pressure antinode asymptotically as the amplitude of the acoustic pressure increases. SBSL bubbles, however, do not experience linear radial pulsations; they oscillate non-linearly.

Once the non-linear nature of the bubble's behavior was taken into account, an equilibrium position could be found by using numerical solutions to a bubble's radial motion. The locations of the vertical equilibrium positions for SBSL bubbles, it turns out, move away from the location of the antinode. The predictions for the equilibrium position given by this non-linear approach were verified experimentally. Furthermore, it was demonstrated that the balance between Bjerknes and buoyancy forces provides a theoretical limit to the amplitude of the acoustic pressure that can be applied to a bubble. (See Chapter 3 for details.)

6.2 Translational Motion

In this chapter, the vertical location of a SBSL bubble was treated in a dynamic way, building on the work of Watanabe and Kukita [48], who investigated the translation of bubbles of near-resonance size and found a regime of "chaotic" translation. This work has suggested that the motion of such bubbles is probably not "chaotic", but periodic; the difference is due to use by Watanabe and Kukita of a less-accurate bubble dynamics equation. Numerical studies of the translation of SBSL bubbles indicates that the bubbles could experience accelerations with magnitudes of thousands of "g's" during the collapse of the bubble. These high accelerations occur when the pressure amplitude on the bubble is

increased and the bubble must move from one position of vertical equilibrium to another.

SBSL bubbles can suffer extinction if the applied acoustic pressure amplitude is too large; this extinction threshold is very sharply defined. Investigation of the translation of SBSL bubbles has revealed a possible mechanism for the extinction threshold: rapid translation during bubble collapse can lead to a loss of spherical integrity of the bubble. If the extent of the loss of sphericity is significant enough, it can lead to the destruction of the bubble during the final stages of collapse. Implementing these ideas had mixed success when trying to reproduce the extinction thresholds seen in the laboratory.

6.3 Sights and Sounds

SBSL bubbles emit both sound and light. The light is generated upon bubble collapse via a mechanism which is subject to debate. The sound radiated by the bubble is also generated by the collapse of the bubble: the bubble collapse radiates a shock-wave into the fluid as well as shock-exciting the bubble so that it "rings" at a certain frequency. The emitted light can be quantitatively evaluated using a photomultiplier tube; the sound also, via a small hydrophone placed near the bubble. Measurements of the acoustic energy and the number of photons radiated by the bubble were made over a variety of different experimental conditions.

The observed role of the frequency in this limited study was to alter the range of operational acoustic amplitudes. The lower frequency data had a shorter and lower range than the higher frequency. Although the maximum radius attained by SBSL bubbles was observed to increase with decreasing frequency, the equilibrium radius, and consequently the number of gas molecules, decreased.

In this study, dissolved gas concentration was found to have little effect upon the light

and sound emitted. The water temperature has little effect on the sound produced, but a very strong effect on light production. Hiller [1] first studied the effects of temperature on the quantity of light produced by a SBSL bubble. Since the acoustic energy radiated by the bubble seemed unaffected by the temperature of the water, a reasonable conclusion to be drawn is that the mechanism responsible for the observed temperature-related effects is related to the gas dynamics inside the bubble, most likely the role of water vapor. The vapor pressure, which depends strongly on the temperature of the water, determines the amount of water vapor inside the bubble. If the vapor pressure is low, then there will be little water vapor inside the bubble. The presence of the water vapor reduces the temperatures and pressures generated by an interior shock-wave.

6.4 Closing Remarks

This study has examined three previously unexplored aspects of SBSL. The data obtained and the theories developed here have expanded the body of knowledge of SBSL behavior and revealed new questions to be addressed in the future. This work is one of many steps, past, present and future, leading to a complete understanding of the phenomenon of single-bubble sonoluminescence.

Bibliography

Bibliography

[1] R. Hiller, S. J. Putterman, and B. P. Barber, "Spectrum of synchronous picosecond sonoluminescence," Phys. Rev. Lett. **69**, 1182 (1992).

[2] S. D. Lewia, Master's thesis, Naval Postgraduate School, 1992.

[3] K. S. Suslick, "Sonochemistry.," Science **247**, 1373 (1990).

[4] K. S. Suslick and D. A. Hammerton, "The site of sonochemical reactions," IEEE Transactions on Ultrasonics, Ferroelectrics and Frequency Control - UFFC **33**, 143 (1986).

[5] L. A. Crum, "Sonophysics, sonochemistry and sonoluminescence," J. Acoust. Soc. Am. **95**, 559 (1994).

[6] M. Marinesco and J. J. Trillat, Comptes. Rendus Acad. Sci. **196**, 858 (1933).

[7] J. Frenzil and H. Schultes, Zeit fur Phys. Chem. **B26**, 421 (1934).

[8] E. Meyer and H. Kuttruff, Zeit angew. Phys. **11**, 325 (1959).

[9] D. F. Gaitan, L. A. Crum, C. C. Church, and R. A. Roy, "Sonoluminescence and bubble dynamics for a single, stable, cavitation bubble," J. Acoust. Soc. Am. **91**, 3166 (1992).

[10] B. P. Barber and S. J. Putterman, "Observation of synchronous picosecond sonoluminescence," Nature **352**, 318 (1991).

[11] B. P. Barber, R. Hiller, K. Arisaka, H. Fetterman, and S. Putterman, "Resolving the picosecond characteristics of sonoluminescence," J. Acoust. Soc. Am. **91**, 3061-3 (1992).

[12] M. J. Moran, R. E. Haigh, M. E. Lowry, D. R. Sweider, G. R. Abel, J. T. Carlson, S. D. Lewia, A. A. Atchley, D. F. Gaitan, and X. K. Mariyama (unpublished).

[13] V. H. Arakeri, "Effect of dissolved gas content on single bubble sonoluminescence," Pramana - J. of Phys. **40**, L145 (1993).

[14] R. Hiller, K. Weninger, S. J. Putterman, and B. P. Barber, "Effect of noble gas doping," Science **266**, 248 (1994).

[15] V. H. Arakeri, "Influence of various gases on single bubble sonoluminescence," Pramana - J. of Phys. **41**, L291 (1993).

[16] B. E. Noltingk and E. A. Neppiras, "Cavitation produced by ultrasonics," Proc. Phys. Sec. B **63B**, 674 (1950).

[17] E. A. Neppiras and B. E. Noltingk, "Cavitation produced by ultrasonics: theoretical conditions for the onset of cavitation," Proc. Phys. Sec. B **64B**, 1032 (1951).

[18] C. C. Wu and P. H. Roberts, "Shock-wave propagation in a sonoluminescent gas bubble," Phys. Rev. Lett. **70**, 3424 (1993).

[19] H. P. Greenspan and A. Nadim, "On sonoluminescence of an oscillating gas bubble," Phys. Fluids A **5**, 1065 (1993).

[20] B. P. Barber and et. al., "Sensitivity of sonoluminescence ot experimental parameters," Phys. Rev. Lett. **72**, 1380–3 (1994).

[21] T. K. Saksena and W. L. Nyborg, "Sonoluminescence from stable cavitation," J. Chem. Phys. **53**, 1722 (1970).

[22] M. A. Margulis, "The nature of sonochemical reaction and sonoluminescence," Advances in Sonochemistry **1**, 39 (1990).

[23] T. LePoint and F. Mullie, "What exactly is cavitation chemistry?," Ultrasonics Chemistry **1**, S13 (1994).

[24] R. A. Roy, "Physical aspects of sonoluminescence from acoustic cavitation," Ultrasonics Sonochemistry **1**, 5 (1994).

[25] L. A. Crum, "Sonoluminescence," Physics Today **47**, 22 (1994).

[26] S. M. Cordry and L. A. Crum, a chapter to appear in "Luminescing Solids," edited by D. R. Vij. (unpublished).

[27] B. K. Novikov, O. V. Rudenko, and V. I. Timoshenko, *Nonlinear Underwater Acoustics* (American Institute of Physics, New York, 1978).

[28] T. Hickling and M. S. Plesset, Phys. Fluids **7**, 7 (1964).

[29] M. S. Plesset and R. B. Chapman, "Collapse of an initially spherical vapour cavity in the neighbourhood of a solid boundary," J. Fluid Mech. **47 Pt. 2**, 283 (1971).

[30] H. C. Pumphrey and J. E. Ffowcs-Williams, "Bubbles as sources of ambient noise," IEEE J. of Oceanic Engineering **15**, 268 (1991).

[31] H. C. Pumphery and P. A. Elmore, "The entrainment of bubbles by drop impacts," J. Fluid Mech. **220**, 539 (1991).

[32] E. A. Neppiras, "Acoustic Cavitation," Phys. Rep. **61**, 1 (1980).

[33] H. G. Flynn, "Caviation dynamics. I. A mathematical formulation," J. Acoust. Soc. Am. **57**, 1379 (1975).

[34] L. A. Crum, "The polytropic exponent of gas contained within air bubbles pulsating in a liquid," J. Acoust. Soc. Am. **73 (1)**, 116 (1983).

[35] D. F. Gaitan, Ph.D. thesis, University of Mississippi, 1990.

[36] M. Strasberg, "On the onset of cavitation in tap water," J. Acoust. Soc. Am. **31**, 163 (1969).

[37] V. F. K. Bjerknes, *Di Kraftfelder* (Vieweg und Sohn, Braunsheig, Germany, 1909).

[38] V. F. K. Bjerknes, *Fields of Force* (Columbia University Press, New York, 1906).

[39] A. Eller, "Force on a bubble in a standing acoustic wave," J. Acoust. Soc. Am. **43**, 170 (1968).

[40] T. J. Asaki and P. L. Marston, "Acoustic radiation force on a bubble driven above resonance," J. Acoust. Soc. Am. **96**, 3096 (1994).

[41] R. K. Gould, "Simple method for calibrating small, omnidirectional hydrophones," J. Acoust. Soc. Am. **43**, 1185 (1968).

[42] L. V. King, Proc. R. Soc. Lond. **Ser. A 147**, 212 (1934).

[43] L. P. Gorkov, "On the forces acting on a small particle in an acoustical field in an ideal fluid," Sov. Phys. Dokl. **6**, 773 (1962).

[44] P. L. Marston, "Shape oscillation and static deformation of drops and bubbles driven by modulated radiation stresses - theory," J. Acoust. Soc. Am. **67**, 15 (1980).

[45] R. Löfstedt and S. J. Putterman, "Theory of long wave-length acoustic radiation pressure," J. Acoust. Soc. Am. **90**, 2027 (1991).

[46] K. Yosioka, T. Kawasima, and H. Hirano, Acustica **5**, 173 (1955).

[47] C. P. Lee and T. G. Wang, "Acoustic radiation force on a bubble," J. Acoust. Soc. Am. **93**, 1637 (1993).

[48] T. Watanbe and Y. Kukita, "Translational and radial motions of a bubble in an acoustic standing wave field," Phys. Fluids A **5 (11)**, 2682 (1993).

[49] A. L. Eller and L. A. Crum, "Instability of the motion of a pulsating bubble in a sound field," J. Acoust. Soc. Am. **47**, 762 (1970).

[50] L. A. Crum, "Bjerknes forces on bubbles in a stationary sound field," J. Acoust. Soc. Am. **57**, 1363 (1975).

[51] N. A. Pelekasis and J. A. Tsamopoulos, "Bjerknes forces between two bubbles. Part 1. Response to a step change in pressure," J. Fluid Mech. **254**, 467 (1993).

[52] N. A. Pelekasis and J. A. Tsamopoulos, "Bjerknes forces between two bubbles. Part 2. Response to an oscillatory pressure field," J. Fluid Mech. **254**, 501 (1993).

[53] R. M. Davies and G. I. Taylor, Proc. R. Soc. Lond. A **200**, 375 (1950).

[54] M. S. Longeut-Higins and H. F. Oguz, "Critical microjets in collapsing cavities," J. of Fluid Mech **290**, 183 (1995).

[55] M. S. Plesset and T. P. Mitchel, "On the stability of the spherical shape of a vapor cavity in a liquid," Q. Appl. Math. **13**, 419 (1956).

[56] A. Prosperettie and G. Seminara, "Linear stability of a growing or collapsing bubble in a slightly viscous liquid," Phys. Fluids **21 (9)**, 1465 (1978), shows role of viscocity in surface wave growth.

[57] A. V. Anilkumar, C. P. Lee, and T. G. Wang, "Stability of an acoustically levitated and flattened drop," Phys. Fluids A **5 (11)**, 2763 (1993).

[58] T. D. Taylor and A. Acrivos, "On the deformation and drag of a falling viscous drop at low Reynolds number," J. Fluid Mech. **18**, 466 (1964).

[59] L. A. Crum, "Rectified diffusion," Ultrasonics, September 215 (1984).

[60] C. C. Church, "Prediction of rectified diffusion during nonlinear bubble pulsations at biomedical frequencies," J. Acoust. Soc. Am. **83**, 2210 (1988).

[61] R. Löfstedt, B. P. Barber, and S. Putterman, "Rectified diffusion and single-bubble sonoluminescence," J. Acoust. Soc. Am. **94 (3 Pt. 2)**, 1793 (1993), paper presentation at 126th ASA meeting.

[62] R. Löfstedt, K. Weninger, S. Putterman, and B. P. Barber, "Does a sonoluminescing bubble obey mass diffusion?," To be published .

[63] A. Eller and H. G. Flynn, "Rectified diffusion during nonlinear pulsations of cavitation bubbles," J. Acoust. Soc. Am. **37**, 493 (1965).

[64] P. Jarman, "Measurements of sonoluminescence from pure liquids and some aqueous solutions," Proc. Phys. Soc. **73**, 628 (1959).

[65] B. P. Barber and S. J. Putterman, "Light scattering measurements of the repetitive supersonic implosion of a sonoluminescent bubble," Phys. Rev. Letters **69**, 3839–42 (1992).

Modes in an infinite binary -gas mixture

Yi Mao

Department of Physics and Astronomy, University of Mississippi, University, MS 38677

Lawrence A. Crum and Ronald A. Roy

Applied Physics Laboratory, University of Washington, Seattle, WA, 98105

Solutions are obtained from fundamental equations for an infinite fluid of two component gases. Thermal conductivity, viscosity and mutual mass diffusion are simultaneously taken into account. Four modes are acquired in solving the linearized equations. Except for a small change in their dispersion relationship, three of them, acoustic, entropy, and vorticity modes, which were found in a mono-gas medium, also exist in a binary-gas medium. Only one of them, mass diffusion mode, is unique in a binary-gas mixture. In a linear region, each mode can independently propagate in a bulk of a binary-gas medium without interactions of one another, and their interactions happens only through a boundary. Because of the independence of these modes, a general solution in a binary-gas mixture is a superposition of these four modes. Dispersion relationship for each mode is derived in the limit of smallness of the three defined parameters $\varepsilon_\mu, \varepsilon_\lambda$ and ε_κ. The classical attenuation coefficient actually contains an additional term reflecting mass-diffusion loss, which is negligible in air but can be comparably large in some other circumstances.

PACS number: 43.25.Yw, 43.20.Ks

Introduction

Modal wave fields in a simple mono-gas medium were solved by Pierce [1989]. Three modes, acoustical, entropy and vorticity modes, were found independently to propagate in the medium. Conceptually, these three modes were treated equally and were similar to a longitudinal wave and shear waves in a homogeneous solid. They were directly derived from linear fundamental equations with fewer assumptions. Therefore, the solutions were more mathematically rigorous than that obtained when sound propagation, thermal conduction and viscosity was considered separately. The decomposition of wave fields in a simple gas medium was according to these modes as component fields rather than physical parameters such as temperature, pressure, densities, velocity because each mode may involve the variations of all these physical parameters. This description of wave fields has wide applications in study of acoustical properties near a interface, for example sound reflection from a surface, sound propagation in a duct, etc.[Pierce, 1989 and references mentioned].

In this paper, we will show that the modal wave field decomposition in a binary-gas mixture is also possible. First, fundamental equations are introduced for a binary-gas fluid. They include equations of the mass conservation for each constituent gas, the Navier-Stokes equation, the Kirchhoff-Fourier (thermal diffusion and energy conservation) equation, the mutual mass diffusion equation, and some thermodynamic relations. Then, these fundamental equations are linearized. The rotational motion and irrotational motiom were separated at first. By assuming a simple harmonic frequency field in these linear equations, we abtain the conditions for the linear equations to have a solution. These conditions result in only four dispersion relations: one for rotational motion and three for irrotational motion. Each dispersion relation gives rise a solution of the linear equations, i.e., a mode propagating independently in the mixture. Therefore, any harmonic wave can be represented as a superposition of these four modes.

The solutions are typically useful in handling acoustical properties near a wet interface. The medium near a wet surface can be viewed as a mixture of two gases--vapor and un-condensable gas. One application of the solutions is to an bubble system, which has two regions separated by an interface. The inner region is a vapor-gas mixture and the solutions are applicable. By joining two region solutions at the bubble surface, we are able to calculate the natural frequency and the damping constant of a bubble of any composition of vapor and gas [Mao, et al., 1996a]. Another application is in the study of sound attenuation due to evaporation and condensation in a narrow tube [Mao, et al., 1996b]. This is the simplest model for the investigation of sound propagation in a wet porous medium such as soil, sediment, etc..

Finally, we brief an additional term in the classical attenuation coefficient in a binary-gas mixture. The term is negligible small in air (considered as a binary-gas mixture of N_2 and O_2). It become comparatively large when two gases have nearly equal densities but a big difference of molecular masses.

Fundamental equations

We denote the molecular mass by m, the molecular number density by n, the density by ρ, and the velocity by $\vec{\mathbf{v}}$. The quantities for the two gases will be labeled by subscript *1* and subscript *2*. respectively. The quantities without a subscript are for the mixture. We have the following relations among those quantities:

$$\rho = \rho_1 + \rho_2, \tag{1}$$

$$n = n_1 + n_2, \tag{2}$$

$$n_1 = \frac{\rho_1}{m_1}, \tag{3}$$

$$n_2 = \frac{\rho_2}{m_2}, \tag{4}$$

and, $$\vec{\mathbf{v}} = \frac{\rho_1}{\rho}\vec{\mathbf{v}}_1 + \frac{\rho_2}{\rho}\vec{\mathbf{v}}_2 . \tag{5}$$

The fundamental fluid equations for a binary-gas mixture [Hsieh, 1965] contain the mass conservation law for each individual gas,

$$\frac{\partial \rho_1}{\partial t} + \nabla \cdot (\rho_1 \vec{\mathbf{v}}_1) = 0, \tag{6}$$

$$\frac{\partial \rho_2}{\partial t} + \nabla \cdot (\rho_2 \vec{\mathbf{v}}_2) = 0, \tag{7}$$

the Navier-Stokes equation,

$$\rho \frac{D\vec{\mathbf{v}}}{Dt} = -\nabla p + \mu \nabla^2 \vec{\mathbf{v}} + (\frac{\mu}{3} + \beta)\nabla(\nabla \cdot \vec{\mathbf{v}}), \tag{8}$$

the Kirchhoff-Fourier equation,

$$\rho \frac{Du}{Dt} - \frac{p}{\rho}\frac{D\rho}{Dt} = \frac{\mu}{2}\sum_{ij}(\frac{\partial v_i}{\partial x_j} + \frac{\partial v_j}{\partial x_i} - \nabla \cdot \vec{v}\,\delta_{ij})^2 + \lambda \nabla^2 T$$

$$- kT[\frac{n_1}{\gamma_1 - 1}\nabla \cdot (\vec{\mathbf{v}}_1 - \vec{\mathbf{v}}) + \frac{n_2}{\gamma_2 - 1}\nabla \cdot (\vec{\mathbf{v}}_2 - \vec{\mathbf{v}})], \tag{9}$$

the mass diffusion equation,

$$\vec{\mathbf{v}}_1 - \vec{\mathbf{v}}_2 = -\frac{n^2}{n_1 n_2} D_{12}(\nabla \frac{n_1}{n} + \frac{n_1 n_2 (m_2 - m_1)}{n\rho P}\nabla P), \tag{10}$$

where μ, β, λ, and D_{12} are respectively the coefficients of shear viscosity, bulk viscosity, thermal conductivity, and mutual diffusion, T the temperature, and $\frac{D}{Dt} = \frac{d}{dt} + \bar{\mathbf{v}} \cdot \nabla$.

Two more equations are about thermodynamic relations (the equation of state and the energy function). If the mixture is assumed as an ideal gas, we have

$$p = (\frac{\rho_1}{m_1} + \frac{\rho_2}{m_2})kT, \tag{11}$$

and

$$\rho u = (\frac{\rho_1}{m_1(\gamma_1 - 1)} + \frac{\rho_2}{m_2(\gamma_2 - 1)})kT. \tag{12}$$

where k is Boltzmann's constant, $\gamma$is the specific-heat ratio, u the internal energy per unit mass.

Linear Equations

For a small amplitude disturbance, we can expand the above fundamental equations at the equilibrium values of physical quantities, keep the zeroth- and the first-order terms, and discard higher-order terms. The zeroth-order terms are for the equilibrium and the first order terms for the disturbances. We assume that the state is homogeneous and quiescent. A bar "-" or a tilde "~" over a physical quantity indicate its equilibrium value or its disturbance respectively. Because the equilibrium values of $\bar{\mathbf{v}}, \bar{\mathbf{v}}_1$ and $\bar{\mathbf{v}}_2$ are zero, no "~" is needed to denote their disturbances. Collecting the first order terms in each expanded equation, we have the linear equations for disturbances as follows:

$$\tilde{\rho} = \tilde{\rho}_1 + \tilde{\rho}_2, \tag{1a}$$

$$\tilde{n} = \tilde{n}_1 + \tilde{n}_2, \tag{2a}$$

$$\tilde{n}_1 = \frac{\tilde{\rho}_1}{m_1}, \tag{3a}$$

$$\tilde{n}_2 = \frac{\tilde{\rho}_2}{m_2}, \tag{4a}$$

$$\bar{\mathbf{v}} = \frac{\bar{\rho}_1}{\bar{\rho}}\bar{\mathbf{v}}_1 + \frac{\bar{\rho}_2}{\bar{\rho}}\bar{\mathbf{v}}_2, \tag{5a}$$

$$\frac{\partial \tilde{\rho}_1}{\partial t} + \bar{\rho}_1 \nabla \cdot \bar{\mathbf{v}}_1 = 0, \tag{6a}$$

$$\frac{\partial \tilde{\rho}_2}{\partial t} + \bar{\rho}_2 \nabla \cdot \bar{\mathbf{v}}_2 = 0, \tag{7a}$$

$$\bar{\rho}\frac{\partial \tilde{\mathbf{v}}}{\partial t} = -\nabla \tilde{p} + \mu \nabla^2 \tilde{\mathbf{v}} + (\frac{\mu}{3} + \beta)\nabla(\nabla \cdot \tilde{\mathbf{v}}), \tag{8a}$$

$$\bar{\rho}\frac{\partial \tilde{u}}{\partial t} - \frac{\bar{p}}{\bar{\rho}}\frac{\partial \tilde{\rho}}{\partial t} = \lambda \nabla^2 \tilde{T} - k\bar{T}[\frac{\bar{n}_1}{\gamma_1 - 1}\nabla \cdot (\tilde{\mathbf{v}}_1 - \tilde{\mathbf{v}}) + \frac{\bar{n}_2}{\gamma_2 - 1}\nabla \cdot (\tilde{\mathbf{v}}_2 - \tilde{\mathbf{v}})], \tag{9a}$$

$$\tilde{\mathbf{v}}_1 - \tilde{\mathbf{v}}_2 = -\frac{\bar{n}^2}{\bar{n}_1 \bar{n}_2} D_{12}(\frac{\bar{n}\nabla \tilde{n}_1 - \bar{n}_2 \nabla \tilde{n}}{\bar{n}^2} + \frac{\bar{n}_1 \bar{n}_2 (m_2 - m_1)}{\bar{n}\bar{\rho}\bar{P}}\nabla \tilde{p}), \tag{10a}$$

$$\frac{\partial \tilde{P}}{\partial t} = \bar{n}k\frac{\partial \tilde{T}}{\partial t} - k\bar{T}(\bar{n}_1 \nabla \cdot \tilde{\mathbf{v}}_1 + \bar{n}_2 \nabla \cdot \tilde{\mathbf{v}}_2), \tag{11a}$$

$$\bar{\rho}\frac{\partial \tilde{u}}{\partial t} = (\frac{\bar{n}_1}{\gamma_1 - 1} + \frac{\bar{n}_2}{\gamma_2 - 1})k\frac{\partial \tilde{T}}{\partial t} + \frac{k\bar{T}}{\bar{\rho}}(\frac{\bar{n}_1 \bar{\rho}_2}{\gamma_1 - 1} - \frac{\bar{n}_2 \bar{\rho}_1}{\gamma_2 - 1})(\nabla \cdot \tilde{\mathbf{v}}_2 - \nabla \cdot \tilde{\mathbf{v}}_1). \tag{12a}$$

The other relationships for the equilibrium are obtained by collecting the zeroth-order terms in each equation. They come from Eqs. (1-4, 11, 12),

$$\bar{\rho} = \bar{\rho}_1 + \bar{\rho}_2 , \tag{1b}$$

$$\bar{n}_1 = \frac{\bar{\rho}_1}{m_1}, \tag{2b}$$

$$\bar{n}_2 = \frac{\bar{\rho}_2}{m_2}, \tag{3b}$$

$$\bar{n} = \bar{n}_1 + \bar{n}_2, \tag{4b}$$

$$\bar{p} = (\frac{\bar{\rho}_1}{m_1} + \frac{\bar{\rho}_2}{m_2})k\bar{T}, \tag{11b}$$

and,

$$\bar{\rho}\bar{u} = (\frac{\bar{\rho}_1}{m_1(\gamma_1 - 1)} + \frac{\bar{\rho}_2}{m_2(\gamma_2 - 1)})k\bar{T}. \tag{12b}$$

Rotational and irrotational waves

Our goal is to find how many modal fields can exist in the medium. The first easy step is to separate irrotational and rotational waves.

1) Irrotational wave

For a irrotational field, the curl of a particle-velocity field of each gas has to be zero by definition,

$$\nabla \times \tilde{\mathbf{v}}_1 = 0, \ \nabla \times \tilde{\mathbf{v}}_2 = 0. \tag{13}$$

Therefore, for an irrotational wave Eq. (8a), Eq. (9a) and Eq. (10a) become a set of equations for $\nabla\cdot\vec{v}_1$, $\nabla\cdot\vec{v}_2$ and $\tilde{T}$ by using the other equations and relationships of the above Eqs. (1a-12a) and (1b-4b, 11b, 12b).

$$\left[\bar{\rho}_1\frac{\partial^2}{\partial t^2}-\bar{n}_1k\bar{T}\nabla^2-(\frac{4\mu}{3}+\beta)\frac{\bar{\rho}_1}{\bar{\rho}}\frac{\partial}{\partial t}\nabla^2\right](\nabla\cdot\vec{v}_1)+$$

$$\left[\bar{\rho}_2\frac{\partial^2}{\partial t^2}-\bar{n}_2k\bar{T}\nabla^2-(\frac{4\mu}{3}+\beta)\frac{\bar{\rho}_2}{\bar{\rho}}\frac{\partial}{\partial t}\nabla^2\right](\nabla\cdot\vec{v}_2)+ \qquad (8c)$$

$$\bar{n}k\frac{\partial}{\partial t}\nabla^2\tilde{T}=0,$$

$$\frac{\bar{p}}{\bar{\rho}}\bar{\rho}_1\nabla\cdot\vec{v}_1+\frac{\bar{p}}{\bar{\rho}}\bar{\rho}_2\nabla\cdot\vec{v}_2+(\frac{n}{\gamma-1}k\frac{\partial}{\partial t}-\lambda\nabla^2)\tilde{T}=0, \qquad (9c)$$

$$\left[\frac{\partial}{\partial t}-D_{12}(1+\frac{\bar{n}_1(m_2-m_1)}{\bar{\rho}})\nabla^2\right]\nabla\cdot\vec{v}_1-$$

$$\left[\frac{\partial}{\partial t}-D_{12}(1+\frac{\bar{n}_2(m_1-m_2)}{\bar{\rho}})\nabla^2\right]\nabla\cdot\vec{v}_2+ \qquad (10c)$$

$$D_{12}\frac{\bar{n}(m_2-m_1)}{\bar{\rho}\bar{T}}\frac{\partial}{\partial t}\nabla^2\tilde{T}=0.$$

where

$$\frac{\bar{n}}{\gamma-1}=\frac{\bar{n}_1}{\gamma_1-1}+\frac{\bar{n}_2}{\gamma_2-1}. \qquad (14)$$

The Eqs. (8c-10c) have to be solved with the other linear equations and the irrotational definition Eq.(13).

2) rotational wave

The rotational wave is obtained by assuming the divergence of a particle velocity field for either gas to be zero,

$$\nabla\cdot\vec{v}_1=0,\ \nabla\cdot\vec{v}_2=0. \qquad (15)$$

With this condition, the linear fundamental equations can be simplified as

$$\frac{\partial \tilde{\rho}_1}{\partial t} = 0, \tag{6d}$$

$$\frac{\partial \tilde{\rho}_2}{\partial t} = 0, \tag{7d}$$

$$\bar{\rho}\frac{\partial \bar{\mathbf{v}}}{\partial t} = -\nabla \tilde{p} + \mu \nabla^2 \bar{\mathbf{v}}, \tag{8d}$$

$$\nabla^2 \tilde{p} = 0, \tag{8d1}$$

$$\bar{\rho}\frac{\partial \tilde{u}}{\partial t} = \lambda \nabla^2 \tilde{T}, \tag{9d}$$

$$\bar{\mathbf{v}}_1 - \bar{\mathbf{v}}_2 = -\frac{\bar{n}^2}{\bar{n}_1 \bar{n}_2} D_{12}\left(\frac{\bar{n}_1 \bar{n}_2 (m_2 - m_1)}{\bar{n}\bar{\rho}\bar{P}} \nabla \tilde{p}\right), \tag{10d}$$

$$\frac{\partial \tilde{P}}{\partial t} = \bar{n} k \frac{\partial \tilde{T}}{\partial t}, \tag{11d}$$

and,
$$\bar{\rho}\frac{\partial \tilde{u}}{\partial t} = \left(\frac{\bar{n}_1}{\gamma_1 - 1} + \frac{\bar{n}_2}{\gamma_2 - 1}\right) k \frac{\partial \tilde{T}}{\partial t}, \tag{12d}$$

where Eqs (6d-7d) and Eqs.(1a-5a) are used to derive Eqs. (9d, 10d) and the applying the divergence operator to Eq. (8d) leads to Eq. (8d1). Similarly to the irrotational wave, these equations have to be solved with Eqs.(1a-5a) and the irrotational definition Eq.(15).

Harmonic oscillation waves

When a simple harmonic disturbance is in the binary-gas mixture, quantities such as $\bar{\mathbf{v}}_1$, $\bar{\mathbf{v}}_2$, $\bar{\mathbf{v}}$, $\nabla \cdot \bar{\mathbf{v}}_1$, $\nabla \cdot \bar{\mathbf{v}}_2$, $\nabla \cdot \bar{\mathbf{v}}$, $\tilde{p}$, $\tilde{T}$, $\tilde{\rho}_1$, $\tilde{\rho}_2$ and $\tilde{\rho}$ have a factor $e^{i\omega t}$. Therefore, we have

$$\frac{\partial}{\partial t} F = i\omega F, \tag{16}$$

where F is any one of these quantities.

We also assume that F satisfies the following equation:

$$\nabla^2 F + \hat{\mathbf{k}}^2 F = 0. \tag{17}$$

where $\hat{\mathbf{k}}$ is a wave vector and $\hat{\mathbf{k}}^2 = \hat{\mathbf{k}} \bullet \hat{\mathbf{k}}$ is the square of the length of the vector. For a given frequency ω, each satisfactory $\hat{\mathbf{k}}^2$ by the above linear fundamental equations corresponds to a component wave field mode in the binary-gas mixture. The quantity $\hat{\mathbf{k}}^2$ is a complex function of

the frequency ω and represents the dispersion relationship of that mode. A similar illustration example is in a homogeneous elastic solid, where the longitudinal and shear waves correspond to two simple values of $\hat{\mathbf{k}}^2$, $(\omega/c_l)^2$ and $(\omega/c_s)^2$, with c_l and $c_s$the sound speeds of he longitudinal and shear waves in the solid respectively. The modal wave fields in a binary-gas mixture are a completely different concept from that of resonance modes in a cavity or transmitting modes in a wave guide, where different modes have a different wave vector $\hat{\mathbf{k}}$ but the same value of $\hat{\mathbf{k}}^2$.

The effect of Eqs. (16-17) is to replace operators in the linear irrotational and rotational wave equations with the following scheme:

$$\frac{\partial}{\partial t} \to i\omega, \tag{18}$$

$$\nabla^2 \to -\hat{\mathbf{k}}^2. \tag{19}$$

We first utilize this replacement scheme for the linear irrotational equations. After the operator replacement, Eqs. (8c-10c15) have the following forms:

$$\begin{aligned}&\left[\bar{n}_1 k\bar{T}\hat{k}^2 + i(\frac{4\mu}{3}+\beta)\frac{\bar{\rho}_1}{\bar{\rho}}\omega\hat{k}^2 - \bar{\rho}_1\omega^2\right](\nabla\cdot\bar{\mathbf{v}}_1)+\\ &\left[\bar{n}_2 k\bar{T}\hat{k}^2 + i(\frac{4\mu}{3}+\beta)\frac{\bar{\rho}_2}{\bar{\rho}}\omega\hat{k}^2 - \bar{\rho}_2\omega^2\right](\nabla\cdot\bar{\mathbf{v}}_2)-\\ &i\bar{n}k\omega\hat{k}^2\tilde{T}=0,\end{aligned} \tag{20}$$

$$\frac{\tilde{p}}{\bar{\rho}}\bar{\rho}_1\nabla\cdot\tilde{v}_1 + \frac{\tilde{p}}{\bar{\rho}}\bar{\rho}_2\nabla\cdot\tilde{v}_2 + (i\frac{n}{\gamma-1}k\omega + \lambda\hat{k}^2)\tilde{T}=0, \tag{21}$$

$$\begin{aligned}&\left[i\omega + D_{12}(1+\frac{\bar{n}_1(m_2-m_1)}{\bar{\rho}})\hat{k}^2\right]\nabla\cdot\bar{\mathbf{v}}_1 -\\ &\left[i\omega + D_{12}(1+\frac{\bar{n}_2(m_1-m_2)}{\bar{\rho}})\hat{k}^2\right]\nabla\cdot\bar{\mathbf{v}}_2 -\\ &iD_{12}\frac{\bar{n}(m_2-m_1)}{\bar{\rho}\bar{T}}\omega\hat{k}^2\tilde{T}=0.\end{aligned} \tag{22}$$

Further simplification of Eqs. (21-23) is achieved by introducing the dimensionless quantities:

$$
\begin{aligned}
&x=\frac{\hat{k}^2c^2}{\omega^2},\quad \bar{p}_1^*=\frac{\bar{n}_1k\bar{T}}{\bar{\rho}c^2},\qquad \bar{p}_2^*=\frac{\bar{n}_2k\bar{T}}{\bar{\rho}c^2},\\
&\nabla^*\cdot\vec{\mathbf{v}}_1^*=i\frac{\nabla\cdot\vec{\mathbf{v}}_1}{\omega},\qquad \nabla^*\cdot\vec{\mathbf{v}}_2^*=i\frac{\nabla\cdot\vec{\mathbf{v}}_2}{\omega},\\
&\bar{\rho}_1^*=\frac{\bar{\rho}_1}{\bar{\rho}},\qquad \bar{\rho}_2^*=\frac{\bar{\rho}_2}{\bar{\rho}},\qquad \tilde{\rho}_1^*=\frac{\tilde{\rho}_1}{\bar{\rho}},\qquad \tilde{\rho}_2^*=\frac{\tilde{\rho}_2}{\bar{\rho}},\\
&m_1^*=\frac{m_1}{m_1+m_2},\quad m_2^*=\frac{m_2}{m_1+m_2},\\
&\tilde{p}^*=\frac{\tilde{p}}{\bar{\rho}c^2},\qquad \tilde{T}^*=\frac{\tilde{T}}{\bar{T}},\qquad \nabla^*\cdot\vec{\mathbf{v}}^*=i\frac{\nabla\cdot\vec{\mathbf{v}}}{\omega},\\
&\varepsilon_\mu=\frac{i\omega(\frac{4}{3}\mu+\beta)}{\bar{\rho}c^2},\quad \varepsilon_\lambda=\frac{i\omega\lambda}{\bar{\rho}c_pc^2},\quad \varepsilon_\kappa=\frac{i\omega D_{12}(m_1+m_2)n}{\bar{\rho}c^2},
\end{aligned}
\tag{23}
$$

where c_p is the specific-heat coefficient at constant pressure, and the sound velocity squared $c^2=\gamma\bar{p}/\bar{\rho}$. With these dimensionless quantities, solution for $\hat{\mathbf{k}}^2$ is changed to for the dimensionless quantity x. The three ε's are usually much smaller than 1 and this property is helpful in arriving at concise analytical solutions for x.

In terms of these dimensionless quantities, Eqs. (21-23) become

$$[(\bar{p}_1^*+\bar{\rho}_1^*\varepsilon_\mu)x-\bar{\rho}_1^*]\nabla^*\cdot\vec{\mathbf{v}}_1^*+[(\bar{p}_2^*+\bar{\rho}_2^*\varepsilon_\mu)x-\bar{\rho}_2^*]\nabla^*\cdot\vec{\mathbf{v}}_2^*+(\bar{p}_1^*+\bar{p}_2^*)x\tilde{T}=0, \tag{24}$$

$$\bar{\rho}_1^*\nabla^*\cdot\vec{\mathbf{v}}_1^*+\bar{\rho}_2^*\nabla^*\cdot\vec{\mathbf{v}}_2^*-\frac{1-\gamma\varepsilon_\lambda x}{\gamma-1}\tilde{T}^*=0, \tag{25}$$

$$(1-m_2^*\varepsilon_\kappa x)\nabla^*\cdot\vec{\mathbf{v}}_1^*-(1-m_1^*\varepsilon_\kappa x)\nabla^*\cdot\vec{\mathbf{v}}_2^*-(m_2^*-m_1^*)\varepsilon_\kappa x\tilde{T}^*=0. \tag{26}$$

Once we get solutions for $\nabla^*\cdot\vec{\mathbf{v}}_1^*$, $\nabla^*\cdot\vec{\mathbf{v}}_2^*$ and $\tilde{T}^*$ from Eqs. (24-26), we can express $\tilde{\rho}_1^*$, $\tilde{\rho}_2^*$, $\tilde{p}^*$ and $\nabla^*\cdot\vec{\mathbf{v}}^*$ in terms of $\nabla^*\cdot\vec{\mathbf{v}}_1^*$, $\nabla^*\cdot\vec{\mathbf{v}}_2^*$ and $\tilde{T}^*$, using Eq. (6a), Eq. (7a) and Eq. (5a).

$$
\begin{aligned}
&\tilde{\rho}_1^*=\nabla^*\cdot\vec{\mathbf{v}}_1^*,\\
&\tilde{\rho}_2^*=\nabla^*\cdot\vec{\mathbf{v}}_2^*\\
&\tilde{p}^*=\frac{1-x\varepsilon_\mu}{x}(\bar{\rho}_1^*\nabla^*\cdot\vec{\mathbf{v}}_1^*+\bar{\rho}_2^*\nabla^*\cdot\vec{\mathbf{v}}_2^*),\\
&\nabla^*\cdot\vec{\mathbf{v}}^*=\bar{\rho}_1^*\nabla^*\cdot\vec{\mathbf{v}}_1^*+\bar{\rho}_2^*\nabla^*\cdot\vec{\mathbf{v}}_2^*.
\end{aligned}
\tag{27}
$$

The velocity fields $\vec{\mathbf{v}}_1^*$, $\vec{\mathbf{v}}_2^*$, $\vec{\mathbf{v}}^*$ have to meet the irrotational condition Eq. (13).

In the same way, the implementation of the operator replacement Eqs. (18-19) in the rotational wave equations Eqs. (6d-12d) results in very simple equations. Eqs. (6d,7d, 8d1) become

$$i\omega\tilde{\rho}_1 = 0, \tag{7e}$$

$$i\omega\tilde{\rho}_2 = 0, \tag{7e}$$

$$-\hat{\mathbf{k}}^2\tilde{p} = 0. \tag{8e1}$$

Thus, these equation have a simple solution since neither ω nor $\hat{\mathbf{k}}^2$ equal to zero is interesting in our objective,

$$\begin{aligned} &\tilde{\rho}_1 = 0, \\ &\tilde{\rho}_2 = 0, \\ &\tilde{p} = 0. \end{aligned} \tag{29}$$

Substituting Eq. (29) in the other equations, we have

$$\begin{aligned} &i\omega\overline{\rho}\vec{\mathbf{v}} = -\mu\hat{\mathbf{k}}^2\vec{\mathbf{v}}, \\ &\tilde{T} = 0, \\ &\vec{\mathbf{v}}_1 = \vec{\mathbf{v}}_2. \end{aligned} \tag{30}$$

In terms of dimensionless quantities, Eqs. (29-39) can be rewritten as the follows:

$$(x - \frac{1}{\varepsilon_{\mu 0}})\vec{\mathbf{v}}^* = 0, \tag{31}$$

$$\begin{cases} \vec{\mathbf{v}}_1^* = \vec{\mathbf{v}}_2^* \\ \tilde{p}^* = \tilde{T}^* = \tilde{\rho}_1^* = \tilde{\rho}_2^* = 0 \end{cases}, \tag{32}$$

where the dimensionless quantity $\varepsilon_{\mu 0}$ is defines as

$$\varepsilon_{\mu 0} = \frac{i\omega\mu}{\overline{\rho}c^2}. \tag{33}$$

Since a length is rescaled by c/ω in this dimensionless system, a dimensionless velocity should be a velocity rescaled by $-ic$ in order to keep the consistency with the definitions in Eq. (23),

$$\vec{\mathbf{v}}_1^{\,*} = \frac{i\vec{\mathbf{v}}_1}{c}, \quad \vec{\mathbf{v}}_2^{\,*} = \frac{i\vec{\mathbf{v}}_2}{c}, \quad \vec{\mathbf{v}}^{\,*} = \frac{i\vec{\mathbf{v}}}{c}. \tag{34}$$

One rotational wave mode and three irrotational wave modes

Zero disturbances of temparature, velocity, etc. are apparently a solution of Eqs. (24-26) for irrotational waves and Eq. (31) for rotational waves. However, no disturbances represent the equalibrium state and, therefore, nothing has be achieved. It is obvious that any wave satisfying Eq. (17) with an arbitrary value of $\hat{\mathbf{k}}^2$ for a given frequency ω will not be supported by the medium. Only a few of values of $\hat{\mathbf{k}}^2$ can serve the purpose. Therefore, a non zero solution only exists only when the relation between the frequency ω and $\hat{\mathbf{k}}^2$(or the dimensionless quantity x) meets a specific condition. This condition is actually the dispersion relationship of the wave of the corresponding solution. Exhausting every possible condition will reveal all the wave modes in the medium.

1) Voracity mode

We start with the simple equation of the rotational wave. Since non zero solution is desirable, the equation (31) can be satisfied only if

$$x = x_v = 1/\varepsilon_{\mu 0}. \tag{35}$$

When this condition is satisfied, there is a non-zero solution , which is a rotational wave mode. Because of Eq. (32), all physical quantities except the velocity fields are zero in the mode. Moreover, the velocities of two gases are equal. This is the vorticity mode exactly the same as the one in a mono-gas medium. For completeness, the equations for the mode are summerized below;

$$\nabla^{*2}\vec{\mathbf{v}}^{\,*} + x_v \vec{\mathbf{v}}^{\,*} = 0$$
$$\nabla^{*} \bullet \vec{\mathbf{v}}^{\,*} = 0 \qquad (36)$$
$$\begin{cases} \vec{\mathbf{v}}_1^{\,*} = \vec{\mathbf{v}}_2^{\,*} = \vec{\mathbf{v}}^{\,*} \\ \tilde{p}^{*} = \tilde{T}^{*} = \tilde{\rho}_1^{\,*} = \tilde{\rho}_2^{\,*} = 0 \,. \end{cases}$$

A proper coordinate system is needed before solving them.

2) acoustical, thermal and mass diffusion modes

The irrotational wave equations Eq. (24-26) are a set of homogenous equations for $\nabla^{*} \cdot \vec{\mathbf{v}}_1^{*}$, $\nabla^{*} \cdot \vec{\mathbf{v}}_2^{*}$ and $\tilde{T}^{*}$. Only when the determinant of the matrix formed by the coefficients of $\nabla^{*} \cdot \vec{\mathbf{v}}_1^{*}$, $\nabla^{*} \cdot \vec{\mathbf{v}}_2^{*}$ and $\tilde{T}^{*}$ is equal to zero will the set of equations have a non zero solution.

$$\begin{vmatrix} (\overline{p}_1^{*} + \overline{\rho}_1^{*}\varepsilon_\mu)x - \overline{p}_1^{*} & (\overline{p}_2^{*} + \overline{\rho}_2^{*}\varepsilon_\mu)x - \overline{p}_2^{*} & (\overline{p}_1^{*} + \overline{p}_2^{*})x \\ \overline{\rho}_1^{*} & \overline{\rho}_2^{*} & -\dfrac{1-\gamma\varepsilon_\lambda x}{\gamma-1} \\ 1 - m_2^{*}\varepsilon_\kappa x & -(1 - m_1^{*}\varepsilon_\kappa x) & -(m_2^{*} - m_1^{*})\varepsilon_\kappa x \end{vmatrix} = 0 \qquad (37)$$

Obviously, Eq. (37) is a cubic equation for x, which has and only has three roots. The three conditions which demand x to be equal to one of the roots provide three solutions for Eq. (24-26), the three modes of irrotational waves.

A cubic equation has routine formula for its roots. However, the expresions of the three roots are so complicated to handle with. Concise expresions are possible due to the fact that ε_μ, ε_κ and ε_λ are usually much smaller than 1. By expanding the solutions in a Taylor series and keeping the two lowest orders in ε_μ, ε_κ and ε_λ , the three solutions of the cubic equation can expressed as the dimensionless quantity x equal to one of the three roots x_A, x_T, x_M,

$$x_A = 1 - (g_2 - \gamma g_1)\varepsilon_\kappa - (\gamma - 1)\varepsilon_\lambda - \varepsilon_\mu, \qquad (38)$$
$$x_T = \frac{1}{\varepsilon_\lambda} + \frac{(\gamma-1)(\varepsilon_\lambda - g_2\varepsilon_\kappa)(\varepsilon_\lambda - \varepsilon_\mu)}{\varepsilon_\lambda(\varepsilon_\lambda - \gamma g_1\varepsilon_\kappa)}, \qquad (39)$$
$$x_M = \frac{1}{\gamma g_1 \varepsilon_\kappa} - \frac{(\gamma g_1 - g_2)(\varepsilon_\lambda - g_1\varepsilon_\kappa)(\gamma g_1\varepsilon_\kappa - \varepsilon_\mu)}{\gamma g_1^{\,2}\varepsilon_\kappa(\varepsilon_\lambda - \gamma g_1\varepsilon_\kappa)}, \qquad (40)$$

when $\varepsilon_\lambda - \gamma g_1 \varepsilon_\kappa$ is the same order as the three ε's, where $g_1 = \bar{p}_1^* m_1^* + \bar{p}_2^* m_2^*$, $g_2 = \bar{\rho}_1^* m_1^* + \bar{\rho}_2^* m_2^*$. In the other cases when ε_λ and $\gamma g_1 \varepsilon_\kappa$ are very close, x_T and x_M take the following expressions instead,

$$x_T = \frac{1}{\varepsilon_\lambda} + \sqrt{\frac{(\gamma-1)(g_2 - \gamma g_1)(\varepsilon_\lambda - \varepsilon_\mu)}{\gamma g_1 \varepsilon_\lambda^{\,2}}}, \tag{41}$$

$$x_M = \frac{1}{\gamma g_1 \varepsilon_\kappa} - \sqrt{\frac{(\gamma-1)(g_2 - \gamma g_1)(\varepsilon_\lambda - \varepsilon_\mu)}{\gamma g_1 \varepsilon_\lambda^{\,2}}}. \tag{42}$$

The roots x_A and x_T, Eqs. (38-39), are similar to those for the acoustical mode and the entropy mode in a mono-gas medium (See Eqs. (10-37a, 10-37b) of Pierce [1989]). Except a different sign in the front of some terms which is due to the temporal variation term $\exp(\omega t)$ instead of $\exp(-\omega t)$ in Pierce's, they become the same as Eqs. (10-37a, 10-37b) if ε_κ is set to zero in Eqs. (38-39). Therefore, the mode with the root x_A is the acoustical mode, the mode with the root x_T has a close connection with the thermal conductivity and is the thermal mode or entropy mode. The last one with x_M is unique in a binary-gas medium and largely due to the mutual mass diffusion; we define this mode as a mass diffusion mode.

When these three roots are quite different and x is substituted for one of three roots, only two of the three linear equations Eqs. (24-26) for $\nabla^* \cdot \bar{\mathbf{v}}_1^*$, $\nabla^* \cdot \bar{\mathbf{v}}_2^*$ and $\tilde{T}^*$ are independent; a three one can be expressed as a linear combination of the other two. Thus, there are total six [two from Eqs. (24-26) plus four in Eq. (27)] independent equations for the seven physical quantities $\nabla^* \cdot \bar{\mathbf{v}}_1^*$, $\nabla^* \cdot \bar{\mathbf{v}}_2^*$, $\tilde{T}^*$, $\tilde{\rho}_1^*$, $\tilde{\rho}_2^*$, $\tilde{p}^*$ and $\nabla^* \cdot \bar{\mathbf{v}}^*$. As a result, only one of seven physical quantities is independent and the others can be expressed in terms of the independent one. If one physical quantity, say $\nabla^* \cdot \bar{\mathbf{v}}^*$, is chosen as the independent one, the whole problem for each of the irrotational modes can be stated in the following equations,

$$\begin{aligned} &\nabla^{*2} \nabla^* \bullet \bar{\mathbf{v}}^* + x \nabla^* \bullet \bar{\mathbf{v}}^* = 0, \\ &\nabla^* \times \bar{\mathbf{v}}^* = 0, \end{aligned} \tag{43}$$

$$\tilde{\rho}_1^* = \nabla^* \cdot \bar{\mathbf{v}}_1^* = \frac{[\bar{\rho}_2^* - x(\bar{p}_2^* + \bar{\rho}_2^* \varepsilon_\mu)]\gamma(1 - \gamma\varepsilon_\lambda x) - x(\gamma-1)\bar{\rho}_2^*}{(\gamma \bar{p}_1^* - \tilde{\rho}_1^*) x (1 - \gamma \varepsilon_\lambda x)} \nabla^* \cdot \bar{\mathbf{v}}^*,$$

$$\tilde{\rho}_2^* = \nabla^* \cdot \vec{\mathbf{v}}_2^* = \frac{[\overline{\rho}_1^* - x(\overline{p}_1^* + \overline{\rho}_1^* \varepsilon_\mu)]\gamma(1-\gamma\varepsilon_\lambda x) - x(\gamma-1)\overline{\rho}_1^*}{(\tilde{\rho}_1^* - \gamma\overline{p}_1^*)x(1-\gamma\varepsilon_\lambda x)} \nabla^* \cdot \vec{\mathbf{v}}^*,$$

$$\tilde{p}^* = \frac{1-x\varepsilon_\mu}{x} \nabla^* \cdot \vec{\mathbf{v}}^*, \qquad (44)$$

$$\tilde{T}^* = \frac{\gamma-1}{1-x\gamma\varepsilon_\lambda} \nabla^* \cdot \vec{\mathbf{v}}^*.$$

where x should be equal to x_A or x_T or x_M.

For the case when x_T and x_M are equal, a set of equations equivalent to Eqs. (43-44) is easy to be established with a knowledge of linear algebra. We will not elaborate this case too much. It is interesting to note that there are two "orthonormal" modes associated with the two equal roots of x. . Two alternative "orthonormal" modes can be constructed by a proper linear combination of the two old "orthonormal" modes and the two new modes are equally good. Hence, the question as to which of the two modes is mainly duo to the thermal conductivity or the mass diffusion becomes meaningless in the case. Each of the two "orthonormal" modes is largely due to the combination effects of the thermal conductivity and the mutual mass diffusion. In other word, it is important that thermal conductivity, viscosity and mutual mass diffusion be simultaneously taken into account to solve the problem in a binary-gas medium.

General solutions and classical attenuation coefficient

The four modes form a set of complete component modal fields. In one hand, a harmonic field can be decomposed into these four modes, which can propagate independently in the binary-gas mixture. A disturbance of a physical quantity can be written as a linear superposition of four components from each modal fields. That means any general solution can be built up with these four basic modes. In the other hand, the family of the solutions based on these four mode contains all the solutions in the medium

Before finishing this paper, we have some comments about the dispersion relationship of the four modes. First, the imaginary parts of the square root of x_v, x_A, x_T, x_M are the attenuation coefficients of the corresponding modes in nepers per $\lambda/2\pi$, where λ is the

acoustical wavelength. Because all ε's are usually small in magnitude and pure imaginary, the vorticity mode, the thermal mode and the mass diffusion mode are highly damping modes. Therefore, these three highly attenuated modes have a significant amplitude near a interface, and only the acoustical mode can survive for a long distance. The four modes will coexist and be equally important, for example, in the vapor-gas mixture inside a bubble or in a narrow wet tube [Mao, et al., 1996a; Mao, et al., 1996b]. Secondly, the expression for root x_A Eq. (38) has an extra term, comparing to that in the mono-gas case (Eq. (10-3.7a) of Pierce [1989]). The extra term brings in one more classical attenuation mechanism for the acoustical wave in a binary-gas medium in addition to the viscosity and the thermal conductivity. It is the attenuation duo to the mutual mass diffusion. The factor $(g_2 - \gamma g_1)$ in the extra term is non-negative,

$$g_2 - \gamma g_1 = \frac{\rho_1 \rho_2}{n\rho} \frac{(m_1 - m_2)^2}{m_1 m_2 (m_1 + m_2)} \geq 0. \tag{45}$$

This gives a consistent conclusion that the additional term has the same sign as the other two damping terms, and the mass diffusion never strengthen the acoustic wave. The factor becomes zero when the two gases have the same molecular masses. Moreover, two favorable conditions for a significant effect of this attenuation mechanism are seen in Eq. (45). They are (1) a large difference of the molecular masses and (2) nearly equal densities of the two gases. With the expression for root x_A Eq. (38), the classical attenuation coefficient α_{cl} has a form as follows:

$$\alpha_{cl} = \frac{\omega^2}{c^3} \delta_{cl}, \tag{46}$$

$$\delta_{cl} = \frac{\mu}{2\rho} [(\frac{4}{3} + \frac{\beta}{\mu}) + \frac{\gamma - 1}{\mu c_p / \lambda} + \frac{\rho_1 \rho_2}{\rho^2} \frac{(m_1 - m_2)^2}{m_1 m_2} \frac{\rho D_{12}}{\mu}]. \tag{47}$$

In the brackets of the above expression Eq. (47), the first two terms in parentheses and the third term are due to, respectively, viscosity and thermal conductivity. They are the same as in a mono-gas medium (see Eq. (10-2.12) of Pierce [1989]) and both have a magnitude of one. The last term is due to the mutual mass diffusion in a binary-gas mixture. The value of this term varies considerably depending the composition of two gases. For example, in the air considered

as a binary-gas mixture of N_2 and O_2 with $\rho_1 \approx .25\rho$, $\rho_2 \approx .75\rho$, $m_1 = 32$, $m_2 = 28$, $\rho D_{12} / \mu = 0.00125 \times 0.181 / 1.719 \times 10^{-3} \approx 0.126$, the last term is roughly 4.2×10^{-4}. Therefore, the classical attenuation coefficient in the air has a negligible contribution from the mutual mass diffusion. However, if the mixture is composed of He and Kr gases with $\rho_1 \approx .50\rho$, $\rho_2 \approx .50\rho$, $m_1 = 4$, $m_2 = 84$, $\rho D_{12} / \mu = 0.00034 \times 0.558 / (2.328/2 + 1.865/2) \times 10^{-3} \approx 0.09$, the term is about 0.43, which is comparable to the other two terms. Therefore, the energy dissipated by the mutual mass diffusion may not neglected in the calculation of the classical attenuation coefficient in a mixture of two gases with nearly equal densities but a large difference of their molecular masses.

Acknowledgments

The authors wish to gratefully acknowledge the financial support by the Office of Naval Research.

REFERENCES

Hsieh, D. Y., " Some analytical aspects of bubble dynamics, " J. Basic Eng. Am. **87**, 991-1005, (1965).

Mao, Y., Crum, L. A., and Roy, R. A., "Resonance frequency and damping constant of a gas-vapor Bubble," submitted to J. Acoust. Soc. Am. (1996a).

Mao, Y., Sabatier, J. M., and Raspet, R., "Sound attenuation in a cylindrical tube due to evaporation-condensation," submitted to J. Acoust. Soc. Am. (1996b).

Pierce, A. D., Acoustics: An introduction to its physical principles and applications, (Acoust. Soc. Am., 1989), pp. 515-538.

DISTRIBUTION LIST FOR
No. 1.LC.APL.96
UNDER GRANT N00014-93-1-0322
FINAL REPORT

Name	No. of Copies
DR. LOGAN HARGROVE OFFICE OF NAVAL RESEARCH PHYSICS DIVISION ONR 312 800 NORTH QUINCY STREET ARLINGTON VA 22217-5660	2
DEFENSE TECHNICAL INFORMATION CENTER BUILDING 5 CAMERON STATION ALEXANDRIA VA 22314	2
ADMINISTRATIVE GRANTS OFFICER OFFICE OF NAVAL RESEARCH RESIDENT REPRESENTATIVE N63374 UNIV. OF WASHINGTON, UNIV. DISTRICT RM 410, 1107 NE 45TH ST SEATTLE, WA 98105-4631	1
NAVAL RESEARCH LABORATORY ATTN CODE 2667 4555 OVERLOOK AVENUE SW WASHINGTON DC 20375-5320	1
NAVAL POSTGRADUATE SCHOOL TECHNICAL LIBRARY CODE 0212 MONTEREY CA 93943	1
PROF. ANTHONY A. ATCHLEY DEPT OF PHYSICS CODE PH/AY NAVAL POSTGRADUATE SCHOOL MONTEREY, CA 94943-5000	1
PROFESSOR PHILIP MARSTON DEPT. OF PHYSICS WASHINGTON STATE UNIVERSITY PULLMAN, WA 99164-2814	1
PROF. ANDREA PROSPERETTI DEPT. OF MECHANICAL ENGINEERING JOHNS HOPKINS UNIVERSITY BALTIMORE, MD 21218	1